Analysis of weakly chromophore impurities by means of liquid chromatography coupled with charged aerosol detection and mass spectrometry

Dissertation zur Erlangung des naturwissenschaftlichen

Doktorgrades der Julius-Maximilians-Universität Würzburg

vorgelegt von

Rasmus Walther

aus Coburg

Würzburg 2023

Eingereicht bei der Fakultät für Chemie und Pharmazie am

_____

Gutachter der schriftlichen Arbeit

1. Gutachter: _____

2. Gutachter: _____

Prüfer des öffentlichen Promotionskolloquiums

1. Prüfer: _____

2. Prüfer: _____

3. Prüfer: _____

Datum des öffentlichen Promotionskolloquiums

_____

Doktorurkunde ausgehändigt am

_____

„The ability to speak does not make you intelligent."

– *Qui-Gon Jinn, The Phantom Menace* –

Für meinen Vater

DANKSAGUNG

Die vorliegende Arbeit wurde auf Anregung und unter Anleitung von

Frau Prof. Dr. Ulrike Holzgrabe

am Lehrstuhl für Pharmazeutische und Medizinische Chemie

des Instituts für Pharmazie und Lebensmittelchemie

der Julius-Maximilians-Universität Würzburg angefertigt.

Ich möchte mich an dieser Stelle bei Ihr für die freundliche Aufnahme in den Arbeitskreis, ihren Anregungen und Ideen sowie für das in mich gesetzte Vertrauen bedanken, welches mir das selbständige und eigenverantwortliche Anfertigen dieser Arbeit ermöglichte.

Ebenso bedanken möchte ich mich bei Herrn Prof. Dr. Oliver Scherf-Clavel für seine „offene Tür" und bereitwillige Unterstützung bei allen Fragen und Problemen rund um das Carbocystein-Projekt.

Weiterer Dank gilt Frau Dr. Anette Zamponi von A. Nattermann & Cie. GmbH – a Sanofi Company in Köln für die interessanten Einblicke und die gute Zusammenarbeit, sowie Herrn Prof. Dr. Fritz Sörgel und Frau Dr. Martina Kinzig vom IBMP in Heroldsberg.

Table of contents

TBALE OF CONTENTS

List of abbreviations

AA	amino acid
ACN	acetonitrile
AEX	anion exchange
AmFA	ammonium formate
AmOAc	ammonium acetate
ANOVA	analysis of variance
API	active pharmaceutical ingredient
AQbD	analytical quality by design
A_s	asymmetry factor
ATP	analytical target profile
BBD	Box-Behnken design
CAD	charged aerosol detector
CC	carbocisteine
CCD	central composite design
CEX	cation exchange
CID	collision induced dissociation
CMA	critical method attribute
CMP	critical method parameter
CRS	chemical reference substance
CysTGA	disulfide between *L*-cysteine and thioglycolic acid
D	dwell volume
DAD	diode array detector
DiBA	dibutylamine
DiMBA	*N,N*-dimethylbutylamine
DiMHA	*N,N*-dimethylhexylamine

LIST OF ABBREVIATIONS

DoE	design of experiments
DP	degradation product
DS	design space
ELSD	evaporative light scattering detector
ESI	electrospray ionisation
FA	formic acid (in chapters 3.1 and 3.3)
	fatty acid (in chapter 3.4)
FIA	flow injection analysis
GC	gas chromatography
GUCS	general unknown comparative screening
HILIC	hydrophilic interaction liquid chromatography
HOAc	acetic acid
HPLC	high performance liquid chromatography
HRMS	high-resolution mass spectrometry
ICH	International Council for Harmonisation of Technical Requirements for Pharmaceuticals for Human Use
IDA	information dependent acquisition
IEX	ion exchange
IPC	ion pair chromatography
IPR	ion-pairing reagent
k	capacity/retention factor
LA	carbocisteine lactam
LASO	lactam of the carbocisteine sulfoxides
LC	liquid chromatography
LOQ	limit of quantification/quantitation
MC	Monte Carlo
MeOH	methanol

MMC	mixed-mode chromatography
MODR	method operable design region
MS	mass spectrometry
m/z	mass-to-charge ratio
OFAT	one-factor-at-a-time
p	probability
PFV	power function value
p/v	peak-to-valley ratio
Ph. Eur.	European Pharmacopoeia
PS	polysorbate
QqQ	triple quadrupole
QqTOF	quadrupole time-of-flight
(adj.) R^2	(adjusted) coefficient of determination
RDB	ring double bond equivalent
RF	radio frequency
RP	reversed phase (in chapter 3.1, 3.3 and 3.4)
	reaction product (in chapter 3.2)
R_s	resolution
RSD	relative standard deviation
RSM	response surface methodology
RT	retention time
SAX	strong anion exchange
S criterion	separation criterion
SCX	strong cation exchange
SMD	Sauter mean diameter
S/N	signal-to-noise ratio
SO	carbocisteine sulfoxide

LIST OF ABBREVIATIONS

SWATH	sequential window acquisition of all theoretical fragments
TBAOH	tetrabutylammonium hydroxide
TFA	trifluoroacetic acid
TriBA	tributylamine
TriEA	triethylamine
TriPA	tripropylamine
USP	United States Pharmacopeia
UV	ultraviolet
WAX	weak anion exchange
WCX	weak cation exchange
XIC	extracted ion chromatogram

1. INTRODUCTION

For the approval of a new medicine, the manufacturer is obliged to prove the efficacy, safety and quality through appropriate studies [1-3]. In the ongoing "lifecycle" of a drug, it is therefore essential to monitor the quality of each batch produced, in addition to pharmacovigilance [4,5]. In the globally connected pharmaceutical industry, the three major pharmacopoeias – the *European Pharmacopoeia* (Ph. Eur.), the *United States Pharmacopeia* (USP) and the *Japanese Pharmacopoeia* - and the complementary quality guidelines of the *International Council for Harmonisation of Technical Requirements for Pharmaceuticals for Human Use* (ICH) have become particularly prominent in this regard [6-8]. Since most finished drug products usually consist of only a small amount of the active pharmaceutical ingredient (API) and a large amount of excipients, not only the quality of the individual API but also of all excipients is crucial for the overall quality. In addition, the compatibility of the API with the excipients or of the excipients with each other must be ensured [9]. In the Ph. Eur., therefore, one finds monographs with tests of the identity, purity and assay of drug substances, excipients and, with increasing numbers, finished medicinal products like e.g. sitagliptin tablets [10]. The "purity" must be considered in a sophisticated manner, since a variety of impurities can emerge depending on the production process and can only be covered in their entirety by the appropriate combination of different tests [11]. For example, residual solvents can be controlled using headspace gas chromatography [12]. For acidic or basic impurities, on the other hand, the simple measurement of the pH value is sufficient [13]. However, the focus of this work is on impurities that are structurally similar to the drug substance, the so-called "related substances" [14]. Because of this similarity, the use of (ultra)high-performance chromatographic separation techniques, often with ultraviolet (UV) light detection, has proven to be a reliable workhorse for this purpose [15-17].

The development and validation of efficient liquid chromatography (LC) methods for testing for related substances depends on various factors and requires good planning. The chemical structure of the drug substance and its impurities play a decisive role in the choice of the right chromatographic system and detector type. For compounds that are not UV-active, for example, the charge aerosol detector (CAD) is a promising alternative [18,19]. If, on the other hand, one does not know the structure of the contaminants or wants to obtain a comprehensive picture of the impurity profile, one can resort to high-resolution mass spectrometry (HRMS) [20-22].

1.1. Selection of the appropriate chromatographic systems

Compared to "simple" thin-layer chromatography, the development to modern packed columns as stationary phases brought an enormous improvement in efficiency and selectivity, justifying the name *high-performance liquid chromatography* (HPLC) [16,23]. Nowadays, a wide range of modified column materials in different dimensions is available from various manufacturers for the analysis of small molecules. The selection of an appropriate column as the heart of the chromatographic separation is governed on the structure of the analytes and their physicochemical properties. The mobile phase affects the different distribution of the analytes in the two phases and thus also determines whether a separation is successful [24]. Depending on the selected stationary and mobile phase, individual separation mechanisms come to the fore (see Table 1), which are briefly discussed below [23].

Table 1
Overview of commonly applied liquid chromatographic separation techniques for the analysis of organic small molecules: reversed phase (RP), ion pair chromatography (IPC), hydrophilic interaction liquid chromatography (HILIC) and mixed-mode chromatography (MMC) [16,23-25]

analyte	stationary phase	mobile phase	type
lipophilic	e.g. silica gel modified with C_{18} chains	mixture of water and organic solvents (usually acetonitrile or methanol)*	RP
hydrophilic /ionic	e.g. silica gel modified with C_{18} chains	analogous to RP, but with an ion pairing reagent*	IPC
	e.g. silica gel modified with aminopropyl chains	mixture of high percentage of organic solvent and a small amount of water*	HILIC
	e.g. silica gel modified with alkyl chains and ionizable moieties	analogous to RP, but mandatory with ionic additiva	MMC

* in most applications, a suitable buffer or acid is added for pH control

1.1.1. Reversed phase chromatography

Of the more than 600 reversed phase (RP) columns available on the market, most are silica-based and modified with C_{18} or C_8 alkyl chains. Depending on the manufacturing procedure, there are columns with e.g. different carbon load, pore size or specific surface are, which are better or worse suited for a certain application despite the nominally same column chemistry [26,27]. Another characteristic is the so-called "end-capping" of remaining silanol groups with e.g trimethylchlorosilane [23] Since many drugs are bases, depending on the pH of the mobile phase, undesirable ion-ion interactions of the protonated amines with the remaining free silanol group result in peak tailing. From a mobile phase perspective, the addition of trifluoracetic acid (TFA) with its ion pair-like properties (see section 1.1.2) is an alternative to effectively improve the peak shape of basic analytes [28]. The separation can be fine-tuned by the selection of the type of organic modifier, its percentage and, in the case of ionisable analytes, by the pH value and the type and concentration of the additive.

To achieve a sufficient resolution between structurally closely related critical peak pairs on the one hand, or to shorten the runtime in the case of strongly differing lipophilicity of the analytes and minimize diffusion effects on the other hand, gradient elution offers a feasible solution in many cases [29]. Here, for example, the methanol or acetonitrile percentage is continuously increased to ramp up the eluotropic strength of the mobile phase. For the theoretically prediction of retention, various models such as Snyder´s *linear solvent strength model* have been developed, which facilitate software-assisted optimization in only a limited number of runs and thus accelerate method development [30,31]. As widespread as the aplication of RP LC may be, it reaches its limits in the analysis of hydrophilic, charged analytes that interact little or not at all with the lipophilic stationary phase. Ion pair chromatography (IPC), mixed-mode chromatography (MMC) or hydrophilic interaction liquid chromatography (HILIC) offer interesting solutions for this category of challenging analytes without the need for time-consuming and error-prone derivatisation as is/was often used in compendial amino acid analysis [23,32].

1.1.2. Ion pair chromatography

To increase the retention of hydrophilic, charged analytes on RP columns, oppositely charged ion-pairing reagents (IPR) are added to the mobile phase in IPC. In the first IPC applications, alkylsulfates were employed for the analysis of basic substances and, vice versa, tetraalkylammonium salts can be used for the analysis of acidic, polar APIs (see chapter 3.1) under otherwise RP LC conditions [23]. Due to their non-volatility, the first soap-like IPRs are not compatible with mass spectrometry (MS) or aerosol-based detectors. Perfluorinated carboxylic acids and various volatile alkylamines with high vapor pressure such as triethylamine have proven to be suitable alternatives (see Fig. 1) [23,33-36].
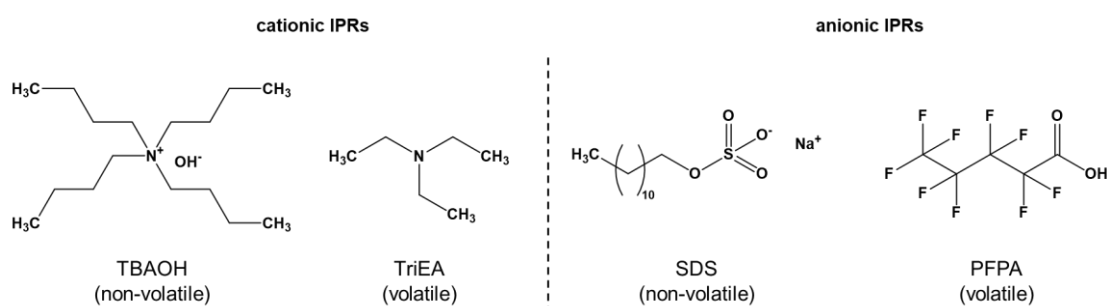
Fig. 1 Chemical structures of commonly used cationic and anionic ion-pairing reagents (IPR) (TBAOH: tetrabutylammonium hydroxide, TriEA: triethylamine, SDS: sodium dodecyl sulfate, PFPA: perfluoropentanoic acid)

All IPRs are amphiphilic molecules and feature a lipophilic tail with an ionized head that is responsible for the formation of an electric neutral "ion pair" with the analyte. Dynamic adsorption of the IPR *via* their alkyl chain modifies the nonpolar surface of the RP columns and creates an electric bilayer that ultimately leads to retention/separation (see Fig. 2a).

Since the equilibrium of adsorption, the composition of the electrical bilayer and ionic interactions are influenced not only by the type and concentration of the IPR but also by the counterions, the pH value, the organic solvent and the temperature, various models for describing and predicting the retention behaviour have been developed over time [37,38]. The large number of influencing factors complicates method development. For laboratory practice, the following disadvantageous points must be considered:

- Due to irreversible adsorption (especially of long-chain IPRs) the selectivity of the RP column is altered permanently, and the column is dedicated for this application [38].
- Even the volatile IPRs influence ionization for mass spectrometric detection (e.g. suppression by TFA in negative ion mode using electrospray ionisation [39]).
- Compared to RP LC, much longer equilibration times and especially re-equilibration times using gradient elution are required in some cases [40].
- The cost of acquiring high-purity IPRs is higher than for standard LC additives.
- Separate waste disposal of reagents (e.g. perfluorinated acids are environmentally persistent and presumably toxic for humans and animals) may be necessary in the future [41,42].

Fig. 2 Simplified overview of the main retention mechanisms in a) ion pair chromatography due to dynamic adsorption of oppositely charged ion-pairing reagents (IPR) onto the reversed phase (RP) column and b) mixed-mode chromatography with embedded ion exchange (IEX) functionalities

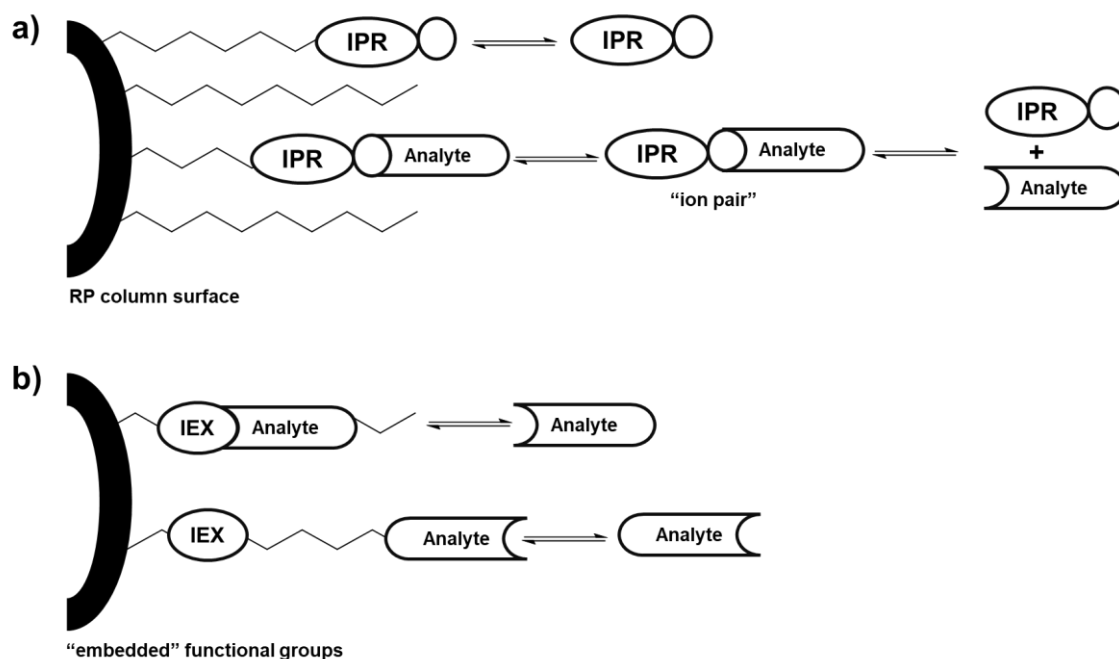Nevertheless, IPC has provided and continues to provide suitable separation technology for many applications in food analysis, life science, environmental analysis or pharmaceutical and clinical research [37]. However, modern mixed-mode columns have gained popularity in all these fields in recent years as they represent an advancement of IPC with, for example, enhanced MS-compatibility [43].

1.1.3. Mixed-mode chromatography

In contrast to IPC, the charged moieties for retention of ionic analytes in MMC are immobilized by chemical modification of the RP column. As illustrated in Fig. 2b, a combination of "classical" RP partition mechanisms and ion exchange interactions (IEX) – or ion exclusion interactions in the case of the same charge – simultaneously contribute to the separation [43]. A current investigation to gain detailed insight in the retention mechanisms *via* quantitative structure-retention relationship models confirmed the involvement of electrostatic and hydrophobic interactions as well as hydrogen bonding, justifying the name "mixed-mode" or "multi-mode", respectively [44]. Depending on the type and pK_a value of the IEX functional group, a distinction can be made between anion (AEX) and cation exchange (CEX) mechanisms as well as weak and strong ion exchange groups (WAX/WCX or SAX/SCX). In addition, the functional group may be at the tip or embedded within the alkyl chain (see Fig. 2b), or even trimodal columns such as the Acclaim Trinity P1 with spatially separated AEX and CEX functionalities are available today [43,45].

The range of possible analytes is consequently very broad (from an/organic counterions to biopharmaceutical macromolecules) and even the simultaneous analysis of ionic and neutral compounds within a single run is possible [46-48]. On the one hand, the constantly growing number of novel mixed-mode columns allows for an increasingly specific analysis of certain compounds [49]. On the other hand, in addition to a high price, poor comparability of columns with a nominally identical mixed-mode functionality from different manufacturers comes into play when selecting a suitable stationary phase. After a fitting column has been identified, the method is optimized regarding the composition of the mobile phase, as with other LC separation techniques. In particular, pH is a critical parameter for many applications as it controls not only the degree of ionisation of the analytes, but also of the additive species and, in the case of WAX/WCX columns even the charge of the stationary phase [50,51]. In addition, practical requirements must be considered during method development, such as the fact that methanol is not compatible for some SCX columns because of the risk of transesterification [52]. For a long-lasting column performance, it is recommended to avoid extreme pH values and mandatory storage in a mixture with buffer.

Moreover, some column materials differ in the extent of column bleed when coupling with aerosol-based detectors or MS is intended [53]. Nevertheless, there are many MMC applications for the analysis of polar, charged analytes with these detector types [43]. Using impurity profiling of vigabatrin as an example, MMC with hyphenated UV and charged aerosol detection was able to demonstrate its advantages in a direct comparison with IPC [54].

1.1.4. Hydrophilic interaction liquid chromatography

For HILIC, the presence of (low) percentages of water in the otherwise organic-rich mobile phase is crucial, as this creates a water-enriched layer onto the surface of the polar stationary phase, which ultimately enables the retention of polar compounds. The separation is the result of partitioning processes between the lipophilic mobile phase and this polar layer and, to a smaller extent, electrostatic interactions and hydrogen bonding [23,25,55]. Extra low-bleeding HILIC columns are now also available for sensitive applications with these detector types as well as computer-assisted method development tools for a more straightforward method development [56,57]. While the high organic content is advantageous for coupling with aerosol-based detectors or MS, it limits the application to polar analytes that nevertheless are sufficiently soluble [18,25,58].

1.2. Challenges and opportunities of modern detector types

Although the UV detector possesses favourable characteristics as low cost, ease of use and wide dynamic range, the limitation is that only analytes with a suitable chromophore can be detected with sufficient sensitivity [23,59]. An interesting alternative to this is the CAD as a so-called *universal detector* [59,60]. However, when the exact composition of a sample is not known, the application of untargeted HRMS approaches can still provide powerful and sensitive characterisation [61,62]. Assuming a successful LC separation, more factors besides the volatility of the mobile phase have to be carefully considered during method development/optimization for a (reasonable) applicability of these high sophisticated detectors.

1.2.1. Charged aerosol detection

According to the IUPAC Gold Book, a *universal detector* in liquid chromatography is "a detector which responds to every component in the column effluent except the mobile phase" [63]. This requirement is met by the class of aerosol-based detectors such as the evaporative light scattering detector (ELSD), the condensation nucleation light scattering detector and CAD with the limitation that only non-volatile or at least semi-volatile analytes can be detected. Since the introduction of the ELSD in the 1980s, the CAD, as the latest development, has some improved performance characteristics (e.g. no spike peaks, wider dynamic range) [19,64,65]. Reflecting its universal response, it enjoys diverse applications, from the analysis of (in)organic ions to polymers or large biomolecules and has found its way into the USP and Ph. Eur. [17,18,66].

1.2.1.1. Technical features

The process of CAD signal generation can be divided into several steps (see Fig. 3). At the beginning, the mobile phase (containing the solute analyte) is nebulised pneumatically (1) into droplets of different sizes using nitrogen gas (≙ primary aerosol). Too large, heavy drops collide with the rear wall of the spray chamber (2), coalesce, and are removed. The remaining fraction (≙ secondary aerosol) enters the heatable evaporation tube (3) *via* a curved connector. Here, the aerosol droplets are dried by removing the volatile components of the mobile phase, and the non-volatile analytes (but also non-volatile/semi-volatile impurities) remain as residue particles with varying diameters. Now, in contrast to ELSD, a positive diffusion charging process of the surface of the residue particles takes place in the mixing chamber (4). This is realized by a secondary nitrogen gas, which flows past a corona high-voltage discharge needle. After passage of an ion trap to remove excessive charge, the now positively charged analyte particles enter the electrometer (5) and produce a signal.
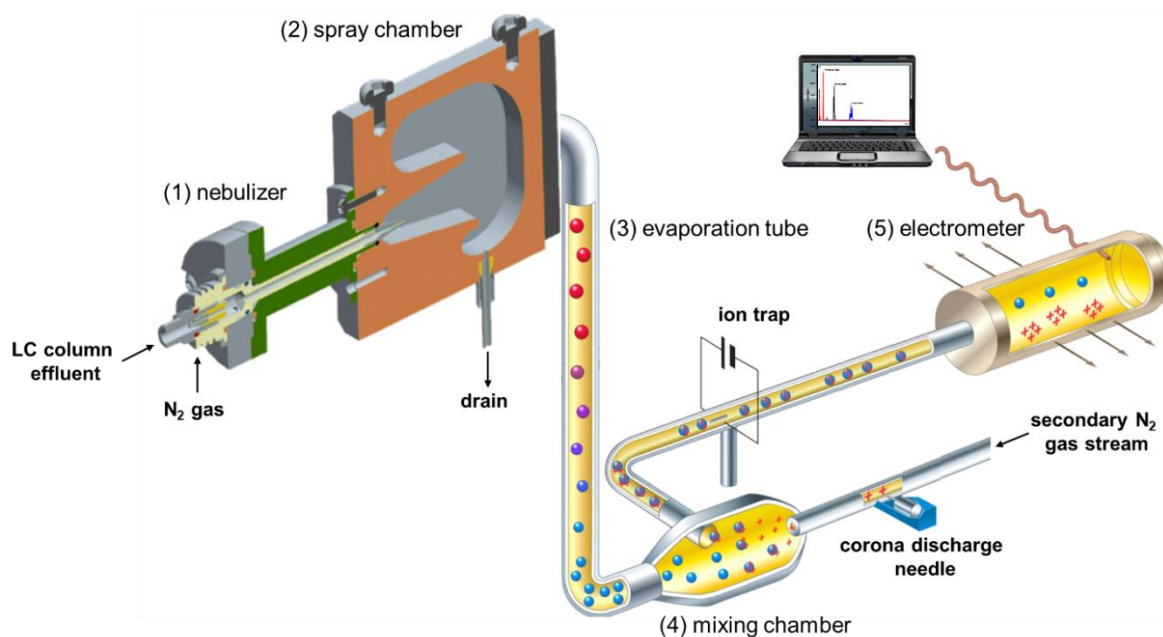
Fig. 3 Schematic illustration of the operation principle of the Vanquish™ charged aerosol detector (reproduced with permission of Thermo Fisher Scientific)

In contrast to the UV detector, the CAD is a mass flow-dependent detector. The relationship between the injected mass ($m_{inj.}$) and the CAD signal (A) follows, analogue to the other aerosol-based detectors, a power law function (see Eq. I)

$$A = a * \left(m_{inj.}\right)^{b}$$

Eq. (I)

where the factors a and b are experimentally influenced by the analyte and the chromatographic factors [19,67]. Despite this non-linear relationship in theory, a quasi-linear relationship for low concentrations (approx. two orders of magnitude) could be demonstrated for several applications [19,67,68]. Other strategies for linearization are a double-logarithmic transformation of Eq. (I) or, in the case of newer CAD models, the built-in power function value (PFV) setting. The latter procedure is compliant with the requirements of *good manufacturing practice*, as it works without subsequent data manipulation. The aim of the PFV is to correct the *b*-factor from Eq. (I) by means of a modified signal output [19,69,70]. The two main reasons for this non-linear behaviour of the CAD are, on the one hand, the equally non-linear relationship between the diameter of the residue aerosol particles (d_p) after drying and the concentration of the non-volatile solutes (see Eq. II) and, on the other hand, the subsequent process of diffusion charging of these particles.

$$d_p = \sqrt[3]{\frac{\beta_s}{\rho_s}} * d_d$$

Eq. (II)

d_p is dependent on the diameter of the primary aerosol droplets (d_d) and the cubic root of the mass concentration (β_s) of the non-volatile solutes (analyte and impurities), which has to be corrected for its density (ρ_s) [71]. The dependence of the *Sauter* mean diameter (*SMD*) of the primary aerosol droplets on both the LC conditions and the nebulizer settings are routinely described by the semiempirical *Nukiyama-Tanasawa* model (see Eq. III) [19]:

$$SMD = \frac{585 * \sqrt{\sigma}}{(v_g - v_l) * \sqrt{\rho}} + 597 * \left[\frac{\eta}{\sqrt{\sigma * \rho}}\right]^{0.45} * \left(1000 * \frac{Q_l}{Q_g}\right)^{1.5} \qquad \text{Eq. (III)}$$

For a given nebulizer design, on the one hand, the axial velocity ($v_{g/l}$) and the volumetric flow rate ($Q_{g/l}$) of the N$_2$ gas as well as of the LC eluent determines the size of the resulting primary aerosol droplets. On the other hand, the surface tension (σ), the liquid density (ρ) and the dynamic viscosity (η) are included in the model as mobile phase parameters. Since too large droplets are withdrawn from the further detection process and smaller droplets/particles have an improved aerosol transport, organic-rich mobile phases with low viscosity/surface tension and high vapour pressure are preferable [19].

These considerations apply equally to the ELSD, and it is only the last step of uniform diffusion charging, generates a wider dynamic range of the CAD. In contrast to light scattering detection, the mean charge of the residue particles of varying size (and thus the signal) is proportional to its diameter by a power law exponent between 1.133 and 2.25 (depending on the particle size). When using ELSD, the proportionality is expressed by power law exponents between 2 and 6 for varying particle sizes, resulting in a smaller quasi-linear range [19].

1.2.1.2. Performance features

As can be deducted from Eq. (III), the CAD response increases with higher organic percentages. This fact is reflected in the increased sensitivity of HILIC methods for the analysis of polar substances [18,58]. If a second pump is available, the organic percentage after the column can be increased and thus improved signal intensities can be achieved [72]. With this more complex equipment set-up (see Fig. 4a), it is also possible to run inverse gradient programmes so that the composition of the mobile phase and thus the response remains constant, which would otherwise rise during gradient elution [73,74]. This setup can furthermore be used to dilute the concentration of IPRs that "interfere" with the CAD´s sensitivity [54]. In addition to the limitations (volatility and mobile phase composition) regarding the nearly universal response of CAD, the special importance of the particle surface area was demonstrated experimentally and through computational modelling approaches [75-77].

One drawback of HILIC applications, however, is the increased occurrence of column bleeding, which negatively influences the signal-to-noise ratio [19,78]. The background noise is the result of all non-volatile and semi-volatile impurities present in the sample and mobile phase. Since in the newer CAD models the evaporation tube can be heated, the influence of semi-volatile impurities on the background noise can be reduced by a higher evaporation temperature provided that the analyte is non-volatile at this temperature [18,19]. The transition between semi-volatile and non-volatile behaviour of analytes/impurities depends on various factors (e.g. boiling point, molecular weight, enthalpy of vaporisation) and is also influenced by the other components of the mobile phase (e.g. ion pair formation). Therefore, in practice, the experimental determination of the optimal evaporation temperature is inevitable. For a uniform response, it is recommended to choose the lowest possible temperature for sufficient sensitivity [19].

The hyphenation of UV (non-destructive) and CAD (destructive) results in a very useful detection system, which can be used for the simultaneous detection of UV-active and non-chromophore (non-volatile) impurities [54,79-81]. Moreover, this tandem detection system enables the simplified determination of relative UV response factors in the case of unknown impurities without the need for laborious isolation steps [82]. If volatile compounds without chromophores are also to be detected, the application of high sophisticated triple UV-CAD-MS detection systems (see Fig. 4b) represent a unique chance for comprehensive sample characterisations [22,79]. Since the mobile phase is volatile, a method transfer to MS is in most cases straightforward, e.g. to elucidate the structure of a newly emerging impurity during the lifecycle of an API [83].
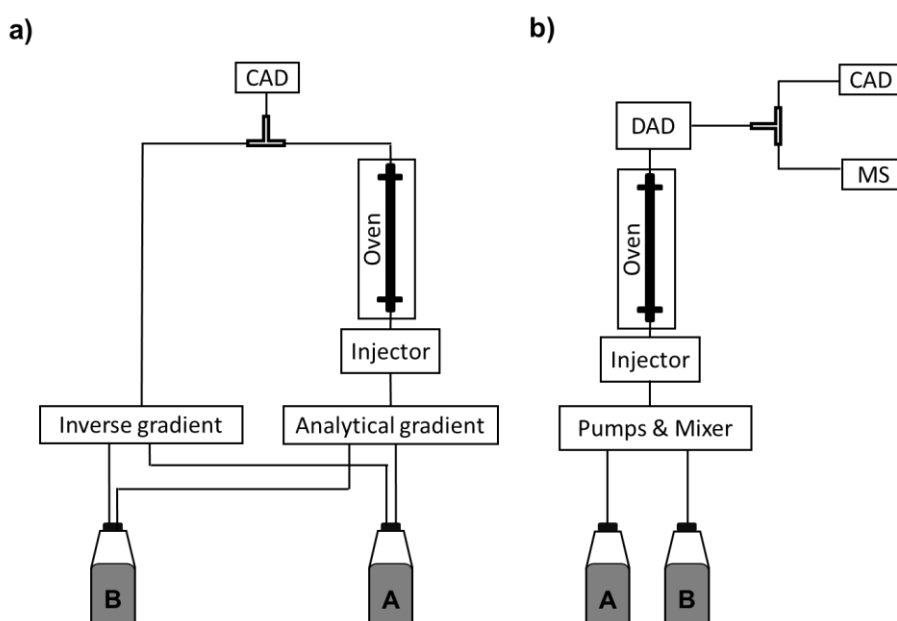

Fig. 4 Schematic instrumental setup for a) inverse gradient compensation (reproduced with permission from [81]) and b) triple detection using a diode array detector (DAD) in connection with a mass spectrometer (MS) or charged aerosol detector (CAD)

1.2.2. High resolution mass spectrometry

Nowadays, the combination of LC with MS is common practice and has become indispensable for many applications, such as therapeutic drug monitoring or structural elucidation of unknown compounds [20,84,85]. A mass spectrometer consists of an ion source, a mass analyser and the ion detection system (usually an electron multiplier). To remove the mobile phase and generate desolvated, charged molecular ions, atmospheric pressure ionisation techniques such as *electrospray ionization* (ESI), *atmospheric pressure chemical ionisation* and *atmospheric pressure plasma ionisation* are the most common interfaces for LC-MS coupling. For the subsequent separation of the molecular ions based on their mass-to-charge ratio (m/z), there are various types of mass analysers available (see Table 2).

Table 2
Operation principle and common application examples of selected mass analysers [86-92]

type	operation principle	application
sector field	deflection of ions in a static magnetic and/or electric field	e.g. gas chromatography analysis of dioxin
quadrupole	trajectories of ions in oscillating electric fields	e.g. therapeutic drug monitoring
FT[1] Orbitrap	axial oscillation of ions around an inner spindle electrode	e.g. proteomics, metabolomics
FT[1] ion cyclotron resonance	cyclotron resonance of ions in a fixed magnetic field	e.g. proteomics, metabolomics
time-of-flight	time of flight of ions after electrostatic acceleration	e.g. with MALDI[2] for analysis of large biomolecules

[1] Fourier transform
[2] matrix assisted laser desorption ionisation

Depending on the aim of the application, certain mass analysing techniques are more suited, or can be used in combination as extremely powerful hybrid instruments, such as the triple quadrupole (QqQ) for quantification at highest sensitivity or the quadrupole-TOF (QqTOF) for structural elucidation based on HRMS data [20,87]. The operation principle of combining ESI (ion source) with a QqTOF instrument (mass analyser) will now be explained in more detail.

1.2.2.1. ESI-QqTOF instrumentation

ESI is the preferred ionisation technique for polar substances that are already present as charged species in the mobile phase. The first step inside the interface is the nebulization of the LC eluent with a nebulizer gas at the capillary tip of the ESI probe, to which either a high positive or negative potential (3–5 kV) is applied. The orifice plate serves as the counter-electrode. The exact processes that contribute to the formation of free molecular ions from the multiply charged aerosol droplets from the *Taylor cone* are not yet fully understood [93]. However, the ionisation efficiency of different analytes with their varying properties such as logP, pK_a and non-polar surface area are significantly influenced by both LC factors (especially the mobile phase composition and flow rate) and source settings (e.g. gas flow, temperature, voltage) [94].
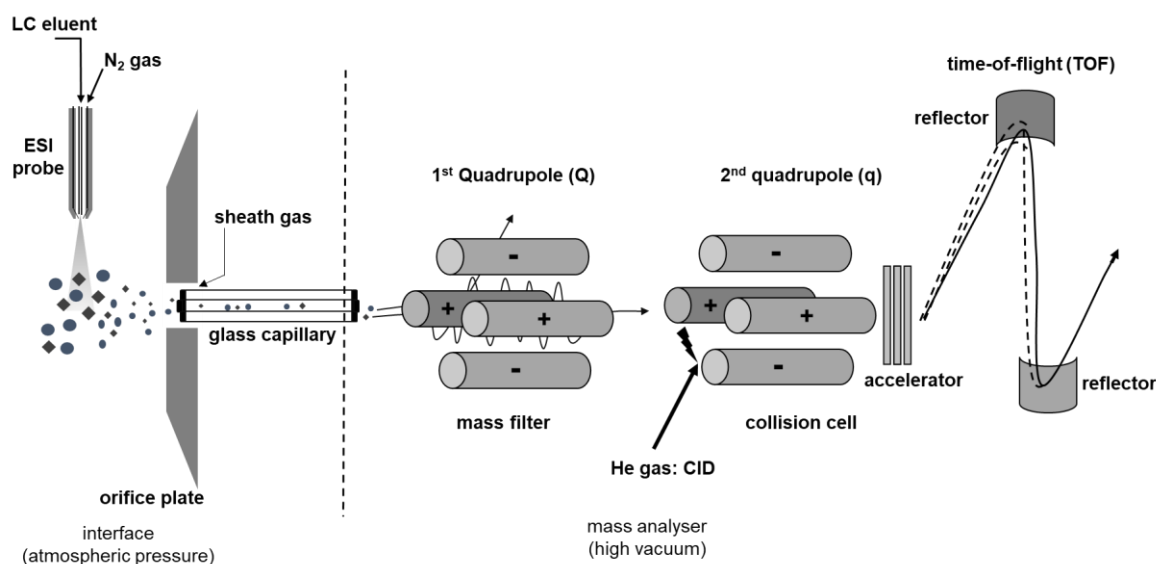
Fig. 5 Schematic setup of an ESI-QqTOF instrument (adapted from [86,93])

The desolvated molecular ions are transported *via* a fine glass capillary into the high vacuum of the mass analyser. Inside the first quadrupole (Q), the trajectories of the molecular ions can be varied so that they are stable or collide with a rod by suitably changing a direct current and a radio frequency (RF) to the pairwise arranged electrodes. In contrast, the second quadrupole (q) serves as a collision cell, where the molecular ions are fragmented by collision induced dissociation (CID) with N_2, argon or helium gas. To ensure that all fragments formed can be detected, this q is operated as "RF-only", and all trajectories are stable. The resulting ions are subsequently accelerated with defined kinetic energy (10–20 kV) and, depending on their m/z, arrive at the end of the flight tube after different flight times. To reduce signal broadening due to ion diffusion, ring-shaped electrodes with rising potential are installed as reflectors/electrostatic mirrors in modern TOF instruments [86,87,95].

1.2.2.2. Untargeted HRMS approaches

For the determination of the exact concentration of a certain API in such a complex matrix as blood, QqQ instruments are the method of choice. Using multiple reaction monitoring, the precursor ions of the drug and its isotopically labelled standard are filtered (1st Q) and after CID (2nd q), the specific fragments can be selectively (3rd Q) detected [84-87]. However, if one wants to use MS to elucidate structures of unknown analytes, one requires a so-called HRMS instrument such as a Fourier transform Orbitrap or QqTOF. The term "high-resolution" refers to the mass resolving power (R) and describes whether two peaks of equal height of the masses m_1 and m_2 can be separated (see Eq. IV; 10 % valley is recommended) [96].

$$R = \frac{m_1}{m_2 - m_1}$$
<div align="right">Eq. (IV)</div>

Modern HRMS instruments with R > 10,000 are capable of measuring the exact mass of a molecular ion with an accuracy of 4 decimal digits (error < 5 ppm). Based on this, sum formulae corresponding to this m/z can be calculated. If one also has information regarding the isotopic pattern and characteristic MS/HRMS fragment spectra, plausible suggestions for the possible structure can be given [20,97]. Even if huge MS/MS databases are available or the plausibility of structural proposals is checked by software-assisted *in silico* fragmentation, the analysis of reference substances is still the gold standard for an unambiguous identification of an unknown compound. As a "shortcut" to structural elucidation of unknown API degradation products (DP) by NMR spectroscopy, which usually requires isolation and purification, the structural proposals have been developed based on HRMS experiments [95-98]. With the so-called untargeted approaches, on the other hand, the goal is to detect all compounds present in sample and not only the structure that belongs to a particular DP in the chromatogram. This is particularly useful for complex unknown samples such as in forensics or "omics" and has led to new comprehensive data acquisition modes in these fields like *MS/MS^all*, *information dependent acquisition*, *data independent acquisition* or *sequential window acquisition of all theoretical fragments* [62,102-104]. Not least, the occurrence of nitrosamine impurities in various drugs has demonstrated the importance of untargeted approaches for comprehensive sample characterization to ensure the best quality and patient safety [105].

With all these advantages, however, one should not forget the high costs of acquisition and maintenance as well as the need for highly trained personnel. To facilitate data handling, the *general unknown comparative screening* (GUCS) offers a structured workflow. Using GUCS, peaks of impurities in a sample are detected by comparing the LC and HRMS data with a "clean" gold standard reference supported by software (see Fig. 6) [105,106].
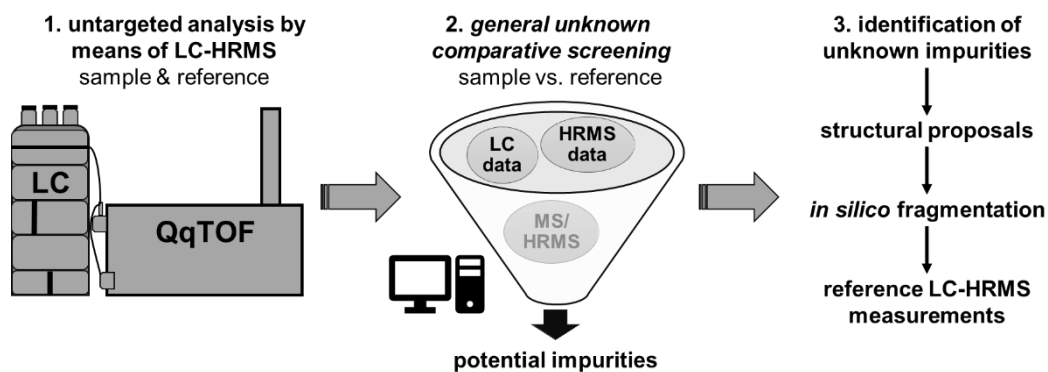

Fig. 6 Workflow for untargeted identification of unknown impurities with the help of general unknown comparative screening for evaluation of liquid chromatography-high-resolution mass spectrometry (LC-HRMS) data (reproduced with permission from [107])

1.3. Design of experiments for method development

When developing any chromatographic separation method, a variety of factors must be considered, starting with the selection of the stationary phase (see section 1.1) and ending with the proper detector settings (see 1.2). For the suitability of the method for its intended application (fortunately) not all factors are always of critical importance. In many cases, a more or less systematic procedure is followed to find the adequate parameters. In order to be able to draw reliable conclusions about the effect, only one factor may be changed at a time. With this so-called *one-factor-at-a-time* approach (OFAT), a large number of experiments is necessary, which is both time-consuming and increases the consumption of chemicals and reagents. Even if a feasible method was found with this approach, one never knows whether these are the optimal conditions, how individual factors may influence each other or which factors are critical in which ranges. This increases the probability of method failure, which in turn leads to (costly) troubleshooting. As an alternative, statistical *design of experiments* (DoE) in combination with *response surface methodology* (RSM) can be used to generate mathematical models, which describe the effects of selected factors [108-112]. The use of DoE is given special attention in the revised ICH Guideline Q2 (R2) "Validation of Analytical Procedures" and in the draft of the new ICH Guideline Q14 "Analytical Procedure Development" [113,114]. In contrast to the OFAT approach, several factors are changed at the same time according to a pre-defined plan, thus reducing the number of experiments to a minimum. To be able to evaluate the influence of the studied factors or their interactions on any number of variables, the data must first be statistically evaluated, and the validity of the models assessed.

1.3.1. Screening and robustness studies

At the beginning of method development and when assessing robustness of the final method, 2-level (low/high) screening designs such as fractional factorial or Plackett-Burman designs are preferred [108,109]. Since each factor is investigated at only two levels (-1/+1), many factors can be studied in only a few experimental runs e.g., using a Plackett-Burman design the influence of seven factors (A-G) can be studied in eight runs (see Table 3). The number of dependent variables is naturally not limited, and for LC applications, retention factor, symmetry factor, resolution, peak-to-valley ratio, number of theoretical plates, among others, have been reported in the literature [111]. With this type of design and the derived main effect models, it is not possible to cover non-linear relationships and interactions of factors. However, in the screening phase, the goal is to determine the critical factors among the many factors to be theoretically considered, such as pH, percentage of the organic modifier, concentration of additives, flow rate, column temperature, slope of the gradient, etc. [115].

In a subsequent reduced experimental design, the statistically significant factors and their interactions are investigated in more detail allowing the optimal settings to be predicted. Likewise, when determining robustness by means of DoE, it should be proven that the selected factors have no statistically significant effect on the selected variables. The interpretation of the (normalised) effects can be done both graphically, for example with a half-normal probability plot, and mathematically, usually with the *t*-test statistic based on the estimation of the experimental error of the effects. In addition, a statistically based prediction of the limits of the system suitability criteria is possible and advisable [115].

Table 3
2-level Plackett-Burman design for 7 factors (A-G)

run	factor						
	A	B	C	D	E	F	G
1	+1	+1	+1	-1	+1	-1	-1
2	-1	+1	+1	+1	-1	+1	-1
3	-1	-1	+1	+1	+1	-1	+1
4	+1	-1	-1	+1	+1	+1	-1
5	-1	+1	-1	-1	+1	+1	+1
6	+1	-1	+1	-1	-1	+1	+1
7	+1	+1	-1	+1	-1	-1	+1
8	-1	-1	-1	-1	-1	-1	-1

1.3.2. Optimization studies

To gain detailed information on the influence of the significant factors and possible interactions, other designs with usually three levels (low-middle-high) must be applied. For the creation of multi-dimensional response surface models, full/fractional factorial designs, central composite designs (CCD), Box-Behnken designs (BBD), Doehlert matrix or mixture designs are suited. For optimisation of chromatographic methods, CCD and BBD with three or more factors at three levels each (-1/0/+1) are commonly employed [116-120]. The experimental space can be represented as a cube in a 3D coordinate system in which the axes correspond to the factors (see Fig. 7a) [116]. The CCD combines factorial with axial points (see points or stars in Fig. 7b) and thus covers both the extreme (vertices of the cube) and intermediate experimental conditions. For some applications, for example, if a high organic percentage is to be tested with a high buffer concentration (danger of precipitation), this can lead to LC conditions that are not feasible. The BBD, on the other hand, only works at medium conditions (see points in Fig. 7c) with the risk that information at the limits of the experimental space is insufficiently represented in the model [117]. Depending on the data of the screening experiments, one should carefully choose the factor levels and the most suitable design.
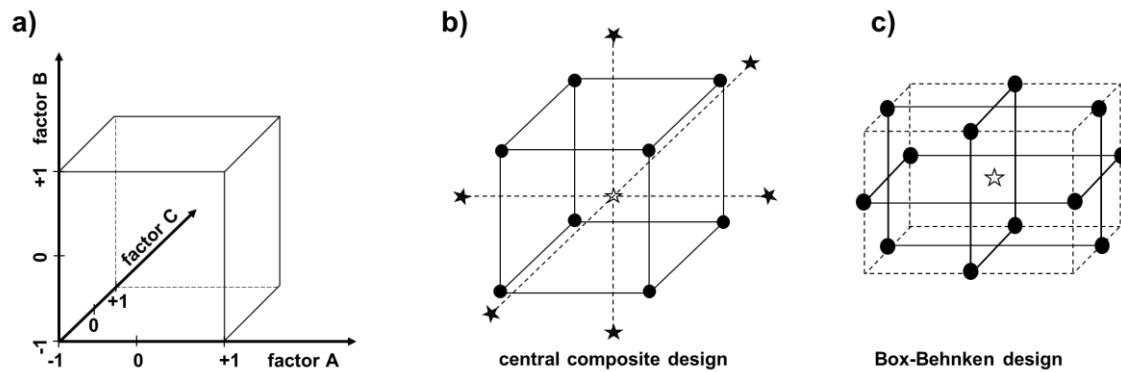
Fig. 7 Schematic illustration of the experimental space in general (a), the central composite design (b) and Box-Behnken design (c) with three factors (experimental runs marked as points/stars) (adapted from [111,115,116])

Compared to a 3x3 full factorial design, CCD or BBD require fewer runs for comparable validity [117]. After all runs have been performed in randomised order according to a predefined experimental plan, multiple linear regression is carried out to create suitable polynomial models. Based on the model coefficients and their standard errors, the quality of the regression models should be checked by means of *analysis of variance* (ANOVA). The statistical significance of the models and, if applicable, the lack-of-fit of the models are then demonstrated by an *F*-test. Eliminating non-significant coefficients from the model usually improves the quality of the model, which is evident from higher values of the (adjusted) coefficient of determination [111,112,121]. The complex polynomial models can be visualised in 3D plots, which allow a concise representation of the effects of factors and their interactions on certain factors. For the calculation of the optimal factor setting, the individual model equations are merged in a multi-criteria algorithm such as the desirability function [116,122,123]. Afterwards, however, experimental confirmation of the prediction should be carried out since each model always represents only an estimate. Another exciting possibility is the creation of the so-called *method operable design region* (MODR) within the design space in terms of the *analytical quality by design* (AQbD) concept [121,124,125]. For this purpose, the RSM data are submitted to a suitable probabilistic approach such as Monte Carlo simulation or Bayesian regression [120,126]. A beneficial consequence of AQbD is that variations within the MODR do not have to be reported as a change to the regulatory authorities, thus allowing for more flexible operation [114,127].

1.4. References

[1]   International Council for Harmonisation of Technical Requirements for Pharmaceuticals for Human Use, Guideline M4E (R2) Efficacy (2016).

[2]   International Council for Harmonisation of Technical Requirements for Pharmaceuticals for Human Use, Guideline M4S (R2) Safety (2002).

[3]   International Council for Harmonisation of Technical Requirements for Pharmaceuticals for Human Use, Guideline M4Q (R1) Quality (2002).

[4]   European Commission, EudraLex Volume 4 Good Manufacturing Practice, Chapter 6: Quality Control (2014). Available from: https://www.gmp-compliance.org/files/guidemgr/2014-03_gmp_chapter_6.pdf (accessed 09.02.2023).

[5]   Council of Europe, Directive 2010/84/EU, Official Journal of the European Union, L 348 74-99 (2010). Available from: https://eur-lex.europa.eu/LexUriServ/LexUriServ.do?uri=OJ:L:2010:348:0074:0099:EN:PDF (accessed 09.02.2023).

[6]   European Directorate for the Quality of Medicines & HealthCare, European Pharmacopoeia, 11.0 edition, Strasbourg, France (2023).

[7]   The United States Pharmacopeial Convention, United States Pharmacopeia, USP-NF online (2023) Rockville, Maryland, USA.

[8]   Society of Japanese Pharmacopoeia, Japanese Pharamcopoeia, 18 edition, Tokyo, Japan (2021).

[9]   International Council for Harmonisation of Technical Requirements for Pharmaceuticals for Human Use, Guideline Q3B (R2) Impurities in New Drug Products (2006).

[10]   Council of Europe, European Pharmacopoeia, 11.0 edition, Monograph no. 2927, Sitagliptin tablets, Strasbourg, France (2023).

[11]   Council of Europe, European Pharmacopoeia, 11.0 edition, General Monographs Substances for pharmaceutical use, Strasbourg, France (2023).

[12]   Council of Europe, European Pharmacopoeia, 11.0 edition, Chapter 2.4.24 Identification and control of residual solvents, Strasbourg, France (2023).

[13]   Council of Europe, European Pharmacopoeia, 11.0 edition, Chapter 2.2.4 Approximate pH of solutions, Strasbourg, France (2023).

[14]   Council of Europe, European Pharmacopoeia, 11.0 edition, Chapter 5.10 Control of impurities in substances for pharmaceutical use, Strasbourg, France (2023).

[15]   S. Görög, The changing face of pharmaceutical analysis, Trends Anal. Chem. 26(1) (2007) 12-17.

[16]   Y. Kazakevich, R. LoBrutto, HPLC for pharmaceutical scientists, 1st edition, John Wiley & Sons, Hoboken, New Jersey, USA (2007).

[17] B. Davani, Common Methods in Pharmaceutical Analysis: Pharmaceutical Analysis for Small Molecules, 1st edition, John Wiley & Sons, Hoboken, New Jersey, USA (2017).

[18] K. Schilling, U. Holzgrabe, Recent applications of the Charged Aerosol Detector for liquid chromatography in drug quality control, J. Chromatogr. A 1619 (2020) 460911.

[19] P. H. Gamache, Charged aerosol detection for liquid chromatography and related separation techniques, 1st edition, John Wiley & Sons, Hoboken, New Jersey, USA (2017).

[20] T. Kind, O. Fiehn, Advances in structure elucidation of small molecules using mass spectrometry, Bioanal. Rev. 2 (2010) 23-60.

[21] L. Lin, H. Lin, M. Zhang, X. Dong, X. Yin, C. Qu, J. Ni, Types, principle, and characteristics of tandem high-resolution mass spectrometry and its applications, RSC Adv. 5(130) (2015) 107623-107636.

[22] H. Thakkar, S. Jain, S. Kumar, V. S. Bhalekar, S. Gangakhedkar, R. P. Shah, Hyphenated liquid chromatography - diode array detection - charged aerosol detection - high resolution - multistage mass spectrometry with online hydrogen/deuterium exchange: One stop solution for pharmaceutical impurity profiling, J. Chromatogr. A 1689 (2023) 463725.

[23] L. R. Snyder, J. J. Kirkland, J. W. Dolan, Introduction to modern liquid chromatography, 3rd edition, John Wiley & Sons, Hoboken, New Jersey, USA (2010).

[24] B. E. Boyes, M. W. Dong, Modern Trends and Best Practices in Mobile-Phase Selection in Reversed-Phase Chromatography, LCGC N. Am. 36(10) (2018) 752-768.

[25] B. Buszewski, S. Noga, Hydrophilic interaction liquid chromatography (HILIC) - a powerful separation technique, Anal. Bioanal. Chem. 402 (2012) 231-247.

[26] C. S. Young, R. J. Weigand, An efficient approach to column selection in HPLC method development, LCGC N. Am. 20(5) (2002) 464-473.

[27] P. Žuvela, M. Skoczylas, J. J. Liu, T. Bączek, R. Kaliszan, M. W. Wong, B. Buszewski, Column Characterisation and Selection Systems in Reversed-Phase High-Performance Liquid Chromatography, Chem. Rev. 119(6) (2019) 3674-3729.

[28] D. V McCalley, Effect of buffer on peak shape of peptides in reversed-phase high performance liquid chromatography, J. Chromatogr. A 1038(1-2) (2004) 77-84.

[29] D. Guillarme, D. T. T. Nguyen, S. Rudaz, J.-L. Veuthey, Method transfer for fast liquid chromatography in pharmaceutical analysis: Application to short columns packed with small particle. Part II: Gradient experiments, Eur. J. Pharm. Biopharm. 68(2) (2008) 430-440.

[30] L. R. Snyder, J. W. Dolan, J. R. Gant, Gradient elution in high-performance liquid chromatography. I. Theoretical basis for reversed-phase systems, J. Chromatogr. A 165(1) (1979) 3-30.

[31]   I. Molnar, Computerized design of separation strategies by reversed-phase liquid chromatography: Development of Dry-Lab software, J. Chromatogr. A 965(1-2) (2002)175-94.

[32]   O. Wahl, U. Holzgrabe, Amino acid analysis for pharmacopoeial purposes, Talanta, 154 (2016) 150-163.

[33]   K. Petritis, C. Elfakir, M. Dreux, A comparative study of commercial liquid chromatographic detectors for the analysis of underivatized amino acids, J. Chromatogr. A 961(1) (2002) 9-21.

[34]   S. Furota, N. O. Ogawa, Y. Takano, T. Yoshimura, N. Ohkouchi, Quantitative analysis of underivatized amino acids in the sub- to several-nanomolar range by ion-pair HPLC using a corona-charged aerosol detector (HPLC-CAD), J. Chromatogr. B 1095 (2018) 191-197.

[35]   Z. Xie, Y. Jiang, D. Zhang, Simple analysis of four bisphosphonates simultaneously by reverse phase liquid chromatography using n-amylamine as volatile ion-pairing agent, J. Chromatogr. A 1104(1-2) (2006) 173-178.

[36]   N. Li, N. M. El Zahar, J. G. Saad, E. R. E. van der Hage, M. G. Bartlett, Alkylamine ion-pairing reagents and the chromatographic separation of oligonucleotides, J. Chromatogr. A 1580 (2018) 110-119.

[37]   T. Cecchi, Ion pairing Chromatography, Crit. Rev. Anal. Chem. 38(3) (2008) 161-213.

[38]   T. Cecchi, P. Passamonti, Retention mechanism for ion-pair chromatography with chaotropic reagents, J. Chromatogr. A 1216(10) (2009) 1789-1797.

[39]   C. R. Mallet, Z. Lu, J. R. Mazzeo, A study of ion suppression effects in electrospray ionization from mobile phase additives and solid-phase extracts, Rapid Commun. Mass Spectrom. 18(1) (2004) 49-58.

[40]   M. Patthy, Gradient elution with shorter equilibration times in reversed-phase ion-pair chromatography, J. Chromatogr. A 592(1–2) (1992) 143-156.

[41]   T. Buhrke, A. Kibellus, A. Lampen, In vitro toxicological characterization of perfluorinated carboxylic acids with different carbon chain lengths, Toxicol. 218(2) (2013) 97-104.

[42]   I. T. Cousins, J. H. Johansson, M. E. Salter, B. Sha, M. Scheringer, Outside the Safe Operating Space of a New Planetary Boundary for Per- and Polyfluoroalkyl Substances (PFAS), Environ. Sci. Technol. 56(16) (2022) 11172-11179.

[43]   K. Zhang, X. Liu, Reprint of Mixed-mode chromatography in pharmaceutical and biopharmaceutical applications, J. Pharm. Biomed. Anal. 130 (2016) 19-34.

[44]   B. Svrkota, J. Krmar, A. Protić, B. Otašević, The secret of reversed-phase/weak cation exchange retention mechanisms in mixed-mode liquid chromatography applied for small drug molecule analysis, J. Chromatogr. A 1690 (2023) 463776.

[45] X. Liu, C. A. Pohl, Comparison of reversed-phase/cation-exchange/anion-exchange trimodal stationary phases and their use in active pharmaceutical ingredient and counterion determinations, J. Chromatogr. A 1232 (2012) 190-195.

[46] K. Zhang, L. Dai, N. P. Chetwyn, Simultaneous determination of positive and negative pharmaceutical counterions using mixed-mode chromatography coupled with charged aerosol detector, J. Chromatogr. A 1217(37) (2010) 5776-5784.

[47] S. Aoyama, Y. Matsumoto, C. Mori, K. Sota, Application of novel mixed mode chromatography (MMC) resins having a hydrophobic modified polyallylamine ligand for monoclonal antibody purification, J. Chromatogr. B 1191 (2022) 123072.

[48] J. Li, S. Shao, M. S. Jaworsky, P. T. Kurtulik, Simultaneous determination of cations, zwitterions and neutral compounds using mixed-mode reversed-phase and cation-exchange high-performance liquid chromatography, J. Chromatogr. A 1185(2) (2008) 185-193.

[49] D. Sýkora, P. Rezanka, K. Záruba, V. Král, Recent advances in mixed-mode chromatographic stationary phases, J. Sep. Sci. 42(1) (2019) 89-129.

[50] J. L. Dores-Sousa, J. De Vos, W. Th. Kok, S. Eeltink, Probing selectivity of mixed-mode reversed-phase/weak-anion-exchange liquid chromatography to advance method development, J. Chromatogr. A 1570 (2018) 75-81.

[51] J. Wang, J. Wang, X. Ning, J. Liu, H. Xia, G.Wan, Q. Bai, pH-dependent selective separation of acidic and basic proteins using quaternary ammoniation functionalized cysteine-zwitterionic stationary phase with RPLC/IEC mixed-mode chromatography, Talanta 225 (2021) 122084.

[52] SIELC Technologies, FAQ Columns Care Instructions, Wheeling, Illinois, USA. Available from: https://sielc.com/FAQ_Column_Care (accessed 29.03.2023).

[53] T. H. Walter, M. M. T. Blaze, C. Boissel, Electrospray ionization mass spectrometry ion suppression/enhancement caused by column bleed for three mixed-mode reversed-phase/anion-exchange high-performance liquid chromatography columns, Rapid Commun. Mass Spectrom. 35(12) (2021).

[54] R. Pawellek, U. Holzgrabe, Influence of the mobile phase composition on hyphenated ultraviolet and charged aerosol detection for the impurity profiling of vigabatrin, J. Pharm. Biomed. Anal. 201 (2021) 114110.

[55] B. Dejaegher, Y. Vander Heyden, HILIC methods in pharmaceutical analysis, J. Sep. Sci. 33(6-7) (2010) 698-715.

[56] K. Quian, Z. Yang. F. Zhang, B. Yang, P. K. Dasgupta, Low-Bleed Silica-Based Stationary Phase for Hydrophilic Interaction Liquid Chromatography, Anal. Chem. 90(15) (2018) 8750-8755.

[57] M. Taraji, P. R. Haddad, R. I. J. Amos, M. Talebi, R. Szucs, J. W. Dolan, C. A. Pohl, Chemometric-assisted method development in hydrophilic interaction liquid chromatography: A review, Anal. Chim. Acta 1000 (2018) 20-40.

[58] R. Pawellek, U. Holzgrabe, Performance of ion pairing chromatography and hydrophilic interaction liquid chromatography coupled to charged aerosol detection for the analysis of underivatized amino acids, J. Chromatogr. A 1659 (2021) 462613.

[59] M. Swartz, HPLC Detectors: A Brief Review, J. Liq. Chromatogr. 33(9-12) (2010) 1130-1150.

[60] K. Zhang, K. L. Kurita, C. Venkatramani, D. Russell, Seeking universal detectors for analytical characterizations, J. Pharm. Biomed. Anal. 162 (2019) 192-204.

[61] G. Hopfgartner, D. Tonoli, E. Varesio, High-resolution mass spectrometry for integrated qualitative and quantitative analysis of pharmaceuticals in biological matrices, Anal. Bioanal. Chem. 402 (2012) 2587.2596.

[62] F. Fenaille, P. B. Saint-Hilaire, K. Rousseau, C. Junot, Data acquisition workflows in liquid chromatography coupled to high resolution mass spectrometry-based metabolomics: Where do we stand?, J. Chromatogr. A 1526 (2017) 1-12.

[63] IUPAC, Compendium of Chemical Terminology, 2nd ed. (the "Gold Book"). Compiled by A. D. McNaught and A. Wilkinson. Blackwell Scientific Publications, Oxford (1997). Available from: https://goldbook.iupac.org/terms/view/U06565 (accessed 20.03.2023).

[64] J. Shaodong, W. J. Lee, J. W. Ee, J. H. Park, S. W. Kwon, J. Lee, Comparison of ultraviolet detection, evaporative light scattering detection and charged aerosol detection methods for liquid-chromatographic determination of anti-diabetic drugs, J. Pharm. Biomed. Anal. 51(4) (2010) 973-978.

[65] S. Almeling, U. Holzgrabe, Use of evaporative light scattering detection for the quality control of drug substances: Influence of different liquid chromatographic and evaporative light scattering detector parameters on the appearance of spike peaks, J. Chromatogr. A 1217(14) (2010) 2163-2170.

[66] Council of Europe, European Pharmacopoeia, 11.0 edition, Chapter 2.2.29 Liquid chromatography, Strasbourg, France (2023).

[67] T. Vehovec, A. Obreza, Review of operating principle and applications of the charged aerosol detector, J. Chromatogr. A 1217(10) (2010) 1549-1556.

[68] S. Almeling, D. Ilko, U. Holzgrabe, Charged aerosol detection in pharmaceutical analysis, J. Pharm. Biomed. Anal. 69 (2012) 50-63.

[69] I. A. Haidar Ahmad, A. Blasko, J. Tam, N. Variankaval, H. M. Halsey, R. Hartman, E. L. Regalado, Revealing the inner workings of the power function algorithm in Charged Aerosol Detection: A simple and effective approach to optimizing power function value for quantitative analysis, J. Chromatogr. A 1603 (2019) 1-7.

[70] R. Pawellek, T. Muellner, P. Gamache, U. Holzgrabe, Power function setting in charged aerosol detection for the linearization of detector response – optimization strategies and their application, J. Chromatogr. A 1637 (2021) 461844.

[71] R. Dixon, D. S. Peterson, Development and Testing of a Detection Method for Liquid Chromatography Based on Aerosol Charging, Anal. Chem. 74 (2002) 2930-2937.

[72] O. Wahl, U. Holzgrabe, Impurity profiling of carbocisteine by HPLC-CAD, qNMR and UV/vis spectroscopy, J. Pharm. Biomed. Anal. 95 (2014) 1-10.

[73] T. Górecki, F. Lynen, R. Szucs, P. Sandra, Universal Response in Liquid Chromatography Using Charged Aerosol Detection, Anal. Chem. 78(9) (2006) 3186-3192.

[74] S. Grosse, T. Muellner, K. Lovejoy, I. Acworth, P. Gamache, Why use charged aerosol detection with inverse gradient?, Thermo Fisher Scientific Technical note 73449 (2020). Available from: https://assets.thermofisher.com/TFS-Assets/CMD/Technical-Notes/tn-73449-cad-inverse-gradient-tn73449-en.pdf (accessed 20.03.2023).

[75] S. Matsuyama, Y. Orihara, S. Kinugasa, H. Ohtani, Effects of Densities of Brominated Flame Retardants on the Detection Response for HPLC Analysis with a Corona-charged Aerosol Detector, Anal. Sci. 31 (2015) 61-65.

[76] M. W. Robinson, A. P. Hill, S. A. Readshaw, J. C. Hollerton, R. J. Upton, S. M. Lynn, S. C. Besley, B. J. Boughtflower, Use of Calculated Physicochemical Properties to Enhance Quantitative Response When Using Charged Aerosol Detection, Anal. Chem. 89(3) (2017) 1722-1777.

[77] K. Schilling, J. Krmar., N. Maljurić, R. Pawellek, A. Protić, U. Holzgrabe, Quantitative structure-property relationship modeling of polar analytes lacking UV chromophores to charged aerosol detector response, Anal. Bioanal. Chem. 411 (2019) 2945-2959.

[78] T. Teutenberg, J. Tuerk, M. Holzhauser, T. K. Kiffmeyer, Evaluation of column bleed by using an ultraviolet and a charged aerosol detector coupled to a high-temperature liquid chromatographic system, J. Chromatogr. A 1119(1-2) (2006) 197-201.

[79] K. Zhang, Y. Li, M. Tsang, N. P. Chetwyn, Analysis of pharmaceutical impurities using multi-heartcutting 2D LC coupled with UV-charged aerosol MS detection, J. Sep. Sci. 36 (2013) 2986-2992.

[80] R. Pawellek, K. Schilling, U. Holzgrabe, Impurity profiling of l-aspartic acid and glycine using high-performance liquid chromatography coupled with charged aerosol and ultraviolet detection, J. Pharm. Biomed. Anal. 183 (2020) 113149.

[81] R. Walther, U. Holzgrabe, Simplification of pharmacopoeial liquid chromatography methods for related substances of statins by hyphenated ultraviolet and charged aerosol detection, J. Pharm. Biomed. Anal. 225 (2023) 115218.

[82] P. Sun, X. Wang, L. Alquier, C. A. Maryanoff, Determination of relative response factors of impurities in paclitaxel with high performance liquid chromatography equipped with ultraviolet and charged aerosol detectors, J. Chromatogr. A 1177(1) (2008) 87-91.

[83] P. K. Ragham, K. B. Chandrasekhar, Development and validation of a stability-indicating RP-HPL C-CAD method for gabapentin and its related impurities in presence of degradation products, J. Pharm. Biomed. Anal. 125 (2016) 122-129.

[84] T. Tuzimski, A. Petruczynik, Review of Chromatographic Methods Coupled with Modern Detection Techniques Applied in the Therapeutic Drugs Monitoring (TDM), Molecules 25(17) (2020) 4026.

[85] M. Shipkova, D. Svinarov, LC–MS/MS as a tool for TDM services: Where are we?, Clin. Biochem. 49(13–14) (2016) 1009-1023.

[86] J. H. Gross, Massenspektrometrie – Spektroskopiekurs kompakt, 1st edition, Springer, Heidelberg, Germany (2019).

[87] Council of Europe, European Pharmacopoeia, 11.0 edition, Chapter 2.2.43 Mass spectrometry, Strasbourg, France (2023).

[88] H. Fiedler, I. van der Veen, J. de Boer, Interlaboratory assessments for dioxin-like POPs (2016/2017 and 2018/2019), Chemosphere 288(1) (2022) 132449.

[89] M. Scigelova, A. Makarov, Orbitrap Mass Analyzer – Overview and Applications in Proteomics, Proteomics 6 (2006) 16-21.

[90] M. Ghaste, R. Mistrik, V. Shulaev, Applications of Fourier Transform Ion Cyclotron Resonance (FT-ICR) and Orbitrap Based High Resolution Mass Spectrometry in Metabolomics and Lipidomics, Int. J. Mol. Sci. 17(6) (2016) 816.

[91] S. C. Brown, G. Kruppa, J.-L. Dasseux, Metabolomics applications of FT-ICR mass spectrometry. Mass Spectrom. Rev. 24 (2005) 223-231.

[92] M. Karas, F. Hillenkamp, Laser Desorption ionization of proteins with molecular masses exceeding 10,000 daltons, Anal. Chem. 60(20) (1988) 2299-2301.

[93] L. Konermann, E. Ahadi, A. D. Rodriguez, S. Vahidi, Unraveling the Mechanism of Electrospray Ionization, Anal. Chem. 85(1) (2013) 2-9.

[94] P. Liigand, J. Liigand, K. Kaupmees, A. Kruve, 30 Years of Research on ESI/MS response: trends, contradictions and applications, Anal. Chim. Acta (2020) 238117.

[95] G. L. Glish, D. J. Burinsky, Hybrid mass spectrometers for tandem mass spectrometry, J. Am. Soc. Mass Spectrom. 19 (2008) 161-172.

[96] IUPAC, Compendium of Chemical Terminology, 2nd ed. (the "Gold Book"). Compiled by A. D. McNaught and A. Wilkinson. Blackwell Scientific Publications, Oxford (1997). Available from: https://goldbook.iupac.org/terms/view/M03730 (accessed 31.03.2023).

[97] L. Lin, H. Lin, M. Zhang, X. Dong, X. Yin, C. Qu, J. Ni, Types, principle, and characteristics of tandem high-resolution mass spectrometry and its applications, RSC Adv. 5(130) (2015) 107623-107636.

[98] R. P. Shah, A. Sahu, S. Singh, Identification and characterization of degradation products of irbesartan using LC–MS/TOF, MSn, on-line H/D exchange and LC–NMR, J. Pharm. Biomed. Anal. 51(5) (2010) 1037-1046.

[99] R. Rapolu, C. K. Raju, K. Srinivas, A. Awasthi, S. G. Navalgund, K. V. Surendranath, Isolation and characterization of a novel acid degradation impurity of

Amlodipine Besylate using Q-TOF, NMR, IR and single crystal X-ray, J. Pharm. Biomed. Anal. 99 (2014) 59-66.

[100] M. Narayanam, A. Sahu, S. Singh, Use of LC–MS/TOF, LC–MSn, NMR and LC–NMR in characterization of stress degradation products: Application to cilazapril, J. Pharm. Biomed. Anal. 111 (2015) 190-203.

[101] Q. Zhang, J. Guan, R. Rong, Y. Zhao, Z. Yu, Study on degradation kinetics of 2-(2-hydroxypropanamido) benzoic acid in aqueous solutions and identification of its major degradation product by UHPLC/TOF–MS/MS, J. Pharm. Biomed. Anal. 112 (2015) 1-7.

[102] H. H. Maurer, M. R. Meyer, High-resolution mass spectrometry in toxicology: current status and future perspectives, Arch. Toxicol. 90 (2016) 2161–2172.

[103] A. T. Roemmelt, A. E. Steuer, M. Poetzsch, T. Kraemer, Liquid chromatography, in combination with a quadrupole time-of-flight instrument (LC QTOF), with sequential window acquisition of all theoretical fragment-ion spectra (SWATH) acquisition: systematic studies on its use for screenings in clinical and forensic toxicology and comparison with information-dependent acquisition (IDA), Anal. Chem. 86(23) (2014) 11742-11749.

[104] R. Bonner, G. Hopfgartner, SWATH acquisition mode for drug metabolism and metabolomics investigations, Bioanalysis 8(16) (2016) 1735-1750.

[105] O. Scherf-Clavel, M. Kinzig, A. Besa, A. Schreiber, C. Bidmon, M. Abdel-Tawab, J. Wohlfart, F. Sörgel, U. Holzgrabe, The contamination of valsartan and other sartans, Part 2: Untargeted screening reveals contamination with amides additionally to known nitrosamine impurities, J. Pharm. Biomed. Anal. 172 (2019) 278-284.

[106] J. Wohlfart, E. Jäckel, O. Scherf-Clavel, D. Jung, M. Kinzig, F. Sörgel, U. Holzgrabe, Impurity profiling of bisoprolol fumarate by liquid chromatography-high-resolution mass spectrometry: A combination of targeted and untargeted approaches using a synthesis reaction matrix and general unknown comparative screening, J. Chromatogr. Open 1 (2021) 100012.

[107] R. Walther, M. Kinzig, A. Zamponi, F. Sörgel, O. Scherf-Clavel, U. Holzgrabe, Identification of low-level impurities in drug prototypes of carbocisteine by means of liquid chromatography-high-resolution mass spectrometry and general unknown comparative screening, submitted manuscript.

[108] B. Dejaegher, Y. Vander Heyden, Experimental designs and their recent advances in set-up, data interpretation, and analytical applications, J. Pharm. Biomed. Anal. 56(2) (2011) 141-158.

[109] D. B. Hibbert, Experimental design in chromatography: A tutorial review, J. Chromatogr. B 910 (2012) 2-13.

[110] P. K. Sahu, N. R. Ramisetti, T. Cecchi, S. Swain, C. Sekhar Patro, J. Panda, An overview of experimental designs in HPLC method development and validation, J. Pharm. Biomed. Anal. 147 (2018) 590-611.

[111] S. B. Ganorkar, A. A. Shirkhedkar, Design of experiments in liquid chromatography (HPLC) analysis of pharmaceuticals: analytics, applications, implications and future prospects, Rev. Anal. Chem. 36(3) (2017) 20160025.

[112] Wilhelm Kleppmann, Versuchsplanung, Produkte und Prozesse optimieren, 10th edition, Hanser, München (2020).

[113] International Council for Harmonisation of Technical Requirements for Pharmaceuticals for Human Use, Draft Guideline Q2 (R2) Validation of Analytical Procedures (2022).

[114] International Council for Harmonisation of Technical Requirements for Pharmaceuticals for Human Use, Draft Guideline Q14 Analytical Procedure Development (2022).

[115] Y. Vander Heyden, A. Nijhuis, J. Smeyers-Verbeke, B. G. M. Vandeginste, D. L. Massart, Guidance for robustness/ruggedness tests in method validation, J. Pharm. Biomed. Anal. 24(5-6) (2001) 723-753.

[116] S. L. C. Ferreira, R. E. Bruns, E. G. Paranhos da Silva, W. N. L. dos Santos, C. M. Quintella, J. M. David, J. B. de Andrade, M. C. Breitkreitz, I. C. S. Fontes Jardim, B. B. Neto, Statistical designs and response surface techniques for the optimization of chromatographic systems, J. Chromatogr. A 1158(1-2) (2007) 2-14.

[117] S. L. C. Ferreira, R. E. Bruns, H. S. Ferreira, G. D. Matos, J. M. David, G. C. Brandão, E. G. P. da Silva, L. A. Portugal, P. S. dos Reis, A. S. Souza, W. N. L. dos Santos, Box-Behnken design: An alternative for the optimization of analytical methods, Anal. Chim. Acta 597(2) (2007) 179-186.

[118] S. L. C. Ferreira, W. N. L. dos Santos, C. M. Quintella, B. B. Neto, J. M. Bosque-Sendra, Doehlert matrix: a chemometric tool for analytical chemistry-review, Talanta 63(4) (2004) 1061-1067.

[119] R. Walther, O. Scherf-Clavel, U. Holzgrabe, Method transfer from ion pair chromatography to charged aerosol detector-compatible mixed-mode chromatography: A case study using carbocisteine, J. Chromatogr. Open 1 (2021) 100014.

[120] R. Walther, J. Krmar, A. Leistner, B. Svrkota, B. Otašević, A. Malenović, U. Holzgrabe, A. Protić, Analytical Quality by Design: Achieving Robustness of an LC-CAD Method for the Analysis of Non-Volatile Fatty Acid, Pharmaceuticals 16(4) (2023) 478.

[121] T. Tome, N. Žigart, Z. Časar, A. Obreza, Development and Optimization of Liquid Chromatography Analytical Methods by Using AQbD Principles: Overview and Recent Advances. Org. Process Res. Dev. 23 (2019) 1784-1802.

[122] G. Derringer, R. Suich, Simultaneous optimization of several response variables, J. Qual. Technol. 12(4) (1980) 214-219.

[123] N. García-Villar, J. Saurina, S. Hernández-Cassou, High-performance liquid chromatographic determination of biogenic amines in wines with an experimental design optimization procedure, Anal. Chim. Acta 575(1) (2006) 97-105.

[124] E. Rozet, P. Lebrun, P. Hubert, B. Debrus, B. Boulanger, Design Spaces for analytical methods, Trends Anal. Chem. 42 (2013) 157-167.

[125] R. Deidda, S. Orlandini, P. Hubert, C. Hubert, Risk-based approach for method development in pharmaceutical quality control context: A critical review, J. Pharm. Biomed. Anal. 161 (2018) 110-121.

[126] B. Otašević, J. Šljivić, A. Protić, N. Maljurić, A. Malenović, M. Zečević, Comparison of AQbD and grid point search methodology in the development of micellar HPLC method for the analysis of cilazapril and hydrochlorothiazide dosage form stability, Microchem. 145 (2019) 655-663.

[127] P. Jackson, P. Borman, C. Campa, M. Chatfield, M. Godfrey, P. Hamilton, W. Hoyer, F. Norelli, R. Orr, T. Schofield, Using the Analytical Target Profile to Drive the Analytical Method Lifecycle, Anal. Chem. 91 (2019) 2577–2585.

2. AIM OF THE THESIS

In all projects of this thesis, different APIs and excipients, which feature no or only a weak chromophore, are characterized with novel methods for quality assessment with regard to the chromatographic separation technique and/or detection. Today, software-based tools such as DoE are available for time- and resource-efficient method development and data evaluation and are therefore also incorporated to facilitate certain project steps.

CAD has made a name for itself in recent years as a powerful alternative to UV detection of weakly chromophore analytes at low wavelengths. The first project therefore aims to find a CAD-compatible substitute to the non-volatile cationic IPR tetrabutylammonium hydroxide for the separation and sensitive detection of carbocisteine and its two main degradation products. In addition to IPC with volatile alkylamines, a modern mixed-mode column with AEX functionalities should be evaluated as solution for coupling with aerosol-based detectors and MS.

Based on the results of the first project, the stability of two carbocisteine-containing syrup prototype formulations after 9 months of storage at 40 °C and 75 % relative humidity should be studied by means of LC-HRMS. For comprehensive sample characterisation, untargeted approaches are available for data acquisition. Since corresponding placebo prototype formulations are available, the GUCS workflow is a sophisticated option to systematically evaluate data evaluation and identify possible impurities. In addition, with HRMS and informative MS/HRMS spectra, structural elucidation of unknown degradation products in the syrup prototypes is feasible.

The objective of the third project is a possible simplification of the existing Ph. Eur. monographs of simvastatin and lovastatin by using a hyphenated UV-charged aerosol detection system. For both APIs, in addition to UV-active related substances, the corresponding *4,4a*-dihydro compound is separately tested for as a specified impurity. A transfer to gradient LC UV CAD methods would allow the control of all impurities in a single run. However, the need for inverse gradient compensation must be considered to ensure the validity of this approach.

The final project focuses on the AQbD approach for the development of an LC-CAD method for the analysis of non-volatile fatty acids as an alternative to the extremely laborious Ph. Eur. GC method, which requires derivatisation. In a systematically planned process, a suitable RP-LC method should be developed and the MODR determined. In addition to a batch of polysorbate 80, the fatty acid composition of the excipient magnesium stearate is to be analysed in order to broaden the possible application.

3. RESULTS

3.1. Method transfer from ion pair chromatography to charged aerosol detector-compatible mixed-mode chromatography: A case study using carbocisteine

Rasmus Walther, Oliver-Scherf-Clavel, Ulrike Holzgrabe

Abstract

To take advantage of the charged aerosol detector (CAD) for sensitive LC analysis of analytes with weak chromophore, the volatility of the entire mobile phase is a prerequisite. Therefore, it is not feasible to use common non-volatile ion-pairing reagents such as tetrabutylammonium hydroxide for the analysis of polar, acidic amino acids.

This case study presents a possible procedure for transferring an ion pair chromatography to an HPLC-CAD method using the example of carbocisteine and its two main degradation products, carbocisteine sulfoxide and carbocisteine lactam. In screening experiments, substitution by various volatile alkylamines resulted in inferior chromatographic separation. As an alternative, mixed-mode chromatography using a column with strong anion exchange functionalities and a mobile phase containing 12 mM formic acid and 2 mM trifluoroacetic acid, led to a selectivity equivalent to ion pair chromatography with tetrabutylammonium hydroxide. A change in the level of background noise generated by non-volatile impurities eluting from the column during measurements – often called column bleeding – invalidated the settings predicted from response surface methodology experiments in terms of modelling chromatographic selectivity and CAD sensitivity, and a reduction of the acetonitrile ratio to 22 % (v/v) was required. At a flow rate of 1.2 mL/min and an evaporation temperature of 65 °C, the experimentally determined LOQs of both degradation products were below 50 ng on column. The combination of mixed-mode chromatography with CAD offers a viable alternative to ion pair chromatography with UV detection in the analysis of acidic analytes with a weak chromophore such as amino acids and impurities thereof.

Graphical abstract

Method transfer from ion pair to CAD-compatible mixed-mode chromatography: a case study using carbocisteine

Walther et al. (2021)
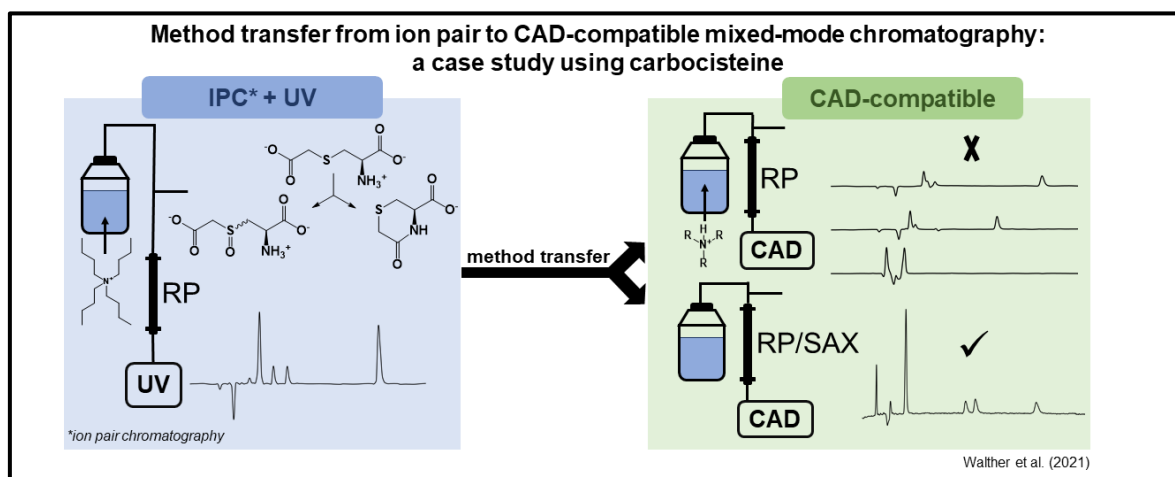
1. Introduction

The analysis of non-aromatic amino acids (AA) and their derivatives is challenging with regard to both the separation of these polar, charged analytes and their sensitive detection. Various derivatization techniques have played an important role in the past to enable the use of UV/vis or fluorescence detectors [1] and are still employed in compendial amino acid analysis [2]. In the case of post-column derivatisation with e.g. ninhydrin, an ion exchange resin is used as a stationary phase with an aqueous, ionic mobile phase for separation. On the other side, pre-column derivatisation allows separation on reversed-phase (RP) columns, as the lipophilicity of the analytes is increased by the chromophore. However, these techniques are not only time-consuming and require more equipment, but are also complex and error-prone, as illustrated by the large number of different derivatization procedures in the literature [1,2]. Another strategy to achieve selective separation of zwitterionic analytes on conventional RP columns is to add either acidic alkyl sulfonates or basic tetraalkylammonium salts as ion-pairing reagents (IPR) to the mobile phase [3]. Due to their low UV cut-off, sufficient limits of quantification (LOQ) could be achieved at low wavelength with acetonitrile as organic modifier in some cases [4].

A promising alternative to compensate for the weak chromophore of non-aromatic AA is the application of aerosol-based detectors [5]. With the corona charged aerosol detector (CAD) in particular, LOQs have been achieved that are comparable or even superior to UV-detection – both for APIs and excipients with weak chromophore [6,7]. However, neither the standard ion exchange methods nor the soap-like IPRs allow direct coupling to the CAD, since the mobile phases are not volatile. Alternatively, various perfluorinated carboxylic acids have been established as anionic volatile IPRs for the analysis of AA with MS or aerosol-based detection [1,5-8].

The fact that these reagents significantly impair the sensitivity of the CAD despite their sufficiently high vapour pressure was recently discussed by Pawellek and Holzgrabe [9]. Taking the new monograph of the anticonvulsant vigabatrin in the European Pharmacopoeia as an example [10], a significant improvement of this CAD method was possible by switching to a mixed-mode column with cation exchange functionalities.

Less common, however, is the substitution of cationic tetraalkylammonium salts by volatile alkylamines for the separation of acidic analytes. In addition, from the routine use of various secondary and tertiary alkylamines in combination with hexafluoroisopropanol for the LC-MS/MS analysis of oligonucleotides [11,12], HPLC-ELSD analysis of bisphosphonates has been published [13]. To the best of our knowledge, this is the only example of a separation of acidic, small molecule APIs.

Using the example of carbocisteine (CC), this case study sketches a procedure for transferring an ion pair chromatography (IPC) method based on the non-volatile tetrabutylammonium hydroxide (TBAOH) to a CAD-compatible HPLC method with equivalent selectivity. In comparison to the natural AA cysteine, CC features an additional carboxylic acid moiety and is used as a mucolytic agent with anti-oxidative and anti-inflammatory effects in the treatment of chronic obstructive pulmonal disease [14]. In the European Pharmacopoeia, simple testing for ninhydrin-positive substances with a limit of 0.5 % (m/m) is currently performed using thin-layer chromatography, which only covers impurities with AA structure [15]. For the selective separation of CC and its two main degradation products, i.e. the sulfoxides (SO I + II) and the lactam (LA) (see Fig. 1) [16], different volatile alkylamines and a reversed-phase/strong anion exchange mixed-mode column (RP/SAX) were tested as CAD-compatible alternatives. In addition to the evaluation of the chromatographic performance, factors that influence the background noise of the CAD and thus the sensitivity were studied.
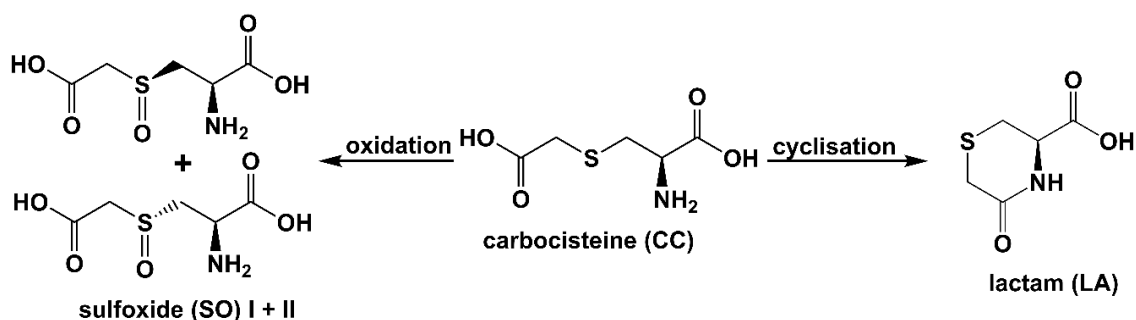

Fig. 1 Molecular structures of carbocisteine and the two main degradation products [16]

2. Material and methods

2.1 Chemicals and reagents

High-purity deionized water for HPLC was produced by a water purification system from Merck Millipore (Schwalbach, Germany). Acetonitrile for HPLC (ACN), glacial acetic acid (HOAc), disodium hydrogen phosphate, tetrabutylammonium hydroxide 40 % solution in water (TBAOH), *N,N*-dimethylbutylamine (DiMBA), dibutylamine (DiBA), *N,N*-dimethylhexylamine (DiMHA), tripropylamine (TriPA) and tributylamine (TriBA), formic acid (FA), trifluoroacetic acid (TFA), ammonium formate (AmFA) and ammonium acetate (AmOAc) were purchased from Sigma Aldrich (Steinheim, Germany). Phosphoric acid 85 %, ammonia 32 % and triethylamine HiPerSolv® (TriEA) were bought from VWR International S.A.S. (Fontenay-sous-Bois, France). The purity of the volatile alkylamines used was at least 98 % and the quality of all other mobile phase additives was HPLC grade. Chemical reference substances of carbocisteine (CC), carbocisteine sulfoxides (SO) and carbocisteine lactam (LA) were obtained from the EDQM (Strasbourg, France).

2.2 Apparatus

A 1295 Alliance Waters separation module with online degasser, autosampler, column thermostat and 995 diode array detector (DAD) was used to examine the chromatographic performance of the different alkylamine IPR (see next section 2.4). Data obtained from the chromatograms were evaluated using Empower 3, 2010 software (Waters, Eschborn, Germany).

CAD experiments using the mixed-mode column were conducted on a Thermo Scientific Vanquish Flex modular chromatographic system equipped with a binary pump with online degasser, an autosampler, a thermostatted column compartment and a variable wavelength detector in-line with a Vanquish Horizon CAD. For instrument control and data evaluation the Chromeleon Data System 7.2.6 Software was applied. Nitrogen was produced (35.0 psi inlet pressure, filter: "none", range: 100 pA) using an ESA nitrogen generator (all Thermo Fisher Scientific, Germering, Germany). A 744 pH-meter (Metrohm, Villebon-sur-Yvette, France) was used for accurate pH adjustment.

2.3 Preparation of solutions

Stock solutions of the two main degradation products were prepared by weighing exactly 2.5 mg of each impurity and diluting with water to 10.0 mL. The API stock solution was prepared by dissolving 5.0 mg CC in 30 µL of ammonia (32 %) and subsequent dilution to 10.0 mL with water. The stock solutions were stored at 2 – 8 °C. For chromatographic method development, a test solution was prepared by mixing equal volumes of the stock solutions. For the RSM experiments a sample consisting of 0.05 mg/mL of SO I + II and LA was used. For the API sample solution, 50 mg was dissolved in 0.3 mL ammonia (32 %)

and spiked (0.1 %) with the impurity stock solutions before making up to 10.0 mL with water. All samples were kept in the autosampler at 8 °C and reused for up to 1 week.

2.4 Screening of the alkylamine IPRs

A Waters XBridge C_{18} column (150 x 4.6 mm; 3.5 µm) was used for the chromatographic separation. All experiments were carried out isocratically (n = 2) at 25 °C with a flow rate of 1.0 mL/min, an injection volume of 20 µL and a detection wavelength of 230 nm. Mobile phase A consisted of either 25 mM TBAOH pH 7.0 (adjusted with concentrated phosphoric acid) or 25 mM of a volatile IPR pH 7.0 (adjusted with glacial acetic acid) in a mixture with 5 % (v/v) ACN. By mixing with mobile phase B, which was a mixture of water with 5 % (v/v) ACN, the concentration of the IPR was varied. The column was flushed thoroughly between the different IPR types applying a three-step procedure: first, the column was purged with 30 column volumes of a 25 mM phosphate or ammonium acetate buffer (pH 7.0) in a mixture containing 5 % (v/v) ACN (≙ mobile phase C). Second, the ACN ratio was then gradually increased to 65 % (v/v), and the column was flushed with an additional 30 column volumes of a 65/35 % (v/v) ACN/water mixture. Third, before changing the IPR type, the test solution was re-injected at 100 % mobile phase C and the chromatogram was checked for increased retention of analytes. In case of insufficient purification, the second and the third steps were repeated, but more than two cycles were never required.

2.5 Mixed-mode chromatography

2.5.1 Method development

For mixed-mode chromatography (MMC), an RP/SAX mixed-mode column, SIELC Primesep SB (150 x 4.6 mm, 5 µm, SIELC Technologies, Wheeling IL, USA) was chosen. To investigate the effects of the pH, the type and the ionic strength of the additive used on the chromatographic performance 20 mM aqueous solutions of AmFA (pH 3.0), AmOAc (pH 4.5) and FA (pH 2.7) were prepared, as well as a 0.1 % (v/v) TFA (13 mM; pH 2.0) solution. By mixing with water and/or ACN, the ionic strength could be reduced and the ratio of the organic modifier increased. The influence of the column temperature was tested between 15 and 35 °C. All experiments were performed isocratically with an injection volume of 10 µL and a detection wavelength of 230 nm.

Response surface methodology (RSM) was applied to investigate the resolution (R_s) between SO I and SO II as well as the signal-to-noise ratio (S/N) of the LA as a function of the flow rate, the ACN proportion and the evaporation temperature [17] using the design of experiments tool of the software STATISTICA (StatSoft Inc., Tulsa, OK, US) for the experimental plan and statistical analysis. The noise was calculated based on a 2 min interval at the end of each run with a CAD filter constant of 5 s and a data collection rate of 10 Hz. A symmetrical, rotatable central composite design (CCD) with three factors at three levels was selected (see Table S1). The centre point was measured in triplicate to estimate

the experimental error, and the resulting 17 runs (see Table S2) were performed in random order. After changing the experimental conditions, the column was flushed for 30 min. Quadratic models including only the statistically significant terms were used to predict the desired factor settings.

2.5.2 Investigation of column bleed

As mobile phases, water and ACN were each mixed with the combination of 12 mM FA and 2 mM TFA. All runs were performed isocratically with a flow rate of 1.2 mL/min at a column temperature of 25 °C and an evaporation temperature of 65 °C. Using a restriction capillary instead of column for flow injection analysis (FIA) at sufficient back pressure (> 100 bar), 10 µL of mobile phase (n = 2) were injected and the background noise was monitored for 5 min while varying the ACN ratio between 15 and 30 % (v/v). After changing the concentration of the organic modifier, the system was rinsed for 10 min.

In addition to the first column used (SB#1), a second Primesep SB column (SB#2) from a different manufacturing lot was used for comparison. In analogy to the FIA experiments (see above), blank injections at varying ACN ratios were performed with the original column SB#1. Three additional cycles of a sequence including API and blank samples were carried out with the SB#2 column, as shown in Table 1.

Table 1
Sequence for the investigation of column bleeding
with the Primesep SB#2 column

No.	Inj.	Sample	ACN % (v/v)	Run time
1	n = 2	blank	20	5 min
2		API		9 min
3	equilibration		25	30 min
4	n = 2	blank	25	5 min
5		API		9 min
6	equilibration		20	30 min

2.5.3 Final chromatographic procedure

The mobile phase consisted of a combination of 12 mM FA and 2 mM TFA in a mixture of 78/22 % (v/v) water/ACN. Runs were performed isocratically with a flow rate of 1.2 mL/min at a column temperature of 25 °C and an injection volume of 10 µL. The CAD was set to an evaporation temperature of 65 °C, a filter constant of 10 and data collection rate of 10 Hz.

3. Results and discussion

3.1 Transfer from IPC to a CAD-compatible MMC method

According to modern architecture of IPC, retention of charged analytes is regarded as a mixture of electrostatic and partition processes. The dynamic adsorption of the alkylamines onto the lipophilic column surface creates an electrical bilayer, which is strongly influenced by the type and concentration of: (1) the IPR, (2) the counter ions and (3) the organic modifier [3]. A pH of 7.0 was set for both the experiments with TBAOH and the volatile alkylamines, as all analytes bear a negative charge and can thus interact strongly with the oppositely charged alkylamines. In the case of TBAOH, concentrated phosphoric acid was added to adjust the pH because of its low UV cut-off.

Baseline separation of all analytes was achieved over the entire tested concentration range of 5 – 25 mM TBAOH with 5 % ACN (v/v) (see Fig. 2). Plotting the logarithm of the capacity factor k against the concentration of TBAOH results in a graph with a parabolic shape (see Fig. S1). This can be explained by the fact that as soon as a monomolecular layer has been formed on the column surface, the remaining alkylamine ions in the mobile phase compete for ion-pair formation with the oppositely charged analytes decreasing their affinity to the adsorbed IPR molecules on the column surface and thus reduce retention [3,18]. The API eluted first, closely followed by the pair of diastereomers of SO I + II and, then, the less polar LA (no basic, protonatable N).
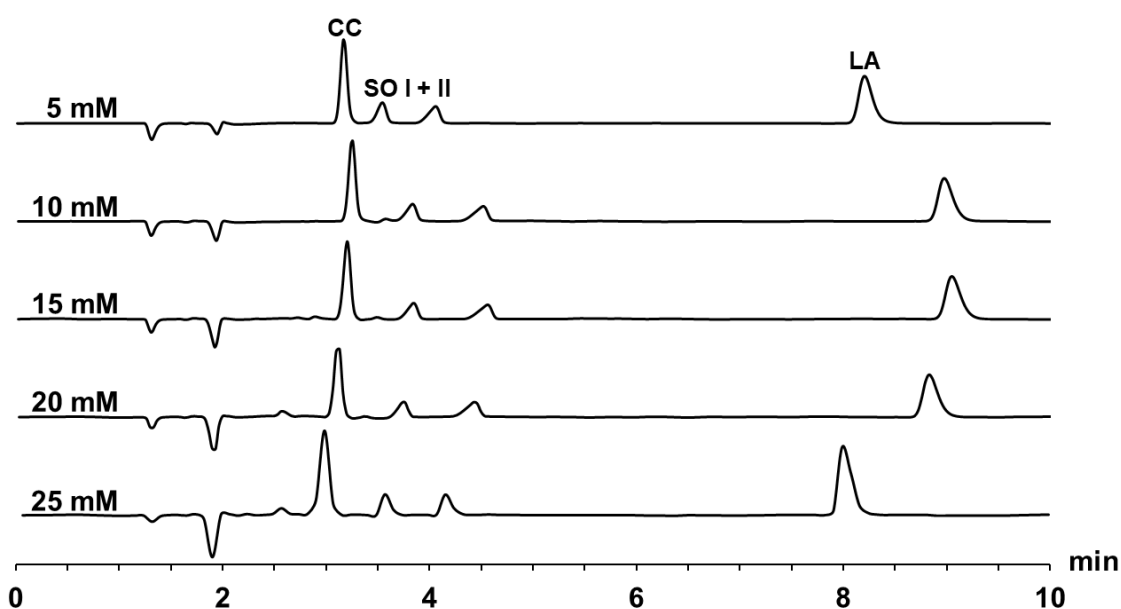
Fig. 2 Influence of the TBAOH concentration on the chromatographic separation
Overlaid chromatograms of the test solution containing carbocisteine (CC), its sulfoxides (SO I + II) and the lactam (LA) with increasing TBAOH concentration at pH 7.0 using a Waters XBridge C_{18} column at a constant ACN ratio of 5 % (v/v) (for further details see section 2.4).

This elution order corresponds to a published anion exchange method [19], but the selectivity with TBAOH is higher, as even baseline separation ($R_s = 2.79$) of the physicochemically very similar diastereomers was possible. Although retention of all

analytes was highest in the range of 10 – 15 mM, better peak symmetry and S/N values were obtained with 25 mM and 5 % ACN (v/v). From the corresponding chromatograms of the blank and the injected test mixture (both 0.083 mg/mL), a S/N of 28 for the SO and 160 for the LA was determined. Based on these values, the LOQs (S/N = 10) were extrapolated to approximately 0.030 mg/mL for SO I + II and 0.0052 mg/mL for the LA due the better chromophore of the lactam structure.

3.1.1 Volatile alkylamine IPRs

Instead of phosphoric acid, HOAc was chosen as a volatile alternative for possible CAD coupling to convert the volatile alkylamines into their protonated, active form. Regarding the IPR, retention should generally rise with increasing its concentration and lipophilicity. However, more precise data on the impact of various volatile alkylamines on separation performance are only available for much larger oligonucleotides. Thus, no baseline separation of e.g., DNA oligomers (n = 24 and n – 1) was possible with the short-chain, more polar IPRs such as *N*-propylamine and only minor chromatographic differences were observed with the more lipophilic derivatives like tripropylamine (TriPA) or *N,N*-dimethylhexylamine (DiMHA) [12].

In contrast, CC and its degradation products are much smaller and have no non-polar substructures. Therefore, in this case, triethylamine (TriEA) with 6 carbon atoms was chosen as the most polar alkylamine and tributylamine (TriBA) with 12 carbon atoms, which is still considered a volatile organic compound [20], was chosen as the largest IPR. To evaluate the influence of chain length, TriPA was included to form a homologous series: TriEA–TriPA–TriBA. In addition, dibutylamine (DiBA), a secondary amine, as well as *N,N*-dimethylbutylamine (DiMBA) and DiMHA, two asymmetrically substituted derivatives, were selected to test whether the type of substitution, and, thus, the steric shielding of the positive charge, affects chromatographic performance. Table 2 summarises the physicochemical properties of the six volatile alkylamines, whose suitability as substitutes for TBAOH in the separation of CC and its main degradation products was investigated.

Table 2
Overview of the volatile alkylamine ion-pairing reagents (IPR) used and selected physicochemical properties

IPR	Formula	Boiling point [a] (°C 1013 hPa)	Vapour pressure [a, b] (hPa 20°C)	log P [a]
Triethylamine (TriEA)		89	69.6	1.45
	$C_6H_{15}N$			
N,N-Dimethylbutylamine (DiMBA)		95	67	1.7
Dibutylamine (DiBA)		161	2.7	2.83
	$C_8H_{19}N$			
N,N-Dimethylhexylamine (DiMHA)		148	n.a. [c]	n.a. [c]
Tripropylamine (TriPA)	$C_9H_{21}N$	156	4.3	2.79
Tributylamine (TriBA)	$C_{12}H_{27}N$	214	0.18	4.6

[a] Data was obtained from the GESTIS Substance Database from the German Social Accident Insurance (accessed 03/2021).
[b] Chemicals with a vapour pressure ≥ 0.1 hPa (20°C) are considered *volatile* [20].
[c] not available

Starting with 25 mM of the respective IPR and 5 % ACN (v/v), the volatile alkylamines were screened in ascending order according to the number of their carbon atoms. In analogy to TBAOH, CC was identified as the first peak and the LA as the last peak based on the UV spectra. It was impossible to separate all analytes with either TriEA or DiMBA (both $C_6H_{15}N$), as SO I + II co-eluted with CC, which was confirmed by the calculated peak purity. Besides, interference with system peaks and insufficient overall retention (< 3 min) impaired chromatography (see Fig. 3A). Using the more lipophilic C_8 derivatives DiBA and DiMHA, SO I + II still co-eluted with the API peak, but as expected, the *k*-values (see Table S3) of all analytes increased. In contrast to the first pair tested (DiMBA > TriEA), the difference between the DiBA and DiMHA was negligible (see Fig. 3A). Not only the length of the alkyl chains is relevant, but also their connection and the steric accessibility of the positive charge. Compared to the sterically more demanding TriEA, the retention of the anionic analytes was more pronounced using the asymmetrically substituted DiMBA, while DiMHA behaved similarly to the secondary DiBA. However, comparing DiMBA and DiMHA, the length of the alkyl chain seems to have the greatest influence on retention (see Table S3). The observed trend of increasing retention continued for TriPA and TriBA, but baseline separation of the four analytes was still not possible (see Fig. 3A). Reducing the concentration of DiMHA, TriPA or TriBA led to an increase in retention analogous to TBAOH, but still no baseline separation of CC and SO I was achieved (see Table S3). For the homologous series TriEA–TriPA–TriBA in a double logarithmic plot of the number of C-

atoms against k, a linear relationship results for CC and LA (see Fig. 3B) [21]. The corresponding values for the quaternary TBAOH are below the regression lines, indicating that the length of the alkyl chain is not the only factor determining retention. Despite the same elution order, none of the volatile alkylamines tested here is a suitable substitute for TBAOH for the analysis of CC. The use of even longer-chain derivatives or a reduction of the ACN proportion did not make sense, as both would be disadvantageous for the CAD sensitivity [22]. If a second pump is available for post-column addition, the organic ratio could be increased without directly affecting chromatography. Due to the reduced viscosity/surface tension of organic-rich eluents, a more efficient nebulization and evaporation takes place, which benefits the particle formation of the analytes and leads to higher CAD responses [7,22].
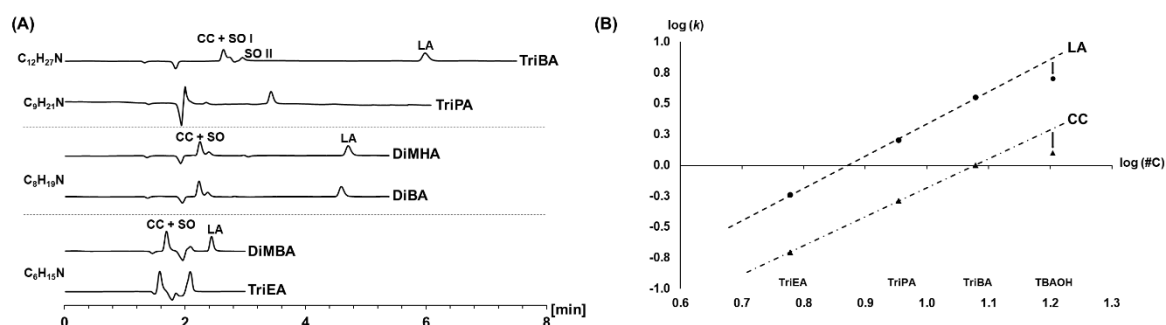

Fig. 3 Evaluation of the volatile alkylamine IPRs
(A) Overlaid chromatograms of the test solution containing carbocisteine (CC), its sulfoxides (SO I + II) and the lactam (LA) for the 6 volatile alkylamine IPRs tested (25 mM, pH 7.0) using a Waters XBridge C_{18} column at a constant ACN ratio of 5 % (v/v) (for further details see section 2.4) (B) Plot of the $\log(k)$ of CC and LA derived from the chromatograms in Fig. 3A against the log of number of C atoms (#C) of the homologue series TriEA–TriPA–TriBA and TBAOH (all 25 mM)

3.1.2 RP/SAX mixed-mode column

A possible CAD-compatible alternative to TBAOH, which works entirely without potentially interfering IPRs, is MMC [9], in this case with anion exchange functionalities. If the mobile phase used is volatile, aerosol-based or MS detectors have been successfully employed for many ionic analytes [1,5-13,16]. However, due to the multiple separation modes, method development and modelling of retention behaviour is complex, so that, for example, a combination of linear solution strength and an empirical stoichiometric displacement net charge model had to be employed for a specific column [23]. The Primesep SB column used in this case study is functionalised with quaternary ammonium moieties (RP/SAX) embedded in a C_{18} chain to interact with the analytes in a manner comparable to TBAOH. The pH of the mobile phase is likely to have a major influence on the chromatography as it defines the ionisation of the analytes as well as the other additives and thus has a direct impact on the ionic interactions with the stationary phase. Furthermore, the type and concentration of a buffer, as well as the ACN ratio, not only affect all interaction modes with the column, but also the sensitivity of the CAD. For a low level of background noise, the

concentration of the additives should be as low as possible and at the same time a high organic ratio of the eluent enhances the signal intensity of the analytes [7,22].

The pH of the mobile phase influenced the chromatography on two levels: first, the elution order of CC and the SO I + II changed at a higher pH, and second, the overall retention increased at lower pH values (see Fig. 4A). Owing to the strong interactions between the analytes and the RP/SAX material, an ACN proportion of more than 20 % (v/v) was required to reduce the run time below 30 min, regardless of the pH, with an additional beneficial effect on CAD sensitivity. Lower concentrations of the additives to further reduce the level of background noise of the CAD caused the retention times (RTs) to increase substantially and could not be compensated by a higher ACN proportion. The fact that RTs shorten at higher pH values despite increasing dissociation of the acidic analytes can be explained by strong ion displacement interactions, which surpass the anion exchange mechanism. This is probably favoured by the embedding of the quaternary ammonium groups in a long, lipophilic chain, so that the interactions with the very polar analytes are weakened.
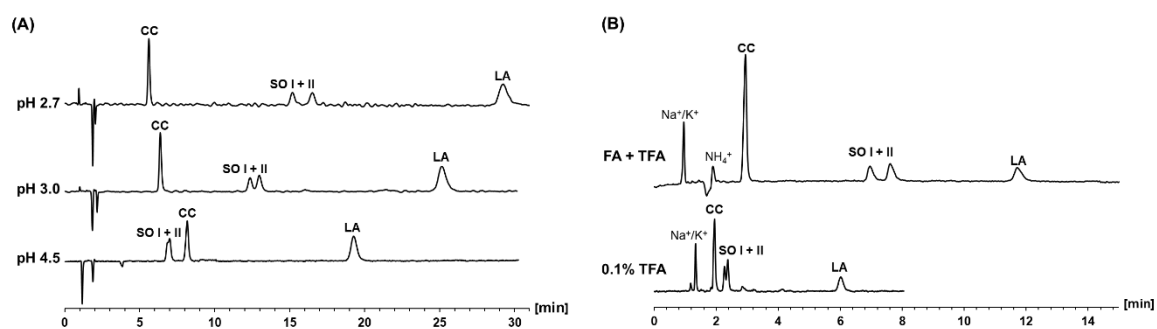

Fig. 4 Overlaid chromatograms of the test solution containing carbocisteine (CC), its sulfoxides (SO) and lactam (LA) using the Primesep SB mixed-mode column with
(A) Mixtures of 25 % (v/v) ACN and 20 mM solutions of ammonium acetate pH 4.5, ammonium formate pH 3.0 or formic acid pH 2.7 using UV detection at 230 nm (further details see sections 2.5.1 and 3.2.1)
(B) Comparison of 0.1 % TFA without ACN (evaporation temperature = 25 °C) and the combination of 12 mM FA + 2 mM TFA with 20 % ACN (v/v) using the CAD (evaporation temperature = 60 °C)

3.2 Optimization of the MMC-CAD method

The influence of the column temperature was small and was therefore set to 25 °C for all further measurements (data not shown).

3.2.1 pH and ionic strength

Further lowering of the pH by addition of 0.1 % (v/v) TFA (13.0 mM; pH 2.0) shortened the run time to only 7 min, but SO I + II were not well resolved (see Fig. 4B). Apart from the lower pH, the chaotropic nature of TFA comes into play here, displacing analyte ions more effectively compared to the hydrophilic FA. Simply reducing the TFA concentration to separate SO I + II caused peak distortion due to the very low ionic strength, and ultimately the combination of 12 mM FA with 2 mM TFA allowed baseline separation of all analytes

(see Fig. 4B). The addition of FA would also reduce ion suppression by TFA when coupled to ESI-MS [24].

3.2.2 CAD sensitivity

3.2.2.1 Response surface methodology

%-ACN, flow and evaporation temperature: Using the above-mentioned additive combination of FA and TFA as a starting point, the sensitivity of the CAD was now investigated in depth. Here, the evaporation temperature is the most influencing variable, as it affects both the level of background noise and the analyte signal intensity. The optimal evaporation temperature depends not only on the chemical structure of each analyte, but also on the exact composition of the mobile phase and flow rate [7,9,22]. Since the latter two factors simultaneously affect chromatographic resolution, the application of response surface methodology (RSM) offers a time- and resource-efficient approach to find the optimal settings [17]. The goal of RSM is to create mathematical models of one or more variables of interest as a function of several factors, which – depending on the model chosen – allow a quantitative description of the effects and of the interactions of the factors. Design of experiments is indispensable to reduce the number of experiments needed by changing all factors simultaneously. To predict the optimum of a chromatographic problem, a Box-Behnken or a central composite design (CCD) are often used with quadratic models for evaluation, whereas other designs have to be applied for screening experiments or robustness studies [17].

In this case, the R_s of the critical peak pair and the S/N of the lactam were selected as variables whose variations were investigated as a function of the three factors ACN ratio, flow rate and evaporation temperature. After the levels of the three factors were specified (ACN: 10– 40 % (v/v), flow: 0.8–1.2 mL/min, evaporation temperature: 50–80 °C; for further details see Table S1) with a few additional screening runs, a CCD (see Table S2) was chosen that experimentally determines the response at the extremes, as opposed to a Box-Behnken design [17,25].

Eliminating all insignificant terms ($p > 0.05$) to improve the models resulted in an adjusted R^2 of 0.9500 for the R_s and 0.9284 for the S/N, respectively (see Table S4). A satisfactory correlation between the experimental data and the models was also confirmed graphically (see Figs. S1 and S2). The final quadratic models were subsequently used to predict the optimal factor settings by a computational multi-criteria approach developed by Derringer and Suich [17,26]. Therefore, the responses first had to be rated between 0 (≙ "undesirable") and 1 (≙ "very desirable"). For the S/N, the minimum and maximal values from Table S2 were chosen, and in terms of R_s, 1.4 was chosen as undesirable and 1.6 as very desirable (no benefit from higher values). The profiles of the predicted values and the desirability are shown in Fig. 5. The upper row illustrates that, on the one hand, the R_s

decreases (negative slope) with increasing ACN ratios as well as flow rates (less pronounced) and, on the other hand, the influence of the evaporation temperature on this chromatographic parameter is negligible. Regarding the S/N (bottom row), a high ACN proportion appears beneficial (ascending straight line). However, to obtain baseline separation of SO I + II as the critical peak pair (R_s > 1.5), a maximum proportion of 25 % (v/v) ACN should not be exceeded. Since all particles – analyte and impurities – arriving in the electrometer per time unit generate a signal [7,22], a plateau for the flow with maximum response is reached (1–1.2 mL/min). The fact, that S/N becomes smaller for an evaporation temperature above 65 °C, can be explained by a semi-volatile behaviour of the lactam, which unlike the other analytes, is not zwitterionic.

To further test the suitability of this MMC method, higher concentrated API samples (5 mg/mL) were injected several times with the determined optimum of 25 % (v/v) ACN + 1.2 mL/min + 65 °C evaporation temperature. Significantly increased column bleeding was observed, invalidating the RSM predictions of the S/N. Interestingly, a reduction of the ACN ratio to 22 % (v/v) almost halved the level of background noise, so this occurrence of column bleeding was investigated in more detail below.
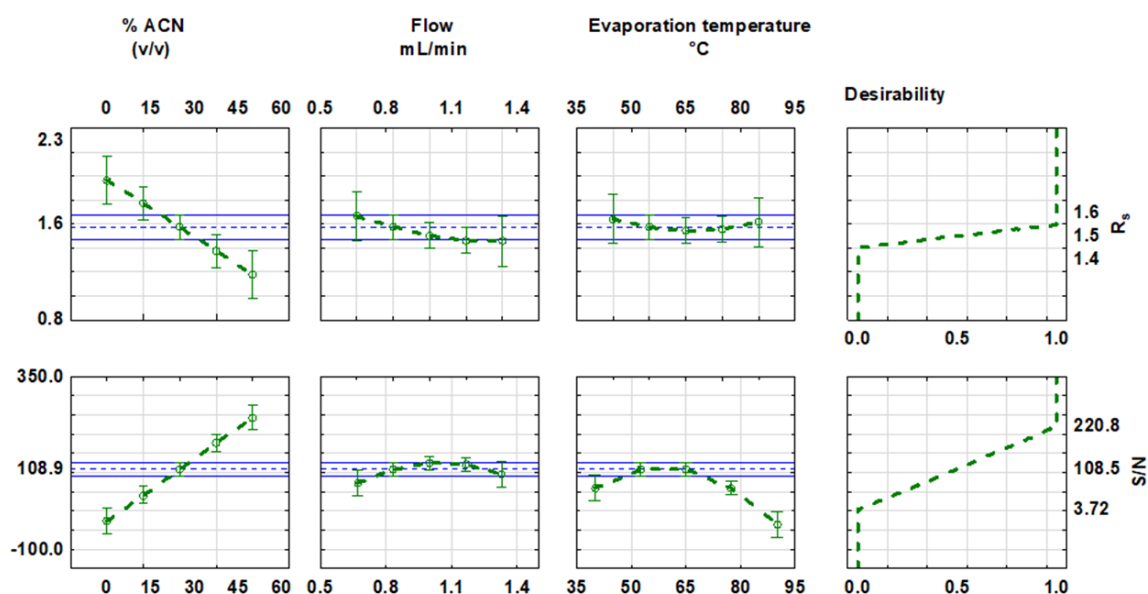
Fig. 5 Profiles of the predicted values and desirability (right column) for the two dependant variables R_s (upper row) and S/N (bottom row)

3.2.2.2 Column bleeding

Bleeding of silica-based mixed-mode columns, especially under HILIC conditions, and their contribution to the CAD background current have already been reported [27]. Currently, Walter et al. were able to confirm the chemical nature as non-volatile hydrolysed column material by means of LC-HRMS, e.g. from a used Primesep B column a molecular ion with m/z = 305.9 was identified as $[C_{15}H_{36}NO_3Si]^+$ [28].

The influence of a more effective particle formation at higher concentrations of the organic solvent and hence increased background current was investigated by flow injection analysis. Without column, changing the ACN ratio from 15 to 30 % (v/v) only resulted in an increase from 0.25 to 0.63 pA. Instead, the background current with column SB#1 was more than 1 pA higher in every case, supporting to the hypothesis of the occurrence of column bleeding. A change in the ACN ratio to 25 % and especially to 30 % was accompanied by a disproportionate increase (see Fig. 6A).
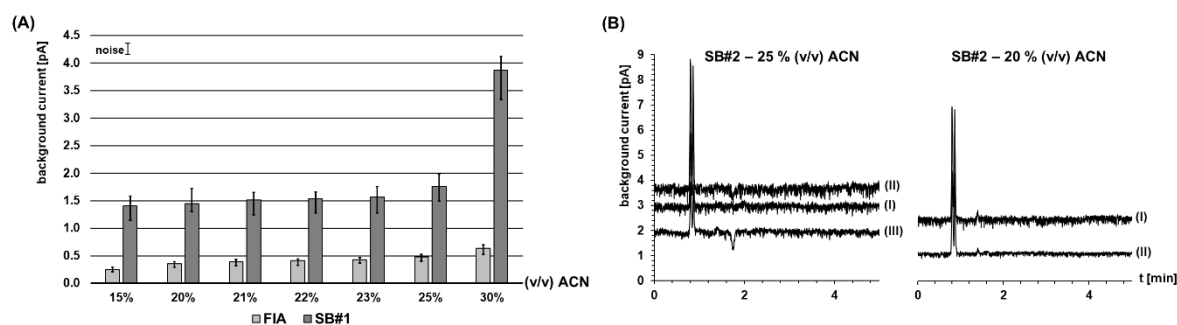

Fig. 6 Investigation of column bleeding
(A) Comparison of the level of background current (noise ranges indicated by vertical bars) by flow injection analysis (FIA) and the Primesep SB#1 column at 15–30 % (v/v) ACN
(B) Chromatogram overlay showing the change in background current at 25 % (left) and 20 % (right) ACN after multiple injection of API samples (for more details see section 3.2.3)

The simulation of column wear for the SB#2 column by multiple injection of concentrated API samples (see Table 1 Section 2.5.2) impressively demonstrated the change in background noise due to column bleeding. When 25 % (v/v) ACN was applied after the third sample injection, the background current increased from 3.0 to 3.6 pA, before decreasing to a constant value of 2.0 pA after the sixth injection (see Fig. 6B left). However, with only 20 % (v/v) ACN, the background current immediately dropped from 2.3 pA after the first two injections to a constant value of 1.0 pA after only one further injection (see Fig. 6B right).

The best S/N for the degradation products were obtained with both columns at 22 % (v/v) ACN and did not change upon the following validation experiments. After conditioning by multiple injection of concentrated API samples, the level of background noise and thus bleeding of both columns reached constant values that remained unchanged (± 0.1 pA) during the validation experiments (see section 3.2.3). The extent of column bleeding was reduced to a robust level, and although this is tantamount to column wear, no progressive loss of efficiency or decreasing *k*-values were observed throughout further measurements. Nevertheless, the level of background noise should be considered in addition to separation performance when defining system suitability criteria. Whether a sensitive control of the impurities is possible at these noise levels was investigated in the following.

3.2.3 Validation of the final MMC-CAD method

Applying the final chromatographic conditions (see section 2.5.3), specificity, LOQ, linearity, accuracy, repeatability and inter-day precision of both main degradation products were determined with both columns (SB#1 and SB#2) according to ICH guideline Q2(R1) [29]. Specificity was demonstrated by comparing spiked samples (see Fig. 7) with a blank solution, obtaining baseline separation between all analytes (R_s > 1.5) with both columns. Applying the second SB#2 column the RT of CC remained unchanged, but the peak pair of SO I + II was shifted forward (– 0.2 and – 0.3 min) and the LA peak was shifted backward (+ 0.2 min).

Limit of quantification was determined by diluting the stock solutions with mobile phase until an S/N ≥ 10 was reached for SO I + II or LA, respectively. On this basis, calibration curves from 0.0050 mg/mL ($\triangleq$ LOQ) to 0.0150 mg/mL for column SB#1 (0.1–0.3 % (m/m)) and 0.0075 mg/mL ($\triangleq$ LOQ) to 0.0175 mg/mL for column SB#2 (0.15–0.35 % (m/m)) with five levels (n = 3) equally distributed were established for both impurities ranging and checked for linearity. The concentration levels "low" ($\triangleq$ LOQ), "middle" (0.010 mg/mL $\triangleq$ 0.2 % (m/m) or 0.0125 mg/mL $\triangleq$ 0.25 % (m/m)) and "high" (0.0150 mg/mL or 0.0175 mg/mL) of the calibration curves were used on the one hand to assess the accuracy (mean recovery rates, n = 3) and on the other hand to investigate the repeatability (RSD, n = 6) and inter-day precision (RSD, n = 12).
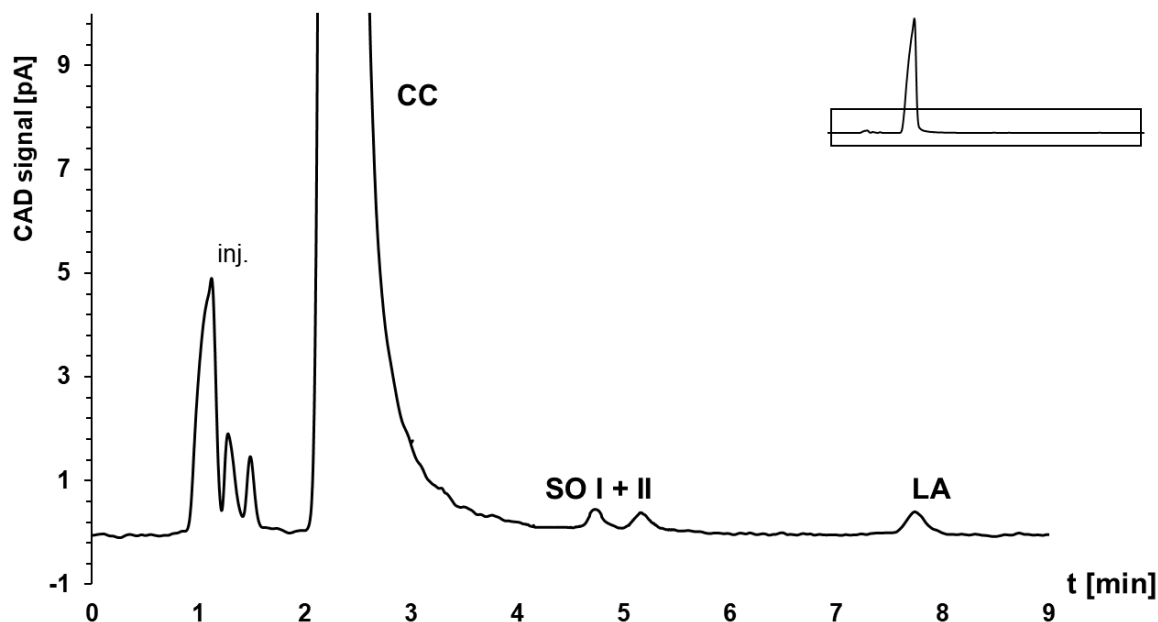
Fig. 7 Chromatogram of a 5 mg/mL CC sample spiked with 0.1 % SO and 0.1 % LA (m/m) using the Primesep SB mixed-mode column, a mobile phase consisting of 2 mM FA, 12 mM TFA with 22 % (v/v) ACN and an evaporation temperature of 65 °C at the CAD

The results summarized in Table 3 show that an accurate and precise control of both main degradation products is possible with both mixed-mode columns in combination with the CAD. However, even after intensive conditioning/priming and a similar level of background

noise, the slope of the linear calibration curve and the LOQs obtained with the second column from a different manufacturing lot are inferior. This has to be taken into account when developing MMC method and for routine applications such as quality control, it is the best to stockpile several columns from the "best" lot, or columns could be tested whose hydrolytic stability have been increased, e.g. by polymer coating or use of ethylene-bridged organic/inorganic hybrid particles [28].

Table 3 Results from validation experiments for both Primesep SB columns applying the final chromatographic conditions described in section 2.5.3

Parameter	Level	Column SB#1			Column SB#2		
		SO I	SO II	LA	SO I	SO II	LA
Recovery rate (n = 3)	low	104 %	101 %	101 %	116 %	115 %	101 %
	middle	103 %	101 %	95 %	99 %	96 %	101 %
	high	104 %	105 %	100 %	106 %	101 %	101 %
Repeatability RSD (n = 6)	low	4.41 %	4.61 %	3.57 %	4..71 %	4.03 %	2.52 %
	middle	3.52 %	4.07 %	3.91 %	3.05 %	4.46 %	3.02 %
	high	4.37 %	1.90 %	4.11 %	4.87 %	3.51%	2.96 %
Inter-day precision RSD (n = 12)	low	4.26 %	8.27 %	4.92 %	7.77 %	6.79 %	5.53 %
	middle	5.32 %	3.91 %	3.85 %	4.77 %	5.48 %	4.76 %
	high	7.55 %	5.90 %	2.94 %	6.03 %	9.45 %	2.97 %
Linearity (n = 3)	y-axis	-0.031	-0.036	-0.017	-0.021	-0.022	-0.007
	slope	11.74	12.71	16.44	6.77	7.21	9.22
	R^2	0.9990	0.9986	0.9960	0.9930	0.9973	0.9953
LOQ	mg/mL	0.00175	0.00175	0.0042	0.00375	0.00375	0.0050
	[%][a]	0.035	0.035	0.084	0.075	0.075	0.10
	ng/column	17.5	17.5	42.0	37.5	37.5	50.0

[a] In per cent (m/m) of the API sample solution

4. Conclusion

In contrast to TBAOH, none of the volatile alkylamines tested here allowed a complete separation of the chemically closely related analytes (CC and SO I + II). As an alternative without an interfering IPR in the mobile phase, a mixed-mode column with anion exchange functionalities can be employed. In this case, IPC-equivalent selectivity was achieved with the Primesep SB and a combination of FA and TFA as with TBAOH. Since injections of highly concentrated API samples altered the intensity of column bleeding and thus the level of background current, the column has to be appropriately pre-conditioned before method optimisation when coupled to the CAD.

Accurate, precise and sensitive (LOQ: 0.035 % SO I + II and 0.084 % LA) control of both main degradation products was demonstrated applying a combination of 2 mM FA and 12 mM TFA in a mixture with 22 % (v/v) ACN as mobile phase, a flow rate of 1.2 mL/min and evaporation temperature of 65 °C. Only after pre-conditioning by multiple injections of CC samples could these results be verified with a second column from a different manufacturing lot. Taken together, this method is appropriate to assess the carbocisteine quality, even for pharmacopoeial purposes.

Conflict of interest statement

None of the authors of this paper does have a financial or personal relationship with other people or organizations that could inappropriately influence or bias the content of the paper.

Acknowledgements

Thanks to Thermo Fisher Scientific for providing the Vanquish Flex UPLC system with Vanquish CAD and for their technical support. Stefanie Gornstein is thanked for her practical support in the lab.

Supplementary material

Table S1
Investigated factors and their opted levels of
the applied central composite design

	Level		
Factor	**- 1**	**0**	**+ 1**
A: % ACN (v/v)	10.0	25.0	40.0
B: Flow (mL/min)	0.80	1.00	1.20
C: ET[a] (°C)	50.0	65.0	80.0

[a] ET: evaporation temperature
The α value was set to 1.683 for rotatability of
the design.

Table S2
Experimental plan of the 3x3 central composite design with the
coded factors A-C (see Table S1) and responses of both
variables R_s and S/N

exp. no	order	A	B	C	R_s	S/N
1	12	- 1	- 1	- 1	1.832	20.64
2	5	- 1	+ 1	+ 1	1.630	13.64
3	6	+ 1	- 1	+ 1	1.324	40.18
4	3	+ 1	+ 1	- 1	1.175	180.6
5	15	- 1	- 1	+ 1	1.856	20.64
6	14	- 1	+ 1	- 1	1.724	31.45
7	8	+ 1	- 1	- 1	1.285	190.5
8	16	+ 1	+ 1	+ 1	1.201	73.87
9	4	- α	0	0	1.607	3.722
10	9	+ α	0	0	1.033	220.8
11	2	0	- α	0	1.663	75.35
12	17	0	+ α	0	1.480	109.9
13	10	0	0	- α	1.631	66.94
14	7	0	0	+ α	1.566	5.214
15*	1	0	0	0	1.596	136.2
16*	11	0	0	0	1.593	1471
17*	13	0	0	0	1.606	126.8

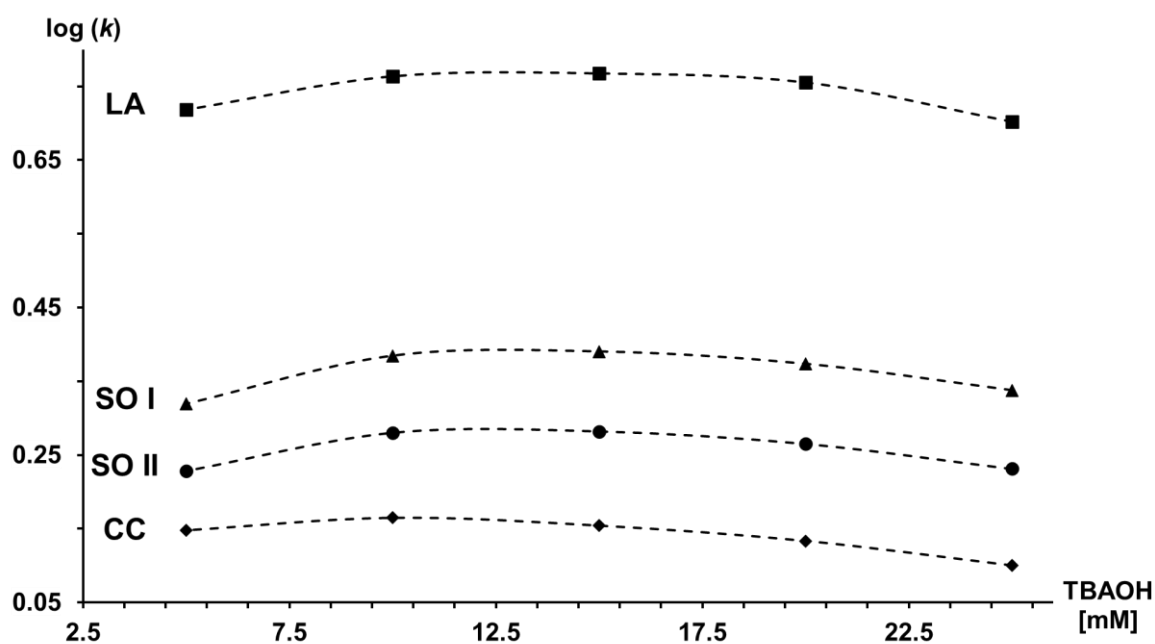* The center point of the CCD was measured in triplicate.

Fig. S1 Influence of the tetrabutylammonium hydroxide (TBAOH) concentration on the
chromatographic separation of carbocisteine (CC), the sulfoxides (SO I + II) and the lactam (LA)
Plot of $\log(k)$ derived from the chromatograms in Fig. 2 for all analytes depending on the TBAOH
concentration in the range from 5 to 25 mM

Table S3
Chromatographic performance of the volatile alkylamine IPRs (calculated according to the European Pharmacopoeia)

IPR + 5 ACN (v/v)	k				R_s		
	CC	SO I	SO II	LA	CC – SO I	SO I – SO II	SO II – LA
25 mM TriEA	0.20	n.a.	n.a.	0.58	n.a.	n.a.	n.a.
25 mM DiMBA	0.28	n.a.	0.58	0.85	n.a.	n.a.	n.a.
25 mM DiBA	0.69	n.a.	0.80	2.47	n.a.	1.18	16.3
25 mM DiMHA	0.70	n.a.	0.81	2.56	1.19	n.a.	16.6
20 mM DiMHA	0.72	n.a.	0.82	2.66	1.13	n.a.	17.7
5 mM DiMHA	0.54	n.a.	0.61	1.62	1.00	n.a.	11.8
25 mM TriPA	0.52	n.a.	0.78	1.60	n.a.	3.08	8.51
15 mM TriPA	0.55	n.a.	0.98	1.65	n.a.	5.16	6.99
25 mM TriBA	1.00	1.07	1.23	3.56	0.76	1.84	19.2
15 mM TriBA	1.16	n.a.	1.40	4.11	n.a.	2.61	20.2

IPR: ion-pairing reagent ACN: acetonitrile k: capacity factor
R_s: resolution CC: carbocisteine SO I/II: carbocisteine sulfoxides
LA: carbocisteine lactam TriEA: triethylamine DiMBA: *N,N*-dimethylbutylamine
DiBA: dibutylamine DiMHA: *N,N*-dimethylhexylamine
TriPA: tripropylamine TriBA: tributylamine
n.a.: not available

Table S4
Effect of all coded terms (A – C) for both quadratic models and their statistical significance

	R_s			S/N		
Term	Effect	95 % CI[a]	p[b]	Effect	95 % CI[a]	p[b]
Constant	1.597	1.51 - 1.683	< 0.0001	137.1	112.4 – 161.9	< 0.0001
A	-0.444	-0.525 - -0.362	< 0.0001	113.7	90.33 - 137.1	< 0.0001
A^2	-0.192	-0.282 - -0.102	0.0015	-20.05	-45.90 - 5.804	0.1093
B	-0.129	-0.211 - -0.047	0.0074	14.12	-9.380 – 37.63	0.1983
B^2	-0.013	-0.105- 0.079	0.7538	-34.92	-61.29 - 8.541	0.0166
C	-0.017	-0.098 - 0.065	0.6431	-57.26	-80.67 - 33.85	0.0007
C^2	0.007	-0.084 - 0.097	0.8624	-74.89	-100.8 - -48.95	0.0002
A x B	0.025	-0.081 - 0.132	0.5919	2.410	-28.06 - -32.88	0.8569
A x C	0.034	-0.073 - 0.140	0.4773	-57.23	-87.70 - -26.75	0.0030
B x C	-0.033	-0.139 - 0.074	0.4900	9.030	-21.44 - 39.50	0.5061

A: % acetonitrile (v/v); B: Flow rate [mL/min]; C: Evaporation temperature [°C]
R_s: resolution; S/N: signal-to-noise ratio [a] CI: confidence interval
[b] p: p-value

Fig. S2 Normal probability plot of the residuals, residuals vs. predicted values plot and predicted vs. actual values plot of the quadratic model for the resolution (R_s)

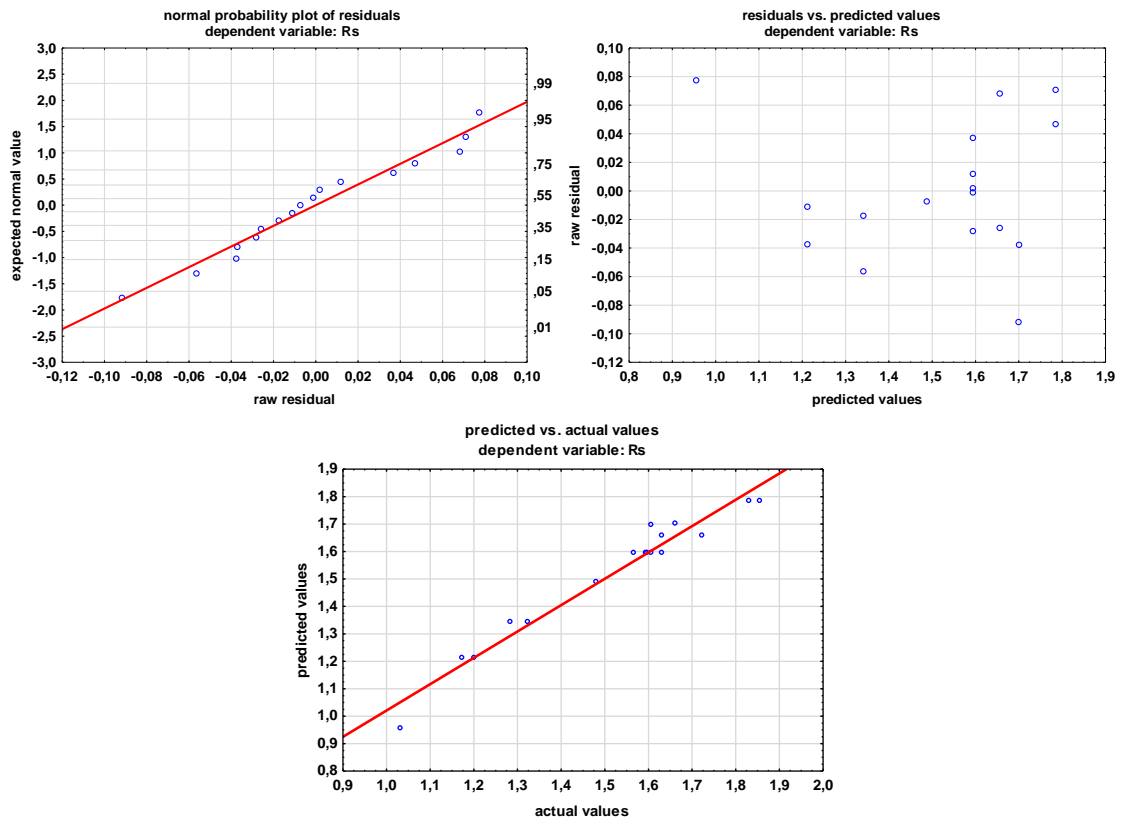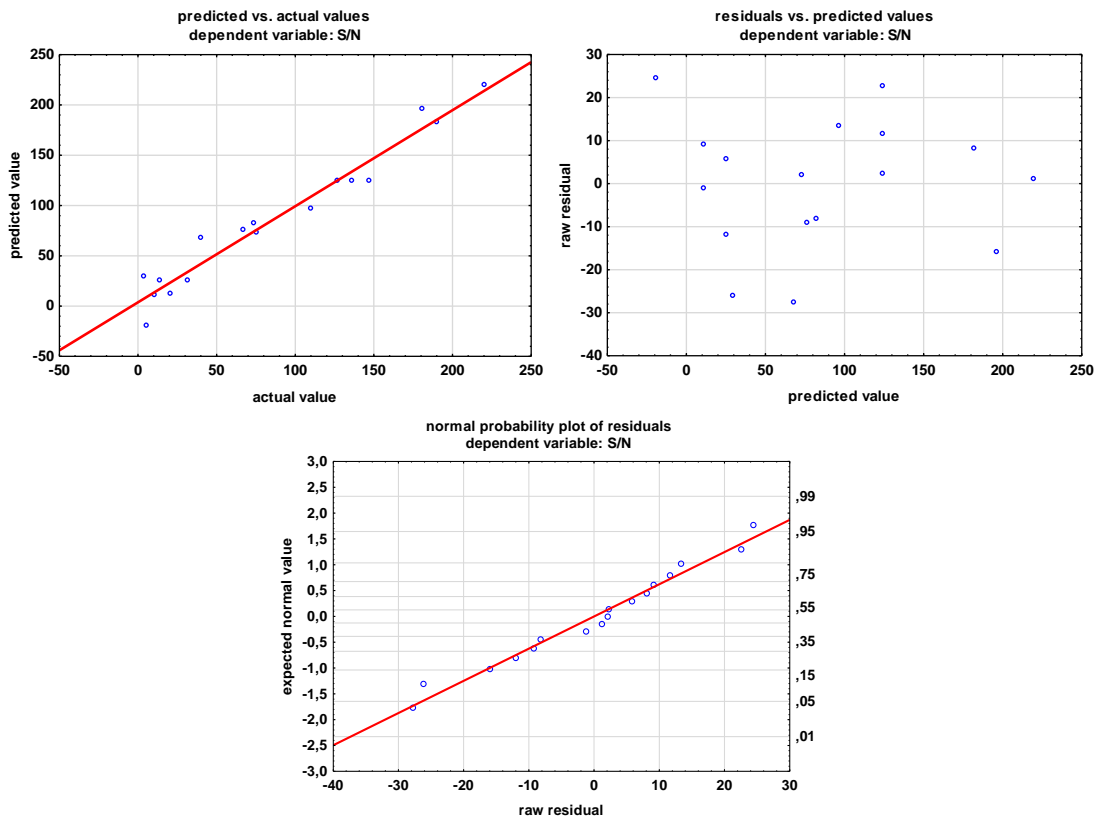**Fig. S3** Normal probability plot of the residuals, residuals vs. predicted values plot and predicted vs. actual values plot of quadratic model for the signal-to-noise (S/N)

References

[1]   S. Ferré, V. González-Ruiz, D. Guillarme, S. Rudaz, Analytical strategies for the determination of amino acids: past, present and future trends, J. Chromatogr. B 1132 (2019) 121819.

[2]   Council of Europe, European Pharmacopeia, 10.5 edition, Chapter 2.2.56 Amino acid analysis, Strasbourg, France (2021).

[3]   T. Cecchi, Ion pairing chromatography, Crit. Rev. Anal. Chem. 38(3) (2008) 161-213.

[4]   K. Schilling, M. C. Amstalden, L. Meinel, U. Holzgrabe, Impurity profiling of l-asparagine monohydrate by ion pair chromatography applying low wavelength UV detection, J. Pharm. Biomed. Anal. 131 (2016) 202-207.

[5]   K. Petritis, C. Elfakir, M. Dreux, A comparative study of commercial liquid chromatographic detectors for the analysis of underivatized amino acids, J. Chromatogr. A 961(1) (2002) 9-21.

[6]   J. Shaodong, W. Jun Lee, J. Won Ee, J. Hill Park, S. Won Kwon, J. Lee, Comparison of ultraviolet detection, evaporative light scattering detection and charged aerosol detection methods for liquid-chromatographic determination of anti-diabetic drugs, J. Pharm. Biomed. Anal. 51(4) (2010) 973-978.

[7]   K. Schilling, U. Holzgrabe, Recent applications of the Charged Aerosol Detector for liquid chromatography in drug quality control, J. Chromatogr. A 1619 (2020) 460911.

[8]   S. Furota, N. O. Ogawa, Y. Takano, T. Yoshimura, N. Ohkouchi, Quantitative analysis of underivatized amino acids in the sub- to several-nanomolar range by ion-pair HPLC using a corona-charged aerosol detector (HPLC–CAD), J. Chromatogr. B 1095 (2018) 191-197.

[9]   R. Pawellek, U. Holzgrabe, Influence of the mobile phase composition on hyphenated ultraviolet and charged aerosol detection for the impurity profiling of vigabatrin, J. Pharm. Biomed. Anal. 201 (2021) 114110.

[10]   Council of Europe, European Pharmacopeia, 10.5 edition, Monograph no. 2305 Vigabatrin, Strasbourg, France (2021).

[11]   A. C. McGinnis, E. C. Grubb, M. G. Bartlett, Systematic optimization of ion-pairing agents and hexafluoroisopropanol for enhanced electrospray ionization mass spectrometry of oligonucleotides, Rapid Commun. Mass Spectrom. 27(23) (2013) 2655-2664.

[12]   N. Li, N. M. El Zahar, J. G. Saad, E. R. E. van der Hage, M. G. Bartlett, Alkylamine ion-pairing reagents and the chromatographic separation of oligonucleotides, J. Chromatogr. A 1580 (2018) 110-119.

[13]   Z. Xie, Y. Jiang, D. Q. Zhang, Simple analysis of four bisphosphonates simultaneously by reverse phase liquid chromatography using n-amylamine as volatile ion-pairing agent, J. Chromatogr. A 1104 (2006) 173-178.

[14]   Z. Zeng, D. Yang, X. Huang, Z. Xiao, Effect of carbocisteine on patients with COPD: a systematic review and meta-analysis, Int. J. Chron. Obstruct. Pulmon. Dis. 12 (2017) 2277-2283.

[15]   Council of Europe, European Pharmacopeia, 10.5 edition, Monograph no. 0885 Carbocisteine, Strasbourg, France (2021).

[16] O. Wahl, U. Holzgrabe, Impurity profiling of carbocisteine by HPLC-CAD, qNMR and UV/vis spectroscopy, J. Pharm. Biomed. Anal. 95 (2014) 1-10.

[17] S. L. C. Ferreira, R. E. Bruns, E. G. Paranhos da Silva, W. N. L. dos Santos, C. M. Quintella, J. M. David, J. B. de Andrade, M. C. Breitkreitz, I. C. S. Fontes Jardim, B. B. Neto, Statistical designs and response surface techniques for the optimization of chromatographic systems, J. Chromatogr. A 1158(1–2) (2007) 2-14.

[18] D. Vaněrková, P. Jandera, J. Hrabica, Behaviour of sulphonated azodyes in ion-pairing reversed-phase high-performance liquid chromatography, J. Chromatogr. A 1143 (2007) 112-120.

[19] A. Fanigliulo, P. De Filippis, O. Curcuruto, P. Repeto, D. Roveda, M. Hartenstein, E. Adams, D. Cabooter, Development and validation of a stability indicating method for S-carboxymethyl-l-cysteine and related degradation products in oral syrup formulation, J. Pharm. Biomed. Anal. 115 (2015) 39-47.

[20] Council directive 2010/75/EU on industrial emissions (integrated pollution prevention and control) (Recast), Off. J. L334 (2010) 17.

[21] B. A. Bidlingmeyer, S. N. Deming, W. P. Price, B. Sachok, M. Petrusek, Retention mechanism for reversed-phase ion-pair liquid chromatography, J. Chromatogr. A 186 (1979) 419-434.

[22] P. H. Gamache, Charged aerosol detection for liquid chromatography and related separation techniques, 1st edition, John Wiley & Sons, Hoboken, New Jersey, USA (2017).

[23] J. L. Dores-Sousa, J. De Vos, W. T. Kok, S. Eeltink, Probing selectivity of mixed-mode reversed-phase/weak-anion-exchange liquid chromatography to advance method development, J. Chromatogr. A 1570 (2018) 75-81.

[24] C. R. Mallet, Z. Lu, J. R. Mazzeo, A study of ion suppression effects in electrospray ionization from mobile phase additives and solid-phase extracts, Rapid Commun. Mass Spectrom. 18 (1) (2004) 49-58.

[25] S. Khodadoust, M. Ghaedi, Optimization of dispersive liquid–liquid microextraction with central composite design for preconcentration of chlordiazepoxide drug and its determination by HPLC-UV, J. Sep. Sci. 36(11) (2013) 1734-1742.

[26] G. Derringer, R. Suich, Simultaneous optimization of several response variables, J. Qual. Technol. 12(4) (1980) 214-219.

[27] K. Zhang, L. Dai, N. P. Chetwyn, Simultaneous determination of positive and negative pharmaceutical counterions using mixed-mode chromatography coupled with charged-aerosol detector, J. Chromatogr. A 1217(37) (2010) 5776-5784.

[28] T. H. Walter, M. M. T. Blaze, C. Boissel, Electrospray ionization mass spectrometry ion suppression/enhancement caused by column bleed for three mixed-mode reversed-phase/anion-exchange high-performance liquid chromatography columns, Rapid Commun. Mass Spectrom. 35(12) (2021).

[29] International Council for Harmonisation of Technical Requirements for Pharmaceuticals for Human Use, Guideline Q2 (R1) Validation of Analytical Procedures (2005).

3.2. Identification of low-level impurities in drug prototypes of carbocisteine by means of liquid chromatography-high-resolution mass spectrometry and general unknown comparative screening
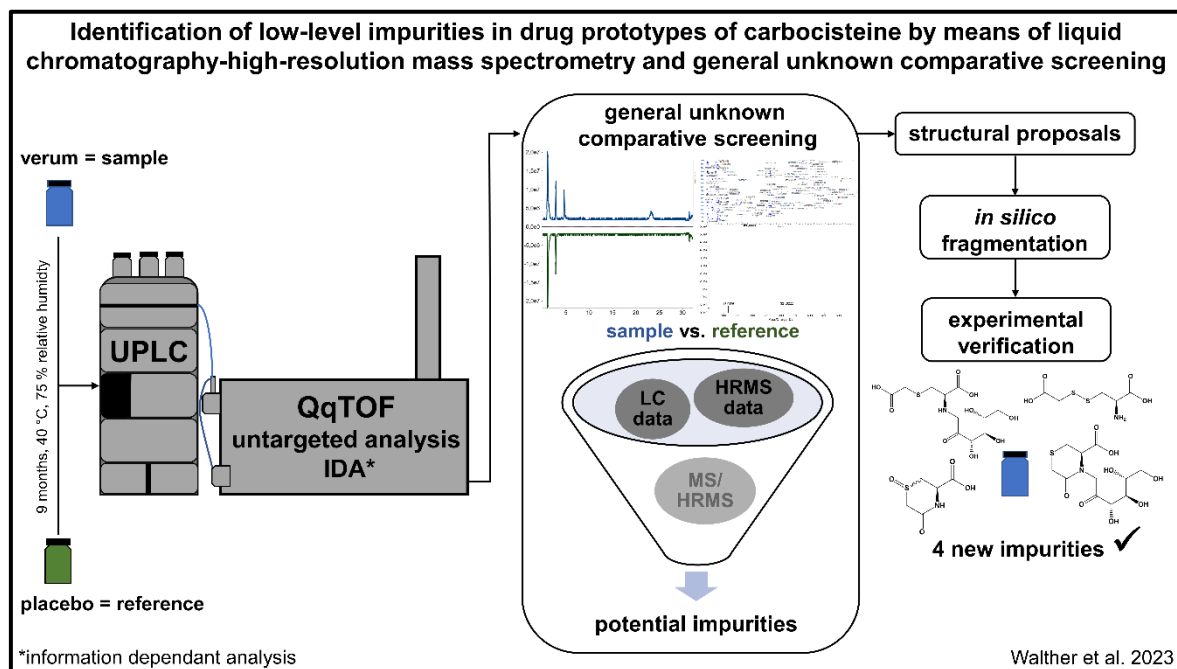
Rasmus Walther, Martina Kinzig, Annette Zamponi, Fritz Sörgel, Oliver Scherf-Clavel, Ulrike Holzgrabe

Abstract

High-resolution tandem quadrupole time-of-flight mass analysers enable new automated workflows for untargeted data evaluation of complex samples like drug products. An example of such procedure is the so-called general unknown comparative screening (GUCS), which is used for software-assisted, automated identification of components that are only present in a sample and not in a reference. We have used this approach to characterize two different carbocisteine containing syrup prototypes – one with sucrose and the other with artificial sweeteners – by comparison with the corresponding placebo samples after nine months of storage at 40 °C and 75 % relative humidity. The samples were analysed chromatographically using a Coresep SB mixed-mode column and high-resolution MS and MS/MS data were recorded in information dependent acquisition mode on a Sciex X500R quadrupole time-of-flight mass spectrometer. With the GUCS approach two hitherto unknown degradation products of carbocisteine, i.e. the carbocisteine lactam of the sulfoxides and the disulfide between *L*-cysteine and thioglycolic acid, were detected at low concentrations in both of the syrup formulations. The presumed structures were confirmed by *in silico* analysis of the fragment spectra and high-resolution LC-MS experiments with reference substances. Two additional impurities were found in the sucrose-containing sample and identified as the *N*-glycosides of carbocisteine and its lactam, respectively, using binary mixtures with a ^{13}C-labelled monosaccharide.

Graphical abstract

Identification of low-level impurities in drug prototypes of carbocisteine by means of liquid chromatography-high-resolution mass spectrometry and general unknown comparative screening

*information dependant analysis

Walther et al. 2023

1. Introduction

Recent improvements in modern mass spectrometers, such as achieving mass resolving powers of more than 10,000 (10 % valley definition) and rapid data acquisition cycles, enable the implementation of untargeted workflows for high-resolution mass spectrometry (HRMS) [1-3]. If one has no or only limited information about a sample, systematic and comprehensive characterization with an untargeted MS/MS method such as *MS/MS[ALL]*, *information dependent acquisition* (IDA), *global precursor ion scan* or *sequential window acquisition of all theoretical fragments* (SWATH) is still possible [1,4-6]. Especially in the "omics" field with its complex samples and vast amount of data, these approaches – in combination with proper statistical analysis – have become indispensable [3,6,7].

Considering the high costs, the time-consuming data evaluation and the necessity of highly qualified personnel, the usage of such sophisticated instruments and analytical methods in the field of quality control of active pharmaceutical ingredients (API) or medicinal products appears exaggerated at first glance. However, if new unknown peaks occur during the life cycle of a drug, e.g. due to a change in manufacturing or a change of supplier, the "classic" approach of targeted isolation and subsequent characterisation by NMR spectroscopy must then be applied in addition to HRMS measurements [8,9]. Although this procedure is equally costly, it does not provide a comprehensive characterisation of the sample as with an untargeted approach. However, as this type of analysis generates large amounts of data (multiple MS or MS/MS experiments are recorded every second of the chromatographic run), automated workflows such as the *general unknown comparative screening* (GUCS) are required for efficient evaluation.

The GUCS workflow comprises an automatic comparison of all chromatographic and mass spectrometric features of an unknown sample with a "gold standard" reference. As a result, differences between sample and reference above a predefined threshold, are displayed in a neat peak list for further evaluation. Using IDA and SWATH as untargeted acquisition modes, samples of sartan drugs containing carcinogenic nitrosamines could be clearly distinguished from tablets free of these impurities [10]. In IDA mode, unlike the unbiased SWATH technique, only the most abundant signals per cycle are selected for fragmentation, which improves the quality of the corresponding MS/MS spectra and facilitates structural elucidation of unknown impurities [3,11]. In addition to a targeted identification of 18 known impurities as well as potential impurities derived from a reaction matrix, this acquisition mode in combination with GUCS was employed for impurity profiling of the API bisoprolol using a blank sample as a reference, resulting in the identification of 17 new additional impurities [12].

Both examples demonstrate the possibilities of untargeted HRMS approaches in quality control/impurity profiling. In this work, we have transferred the concept of GUCS for the identification of unknown degradation products (DP) to a drug product using the identical placebo formulation as reference. According to ICH guideline Q3B, stability studies must be carried out not only for the drug substance but also for the drug products, as the full degradation profile includes both the DPs of the API and reaction products (RP) with excipients or the primary packaging material [13]. As an example for this, two different syrup prototype formulations of the expectorant carbocisteine (CC) with various excipients were subjected to untargeted HRMS analysis after nine months of storage at 40 °C and 75 % relative humidity. The GUCS workflow should then allow the straightforward elaboration of plausible structural proposals for unknown DPs and RPs based on accurate masses, isotopic patterns, and fragment spectra.

2. Materials and methods

2.1 Chemicals and reagents

MS grade formic acid 99 % (m/m) and ammonia solution 25 % (m/m) were bought from VWR International (Darmstadt, Germany). Ultrapure water and acetonitrile for MS as well as *D*-fructose (≥ 99 % GC), *D*-glucose (≥ 99.5 % GC) and *D*-glucose-1,6-^{13}C$_2$ (99 atom % ^{13}C) were purchased from Sigma-Aldrich (Steinheim, Germany). Chemical reference standards of CC, the diastereomeric carbocisteine sulfoxides (SO) and carbocisteine lactam (LA) were obtained from the EDQM (Strasbourg, France). Reference standards of *S*-((carboxymethyl)thio)-*L*-cysteine (disulfide from cysteine and thioglycolic acid: CysTGA; 99.7 % HPLC) and 5-oxothiomorpholine-3-carboxylic acid 1-oxide (lactam of the carbocisteine sulfoxide: LASO; *S,S* and *R,R* enantiomers, 98.5 % HPLC) were purchased from TLC Pharmaceutical Standards (Newmarket, Ontario, Canada).

2.2 Solutions and sample preparation

2.2.1 Reference solutions

Stock solutions (1.0 mg/mL) of CC, SO and LA were prepared by separately weighing 10.0 mg and dissolving ad 10.0 mL of mobile phase A (60/40 v/v ammonium formate buffer pH 2.9 and acetonitrile, see section 2.3.2). For the optimization of the MS source parameters, each stock solution was diluted with the same solvent 1:100 to obtain a concentration of 10 µg/mL. In addition, a mix containing all analytes at a concentration of 100 µg/mL was prepared from the stock solutions by dilution with water. Starting from 1.0 mg/mL CysTGA or LASO stock solution in water, a 10 µg/mL dilution was prepared for both analytes as well as a reference mix with CC (all 10 µg/mL). Aqueous dilutions (1 mg/mL) of all monosaccharides used in the binary mixtures (see section 2.2.3) were prepared from the corresponding stock solutions and used to record reference MS spectra. All stock solutions were stored at -20 °C. Working standard solutions were prepared freshly on the day of analysis.

2.2.2 Syrup samples

A sugar-containing and a sugar-free verum (50 mg/mL CC) and placebo prototype formulation stored for 9 months at 40 °C and 75 % relative humidity in sealed, amber glass bottles were kindly provided by A. Nattermann & Cie. – a Sanofi Company (Köln, Germany). The sugar-containing syrup consisted of 67 % sucrose solution, methyl 4-hydroxybenzoate, caramel flavour, alcoholic aromatic elixir, cinnamon oil and water pH 6.2 and the sugar-free syrup consisted of glycerol, sodium saccharin, sodium methylparaben, caramel/vanilla flavouring elixir and water pH 6.2. 2.0 mL of the two different verum (50 mg/mL) and corresponding placebo formulations were diluted with approx. 80 mL of water and stirred for 2 h before making up to 100.0 mL. From each 1 mg/mL dilution, 3 aliquots were filled into vials and stored in the autosampler at 8 °C until analysis (total samples: 12).

2.2.3 Binary mixtures

The pH value of the aqueous stock solutions of CC (4 mg/mL) was adjusted to 6.2 with ammonia (25 %) before mixing them with the stock solutions (4 mg/mL each) of fructose, glucose or the $^{13}C_2$-labelled glucose in a 1:1 ratio. The resulting three mixtures were then diluted 1:2 with water to obtain a concentration of 1.0 mg/mL and stored at a controlled temperature. These binary mixtures were first stored at 40 °C for a period of 5 weeks, with an aliquot being taken weekly, followed by additional stressing at 60 °C for 2 weeks.

2.3 LC-HRMS experiments

2.3.1 Instrumentation

For chromatographic separation a 2.1 x 100 mm Coresep SB mixed-mode column with 2.7 µm and 90 Å core shell particles (HelixChrom, Prospect Heights IL, USA) was connected to an Agilent Infinity II system (Waldbronn, Germany), consisting of a quaternary pump, a degasser, a thermostatted autosampler and a thermostatted column compartment. The UPLC system was coupled to a Sciex X500R quadrupole time-of-flight (QqTOF) mass spectrometer equipped with a Turbo V™ Ion Source with electrospray ionisation (ESI) interface. For control of the instrument and data evaluation Sciex OS 2.1 software was used (Concord, Ontario, Canada).

2.3.2 Chromatographic procedure

Mobile phase A consisted of a mixture of buffer solution containing 20 mM formic acid in water with pH adjusted to 2.9 and acetonitrile in the ratio 60/40 v/v. The pH of the aqueous portion was adjusted with ammonia (25 %) prior to the addition of acetonitrile. Mobile phase B was a solution of 20 mM formic acid in acetonitrile. The elution was carried out isocratically with 100 % mobile phase A for 30 min at a flow rate of 0.2 mL/min and a column temperature of 35 °C. The percentage of mobile phase B was then increased to 75 % and a flow rate of 0.3 mL/min within 1 min to flush the column for 10 min. The column was re-equilibrated using the initial condition for 10 min prior to the next injection (total run time: 53 min). The injection volume of the syrup samples was set to 2.0 µL.

2.3.3 GUCS experiments

To optimise source parameters for MS and MS/MS experiments, flow injection analysis (FIA) with 10 µg/mL solutions of CC, SO or LA were performed. Therefore, 10 µL of each solution were injected separately at a flow rate of 0.2 or 0.3 mL/min and a run time of 1 min. Changing one factor at a time, settings for both positive and negative mode were adjusted as shown in Table 1.

The samples were then analysed (n = 3) in IDA mode using both ionization modes with these optimised settings. The sequence of verum and placebo samples with or without sucrose was randomized and a blank run (10 µL mobile phase A) was performed after every four injections, followed by automatic calibration of the QqTOF mass spectrometer using the provided tuning mixes for positive or negative ion mode, respectively (Sciex, Concord, Ontario, Canada). Due to the periodic automatic mass calibration, a mass error of less than 5 ppm over the entire mass range was maintained for all measurements. For data evaluation, the GUCS workflow as part of Sciex OS 2.1 software was employed for untargeted peak finding. For this purpose, each verum sample was compared with all three corresponding placebo samples in an automated process and peaks with an area ratio of 100 (verum/placebo) were selected for further analysis.

Table 1
Settings for the time-of-flight (TOF) MS and TOF
MS/MS experiments using the information
dependent acquisition (IDA) mode for ESI in
positive and negative ion mode

Parameter	ESI	
	Positive	Negative
Polarity	+	-
Gas 1	50 psi	
Gas 2	50 psi	
Curtain Gas	20 psi	
CAD gas	7 psi	
Temperature	325 °C	300 °C
Spray voltage	+5500 V	-4500 V
Declustering potential (DP)	+40 V	-40 V
DP spread	5 V	0 V
Mass range	50 – 550 Da	
TOF MS		
Accumulation time (s)	0.25 s	
Collision energy (V)	+10 V	-10 V
Spread (V)	+0 V	0 V
TOF MS/MS: IDA		
Accumulation time (s)	0.1 s	
Collision energy (CE)	+15 V	-10 V
CE spread	5 V	0 V
Max. candidate ions	10	
Intensity threshold	10 cps	
Dynamic background subtraction	true	

2.3.4 Data evaluation and confirmation of impurities

For the hits from the GUCS, sum formulae based on the exact mass (mass error < 5 ppm), ring-double bond equivalents (RDB), isotope pattern (intensity tolerance < 20 %) and known fragments from the analysis of CC, SO and LA were used to develop molecular formulae. To confirm the structures of these presumed impurities, the software´s *in silico* fragmentation tool was used in a first step. Subsequently, the corresponding commercially available substances were analysed regarding their retention times (RT) and MS/MS spectra and compared with the data from the IDA experiments. For commercially unavailable impurities, binary mixtures (see section 2.2.3) were analysed by means of LC-HRMS. To obtain further information about the structures, additional experiments were performed with ^{13}C-labelled monosaccharides, in some cases using an increased injection volume (up to 10 µL).

3. Results and Discussion

3.1 Initial experiments

In our previous work, we developed and validated an LC method coupled with the charged aerosol detector to separate the zwitterionic, highly polar CC and its two main DPs (see Fig. 1) [14]. The reversed-phase/strong-anion exchange mixed-mode column employed in this study is also applicable for ESI, and chromatographic method development was therefore straightforward. A Coresep SB UPLC column with the same chemistry (quaternary ammonium groups embedded into a C_{18} chain) but smaller dimensions was selected to achieve an improved ionization efficiency due to a lower flow rate [15]. Another crucial adjustment compared to the original method was the omission of trifluoroacetic acid (TFA), as this strongly suppresses ionization [16]. Originally, the addition of the highly chaotropic TFA made it possible to shorten the run time to less than 10 min. To replace TFA, 20 mM formic acid adjusted with ammonia to a pH of 2.9 was used to elute the analytes from the strong anion-exchange groups. Furthermore, the acetonitrile percentage was increased to 40 % (v/v).
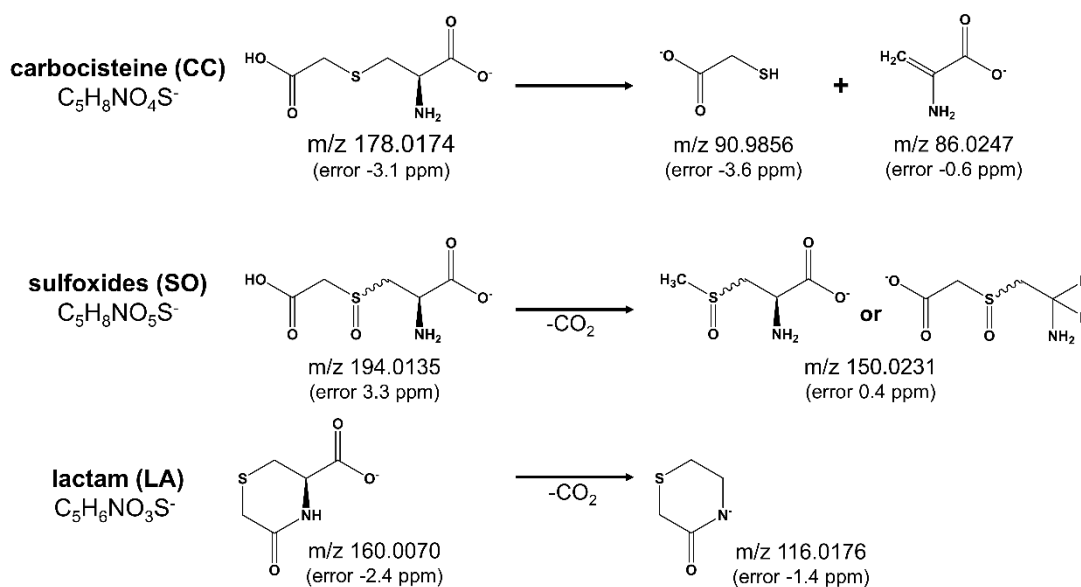

Fig. 1 Structures of the reference substances carbocisteine (CC), carbocisteine sulfoxide diastereomers (SO) and carbocisteine lactam (LA) and their main fragments using the optimised MS settings from Table 1 in the negative ion mode (sum formulae and exact masses of the [M-H]⁻ species)

During FIA for MS parameter optimization, pronounced fragmentation was observed for CC and SO (LA to a lesser extent) even at moderate conditions in negative ion mode, presumably as a result of in-source fragmentation and/or collision induced dissociation [17,18].

With the final settings in Table 1 and a reduced flow rate of 0.2 mL/min, a compromise between sufficient ionisation intensity and moderate fragmentation (e.g. low declustering potential required to minimize decarboxylation) was made. Using the positive ion mode, fragmentation during ionisation/ion transport was less critical.

Subsequently, the MS/MS settings were adjusted so that the signal of the precursor ion was still visible in the fragment spectrum (approx.100 counts per second). In the negative ion mode, a low collision energy (and spread of 0 V) had to be set for the fragmentation experiments because decarboxylation readily occurred for SO and LA. For CC, this played only a minor role and cleavage of the thioether was the main degradation pathway (see Fig. 1 and Fig. S1). In the positive mode (higher collision energy and spread), considerably more complex fragment spectra were obtained due to neutral losses of ammonia, water and/or CO (see Fig. S2-S4). Since the signal intensities were higher in negative ion mode, these data were primarily used to interpret the MS and MS/MS spectra of the unknown impurities.

Finally, before the analysis of the syrup samples a cleaning gradient was tested following the isocratic elution of the analytes to avoid carry-over. As the pressure was only about 130 bar, an increased flow rate of 0.3 mL/min could be used for this part to save time. Since the LA peak eluted after approx. 22 – 23 min, the isocratic part was set to 30 min including a surcharge of 25 % for more strongly retained impurities. After triple injection of a syrup sample applying the cleaning gradient, no components were recovered in the subsequent blank run. Furthermore, a blank run was carried out after every four injections in the sample sequence, confirming that there was no carry-over.

3.2 Results of the GUCS workflow

Following the randomized measurement of the two syrup samples, the data recorded in IDA mode were analysed using GUCS. For this purpose, the sucrose-containing and the sugar-free verum samples were each compared with the corresponding placebo references. As a result, a list is obtained that summarizes all peaks that only occur in the verum samples (peak area ratio > 100) and thus originate from the API. Part of this peak list were, of course, the signals for CC and its two main DPs, as well as the main fragments known from the preliminary experiments (vide supra) that are formed during ionization.

In both negative and positive ion mode, three peaks of unknown DPs were found in both syrup formulations with RTs of 5.84 min (DP1), 11.2 min (DP2.1) and 12.8 min (DP2.2), with the two posterior peaks having the same mass-to-charge ratio (m/z) of 176.0022 for the [M-H]⁻ species and 178.0171 for the [M+H]⁺ species, respectively. Fig. 2a and 2b show the extracted ion chromatograms (XIC) of these DPs compared with the respective placebo samples using the negative mode. For DP1, the peak area was comparable in both syrup formulations, whereas in the case of DP2, less was formed in the sugar-free syrup. Only in the sucrose-containing syrup, were two additional peaks at 4.12 min and 8.26 min detected with m/z above 300 (see Fig 2c and 2d). Since these signals are not present in the sugar-free formulation, they are probably RPs with excipients unique to the sucrose-containing syrup formulation.
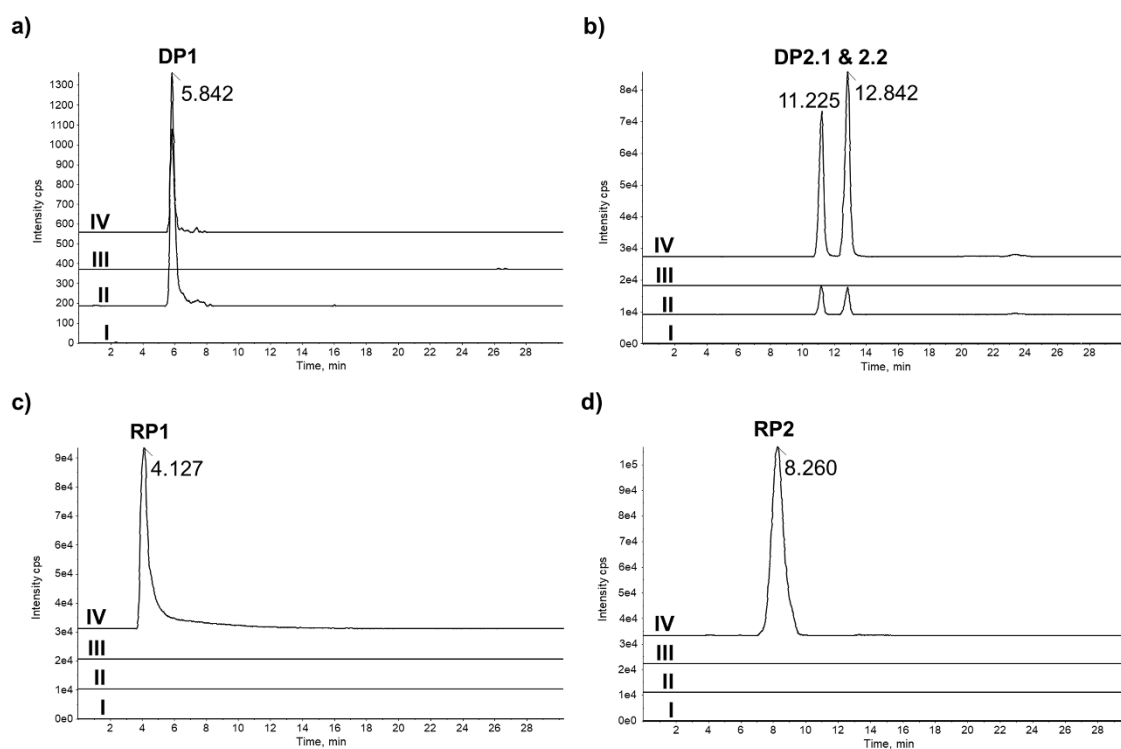

Fig. 2 Overlay of the extracted ion chromatograms [M-H]⁻ of the unknown impurities identified *via* GUCS in the two different syrup formulations (I: placebo sugar-free, II: verum sugar-free, III: placebo sucrose-containing, IV: verum sucrose-containing) for the degradation products DP1 (a) and DP2 (b) as well as the reaction products RP1 (c) and RP2 (d)

Using the positive ion mode, only a small signal was obtained for the second peak of RP2 and instead a signal reduced by - 18.0106 Da was detectable over the same period (see Fig. S5). This was attributed to neutral loss of water leading to a positively charged molecular ion of $[M-H_2O+H]^+$.

3.3 Development of structural proposals

As a first step towards structural elucidation, sum formulae were developed based on the exact masses, the isotope pattern, and logical restrictions (e.g., presence of at least one sulfur atom or the degree of unsaturation), which are summarized in Table 2 with the corresponding errors [2,19]. For these sum formulae, potential structures were developed considering their MS/MS spectra as well as the known fragmentation pathways of CC, SO and LA references. A tabular summary of the main fragments of the unknown impurities is available in the supplementary information (see Table S1-S6).

Table 2
Summary of the most probable sum formulae of the unknown impurities identified *via* GUCS in the two carbocisteine (CC) syrup prototype formulations

rRT[a] (relative to CC)	Peak	Molecular ion	m/z[b]	Sum formula	Error (ppm)	RDB[c]
1.26	DP1	[M-H]⁻	209.9901	$C_5H_8NO_4S_2$	0.4	2.0
		[M+H]⁺	212.0044	$C_5H_{10}NO_4S_2$	-0.8	2.0
2.42	DP2.1	[M-H]⁻	176.0022	$C_5H_6NO_4S$	-0.6	3.0
2.77	DP2.2	[M+H]⁺	178.0171	$C_5H_8NO_4S$	1.4	3.0
0.88	RP1	[M-H]⁻	340.0696	$C_{11}H_{18}NO_9S$	-3.5	3.0
		[M+H]⁺	342.0855	$C_{11}H_{20}NO_9S$	0.5	3.0
1.78	RP2	[M-H]⁻	322.0596	$C_{11}H_{16}NO_8S$	-1.9	4.0
		[M+H]⁺	324.0738	$C_{11}H_{18}NO_8S$	-3.0	4.0

[a] relative retention time
[b] mass-to-charge ratio
[c] ring double bond equivalent

3.3.1 Structural elucidation of the unknown DPs present in both syrup formulations

The proposed sum formula of DP1 differs from CC ($C_5H_9NO_4S$) only by an additional sulfur atom. The two main fragments with an m/z of 120.0124 and 88.9702 correspond to cysteine and thioglycolic acid in negative ion mode (see Fig. 3a). Thus, the precursor ion could be the respective disulfide. The fragmentation pattern in positive ionization mode was more complicated, but similar to CC (see Fig. S2), neutral losses of ammonia or water and CO were the causes of the main fragments besides the cleavage of the disulfide (see Fig. 3b). Applying the *in silico* fragmentation tool included in the Sciex OS software (considering fragments up to 1 % of the max. intensity) to check the plausibility of the proposed structure, CysTGA *in silico* fragmentation explained more than 98 % of the total intensity in both ion modes (see Fig. S6).

Compared to the diastereomeric pair of the SO, the molecular ions of DP2.1 and DP2.2 are reduced by H_2O, which could be explained by an intramolecular cyclisation of SO yielding the lactam of the sulfoxides (LASO). Like in the MS/MS fragment spectra of the LA reference, the main fragment of LASO is formed by either decarboxylation (negative ion mode, see Fig. 3c) or neutral loss of water and carbon monoxide (positive ion mode, see Fig. 3d). The check of the *in silico* fragmentation (considering fragments up to 1 % of the max. intensity) with the LASO structure even resulted in a value of 100 % in the negative ion mode and 94.9 % in the positive ion mode (see Fig. S7). To unambiguously verify these two hitherto unknown DPs of CC, LC-HRMS measurements were performed with both reference substances regarding their chromatographic behaviour and MS fingerprint (see section 3.4).
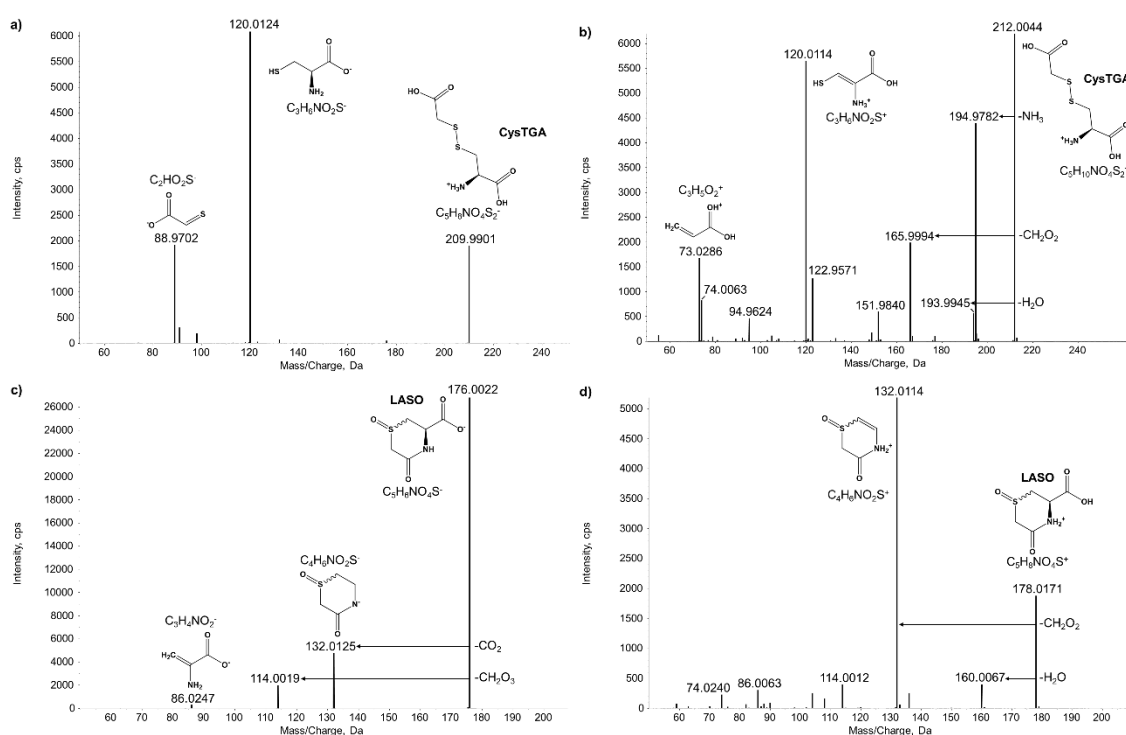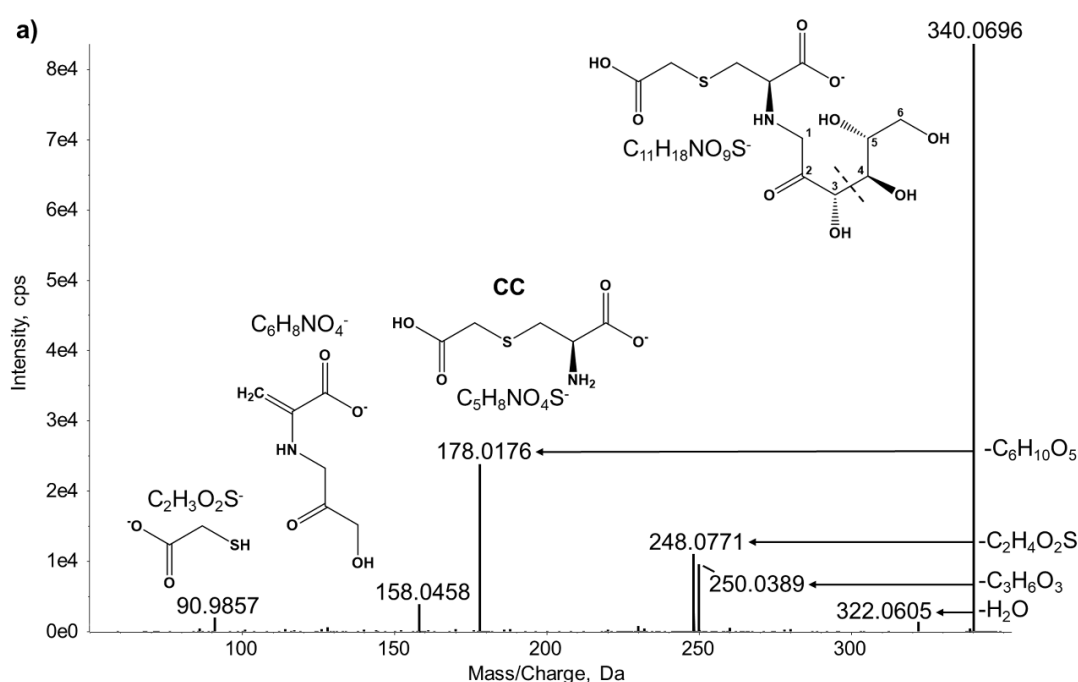

Fig. 3 MS/MS line spectra of the unknown degradation products 1 (a/b) and 2 (c/d) with proposed structures using negative (a/c) or positive (b/d) electrospray ionization

3.3.2 Structural elucidation of the RPs formed only in the sucrose-containing syrup

Six characteristic fragments were visible in the MS/MS spectra of each of the two RPs (see Fig. 4). In the fragment spectra of RP1 and RP2, signals corresponding to CC (m/z = 178.0176) or LA (m/z = 160.0073) precursor ion and their respective fragments (CC: thioglycolic acid; LA: decarboxylation) were assignable (cf. Fig. 1). The occurrence of those signals could be attributed to a neutral loss of $C_6H_{10}O_5$, which is equivalent to a bound monosaccharide. Moreover, the fragments with m/z of 250.0389 and 232.0284 for RP1 and RP2, respectively, can be explained by splitting off "half the sugar chain" ($C_3H_6O_3$) of a hexose. This is a known fragmentation reaction of *N*-glycosides in negative ion mode as a kind of retro aldol reaction between C3-C4 (see Fig. 4) [20]. Likewise, the already described elimination of water in the sugar chain as a neutral loss could be observed for both RPs (m/z = 322.0605 for RP1 in Fig. 4a and m/z = 304.0499 for RP2 in Fig. 4b). As an explanation for the formation of the two remaining fragments of RP1 in Fig. 4a, in the case of the fragment with an m/z of 248.0771, the cleavage of thioglycolic acid is plausible, and for the fragment with m/z = 158.0458, additionally the cleavage of $C_3H_6O_3$.

The two fragments of RP2 in Fig. 4b with m/z of 188.0385 and 186.0231 differ formally by only 2 protons and were formed by the neutral loss of structures containing four C atoms (proposals are given in section 3.5). When using the positive ion mode, more fragments were formed (see Fig. S8-S9), with mainly dehydration reactions taking place (see Table S5-S6), as described in the literature for *N*-glycosides of amino acids with monosaccharides [21,22].
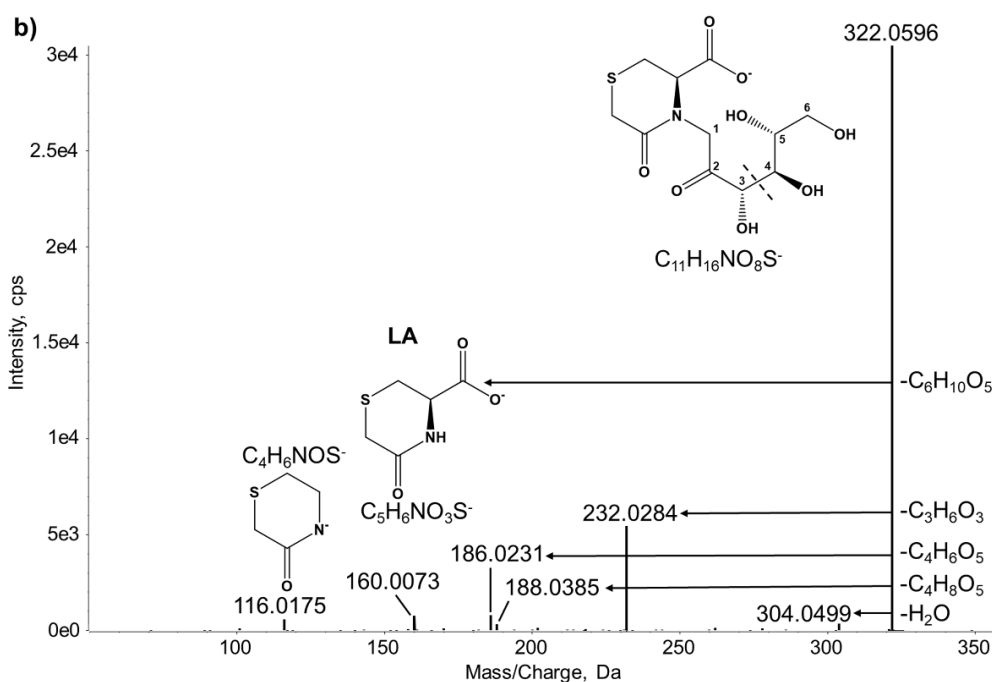
Fig. 4 MS/MS line spectra of the unknown reaction products 1 (a) and 2 (b) with proposed structures of the *N*-glycosides (as Amadori products with *D*-glucose), their main fragments and sum formulae of the corresponding neutral losses using the negative ion mode

The Maillard reaction between a primary amine and a reducing sugar is a well-known reaction and has been observed for lactose and various APIs like hydrochlorothiazide, memantine or gabapentin in tablets or capsules [21,23,24]. In sucrose, however, the two reducing sugars glucose and fructose are linked by an 1,2-β-glycosidic bond, so that a non-reducing disaccharide is formed and no reaction with CC is possible. Apparently, hydrolysis took place here in the aqueous syrup samples over the course of the 9 months at an elevated temperature of 40 °C [25,26]. Since small quantities of these two reducing monosaccharides can occur as impurities of the starting material, special attention should also be paid regarding the quality of this excipient [27]. In a reaction between CC and glucose, a "Schiff base" is formed in the first step with release of water, which is converted into a stable ketosamine as a tautomer by the Amadori rearrangement (see Fig. 5a) [20,21]. According to Xing and Yaylayan the presence of the corresponding C3-C4 retro aldol product is an indicator for the formation of the Amadori product [20]. In the case of fructose, the fructosylamine is formed first, which is converted into the stable Heyns product (aldosamine) (see Fig. 5b) [22,28]. The analogous reaction of LA does not seem chemically plausible because the nitrogen incorporated in the amide does not possess nucleophilic properties. After rearrangement to CC-ketos/aldosamines, cyclization to the corresponding lactam can occur.
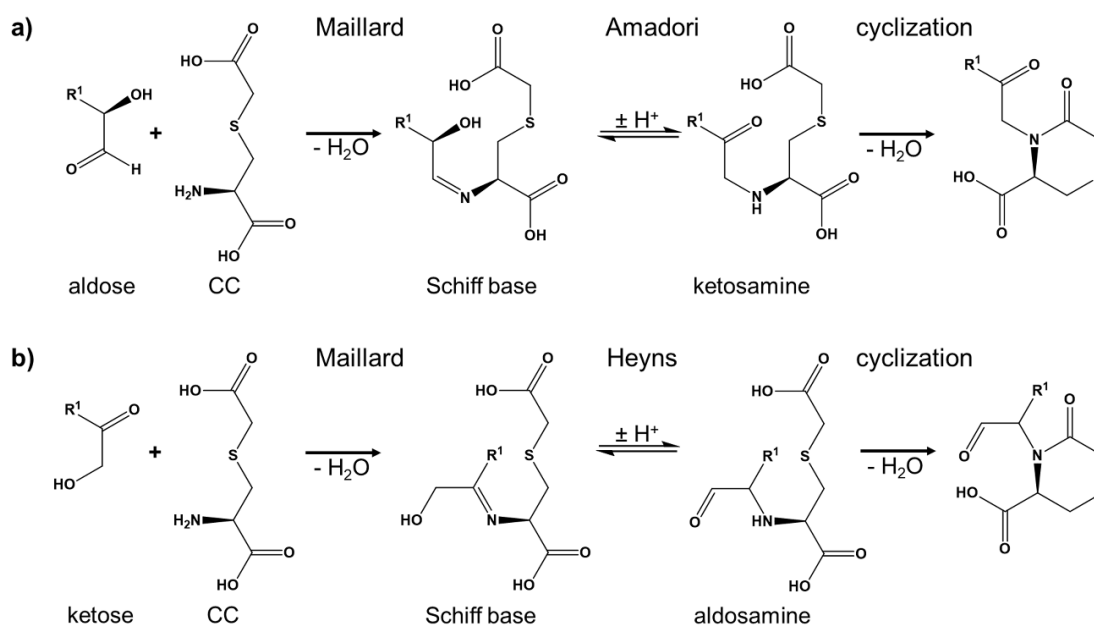
Fig. 5 Schematic illustration of the reaction between carbocisteine (CC) and an aldose (a) or ketose (b) to the Schiff base with subsequent rearrangement and cyclization with loss of water to give lactam *N*-glycosides; (note: for an easier overview, the sugars were drawn in their open-chain form although there is an equilibrium of the several cyclic isomers/anomers in aqueous solution)

Using the *in silico* fragmentation tool, all fragments formed in the negative mode can be explained for both the Amadori products of glucose and the Heyns products of fructose with CC and LA, respectively (see Fig. S10). Neither chromatographically nor under the MS conditions chosen here is it possible to distinguish between the RPs with glucose or fructose, but presumably both react with the primary amino group of CC. However, the assignment of the large number of fragments formed in positive mode seems to overexert the capabilities of the software algorithm (plausibility < 90 %, see Fig. S11). In the MS/MS spectra of both RPs, the program is not able to find possible structures for the relatively intense fragments with a m/z of 258.0518 with 6 RDBs or 270.0435 with 7 RDBs of RP1 and RP2, respectively. A possible explanation for these signals is the formation of aromatic pyrylium *N*-glycosides with a positively charged oxygen atom (see Fig. S8-S9) [22]. Since no reference substances were commercially available, binary mixtures of CC with glucose, a ^{13}C-labelled derivative and fructose were stored at elevated temperature to prove the postulated formation of *N*-glycosides (see section 3.5).

3.4 Reference measurements of the DPs CysTGA and LASO

Both the absolute and relative RTs of the two references CysTGA (rRT = 1.17) and LASO (rRT = 2.65) were slightly shifted compared to the peaks of these DPs in the verum samples, probably due to the wear of the mixed-mode column (see Fig. S12). For a final assessment, the fragment spectra of the references were compared to the MS/MS spectra of the DPs recorded in the IDA experiments and showed complete congruity for all fragments (see Fig. 6). Due to the better ionization efficiency, the positive ion mode was used for CysTGA and the negative ion mode for LASO.
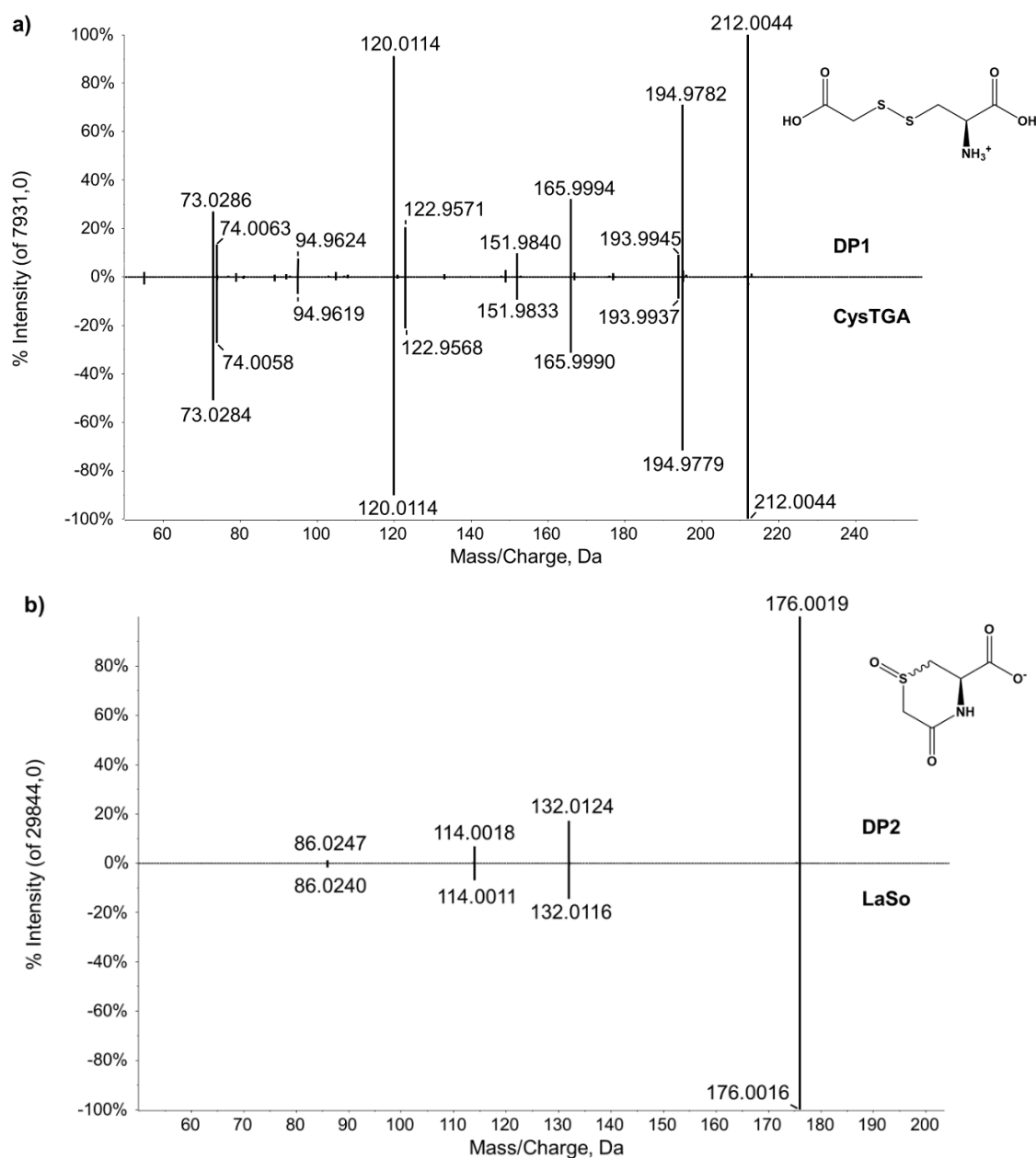

Fig. 6 Comparison of the MS/MS fragment spectra recorded with the syrup samples and the reference substances for a) the unknown degradation product 1 (DP) vs. CysTGA in the positive ion mode and b) the unknown DP2 vs. LASO in the negative ion mode

Based on the comparable chromatographic RTs and especially the matching MS/MS fingerprints, the postulated structural proposals of the two unknown DPs were confirmed with high confidence. The formation of LASO can be plausibly explained chemically in two ways: 1) starting from SO by intramolecular cyclization or 2) starting from LA by oxidation. The CysTGA disulfide could be formed by an asymmetric reaction of L-cystine with chloroacetic acid as a by-product of the synthesis (see Fig. 8) [29].

3.5 Analysis of binary mixtures (N-glycosides)

First, reference solutions of the monosaccharides used in the binary mixtures were analysed to get a better insight into their fragmentation. As expected, these very polar molecules showed no interaction with the mixed-mode stationary phase and all eluted at about 1.1 min. Under the selected MS conditions, no distinct discrimination between fructose and glucose was possible based on the MS/MS pattern (see Fig. S13) and for both sugars the main fragment was formed by symmetrical cleavage between C3 and C4 of each hexose as it was observed for the two RPs.

After five weeks at 40 °C, the amount of the two RPs formed was very low and the samples were therefore stressed again at 60 °C for two weeks. Although no change of colour of the solution was noticed upon visual inspection, a variety of signals appeared in the total ion chromatogram of the binary mixtures. Therefore, harsher conditions were intentionally not chosen to avoid the formation of more complex (yellow/brown) Maillard products [30]. By increasing the injection volume to 10 µL and focusing on the negative ion mode (considerably better ionisation efficiency for the respective RPs), conclusive MS/MS spectra could be recorded for verification of the postulated N-glycoside structures (see section 3.3.2). The resulting XICs of the binary mixtures with glucose, $^{13}C_2$-1,6-glucose, and fructose showed matching peaks with both RPs, although the intensity of the signals in the mix with fructose was significantly lower than with glucose (see Fig. S14). This is probably due to a slower reaction speed of the ketose [31,32]. The peak area of RP2, the lactam of the N-glycoside, was considerably smaller (> 10-fold) than that of RP1, supporting the hypothesis of downstream formation of RP2 by cyclization of RP1. A targeted search for the hypothetical RP with SO ($C_{11}H_{19}NO_{10}S$) in the syrup sample did not reveal any additional peak (both ion modes). Considering the significantly slower rate of formation of SO compared to LA, this is probably a matter of time until a detectable amount has been formed [33].

The direct comparison of the MS/MS pattern isolated from the syrup samples and from the binary mixture, respectively, showed complete congruity for all the main fragments (see Fig. S15). Fig. 7 shows the fragment line spectra for RP1 and RP2 isolated from the mixture with the ^{13}C-labelled glucose. The proposed structures of the fragments were developed using the data summarized in Table 3.

Table 3
Summary of the data of the fragment spectra of the two reaction products (RP) from the mixture with the [13]C$_2$-labelled glucose in the negative ion mode
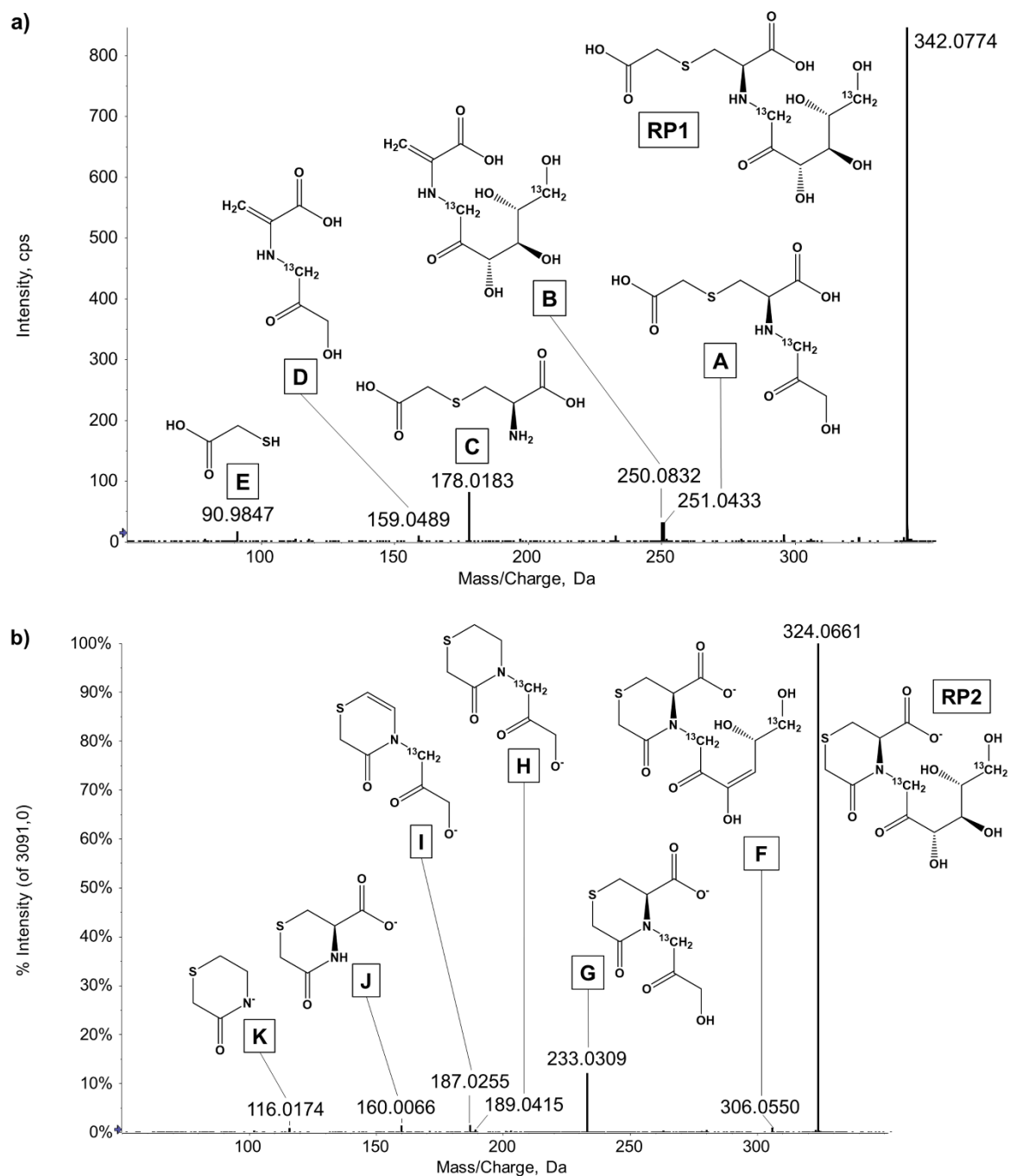
	m/z[a]	sum formulae	error (ppm)	RDB[b]	loss
RP1 [M-H]⁻					
Precursor	342.0774	$^{13}C_2C_9H_{18}NO_9S^-$	-0.3	3.0	n.a.[c]
Fragment A	251.0434	$^{13}CC_7H_{12}NO_6S^-$	3.8	3.0	$^{13}CC_2H_6O_3$
Fragment B	250.0832	$^{13}C_2C_7H_{14}NO_7^-$	-4.3	3.0	$C_2H_4O_2S$
Fragment C	178.0183	$C_5H_8NO_4S^-$	2.0	2.0	$^{13}C_2C_4H_{10}O_5$
Fragment D	159.0489	$^{13}CC_5H_8NO^-_4$	-2.1	3.0	$^{13}CC_4H_{10}O_5S$
Fragment E	98.9859	$C_2H_3O_2S^-$	-0.3	1.0	$^{13}C_2C_7H_{15}NO_7$
RP2 [M-H]⁻					
Precursor	324.0661	$^{13}C_2C_9H_{16}NO_8S^-$	-2.5	4.0	n.a. [c]
Fragment F	306.0550	$^3C_2C_9H_{14}NO_7S^-$	-4.4	5.0	H_2O
Fragment G	233.0309	$^{13}CC_7H_{10}NO_5S^-$	-4.2	4.0	$^{13}CC_2H_6O_3$
Fragment H	189.0415	$^{13}CC_6H_{10}NO_3S^-$	-2.9	3.0	$^{13}CC_3H_6O_5$
Fragment I	187.0264	$^{13}CC_6H_8NO_3S^-$	-4.8	4.0	$^{13}CC_3H_8O_5$
Fragment J	160.0074	$C_5H_6NO_3S^-$	-4.9	3.0	$^{13}C_2C_4H_{10}O_5$
Fragment K	116.0174	$C_4H_6NOS^-$	-1.4	2.0	$^{13}C_2C_5H_{10}O_7$

[a] mass-to-charge ratio
[b] ring double bond equivalent
[c] not applicable

Compared to the MS/MS spectra isolated from the syrup sample, the fragments H and I of RP2 are 1.0033 Da heavier due to the presence of one isotopically labelled ^{13}C atom in the sugar chain. As already mentioned in the interpretation of the MS/MS spectrum of RP2 (see section 3.3.2), these two fragments formally arise from the neutral loss of a structure containing four C atoms. More precisely, however, it is probably the cleavage of the bottom half of the sugar chain *via* retro aldol reaction and additionally the decarboxylation of the LA.

Fig. 7 MS/MS line spectra of precursor ions [M-H]⁻ and supposed structures of fragments according to Table 3 of a) the unknown reaction product 1 (RP) isolated at 4.226 min and b) RP2 isolated at 7.237 min from the binary mixture (1:1) of carbocisteine with glucose-1,6-$^{13}C_2$ after storage at elevated temperature (5 weeks at 40 °C and 2 weeks at 60 °C)

4. Conclusion

Thanks to the identical placebo formulations as a reference sample for the GUCS workflow, an identification of API-related DPs and RPs in two prototypes of syrup samples besides a variety of other excipients was easily possible (see Fig. 8). Owing to the untargeted IDA method, a very sensitive and comprehensive comparison of the stability of different formulations is feasible with the option to predict the chemical structure of possible impurities based on the HRMS data. On the one hand, we were able to identify two previously unknown additional DPs of CC (CysTGA and LASO) and confirm their identity at the highest confidence level possible by means of reference measurements. On the other hand, two *N*-glycosides were identified as RPs with the API after hydrolysis of the excipient sucrose in only one of the two formulations. Thus, the sugar-free formulation seems to be more stable (no *N*-glycosides and less LASO). In the case that no reference substance of RPs with excipients can be purchased or is easy to synthesise, binary mixtures can be a simple but helpful answer. The *N*-glycosides identified here must be clearly distinguished from the carcinogenic "advanced Maillard products" formed at significantly higher temperatures [34,35]. Nevertheless, controlled low storage temperature below e.g. 25°C could minimise the hydrolysis of sucrose as a cause of interaction [25,26].

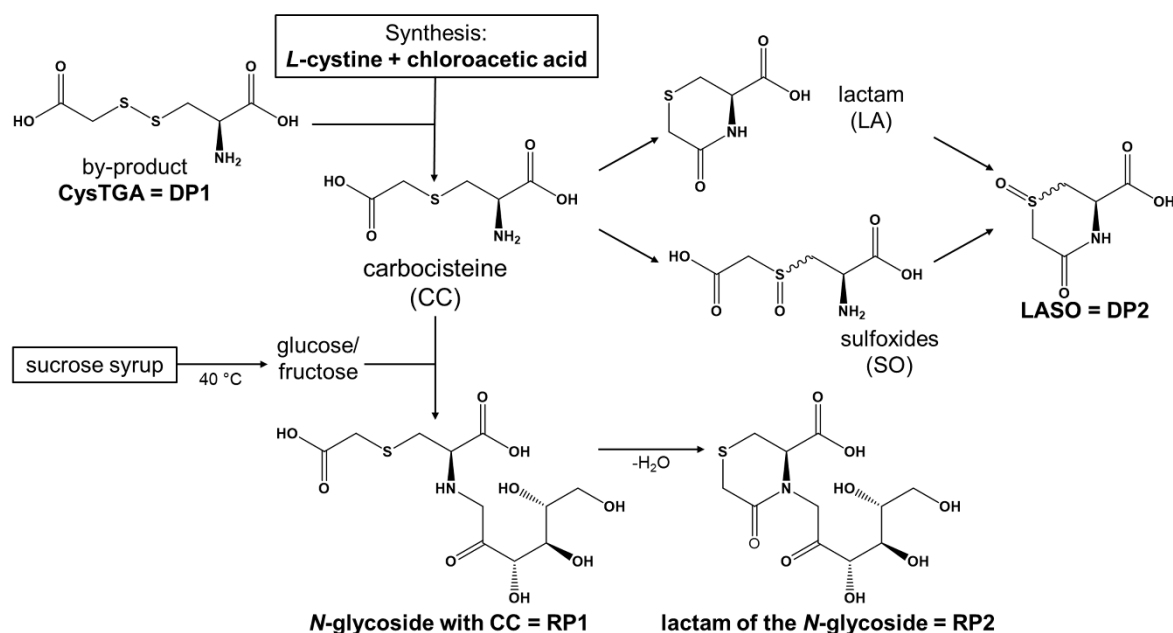
Fig. 8 Schematic overview of the formation of the unknown degradation products (DP) of carbocisteine and reaction products (RP) identified in the sucrose-containing syrup prototype upon storage at 40 °C and 75 % relative humidity for 9 months

Conflict of interest

Acknowledgements

Supplementary material

a) IDA TOF-MS/MS (50-550) from 4.104 min – Precursor: 178.0 Da **carbocisteine**
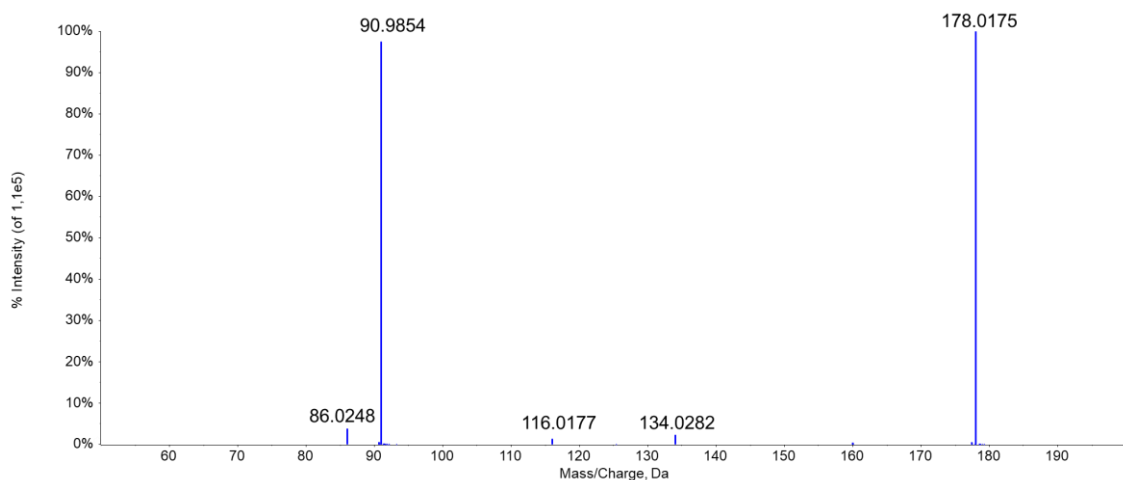
b) IDA TOF-MS/MS (50-550) from 7.348 min – Precursor: 194.0 Da **sulfoxide**
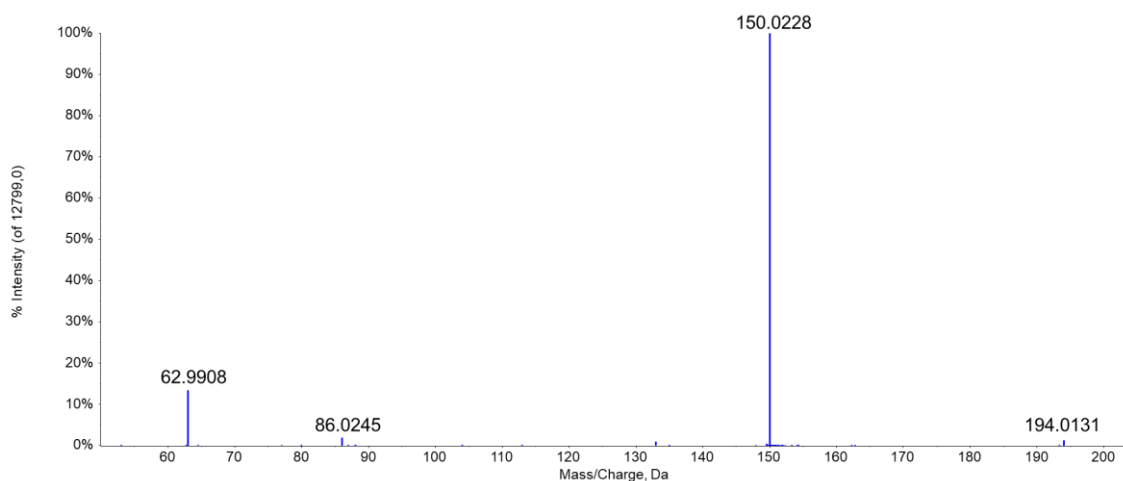
c) IDA TOF-MS/MS (50-550) from 21.061 min – Precursor: 160.0 Da **lactam**
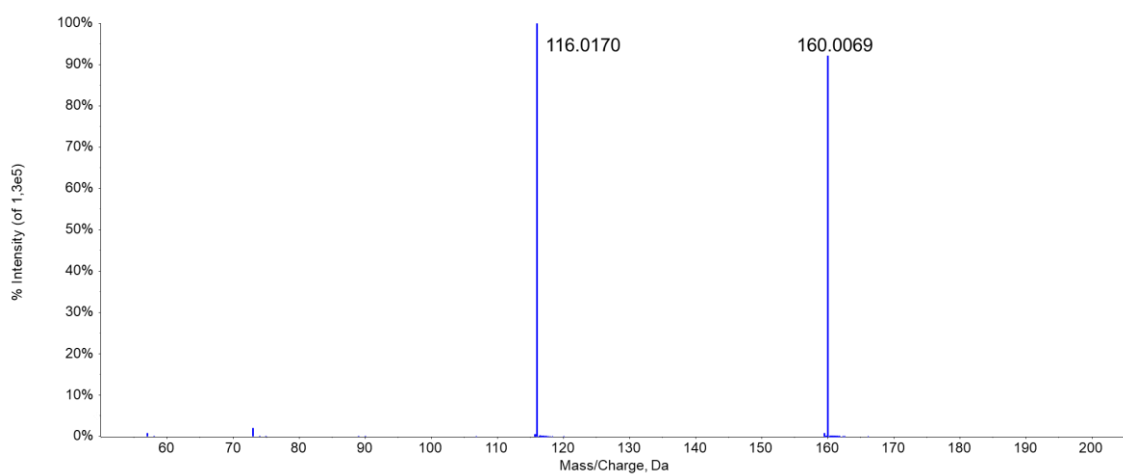
Fig. S1 MS/MS line spectra of the precursor ions [M-H]$^-$ of the reference substances of carbocisteine (a), carbocisteine sulfoxides (b) and carbocisteine lactam (c) using the information dependent acquisition mode (for detailed LC and MS conditions see section 2.3.2 and 2.3.3)

a) IDA TOF-MS/MS from 4.498 min – Precursor: 180.0 Da **carbocisteine**
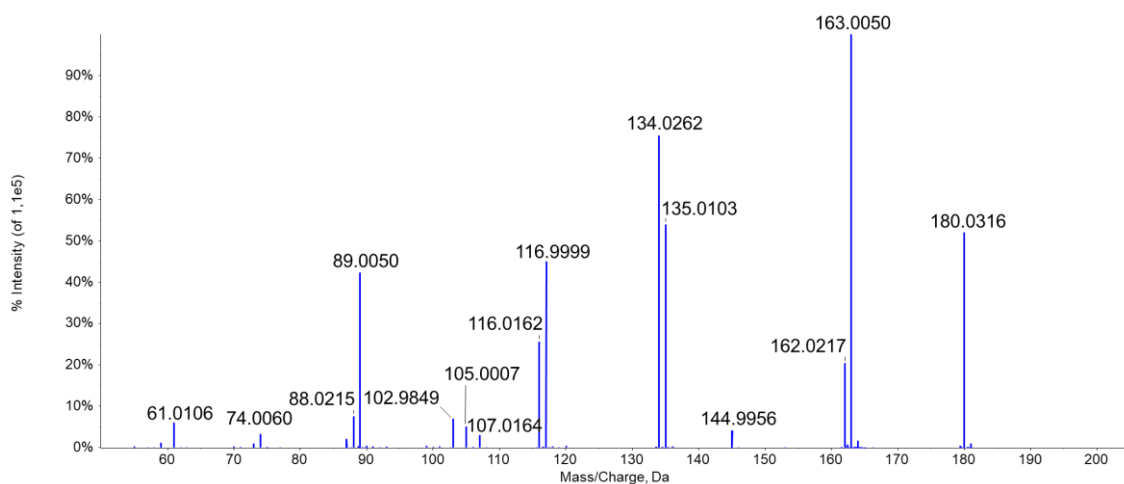
b) IDA TOF-MS/MS from 4.494 min – Precursor: 163.0 Da **carbocisteine - NH$_3$**
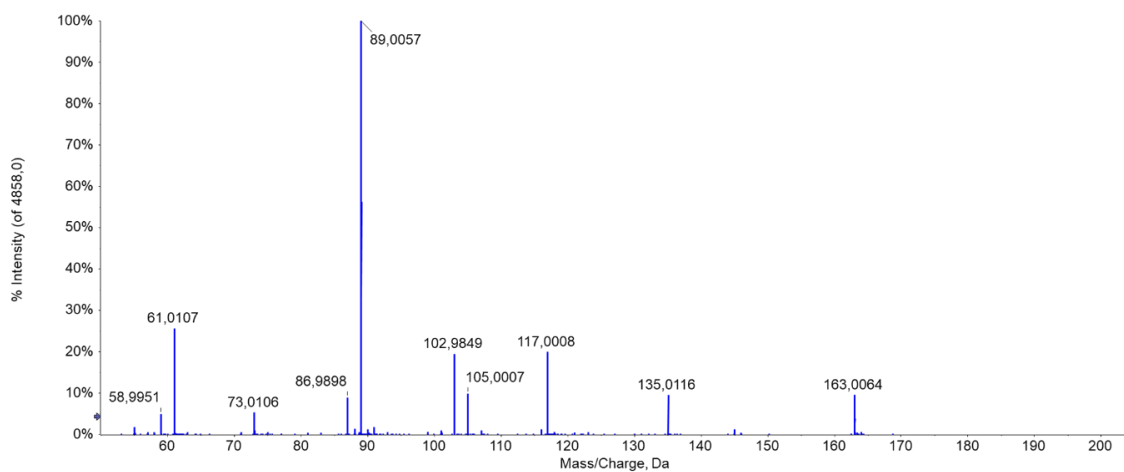
c) IDA TOF-MS/MS from 4.517min – Precursor: 162.0 Da **carbocisteine - H$_2$O**
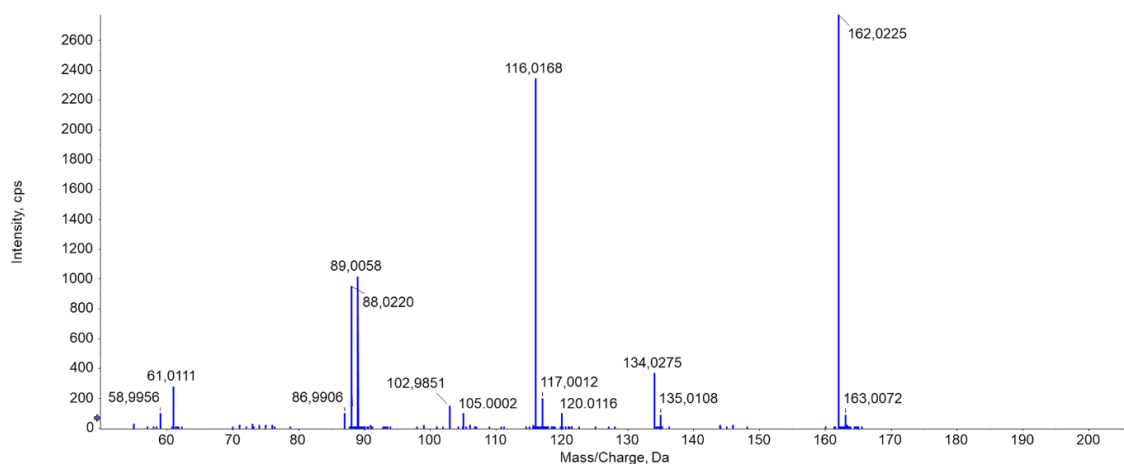
d) IDA TOF-MS/MS from 4.489min – Precursor: 134.0 Da **carbocisteine - H_2O & - CO**
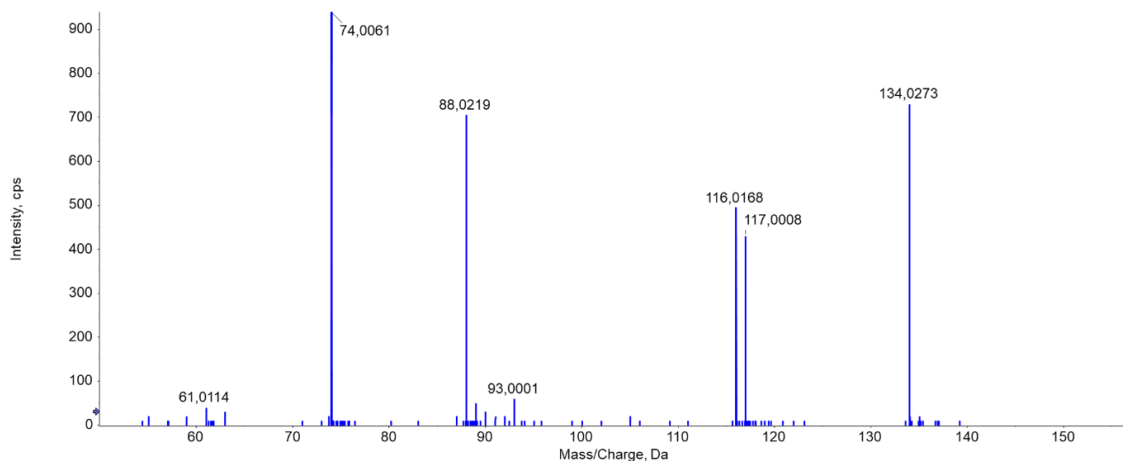
e) IDA TOF-MS/MS from 4.467min – Precursor: 117.0 Da **carbocisteine - NH_3 & - CO & - H_2O**
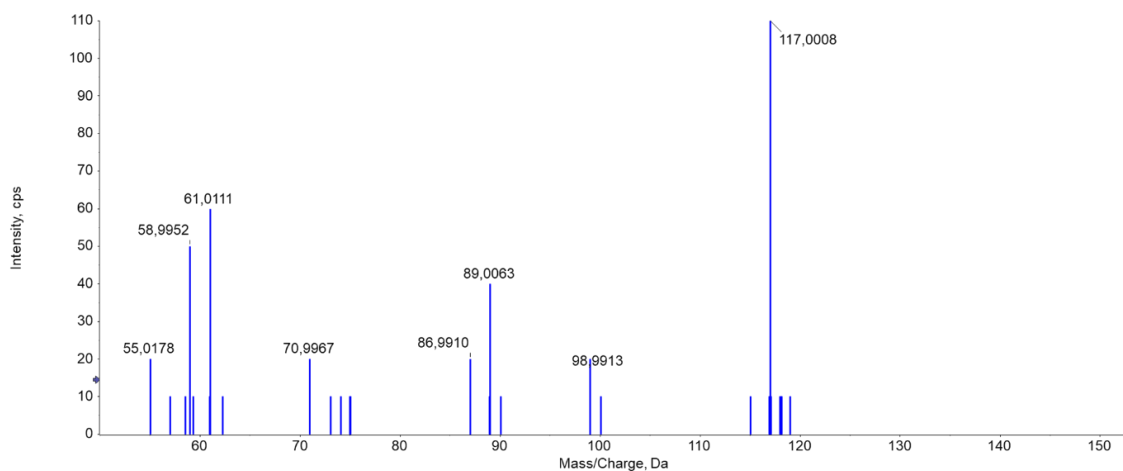
f) IDA TOF-MS/MS from 4.510min – Precursor: 116.0 Da **carbocisteine - H_2O & - CO & - H_2O**
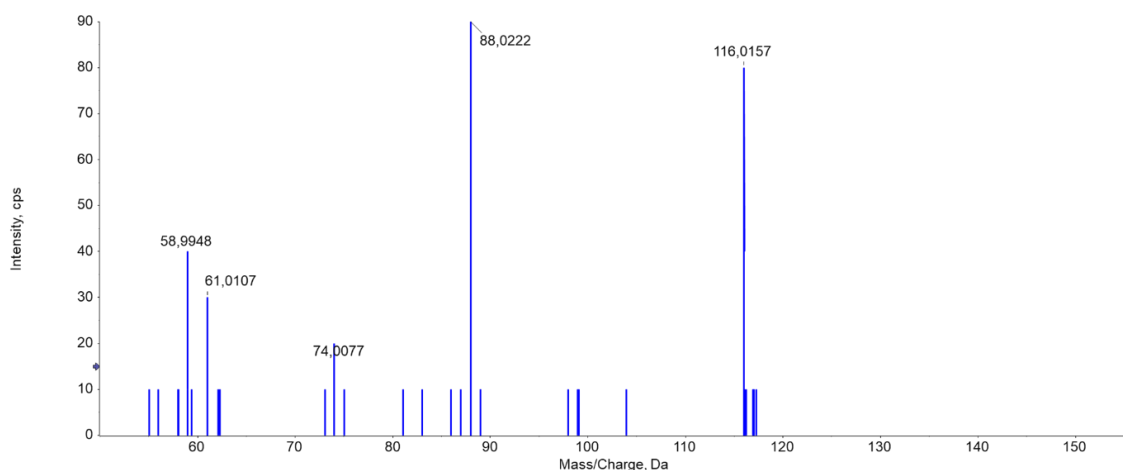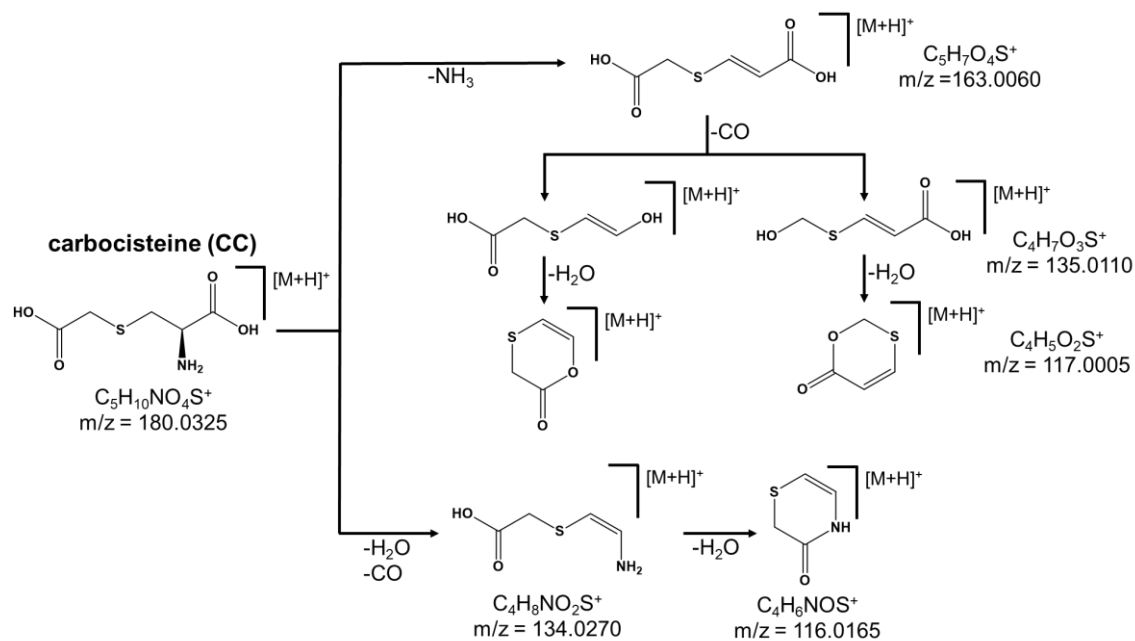
Fig. S2 MS/MS spectra of the precursor ions [M+H]+ of carbocisteine (a) and, if available, its main fragments (b-f) using the information dependent acquisition mode, and a corresponding fragmentation pathway proposal (for detailed LC and MS conditions see section 2.3.2 and 2.3.3)

a) IDA TOF-MS/MS from 6.882 min – Precursor: 196.0 Da **sulfoxide**
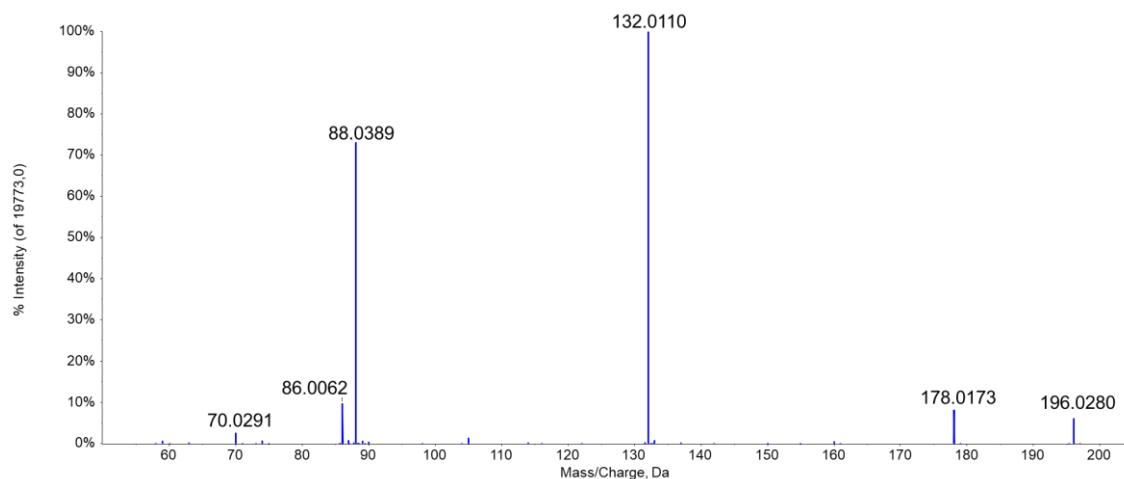
b) IDA TOF-MS/MS from 6.824 min – Precursor: 178.0 Da **sulfoxide - H$_2$O**
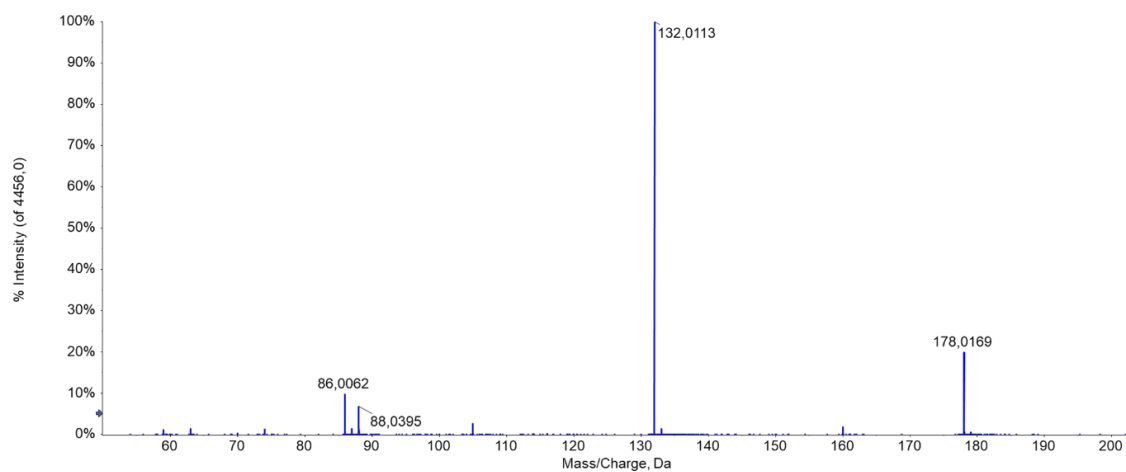
c) IDA TOF-MS/MS from 6.860 min – Precursor: 132.0 Da **sulfoxide - H$_2$O & - CO & - H$_2$O**
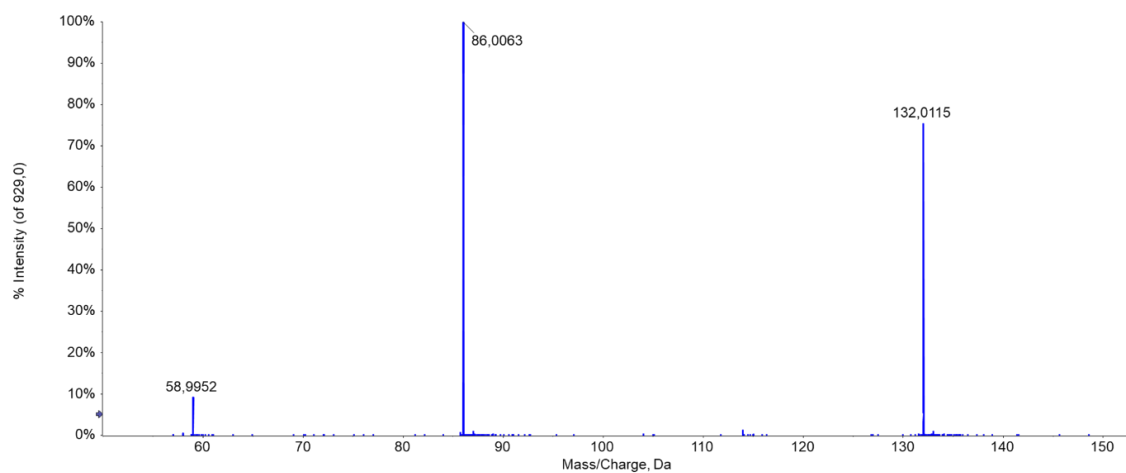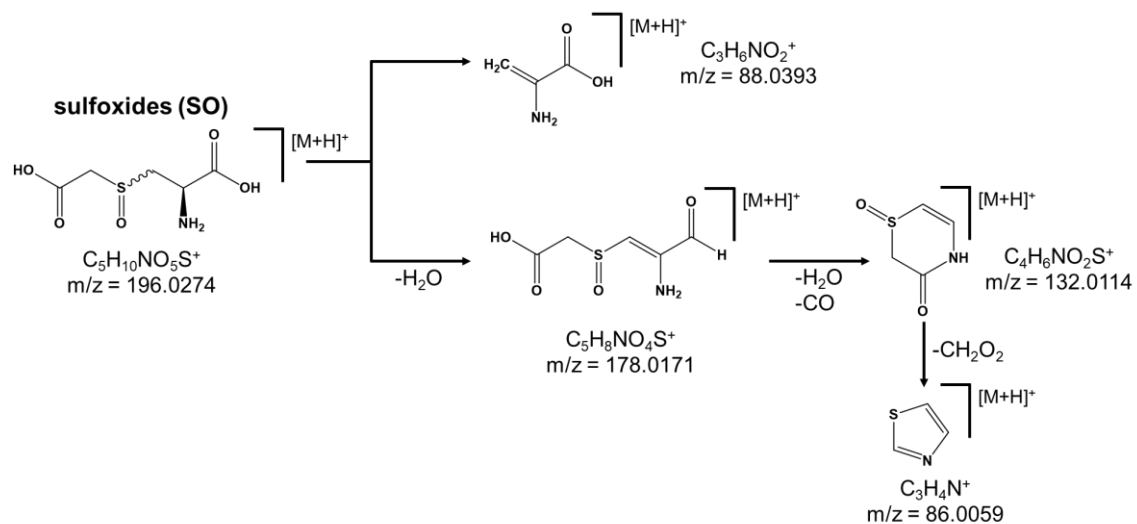
Fig. S3 MS/MS spectra of the precursor ions [M+H]$^+$ of carbocisteine sulfoxides (a) and its two main fragments (b, c) using the information dependent acquisition mode, and a corresponding fragmentation pathway proposal (for detailed LC and MS conditions see section 2.3.2 and 2.3.3)

a) IDA TOF-MS/MS from 23.731 min – Precursor: 162.0 Da **lactam**
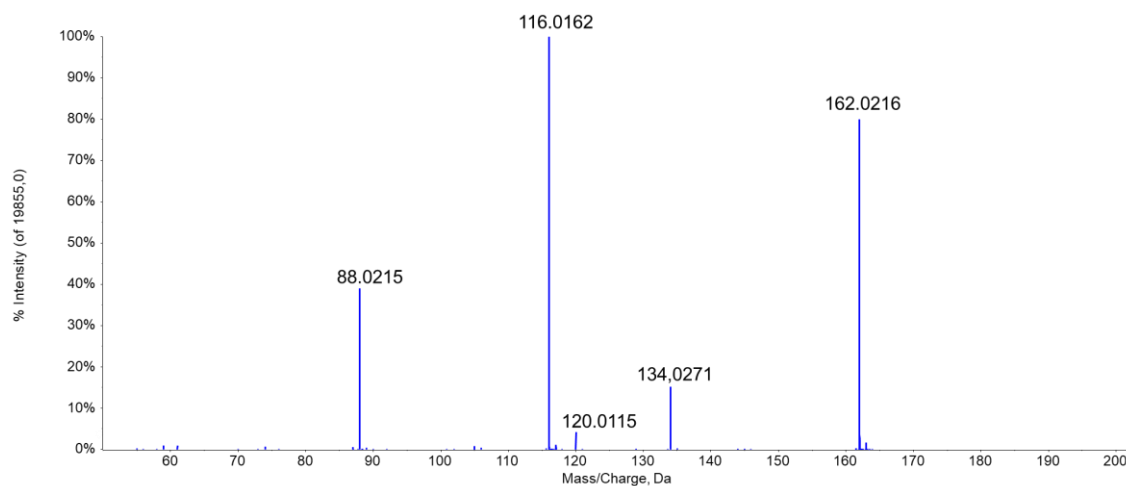
b) IDA TOF-MS/MS from 20.707 min – Precursor: 134.0 Da **lactam - CO**
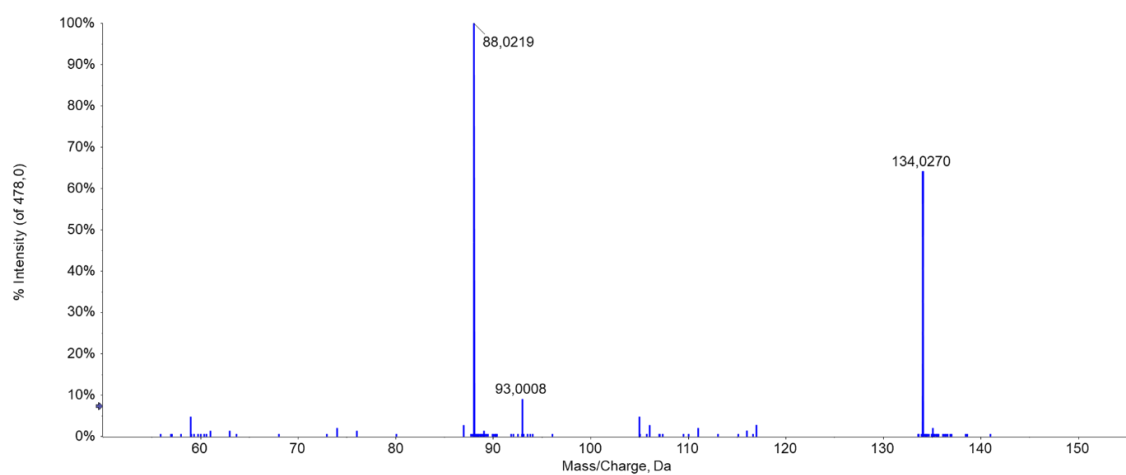
c) IDA TOF-MS/MS from 23.723 min – Precursor: 116.0 Da **lactam - CH$_2$O$_2$**
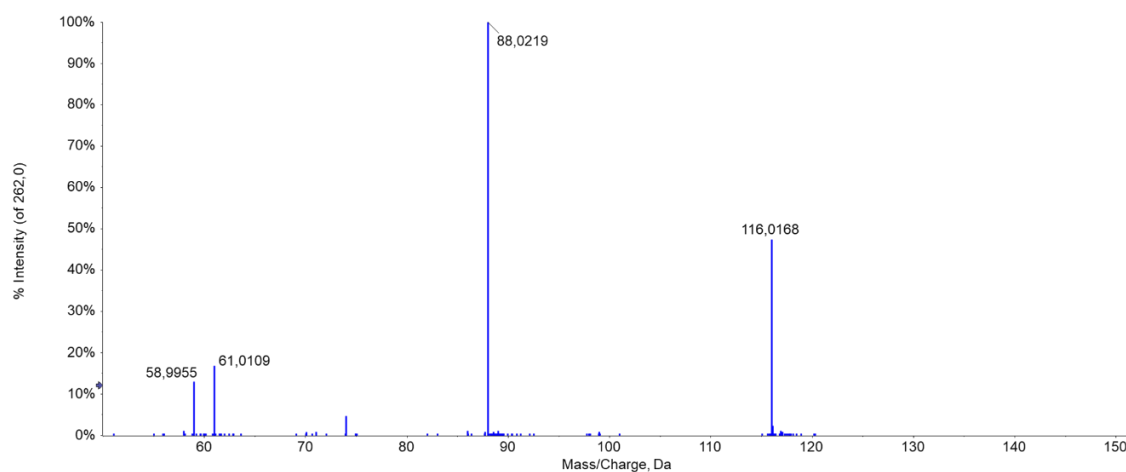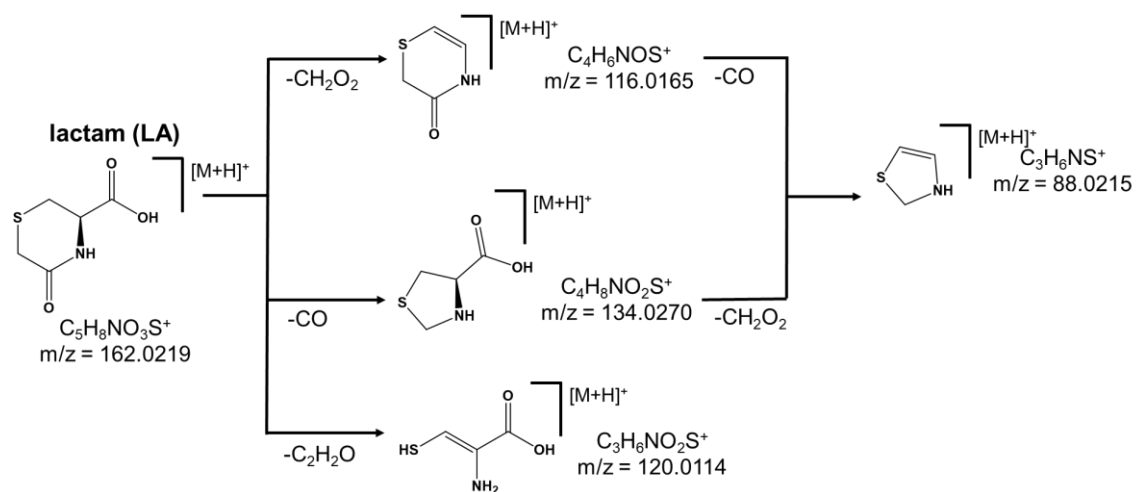
Fig. S4 MS/MS spectra of the precursor ions [M+H]+ of carbocisteine lactam (a) and its two main fragments (b-c) using the information dependent acquisition mode, and a corresponding fragmentation pathway proposal (for detailed LC and MS conditions see section 2.3.2 and 2.3.3)

a) XIC [M+H]$^+$ **DP1**: m/z = 212.0046 ± 0.0025 Da
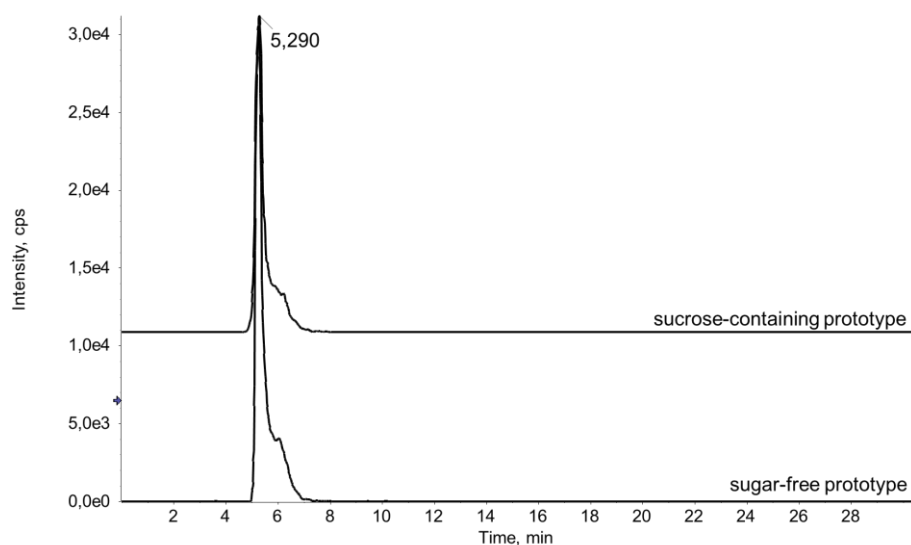
b) XIC [M+H]$^+$ **DP2**: m/z = 178.0169 ± 0.0025 Da
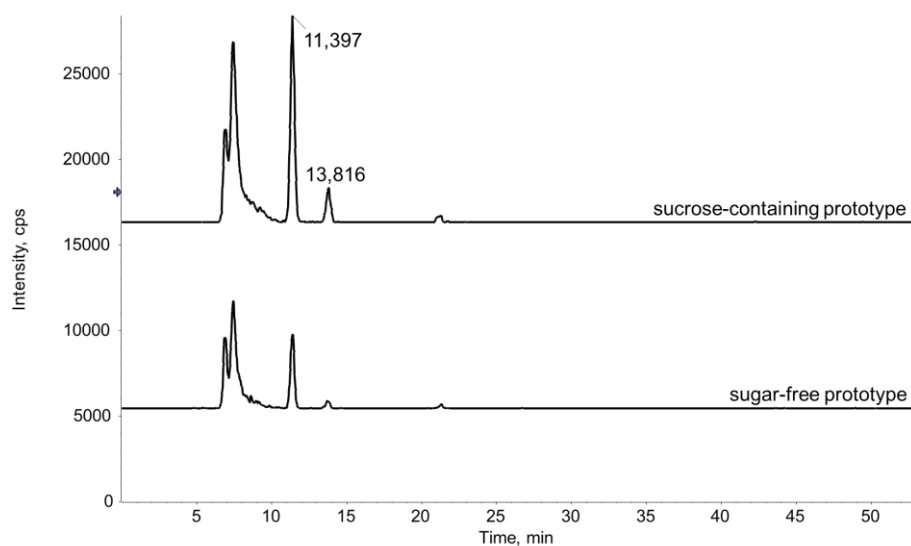
c) XIC [M+H]$^+$ **RP1**: m/z = 342.0853 ± 0.0025 Da
RP2: m/z = 324.0748 ± 0.0025 Da
RP2 -H$_2$O: m/z = 306.0642 ± 0.0025 Da
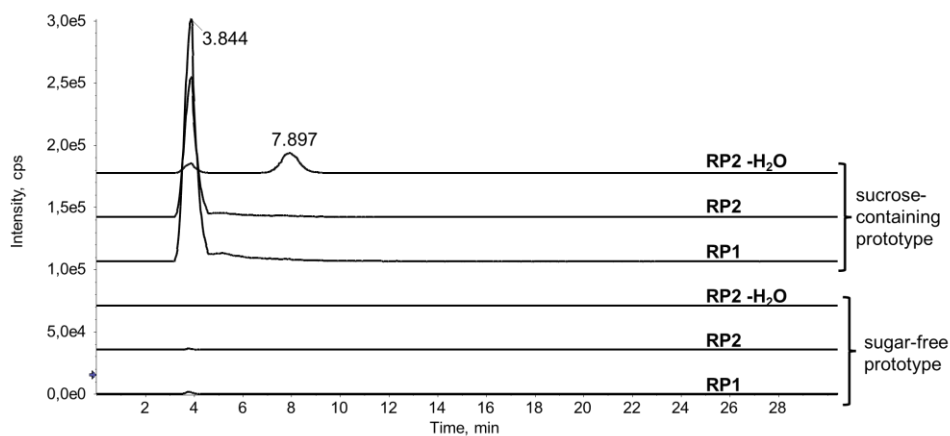
Fig. S5 Overlay of the XICs [M+H]$^+$ of the unknown degradation products DP1 (a), DP2.1 with DP2.2 (b) as well as the unknown reaction products RP1, RP2 and the RP2-H$_2$O (c) in the sugar-free and the sucrose-containing verum prototype, respectively

a) IDA TOF-MS/MS (50-550) from 5.298 min – Precursor [M-H]⁻ 210.0 Da **DP1**

m/z	Int. (%)	Assign.	Error (Da)
88,9702	31,57	True	0,000
90,9858	5,06	True	0,000
98,0248	3,19	False	
120,0124	100,00	True	0,000
132,0127	1,18	True	0,054
209,9901	31,30	True	0,000

Plausibility: 4 of 5 peaks, 98.2 % of total intensity

b) IDA TOF-MS/MS (50-550) from 5.286 min – Precursor [M+H]⁺ 212.0 Da **DP1**

m/z	Int. (%)	Assign.	Error (Da)
55,0181	1,38	False	
73,0285	27,20	True	0,000074
74,0061	14,71	True	0,017556
74,0234	1,10	True	0,000290
78,9673	1,12	True	0,000240
89,0599	1,10	False	
94,9623	6,56	True	0,036103
104,9467	1,62	True	0,053780
120,0113	87,86	True	0,000078
120,9781	1,17	True	0,000451
122,9571	20,40	True	0,000176
133,0861	1,10	False	
148,9728	2,60	True	0,000255
151,9837	10,14	True	0,000204
165,9993	30,11	True	0,000193
166,9838	1,36	False	
176,9676	1,66	True	0,000099
193,9944	8,42	True	0,000382
194,9780	70,49	True	0,000050
195,1230	2,43	True	0,144981
212,0041	100,00	True	0,000488
213,0074	1,12	False	

Plausibility: 17 of 22 peaks, 98.5 % of total intensity

Fig. S6 Application of the *in silico* fragmentation tool for MS/MS spectrum of the unknown degradation product 1 and the CysTGA disulfide structure in the negative (a) or the positive (b) ion mode

Table S1
MS/MS fragments of DP1 ($C_5H_9NO_4S_2$) in the negative ion mode

m/z[a]	sum formula	error [ppm]	RDB[b]	loss
120.0124	$C_3H_6NO_2S^-$	-0.6	1.0	$C_2H_2O_2S$
90.9858	$C_2H_3O_2S^-$	-1.4	1.0	$C_3H_6NO_2S$
88.9702	$C_2HO_2S^-$	-0.8	2.0	$C_3H_8NO_2S$

[a] mass-to-charge ratio
[b] ring double bond equivalent

Table S2
MS/MS fragments of DP1 ($C_5H_9NO_4S_2$) in the positive ion mode

m/z[a]	sum formula	error [ppm]	RDB[b]	loss
194.9782	$C_5H_7O_4S_2^+$	0.9	3.0	NH_3
193.9945	$C_5H_8NO_3S_2^+$	2.5	3.0	H_2O
165.9994	$C_4H_8NO_2S_2^+$	1.8	2.0	CH_2O_2
151.9840	$C_3H_6NO_2S_2^+$	3.0	2.0	$C_2H_4O_2$
122.9571	$C_2H_3O_2S_2^+$	1.6	2.0	C_3H_7N
120.0114	$C_3H_6NO_2S^+$	0.2	2.0	$C_2H_4O_2S$
94.9624	$CH_3OS_2^+$	4.4	1.0	$C_3H_7NO_3$
74.0063	$C_2H_4NS^+$	5.4	2.0	$C_3H_6O_4$
73.0286	$C_3H_5O_2^+$	2.7	2.0	$C_2H_5NO_2S_2$

[a] mass-to-charge ratio
[b] ring double bond equivalent

a) IDA TOF-MS/MS (50-550) from 13.777 min – Precursor [M-H]$^-$ 176.0 Da **DP2**

m/z	Int. (%)	Assign.	Error (Da)
86,0247	1,12	True	0,000
114,0019	7,39	True	0,018
132,0125	17,85	True	0,000
176,0022	100,00	True	0,000

Plausibility: 4 of 4 peaks, 100 % of total intensity

b) IDA TOF-MS/MS (50-550) from 11.352 min – Precursor [M+H]$^+$ 178.0 Da **DP2**

m/z	Int. (%)	Assign.	Error (Da)
58,9952	1,39	True	0,018
74,0240	4,36	True	0,000
82,0293	1,27	False	
86,0063	5,82	True	0,017
88,0397	1,52	True	0,000
90,0011	1,87	True	0,024
104,0170	4,94	True	0,017
108,0117	3,07	False	
114,0012	7,60	True	0,017
132,0114	100,00	True	0,000
133,0142	1,16	True	0,031
136,0066	4,88	False	
160,0067	7,75	True	0,000
178,0171	36,26	True	0,000
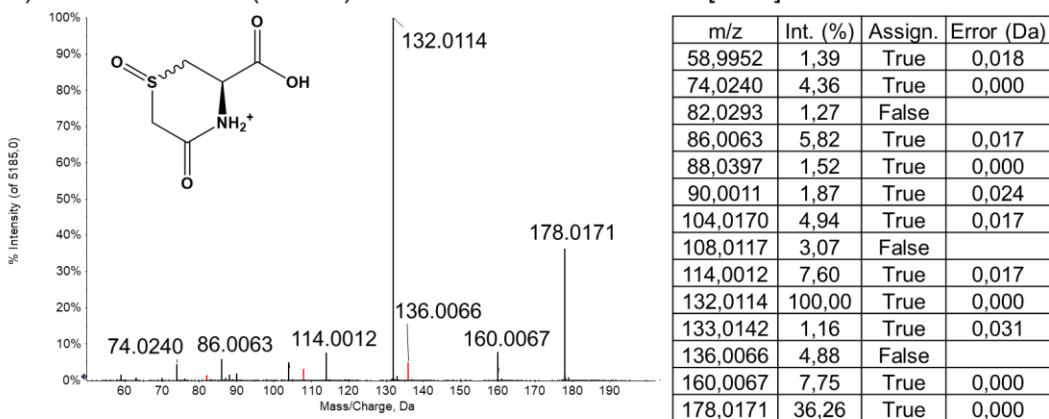
Plausibility: 11 of 14 peaks, 94.9 % of total intensity

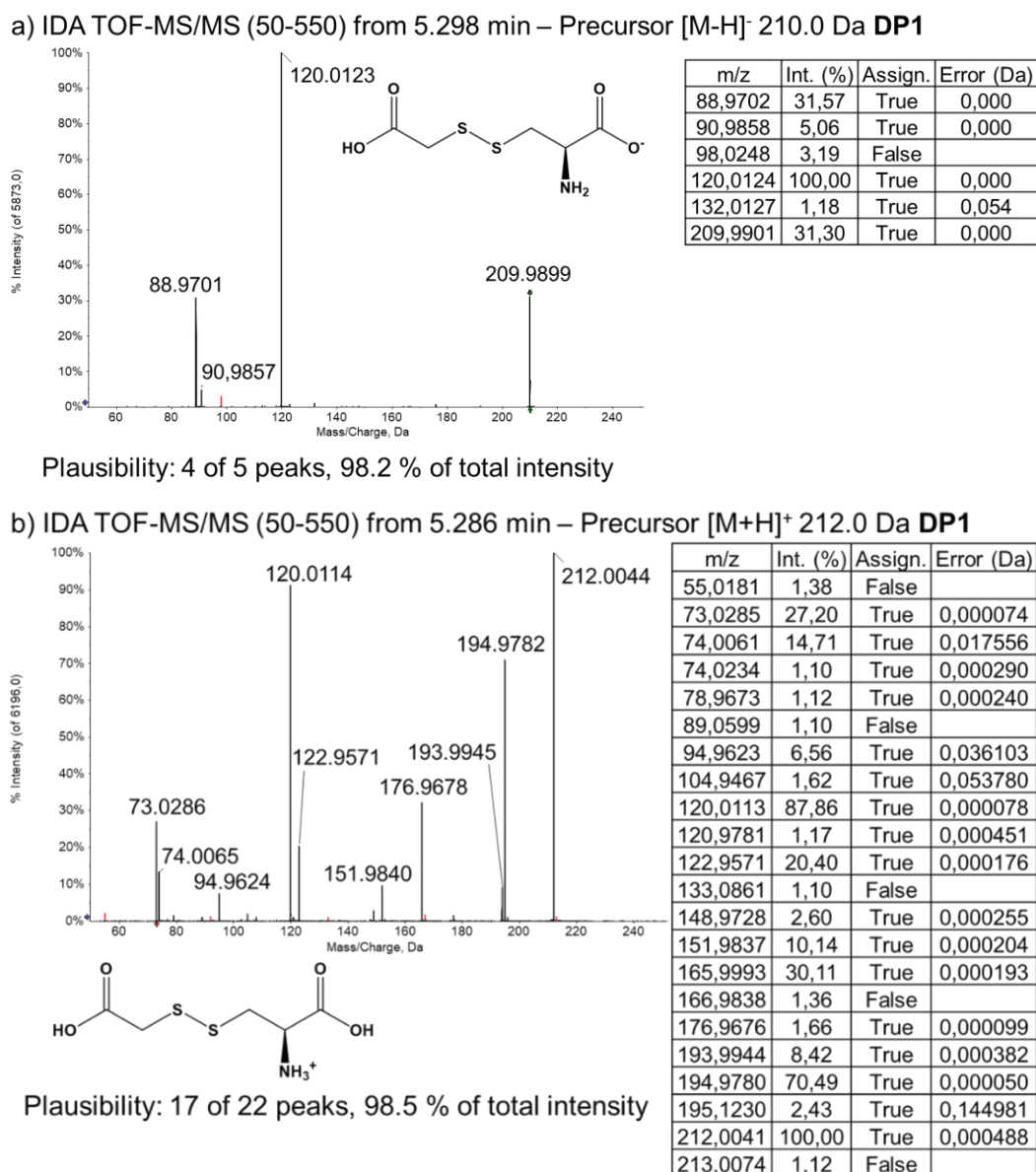**Fig. S7** Application of the *in silico* fragmentation tool for MS/MS spectrum of the unknown degradation product 2 and the LASO structure in the negative (a) or the positive (b) ion mode

Table S3

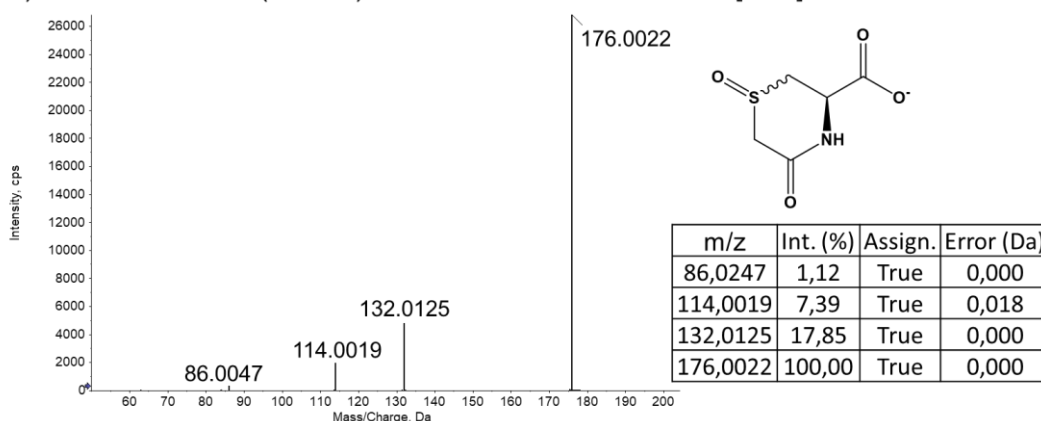MS/MS fragments of DP2 ($C_5H_7NO_4S$) in the negative ion mode

m/z[a]	sum formula	error [ppm]	RDB[b]	loss
132.0125	$C_4H_6NO_2S^-$	0.2	2.0	CO_2
114.0019	$C_4H_4NOS^-$	0.8	3.0	CH_2O_3
86.0247	$C_3H_4NO_2^-$	-0.6	2.0	$C_2H_2O_3S$

[a] mass-to-charge ratio
[b] ring double bond equivalent

Table S4

MS/MS fragments of DP2 ($C_5H_7NO_4S$) in the positive ion mode

m/z[a]	sum formula	error [ppm]	RDB[b]	loss
160.0067	$C_5H_6NO_3S^+$	2.6	4.0	H_2O
132.0114	$C_4H_6NO_2S^+$	0.2	3.0	CH_2O_2
114.0012	C_4H_4NOS	3.4	4.0	CH_4O_3
86.0063	$C_3H_4NS^+$	4.7	3.0	$C_2H_4O_4$
74.0240	$C_2H_4NO_2^+$	4.7	2.0	$C_3H_4O_2S$

[a] mass-to-charge ratio
[b] ring double bond equivalent
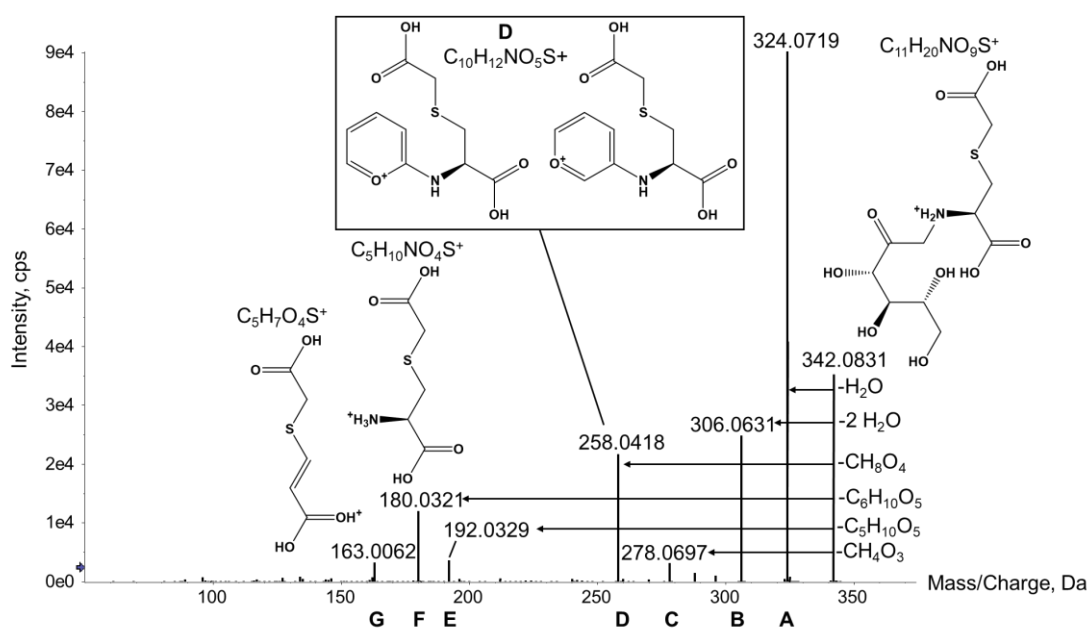
Fig. S8 MS/MS line spectra of RP1 in the positive ion mode with a proposed structure (pyrylium) for the *in silico* unassignable fragment D

Table S5

MS/MS fragments of RP1 ($C_{11}H_{19}NO_9S$) in the positive ion mode

fragment	m/z[a]	sum formula	error [ppm]	RDB[b]	loss
A	324.0719	$C_{11}H_{18}NO_8S^+$	-8.8	4.0	H_2O
B	306.0631	$C_{11}H_{16}NO_7S^+$	-3.6	5.0	$2x\ H_2O$
C	278.0697	$C_{10}H_{16}NO_6S^+$	1.5	4.0	CH_4O_3
D	258.0418	$C_{10}H_{12}NO_5S^+$	-4.9	6.0	CH_8O_4
E	192.0329	$C_6H_{10}NO_4S^+$	2.1	3.0	$C_5H_{10}O_5$
F	180.0321	$C_5H_{10}NO_4S^+$	-2.3	2.0	$C_6H_{10}O_5$
G	163.0062	$C_5H_7O_4S^+$	1.5	3.0	$C_6H_{13}N$

[a] mass-to-charge ratio   [b] ring double bond equivalent
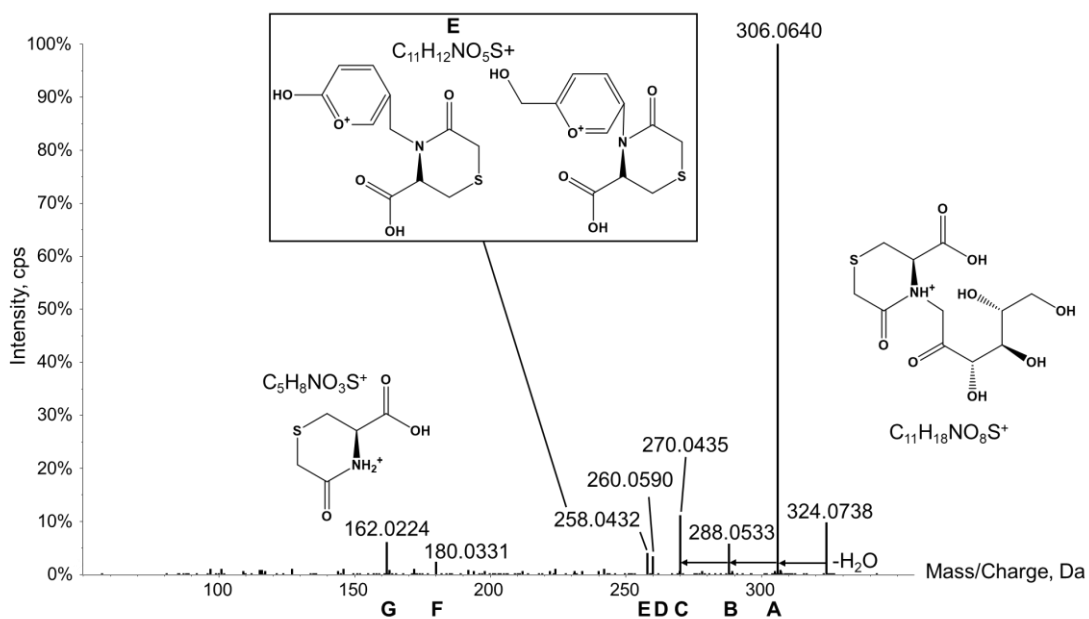
Fig. S9 MS/MS line spectra RP2 in the positive ion mode with a proposed structure (pyrylium) for the *in silico* unassignable fragment E

Table S6
MS/MS fragments of RP2 ($C_{11}H_{17}NO_8S$) in the positive ion mode

fragment	m/z[a]	sum formula	error [ppm]	RDB[b]	loss
A	306.0640	$C_{11}H_{16}NO_7S^+$	-0.7	5.0	H_2O
B	288.0533	$C_{11}H_{14}NO_6S^+$	-1.2	6.0	2x H_2O
C	270.0435	$C_{11}H_{12}NO_5S^+$	1.6	7.0	3x H_2O
D	260.0590	$C_{10}H_{14}NO_5S^+$	1.1	5.0	CH_4O_3
E	258.0432	$C_{10}H_{12}NO_5S^+$	0.5	6.0	CH_6O_3
F	180.0331	$C_5H_{10}NO_4S^+$	3.3	2.0	$C_6H_{10}O_4$
G	162.0224	$C_5H_8NO_3S^+$	2.8	3.0	$C_6H_{10}O_5$

[a] mass-to-charge ratio
[b] ring double bond equivalent

a) IDA TOF-MS/MS (50-550) from 3.746 min – Precursor [M-H]⁻ 340.0 Da **RP1**

Plausibility: 8 of 8 peaks, 100 % of total intensity

CC-Glu
(Amadori product)

CC-Fru
(Heyns product)
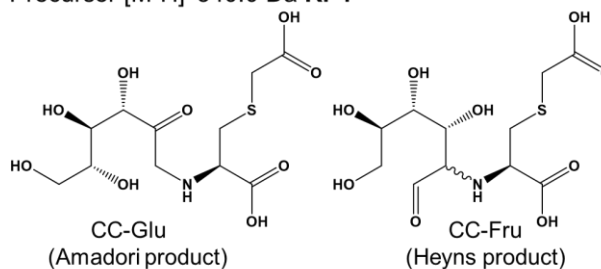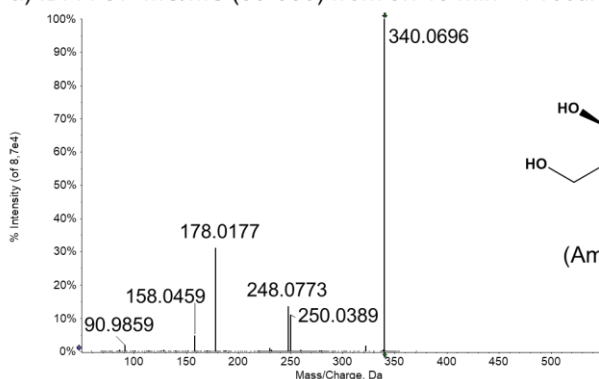
m/z	Int. (%)	Assign.	Error (Da)
90,9859	2,02	True	0,000
158,0459	4,70	True	0,000
178,0177	31,18	True	0,000
230,0669	0,96	True	0,000
248,0773	13,60	True	0,000
250,0389	11,11	True	0,054
322,0606	1,73	True	0,000
340,0696	100,00	True	0,001

b) IDA TOF-MS/MS (50-550) from 7.750 min – Precursor [M-H]⁻ 322.0 Da **RP2**

Plausibility: 8 of 8 peaks, 100 % of total intensity

LA-Glu
(Amadori product)

LA-Fru
(Heyns product)
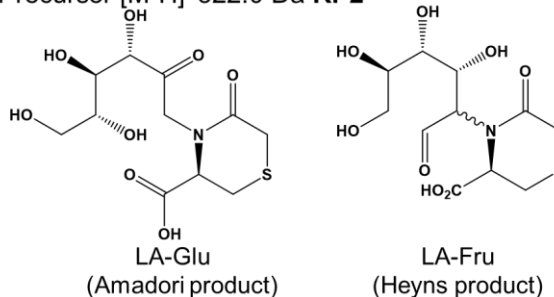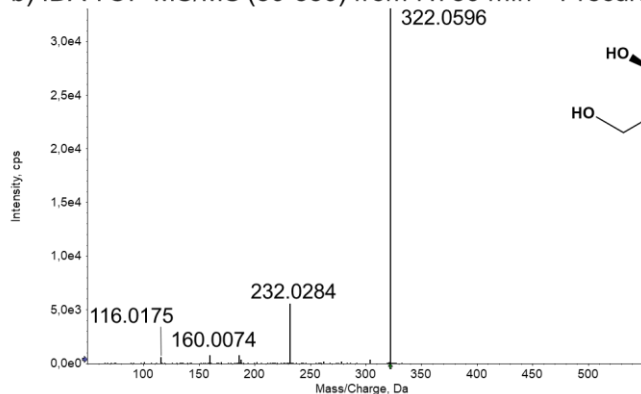
m/z	Int. (%)	Assign.	Error (Da)
116,0175	1,87	True	0,000
160,0073	2,45	True	0,000
186,0231	2,52	True	0,000
188,0385	1,02	True	0,000
232,0284	17,90	True	0,000
304,0499	1,10	True	0,000
322,0596	100,00	True	0,001
322,0979	1,79	True	0,038

Fig. S10 Application of the *in silico* fragmentation tool for MS/MS spectrum of the unknown reaction products RP1 (a) and RP2 (b) with the structures of the *N*-glycosides with glucose or fructose (as Amadori and Heyns rearrangement products) in the negative-ion mode

a) IDA TOF-MS/MS (50-550) from 3.556 min – Precursor [M+H]+ 342.1 Da **RP1**

Plausibility: 8 of 10 peaks, 88.3 % of total intensity

m/z	Int.(%)	Assign.	Error (Da)
163,0058	3,53	True	0,000
180,0320	12,35	True	0,001
192,0326	3,78	True	0,000
258,0414	22,75	False	
278,0692	3,12	True	0,000
288,0538	1,81	False	
296,0802	1,08	True	0,000
306,0627	23,31	True	0,001
324,0715	100,00	True	0,003
342,0827	38,62	True	0,003

CC-Glu (Amadori product)

CC-Fru (Heyns product)

b) IDA TOF-MS/MS (50-550) from 7.428 min – Precursor [M+H]+ 324.1 Da **RP2**

Plausibility: 8 of 10 peaks, 88.3 % of total intensity

m/z	Int.(%)	Assign.	Error (Da)
97,0283	1,03	False	
101,0601	1,03	True	0,037
127,0395	1,03	False	
146,0254	1,03	True	0,002
162,0224	6,09	True	0,000
172,0056	1,03	False	
180,0331	2,37	True	0,054
224,0364	1,03	False	
242,0471	1,03	False	
258,0432	3,96	False	
260,0590	3,40	True	0,000
270,0435	11,08	False	
288,0533	5,78	True	0,000
306,0640	100,00	True	0,000
324,0738	9,73	True	0,001
324,1840	2,61	True	0,109
324,2000	1,58	True	0,125

LA-Glu (Amadori product)

LA-Fru (Heyns product)

Fig. S11 Application of the *in silico* fragmentation tool for MS/MS spectrum of the unknown reaction products RP1 (a) and RP2 (b) with the structures of the *N*-glycosides with glucose or fructose (as Amadori and Heyns rearrangement products) in the positive ion mode
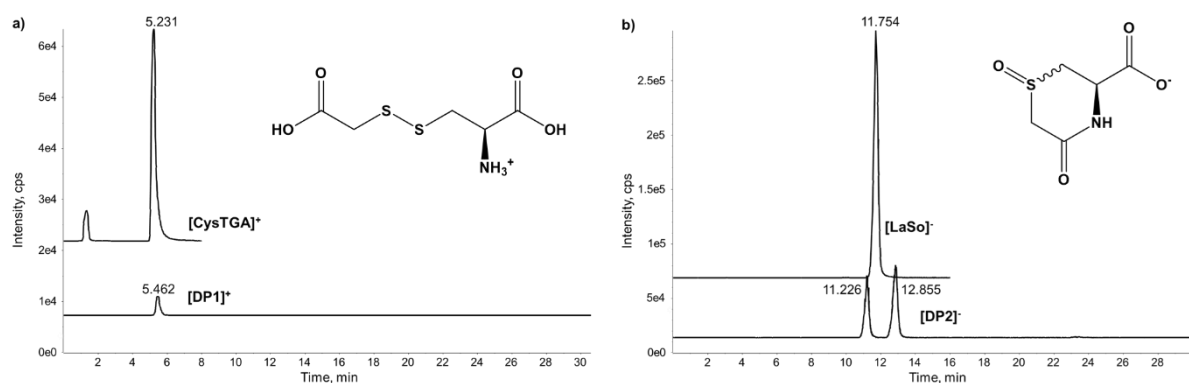
Fig. S12 Overlay of the extracted ion chromatogram of a) the unknown degradation product 1 (DP1) with its postulated reference CysTGA in the positive ion mode [M+H]+ and b) the unknown DP2 with its postulated reference LASO in the negative ion mode [M-H]-
(note: only one peak is visible in the chromatogram of the LASO reference because no diastereomeric mixture was used)

a) Comparison fructose vs. glucose (MS/MS in the negative ion mode)
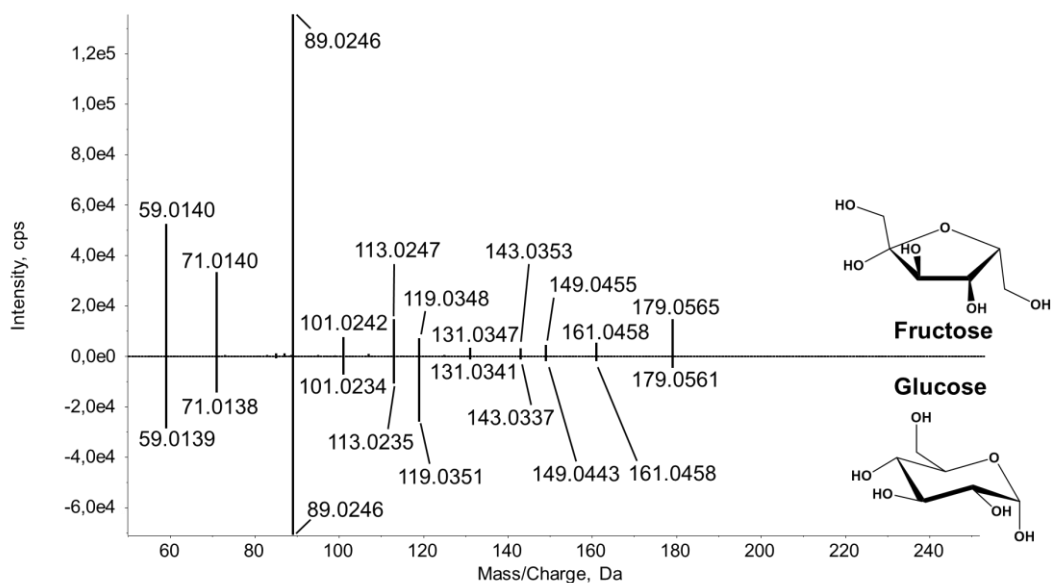
b) Comparison glucose vs. ^{13}C-labelled glucose (MS/MS in the negative ion mode)
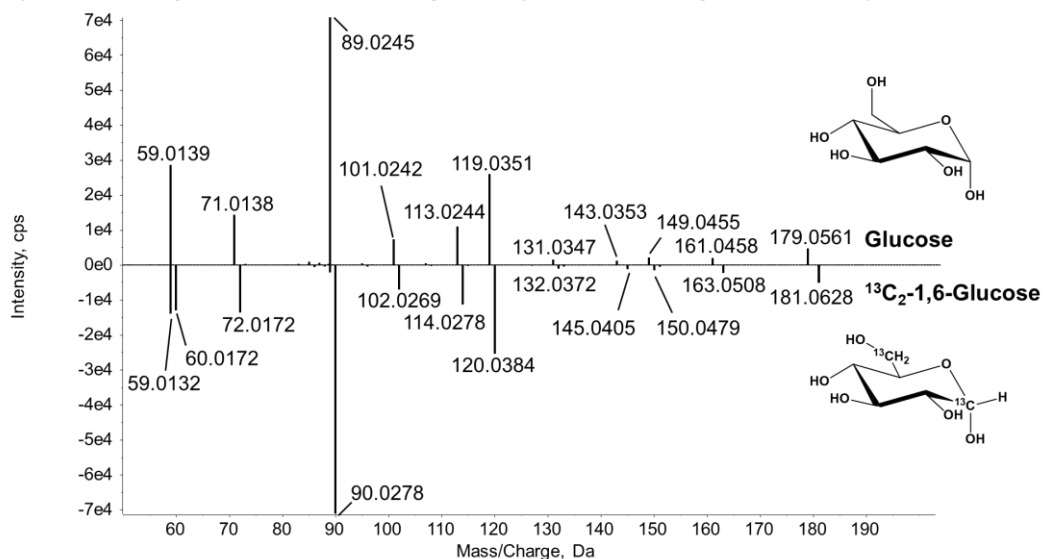
Fig. S13 Comparison of the MS/MS line spectra of the monosaccharide reference substances glucose, fructose and $^{13}C_2$-1,6-glucose in the negative ion mode
(note: the main fragment of glucose/fructose $C_3H_5O_2^-$ without ^{13}C-labelling is also visible, which can only be explained by fragmentation reactions at both ends of the hexose in the open-chain form)

86
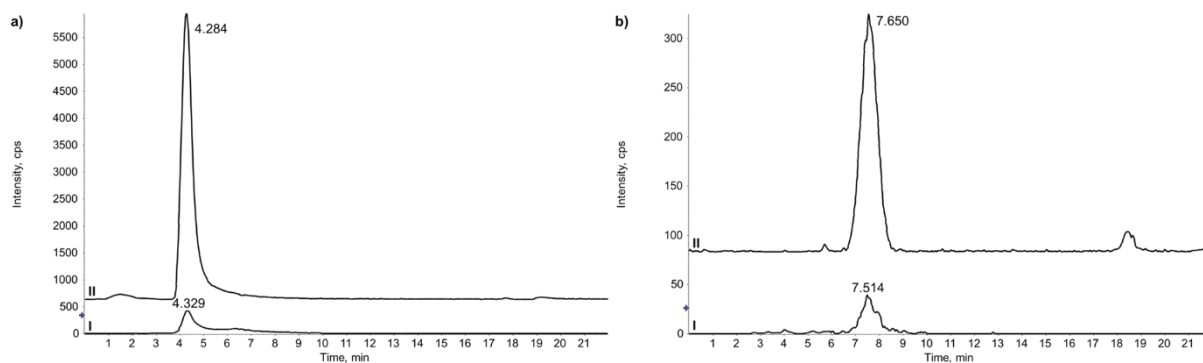
Fig. S14 Overlay of the extracted ion chomratogram [M-H]⁻ of a) the unknown reaction product 1 (RP) and b) RP2 in binary mixtures (1:1) of carbocisteine with fructose (I) or glucose (II) after storage at elevated temperature (4 weeks at 40 °C and 2 weeks at 60 °C)
(note: typical for the chromatographic analysis of sugars at moderate temperature, the peaks of the two RPs were relatively broad (> 2 min) due to the simultaneous presence of the two anomers, which are in equilibrium via the open-chain form)
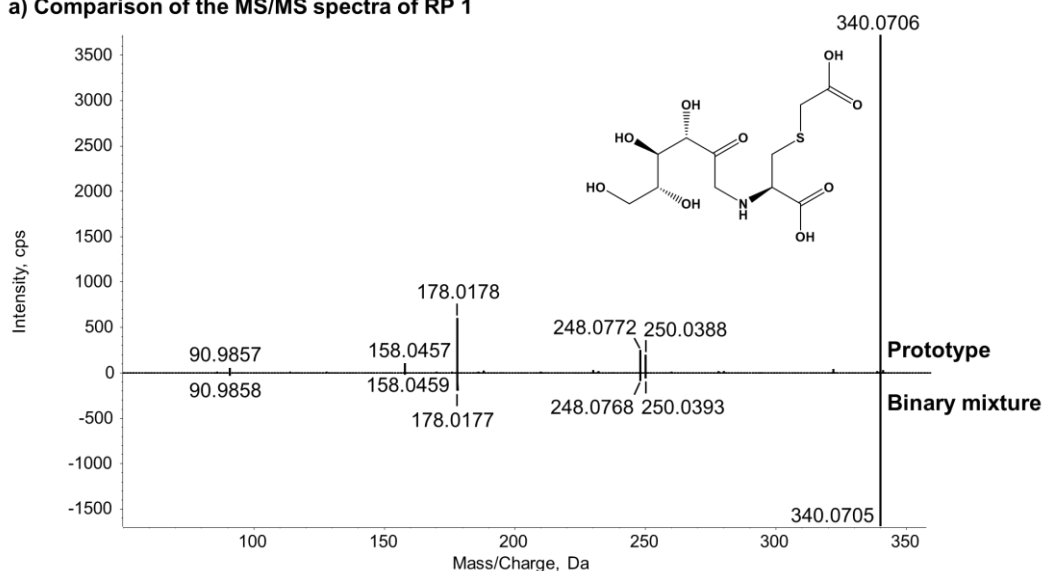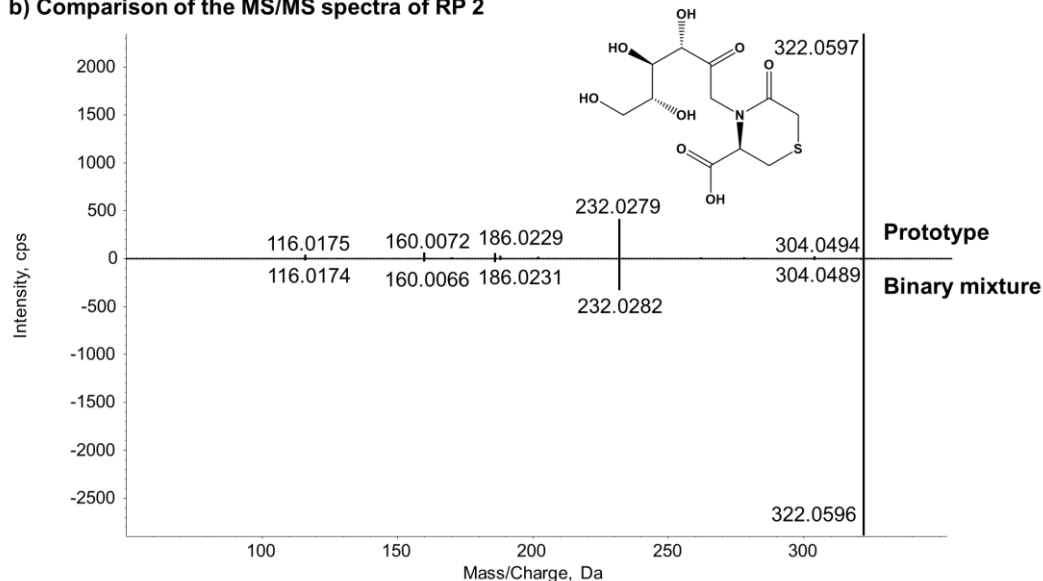
Fig. S15 Comparison of the MS/MS line spectra of RP1 (a) and RP2 (b) isolated from the sucrose-containing prototype and the binary mixture in the negative ion mode

References

[1]   G. Hopfgartner, D. Tonoli, E. Varesio, High-resolution mass spectrometry for integrated qualitative and quantitative analysis of pharmaceuticals in biological matrices, Anal. Bioanal. Chem. 402 (2012) 2587-2596.

[2]   T. Kind, O. Fiehn, Advances in structure elucidation of small molecules using mass spectrometry, Bioanal. Rev. 2 (2010) 23-60.

[3]   F. Fenaille, P. B. Saint-Hilaire, K. Rousseau, C. Junot, Data acquisition workflows in liquid chromatography coupled to high resolution mass spectrometry-based metabolomics: Where do we stand?, J. Chromatogr. A 1526 (2017) 1-12.

[4]   H. H. Maurer, M. R. Meyer, High-resolution mass spectrometry in toxicology: current status and future perspectives, Arch. Toxicol. 90 (2016) 2161-2172.

[5]   A. T. Roemmelt, A. E. Steuer, M. Poetzsch, T. Kraemer, Liquid chromatography, in combination with a quadrupole time-of-flight instrument (LC QTOF), with sequential window acquisition of all theoretical fragment-ion spectra (SWATH) acquisition: systematic studies on its use for screenings in clinical and forensic toxicology and comparison with information-dependent acquisition (IDA), Anal. Chem. 86(23) (2014) 11742-11749.

[6]   R. Bonner, G. Hopfgartner, SWATH acquisition mode for drug metabolism and metabolomics investigations, Bioanalysis 8(16) (2016) 1735-1750.

[7]   L. Lin, H. Lin, M. Zhang, X. Dong, X. Yin, C. Qu, J. Ni, Types, principle, and characteristics of tandem high-resolution mass spectrometry and its applications, RSC Adv. 5(130) (2015) 107623-107636.

[8]   R. Rapolu, C. K. Raju, K. Srinivas, A. Awasthi, S. G. Navalgund, K. V. Surendranath, Isolation and characterization of a novel acid degradation impurity of Amlodipine Besylate using Q-TOF, NMR, IR and single crystal X-ray, J. Pharm. Biomed. Anal. 99 (2014) 59-66.

[9]   M. Narayanam, A. Sahu, S. Singh, Use of LC–MS/TOF, LC–MSn, NMR and LC–NMR in characterization of stress degradation products: Application to cilazapril, J. Pharm. Biomed. Anal. 111 (2015) 190-203.

[10]   O. Scherf-Clavel, M. Kinzig, A. Besa, A. Schreiber, C. Bidmon, M. Abdel-Tawab, J. Wohlfart, F. Sörgel, U. Holzgrabe, The contamination of valsartan and other sartans, Part 2: Untargeted screening reveals contamination with amides additionally to known nitrosamine impurities, J. Pharm. Biomed. Anal. 172 (2019) 278-284.

[11]   J. D. Whitman, K. L. Lynch, Optimization and Comparison of Information-Dependent Acquisition (IDA) to Sequential Window Acquisition of All Theoretical Fragment Ion Spectra (SWATH) for High-Resolution Mass Spectrometry in Clinical Toxicology, Clin. Chem. 65(7) (2019) 862-870.

[12]   J. Wohlfart, E. Jäckel, O. Scherf-Clavel, D. Jung, M. Kinzig, F. Sörgel, U. Holzgrabe, Impurity Profiling of Bisoprolol Fumarate by Liquid Chromatography-High-Resolution Mass Spectrometry: A Combination of Targeted and Untargeted Approaches using a Synthesis Reaction Matrix and General Unknown Comparative Screening, J. Chromatogr. Open (2021) 100012.

[13]   International Council for Harmonisation of Technical Requirements for Pharmaceuticals for Human Use, Guideline Q3B (R2) Impurities in New Drug Products (2006).

[14] R. Walther, O. Scherf-Clavel, U. Holzgrabe, Method transfer from ion pair chromatography to charged aerosol detector-compatible mixed-mode chromatography: A case study using carbocisteine, J. Chromatogr. Open (2021) 100014.

[15] C. R. Mallet, Z. Lu, J. R. Mazzeo, A study of ion suppression effects in electrospray ionization from mobile phase additives and solid-phase extracts, Rapid Commun. Mass Spectrom. 18(1) (2004) 49-58.

[16] A. Schmidt, M. Karas, T. Dülcks, Effect of different solution flow rates on analyte ion signal in nano-ESI MS, or: when does ESI turn into nano-ESI?, J. Am. Soc. Mass Spectrom. 14(5) (2003) 492-500.

[17] V. Gabelica, E. De Pauw, Internal energy and fragmentation of ions produced in electrospray sources, Mass Spectrom. Rev. 24(4) (2005) 566-587.

[18] D. Asakawa, H. Mizuno, E. Sugiyama, K. Todoroki, In-Source Fragmentation of Phenethylamines by Electrospray Ionization Mass Spectrometry: Toward Highly Sensitive Quantitative Analysis of Monoamine Neurotransmitters, Anal. Chem. 92(17) (2020) 12033-12039.

[19] T. Reemtsma, Determination of molecular formulas of natural organic matter molecules by (ultra-) high-resolution mass spectrometry: Status and needs, J. Chromatogr. A 1216(18) (2009) 3687-3701.

[20] H. Xing, V. Yaylayan, Mechanochemical generation of Schiff bases and Amadori products and utilization of diagnostic MS/MS fragmentation patterns in negative ionization mode for their analysis, Carbohydr. Res. 495 (2020) 108091.

[21] R. B. Reddy, K. R. More, M. S. Jha, B. Sharma, L. Magar, Identification, synthesis, isolation and characterization of formulation related impurity of Gabapentin, J. Pharm. Biomed. Anal. 129 (2016) 509-513.

[22] H. Xing, V. V. Mossine, V. Yaylayan, Diagnostic MS/MS fragmentation patterns for the discrimination between Schiff bases and their Amadori or Heyns rearrangement products, Carbohydr. Res. 491 (2020) 107985.

[23] P. A. Harmon, W. Yin, W. E. Bowen, R. J. Tyrrell, R. A. Reed, Liquid chromatography–mass spectrometry and proton nuclear magnetic resonance characterization of trace level condensation products formed between lactose and the amine-containing diuretic hydrochlorothiazide, J. Pharm. Sci. 89(7) (2000) 920-929.

[24] L. Rystov, R. Chadwick, K. Krock, T. Wang, Simultaneous determination of Maillard reaction impurities in memantine tablets using HPLC with charged aerosol detector, J. Pharm. Biomed. Anal. 56(5) (2011) 887-894.

[25] R. Wolfenden, Y. Yuan, Rates of Spontaneous Cleavage of Glucose, Fructose, Sucrose and Trehalose in Water, and the Catalytic Proficiency of Invertase and Trehalas, J. Am. Chem. Soc. 130(24) (2008) 7548-7549.

[26] F. Ghaderi, M. R. S. Shhadbad, M. Hoseinazadeh, Effect of pH and Storage Temperature on 5-(Hydroxymethyl) Furfural (5HMF) Formation in USP Syrup Preparation, Pharm. Sci. 21(1) (2015) 1-5.

[27] Council of Europe, European Pharmacopoeia, 11.0 edition, Monograph no. 2797 Sucrose liquid, Strasbourg, France (2023).

[28]   T. M. Wrodnigg, A. E. Stütz, The Heyns Rearrangement Revisited: An Exceptionally Simple Two-Step Chemical Synthesis of D-Lactosamine from Lactulose, Angew. Chem. Int. Ed. 38(6) (1999) 827-828.

[29]   O. Wahl, U. Holzgrabe, Impurity profiling of carbocisteine by HPLC-CAD, qNMR and UV/vis spectroscopy, J. Pharm. Biomed. Anal. 95 (2014) 1-10.

[30]   M. del Pilar Buera, J. Chirife, S. L. Resnik, G. Wetzler, Nonenzymatic Browning in Liquid Model Systems of High Water Activity: Kinetics of Color Changes due to Maillard´s Reaction Between Different Single Sugars and Glycine and Comparison with Caramelization Browning. J. Food Sci. 52(4) (1987) 1063-1067.

[31]   A. Jakas, A. Katić, N. Bionda, Š. Horvat, Glycation of a lysine-containing tetrapeptide by D-glucose and D-fructose – influence of different reaction conditions on the formation of Amadori/Heyns products, Carbohydr. Res. 343(14) (2008) 2475-2480.

[32]   D. Hemmler, C. Roullier-Gall, J. W. Marshall, M. Rychlik, A. J. Taylor, P. Schmitt-Kopplin, Evolution of Complex Maillard Chemical Reactions Resolved in Time, Sci. Rep. 7 (2017) 3227.

[33]   A. Fanigliulo, P. De Filippis, O. Curcuruto, P. Repeto, D. Roveda, M. Hartenstein, E. Adams, D. Cabooter, Development and validation of a stability indicating method for *S*-carboxymethyl-L-cysteine and related degradation products in oral syrup formulation, J. Pharm. Biomed. Anal. 115 (2015) 39-47.

[34]   Y. Luo, S. Li, C.-T. Ho, Key Aspects of Amadori Rearrangement Products as Future Food Additive*s,* Molecules 26(14) (2021) 4314.

[35]   K. Phuong-Nguyen, B. A. McNeill, K. Aston-Mourney, L. R. Rivera, Advanced Glycation End-Products and Their Effects on Gut Health, Nutrients 15(2) 405.

3.3. Simplification of pharmacopoeial liquid chromatography methods for related substances of statins by hyphenated ultraviolet and charged aerosol detection

Rasmus Walther, Ulrike Holzgrabe

Abstract

For a more comprehensive characterization of a drug substance and its impurities, multidetector approaches are a helpful tool in liquid chromatography. In particular, the relatively inexpensive hyphenation of the ultraviolet (UV) with the charged aerosol detector (CAD) extends the scope from UV-active to non- or weak chromophore analytes, respectively. In this study, the chromatographic methods of the test for related substances of simvastatin and lovastatin in the European Pharmacopoeia were adapted to UV-CAD and thus allowing a more sophisticated detection of the weak chromophore dihydro impurity besides the other UV-active impurities. The compendial gradient program for simvastatin had to be modified (lowered initial acetonitrile percentage and increased gradient slope) because an additional critical peak pair emerged with the Hypersil C_{18} BDS column used here. Therefore, a Plackett-Burman design with 11 factors (including 4 dummy factors) was chosen to evaluate robustness of the adapted method. The flow rate, initial acetonitrile percentage, and column temperature were identified as three critical parameters that had to be carefully observed. Finally, the validity of the method for simultaneous detection of dihydrosimvastatin with CAD and of lovastatin and simvastatin as examples of UV detection was verified according to ICH Q2 (R1). In the case of lovastatin, the direct comparison with the pharmacopoeial method reveal that a determination with CAD is the more sensitive method.

Graphical abstract
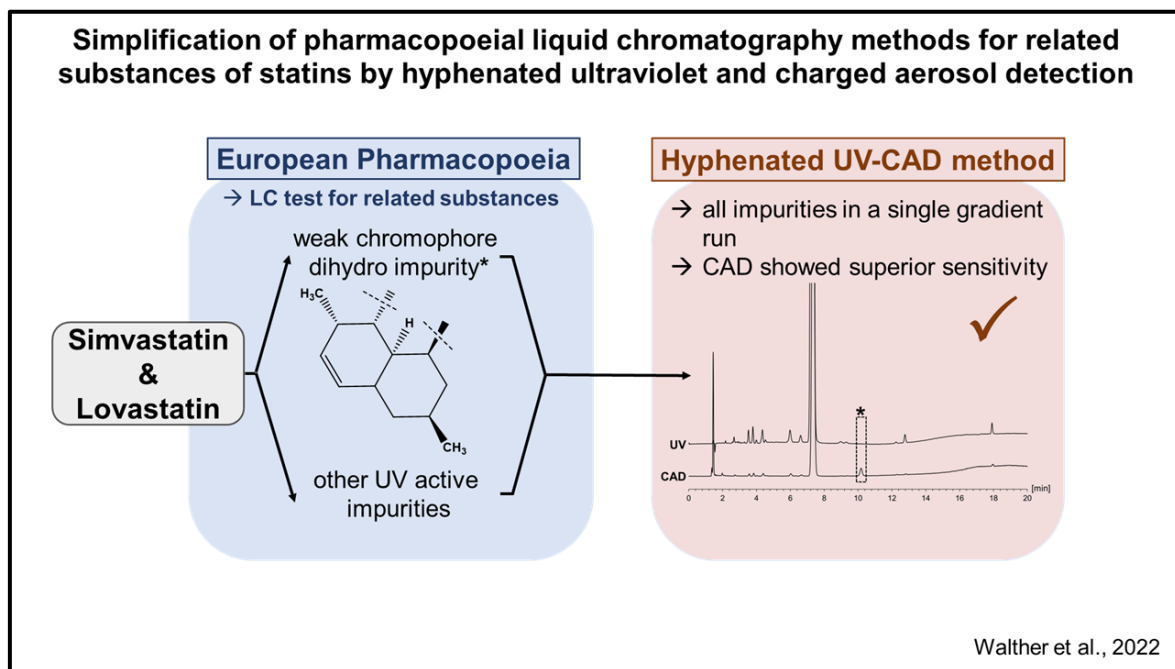
1. Introduction

The search for a universal detector in liquid chromatography (LC) which is able to determine all components of a sample – including analytes with unknown structure and showing uniform responses regardless of the physicochemical properties – has still not come to an end [1,2]. Each type of detector possesses its own requirements, such as a suitable chromophore for ultraviolet (UV) detection, the formation of stable, isolated molecular ions in the case of mass spectrometry or sufficiently low vapour pressures for the application of aerosol-based detectors [3]. By "cleverly" combining different detection principles, the spectrum of detectable analytes can be expanded considerably. If the standard UV detector, which works non-destructively, is connected in series with a mass spectrometer and with the charged aerosol detector (CAD) *via* a splitting T-piece, a detailed search for unknown impurities and the construction of comprehensive impurity profiles is possible [4,5]. Chromatographic systems equipped with tandem UV-CAD can be used to determine the relative response factors of unknown impurities for quality control of active pharmaceutical ingredients (API), eliminating the need for laborious enrichment, isolation, and characterization steps and enabling more precise mass balance studies [6,7]. The dependence of the CAD signal on the composition of the mobile phase can be resolved by the so-called inverse gradient compensation [2] and allows quantification of non-volatile analytes without any internal standard [8]. Moreover, hyphenated UV-CAD methods provide a valuable option for the impurity profiling of APIs with non- or weak chromophore impurities from synthesis [9,10].

In each instance – whether for a possible pharmacopoeial purpose or during drug development – it is desirable to detect all relevant impurities simultaneously with only a single, simple method.

With this in mind, our goal was to simplify the existing chromatographic tests for related substances in the European Pharmacopoeia (Ph. Eur.) for the two cholesterol-lowering drugs simvastatin and lovastatin. In addition to several UV-active impurities (see Figs. S1 and S2), the dihydro compound is described for these two structurally closely related APIs (see Fig. 1) [11,12]. Although complex total syntheses have been described in literature [13], the fermentative semisynthetic production has prevailed as more economical. The fungal natural product lovastatin is formed *via* the polyketide pathway by e.g., *Aspergillus terreus* [14], which can then be converted to the more active simvastatin [15]. As an intermediate product of the biosynthesis, dihydromonacolin L occurs as the origin of the two impurities without the conjugated double bond system [14].

According to the Ph. Eur., in order to control the content of these weak chromophore impurities, detection is carried out at 200 nm and at 238 nm for the other impurities. In the case of simvastatin, the chemical reference substance (*CRS)* of impurity K has to be purchased and an additional reference solution has to be prepared [11] for this purpose, and in the case of lovastatin, a second, isocratic 20 min lasting LC method for impurity E is described [12]. Thus, the alternative use of hyphenated UV and CAD offers cost and time savings. To facilitate a potential adaption of the pharmacopoeial tests, we have tried to stick closely to the existing methods.
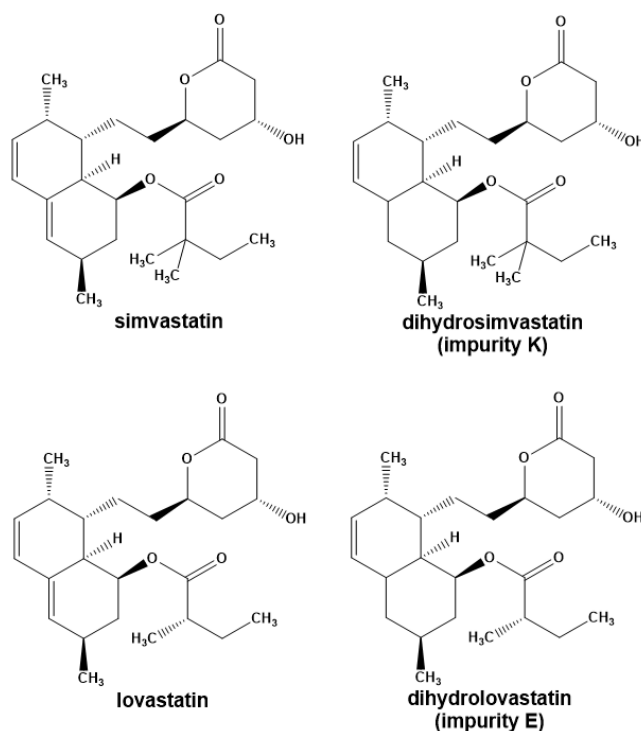

Fig. 1 Molecular structures of simvastatin and lovastatin as well as their weak chromophore dihydro impurities K and E, respectively, without conjugated double bond system

2. Material and methods

2.1 Chemical and reagents

CRS of simvastatin, simvastatin impurity K (dihydrosimvastatin), simvastatin for system suitability (containing simvastatin and impurities A – G, I and J), lovastatin and lovastatin for peak identification (containing lovastatin and impurities A – F) were bought from the EDQM (Strasbourg, France). Acetonitrile (ACN) for HPLC (gradient grade, ≥ 99.9 %), trifluoroacetic acid (TFA) for HPLC (≥ 99.0 %), and uracil (≥ 99 %) were purchased from Sigma Aldrich (Steinheim, Germany). Formic acid (FA) solution in water 49 – 51 % (m/m) for HPLC from Fisher Scientific (Schwerte, Germany) and concentrated 85 % (m/m) phosphoric acid for HPLC was bought from VWR International (Darmstadt, Germany). High-purity deionized water for HPLC was delivered by an in-house water purification system from Milli-Q® system (Merck Millipore, Schwalbach, Germany).

2.2 Apparatus

For hyphenated UV-CAD analysis a Thermo Scientific Vanquish™ Flex modular chromatographic system for inverse gradient compensation was used (Dwell volume 0.96 mL) consisting of a dual pump with online degasser, a thermostatted autosampler, a thermostatted column compartment with active pre-heater, and a diode array detector with standard flow cell in-line with a Vanquish™ Horizon CAD. The Chromeleon® data system Version 7.3 software was used to control the HPLC system and evaluate the data (all Thermo Fisher Scientific, Germering, Germany). The nitrogen gas for the CAD was produced by a Peak Scientific Corona Nitrogen 1010 generator (Düren, Germany) connected to the in-house compressed air system.

Comparative measurements for lovastatin according to the Ph. Eur. method with UV detection only were performed using a 1295 Waters Alliance Separation module with online degasser, thermostatted autosampler, thermostated column compartment and 995 diode array detector. For instrument control and data processing the Empower 3 2010 software was used (all Waters, Eschborn, Germany).

2.3 Preparation of solutions

Stock solutions were prepared by dissolving 20.0 mg of simvastatin in 10.0 mL (2.0 mg/mL), 10.0 mg lovastatin in 10.0 mL (1.0 mg/mL) and 4.0 mg dihydrosimvastatin in 100.0 mL (0.040 mg/mL), respectively. A mixture of equal volume fractions of water and ACN was used as solvent for all solutions. For chromatographic method development, a test solution was prepared by exactly weighing 2.0 mg simvastatin for system suitability and spiking with 200.0 µL of the stock solution of dihydrosimvastatin (corresponds to 0.40 % (m/m) of a 2.0 mg/mL test solution) before filling up to 1.0 mL. For the assessment of robustness, a test solution with 2.0 mg/mL simvastatin for system suitability and 0.050 % (m/m) dihydrosimvastatin was prepared analogue.

The lovastatin solution for peak identification (0.40 mg/mL) was prepared by accurately weighing 4.0 mg and dissolving in 10.0 mL of a mixture 40 % water (v/v) in ACN. This solution was then diluted in the same solvent mixture 1:200 to obtain a concentration of 0.50 % (v/v). All stock solutions and dilutions were stored at 2 – 8 °C and used for up to 3 days.

2.4 Determination of the inverse gradient delay volume

As reported by Scherer and Matysik [8], short 3 s pulses with 0.05 mg/mL uracil in a mixture of 30 % water in ACN (mobile phase B) were performed for the experimental determination of the delay volume between the pump for analytical separation (right side) and the pump for inverse gradient compensation (left side) (see Fig. 2a). At a flow rate of 0.4 mL/min with 30 % water in ACN (mobile phase A), the time delay from the pulse start to maximum CAD response was determined (see. Fig 2b). This was done for both the left pump and the right pump with both columns (n = 6). By multiplication with the flow rate, the delay volume for inverse gradient compensation was calculated from the time delay (Hypersil BDS: 527.6 µL; Hypersil Gold: 564.5 µL).
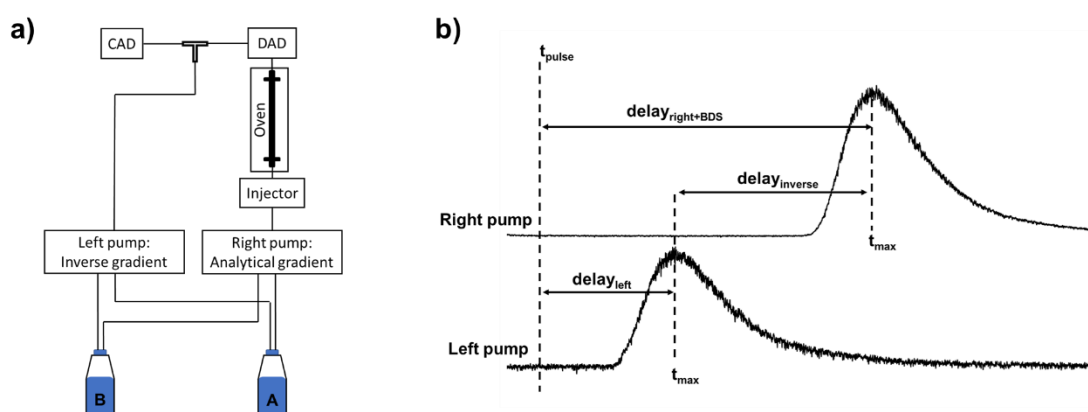
Fig. 2 Inverse gradient compensation
a) Schematic setup of the Vanquish™ LC-system used, consisting of a pump for inverse gradient compensation on the left side and the pump for analytical separation on the right side with injector, thermostatted column, diode array detector (DAD) and CAD after the T-piece
b) Determination of the delay time as the difference between the short pulse (t_{pulse}) with uracil and the maximum detector signal (t_{max}) for the left and right pump

2.5 Adaption of the pharmacopoeial method of simvastatin to UV-CAD

2.5.1 Chromatographic development

The method of the official monograph for the test for related substances [11] provides a 45-minute gradient run and applies a reversed phase column with C_{18} modified silica (end-capped and extra-dense bonded; 150 x 2.1 mm, 3.5 µm), a flow rate of 0.4 mL/min at a column temperature of 35 °C and an injection volume of 5 µL. Water with 0.1 % (v/v) concentrated phosphoric acid mixed with either 40 % (mobile phase A) or 95 % (mobile phase B) ACN (v/v) is used as eluent. To cover all 10 specified impurities (see Fig. S1) UV detection is performed at 238 nm and additionally 200 nm for dihydrosimvastatin.

To calculate the percentage contents of these impurities, a 0.4 % (m/m) solution with the *CRS* of impurity K must be measured at 200 nm in addition to a 0.1 % (m/m) dilution of the API at 238 nm.

For chromatographic separation, two C_{18} column from Thermo Fisher (150 x 2.1 mm, 3 µm), a Hypersil BDS and a Hypersil Gold, were compared. The injection volume (5 µL) and the flow rate (0.4 mL/min) were adopted from the monograph. As volatile alternatives to phosphoric acid, FA and TFA were tested in the concentration range of 0.1 – 0.01 % (v/v). The Ph. Eur. method (see Table 1, left column) was modified to improve the resolution (R_s) between impurity B – J and J – C by varying the column temperature, the ACN percentage and the duration of the three gradient steps (see Table 1), respectively, in addition to adjusting the isocratic hold due to the lower dwell volume of the Vanquish™ LC system. For this purpose, a solvent blank and subsequently the system suitability solution spiked with 0.4 % (m/m) impurity K were injected at respective conditions and peak-to-valley ratios (p/v) were determined. The final gradient conditions (see Table 1, right column) were then used to investigate the influence of the evaporation temperature (50 – 65 °C), the data collection rate (1 – 20 Hz) and the filter constant (1 – 10 s) on the signal-to-noise ratio (S/N) of impurity K.

Table 1
Gradient program of the simvastatin method for the test for related substances from the European Pharmacopoeia (left) and the adapted final UV-CAD method (right)

	European Pharmacopoeia			Final UV-CAD method		
	Time [min]	0.1 % H_3PO_4 (v/v) in water/ACN		Time [min]	0.05 % (v/v) TFA in water	ACN % (v/v)
		40/60 (v/v)	5/95 (v/v)			
Isocratic hold	0 – 4	100	0	0 – 4.6	65	35
1. Step	4 – 5	100 → 80	0 → 20	4.6 – 5.6	65 → 49	35 → 51
2. Step	5 – 33	80 → 60	20 → 40	5.6 – 26	49 → 37	51 → 63
3. Step	33 – 34	60 → 0	40 → 100	26 – 27	37 → 5	63 → 95
Flushing	34 – 45	0	100	27 – 38	5	95
Re-equilibration	45 – 47	0 → 100	100 → 0	38 – 40	5 → 65	95 → 35
	47 – 56	100	0	40 – 48	35	35

2.5.2 Final hyphenated UV-CAD method

For the validation experiments and for the robustness study, the Hypersil BDS column was used. In contrast to the pharmacopoeial method, a 0.05 % (v/v) TFA solution was applied, and the gradient was adapted as shown in Table 1 (right column). The CAD settings were set to 55 °C evaporation temperature, 5 Hz data collection rate, 5 s filter constant and a power function value of 1.0.

2.5.3 Robustness via design of experiments (DoE)

Robustness of the final UV-CAD method was investigated using a two-level (+1, -1) Plackett-Burman design including these 7 factors and 4 dummy factors: concentration of TFA (± 0.005 %), column temperature (± 2 °C), flow rate (± 0.02 mL/min), initial ACN percentage (± 2 %), final ACN percentage (± 2 %), duration of the isocratic hold at the beginning (± 0.5 min) and the evaporation temperature of the CAD (± 3 °C). The resulting 12 runs were performed in random order, with a blank run for equilibration in each case (see Table S1). The dependent variables were, on the one hand, the p/v between the critical peak pairs impurity E – F, B – J as well as J – C and, on the other hand, the S/N of impurity K with the CAD. The design and statistical analysis was carried out using Design Expert 12 software (Stat-Ease Inc., Minneapolis, US).

2.6 Adaption of the pharmacopoeial method of lovastatin to UV-CAD

2.6.1 Pharmacopoeial method as reference

According to the officinal monograph of the Ph. Eur. [12], two separate LC methods are required to control all six specified impurities in lovastatin API. The test for impurity E (dihydrolovastatin) was performed isocratically using an Agilent Eclipse C_8 column (250 x 4.6 mm, 5 µm) at a flow rate of 1.5 mL/min and 40 °C column temperature. The mobile phase consisted of 35 % (v/v) of a 1.1 g/L phosphoric acid solution and 65 % (v/v) ACN. The injection volume was set to 10 µL and UV detection was performed at 200 nm applying a correction factor of 1.6.

Testing for the other related substances (see Fig. S2), gradient elution was carried out with 0.1 % (v/v) concentrated phosphoric acid in water as mobile phase A and ACN as mobile phase B. At a constant flow rate of 1.5 mL/min and after an isocratic hold of 7 min, the percentage of mobile phase B increased from 60 % first to 65 % within 2 min and then to 90 % in the next 6 min. This high organic percentage was maintained for 5 min before the column was re-equilibrated. The injection volume was equally 10 µL, but the UV detection was performed at 238 nm and the column temperature was set to 25 °C.

2.6.2 Transfer to UV-CAD

As stationary phase an Agilent Rx C_8 column (250 x 4.6 mm, 5 µm) was employed for separation and as mobile phase A water with 0.05 % (v/v) TFA. Analogous to the Ph. Eur. monograph, ACN was used as organic modifier, a flow rate of 1.5 mL/min, a column temperature of 40 °C, an injection volume of 10 µL and the same gradient program. For hyphenated UV-CAD detection, on the one hand the wavelength of 238 nm was conserved and on the other hand the CAD settings were adjusted to an evaporation temperature of 60 °C, a data collection rate of 5 Hz, a filter constant of 5 s and a power function value of 1.0. Under otherwise identical conditions, complementary isocratic measurements were carried out with 65 % (v/v) ACN.

3. Results and discussion

3.1. Simvastatin hyphenated UV-CAD method

3.1.1 Chromatographic development

As a starting point, the system suitability solution spiked with dihydrosimvastatin was injected onto both Hypersil C_{18} columns, using 0.1 % (v/v) TFA as a volatile substituent for phosphoric acid and the gradient program of the compendial monograph [11]. Since the elution order with both columns matched the reference chromatogram from the EDQM *Knowledge Database* [16], peak assignment was straightforward. As expected, the weak chromophore impurity K was only detectable with the CAD (see Fig. 3). The UV-active impurities were also visible, but UV detection was superior. Since no co-elution of impurity K with any other analyte was observed in the UV trace at the same time, the simultaneous detection of all specified impurities using the hyphenated UV-CAD approach seems feasible.

The chromatographic selectivity of the two columns tested was similar except for the insufficient separation of the three impurities B, J and C with the Hypersil Gold column (see Fig. 3c and 4a). The observation that the state-of-the-art Hypersil Gold column performed worse in this case may be due to its larger specific surface area of 220 m^2/g. The legacy Hypersil BDS column (170 m^2/g) is more comparable to the Zorbax Eclipse XDB C_{18} column (180 m^2/g) used for compendial method development [16]. Although there are theoretical studies on surface-specific retention factors [17], they are not yet systematically used in method transfer. Since the level of background noise of the CAD was comparable (approx. 0.8 pA) for both columns, the Hypersil BDS was selected for further optimisation. To check the system suitability, the monograph employs p/v between impurity E – F as well as C – J and should be at least 1.5. This requirement was clearly met with the Hypersil BDS column for these two critical peak pairs (p/v: E – F = 17.1 and C – J = 4.6). However, the separation performance between impurity B and J was not satisfactory with a p/v of only 1.1 and the improvement to a value above 1.5 for this third critical peak pair was imperative. That this could be a third critical peak pair can also be seen in one of the chromatograms in the *Knowledge Database* (partial co-elution) [16].
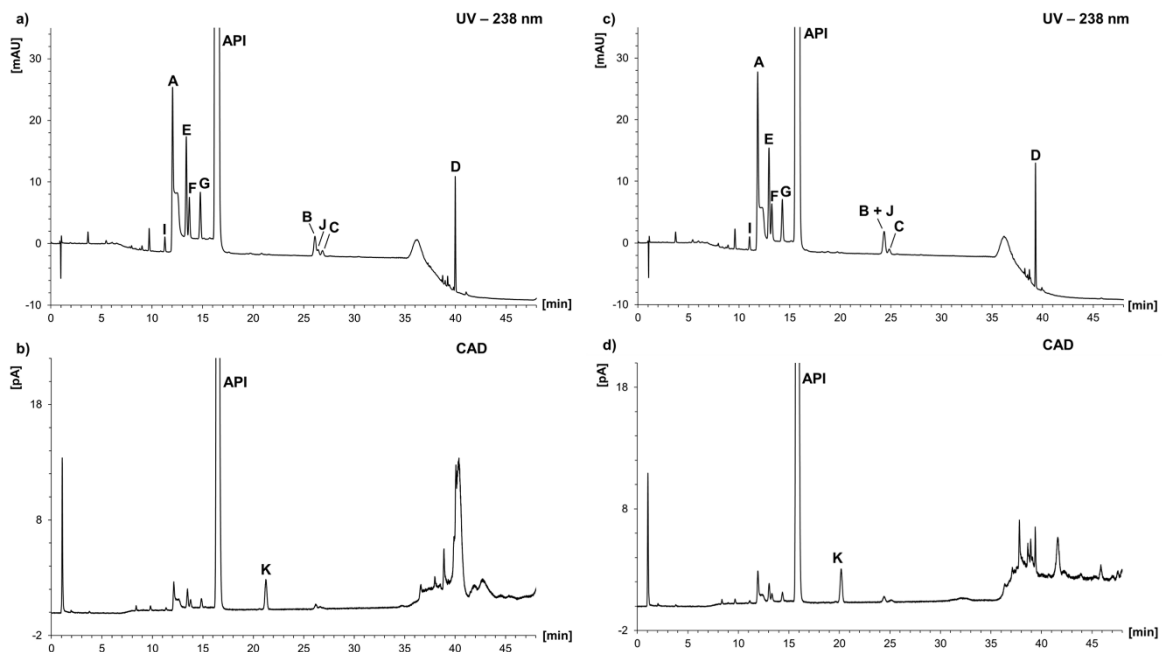
Fig. 3 Chromatograms of the simvastatin system suitability solution (containing impurity A – G + I – J) spiked with dihydrosimvastatin (impurity K) with the Hypersil BDS column applying either UV detection at 238 nm (a) or the CAD (b) and with the Hypersil Gold column applying either UV detection at 238 nm (c) or the CAD (d); the gradient program of the European Pharmacopoeia was used, but phosphoric acid was substituted by TFA (for more details see section 2.5.1)

Initially, FA was evaluated as an alternative to TFA and whether a reduction of the concentration of the two acidic modifiers in favour of the CAD's sensitivity is possible. Even though both acids are considered volatile, they contribute to the level of the background current [18]. Although, except for impurity A with its hydroxy acid function, the other analytes are not ionisable and there were no differences in chromatographic selectivity, FA proved to be disadvantageous. Compared to the stronger acid TFA, a decrease in concentration to lower than 0.05 % (v/v) was impossible, as the peak shape of impurity A deteriorated – evident from the higher value of the asymmetry factor (A_s) of 1.42 compared to A_s = 1.16 with TFA – and at the same time the change of the baseline during the gradient section was more pronounced in UV detection (FA -80 mAU vs. TFA -12 mAU). Further reduction to 0.01 % (v/v) TFA was not reasonable due to an unacceptable peak shape of impurity A (A_s > 2). For the optimisation of the CAD settings (see section 3.1.2) and in the final method, a concentration of 0.05 % (v/v) TFA was therefore used.

To improve the separation of the peak trio of impurities B, J and C, the recommended first step in gradient elution is to adjust the gradient delay or dwell volume [19,20]. According to the *Knowledge Database*, the LC system used for method development had a dwell volume (D) of 1.2 mL [16]. Since the dwell volume of the Vanquish™ LC system (D = 0.96 mL) used here is lower, a difference of + 0.6 min was calculated with the formula in chapter 2.2.46 of the Ph. Eur. [19] by which the gradient time points must be extended. Although this adjustment improved the p/v of the peak pairs E – F and J – C, the separation performance diminished for the additional critical peak pair B – J (see Fig. 4b).
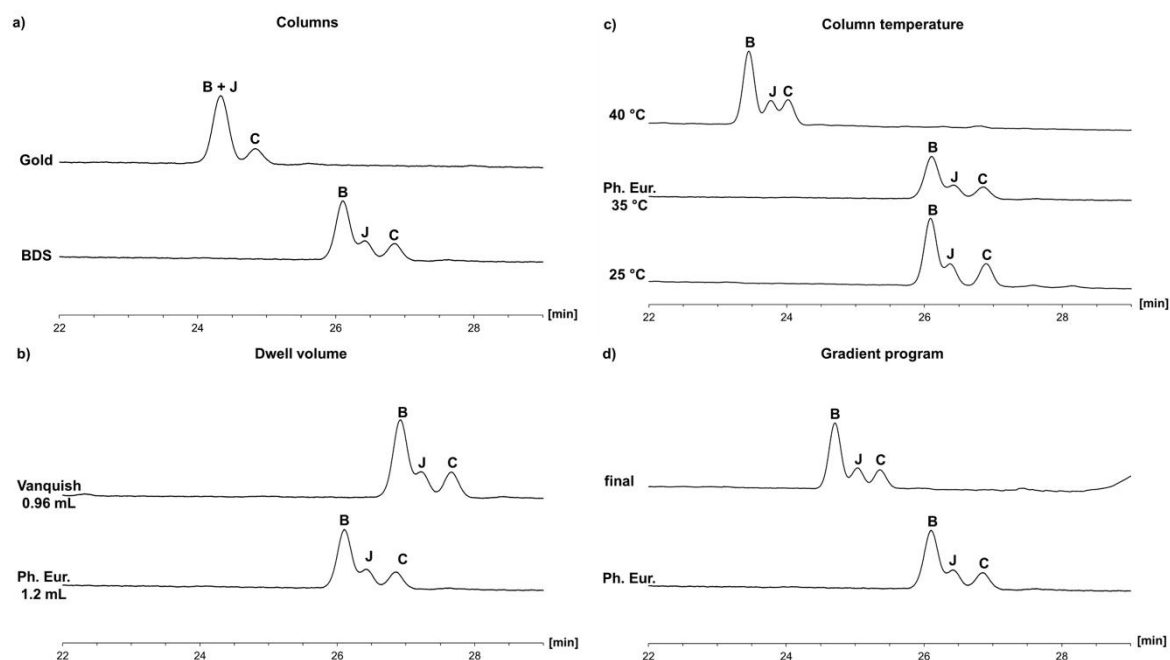
Fig. 4 Sections of the chromatograms showing the separation of impurities B, J and C
a) Comparison of the Hypersil BDS (bottom) and Gold (top) columns applying the gradient program of the European Pharmacopoeia (Ph. Eur.)
b) Comparison of the pharmacopoeial gradient program (bottom) and the gradient program adapted to the lower dwell volume of the chromatographic system used here (top)
c) Comparison of the influence of the column temperature with an increase of 5 °C (top) and a decrease of 10 °C (bottom), respectively, in relation to the Ph. Eur. Method
d) Comparison of the gradient program only adapted to the dwell volume (bottom) and with the final modifications (top) to a lowered initial ACN percentage of 35 % (v/v) and an increased gradient slope during the second step (for more details see section 2.5.2)

3.1.2 Detector settings

Data collection rate of the UV detection at 238 nm was set to 20 Hz based on the peak width of the narrowest peak. Unlike UV detection, the level of background noise of the CAD and the analytes response is more affected by the exact composition of the mobile phase, e.g. particle formation during evaporation is strongly influenced by the viscosity of the mobile phase and thus by the percentage of the organic modifier [10,18]. With the newer CAD instruments, in addition to the data acquisition rate and the filter constant, the evaporation temperature can also be varied.

As expected, increasing the evaporation temperature reduced the level of background current, as less semi-volatile mobile phase impurities arrive at the detector [10,18]. However, the peak height of the analyte decreased at temperature above 55 °C and the S/N worsened because the reduction in background noise was less pronounced (see Table S3).

This semi-volatile behaviour can be explained by a co-evaporation with the ACN fraction from the water/organic aerosol droplets [21]. At an evaporation temperature of 55 °C – with a filter constant of 5 s and a data collection rate of 5 Hz for the best compromise between satisfactory peak shape and low noise – a S/N of 240 was obtained for impurity K at a level of 0.4 % (m/m). This value allows a first estimation that with the applied settings and chromatographic conditions the CAD is capable of sensitive control of this impurity to the compendial reporting threshold of 0.05 % (m/m).

3.1.3 Inverse gradient compensation

Since – as briefly mentioned above – the CAD signal can be influenced by the mobile phase, the detector response during gradient elution increases depending on the ACN percentage [18]. The advantage of the CAD as a universal detector for analytes with comparable physicochemical properties therefore technically speaking applies only to isocratic methods [1-3,8]. This contradicts the idea of dispensing with the additional reference solution of impurity K *CRS* and instead also using the dilution of the simvastatin test solution for calculation of the percentage contents, since the API elutes earlier in the gradient and therefore results in an overestimation.

However, since gradient elution is inevitable in many separation problems, the inverse gradient compensation was successfully developed as early as 2006 by Górecki et al. [2] to account for this phenomenon. Using the setup shown in Fig. 2a and the determined delay volume of 527.6 µL, the composition of the mobile phase entering the CAD is kept constant throughout the gradient elution *via* an inverse gradient. This can be realised by three different approaches: 1) with the "keep solvent composition" approach the gradient programme is exactly run inverted, 2) the "maximize B" approach can be used to increase the percentage of the organic modifier for a higher detector response and 3) the "minimize flow" approach to maintain a constant composition of the mobile phase at the lowest possible flow rate for the inverse gradient [3]. The first two approaches cause the flow rate to double and thus also the absolute amount of semi-volatile impurities in the mobile phase detected per time unit on the electrometer. Since in our case sensitive detection in the ng/column range is required, the minimize flow approach was chosen, resulting in flow rate of 0.24 mL/min and a time delay of 0.64 min for the inverse gradient (see Table S4). Comparing the results with and without inverse compensation in Table 2, there is no significant overestimation of the %-content of impurity K in the relevant concentration range

from the reporting threshold to the pharmacopoeial limit. This is probably due to the low gradient slope of 0.59 %/min, so that the difference between the API peak and the impurity K is only about 2.3 % (v/v) ACN.

Table 2
Comparison of the percentage contents of impurity K using a 0.1 % (m/m) dilution of the API without and with inverse gradient compensation at three different concentration levels

level		analytical gradient	inverse gradient
0.05 %[a] (m/m) (reporting threshold)	n = 3	0.054 %	0.052 %
	RSD [%]	1.30	2.70
	S/N	29	12
0.2 %[a] (m/m)	n = 3	0.19 %	0.20 %
	RSD [%]	1.30	1.42
0.4 %[a] (m/m) (pharmacopoeial limit)	n = 3	0.38 %	0.40 %
	RSD [%]	0.71	1.14

[a] in per cent (m/m) of the API sample solution

Since the inverse gradient compensation increases both the instrumental requirements and the potential for error and at the same time diminished the sensitivity of the CAD (see S/N values in Table 2), it is advantageous not to be reliant on it. Nevertheless, with the inverse compensation in this case, the method would still be sensitive enough, as the limit of quantification (LOQ) with a S/N ≥ 10 is below the reporting threshold of 0.05 % (m/m) [22]. Moreover, since the inverse gradient also leads to increased consumption of reagents, especially organic solvents [3], it is also more sustainable to go without.

3.1.4 Robustness

Although the current ICH guideline on *Validation of Analytical Procedures Q2 (R1)* only strongly recommends the execution of robustness studies [23], this parameter describes the ability of a method to provide reliable results in different laboratories and therefore plays an important role especially for its pharmacopoeial application. To determine the influence of a larger number of factors in a time- and resource-saving way, and since only the significance of the main effects is examined, which are only varied within a limited range, two-level screening designs such as (minimal) fractional factorial or especially Plackett-Burman designs have become established for the evaluation of robustness [24,25].

In addition to the p/v of the three critical peak pairs (E – F, B – J, J – C) from method development work, the S/N of impurity K was also included in the study to prove the suitability of the CAD. Table S5 summarises the measured values of these four variables based on which the statistical evaluation was carried out. Half-normal plots and Pareto charts were used to graphically assess whether one or more of the factors examined had a statistically significant influence [24,26]. In the case of the CAD´s S/N of dihydrosimvastatin, no factor showed a significant effect, and the application of the hyphenated UV-CAD system

can be considered robust. In the half-normal plot, a dummy factor showed the largest deviation from the straight line, but its standardised effect did not intersect the critical *t*-value limit for statistical significance (95 % confidence interval) in the corresponding Pareto chart (see Fig. S3). In contrast, significant effects were identified graphically (see Fig. S3) and mathematically by ANOVA (see Table S6) for the chromatographic separation, which is not surprising in view of the previous findings from method development. Regarding the critical peak pair of impurity E and F, the initial ACN concentration and the column temperature were statistically significant. However, the worst measured p/v of 6.4 in run no. 12 was considerably higher than the required minimum value of 1.5 from the system suitability test in the monograph and variations of both factors within this range (± 2 % and ± 2 °C) are tolerable [26]. Similarly, although column temperature had a statistically significant effect (see Fig. S3) on the resolution between impurities J and C, the limit was not undercut even in the worst cases (see Table S5 runs no. 2 and 12).

By ANOVA, the flow rate, the initial ACN percentage and the column temperature were identified as statistically significant factors in the case of the third critical peak pair B – J, with the first two having a negative effect and only the column temperature having a positive effect on the p/v (see Fig. 5). This is reflected in the two runs no. 1 and 8 (combination of low temperature and low initial ACN content) in which the minimum p/v of 1.5 was not reached. Precise control of flow rate and column temperature is standard on modern LC instruments. In practice, this means that these three factors must be observed particularly closely and the p/v between impurity B and J should be included as an additional system suitability criterion. Based on the model created here (see Table S7), the increase of the column temperature or the decrease of the initial ACN percentage and/or the flow rate may be recommended in case of insufficient separation performance.
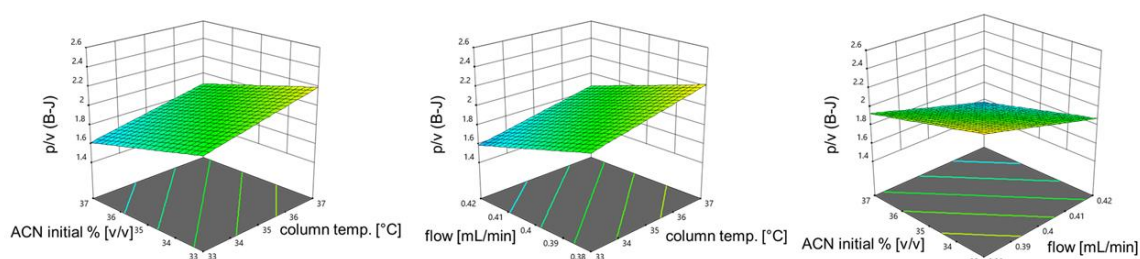
Fig. 5 3D response surface plots showing the dependence of the peak-to-valley ratio (p/v) between impurity B and J as a function of the three statistically significant factor initial ACN percentage, flow rate and column temperature

3.1.5 Validation

To demonstrate the suitability of the LC method adapted to UV-CAD for the simultaneous detection of all specified related substances, the 9 UV-active impurities and dihydrosimvastatin measured by the CAD, in a single, shortened run as an alternative to the current LC-UV method in the Ph. Eur., validation experiments were performed. In addition to impurity K, lovastatin and simvastatin were included as model analytes for UV detection at 238 nm, and specificity, LOQ, linearity, accuracy, and precision were investigated with respect to the ICH guideline Q2 (R1) [23].

The specificity was proven by comparing the UV and CAD trace of a chromatogram of the system suitability solution spiked with impurity K with a blank chromatogram (see Fig. 6).
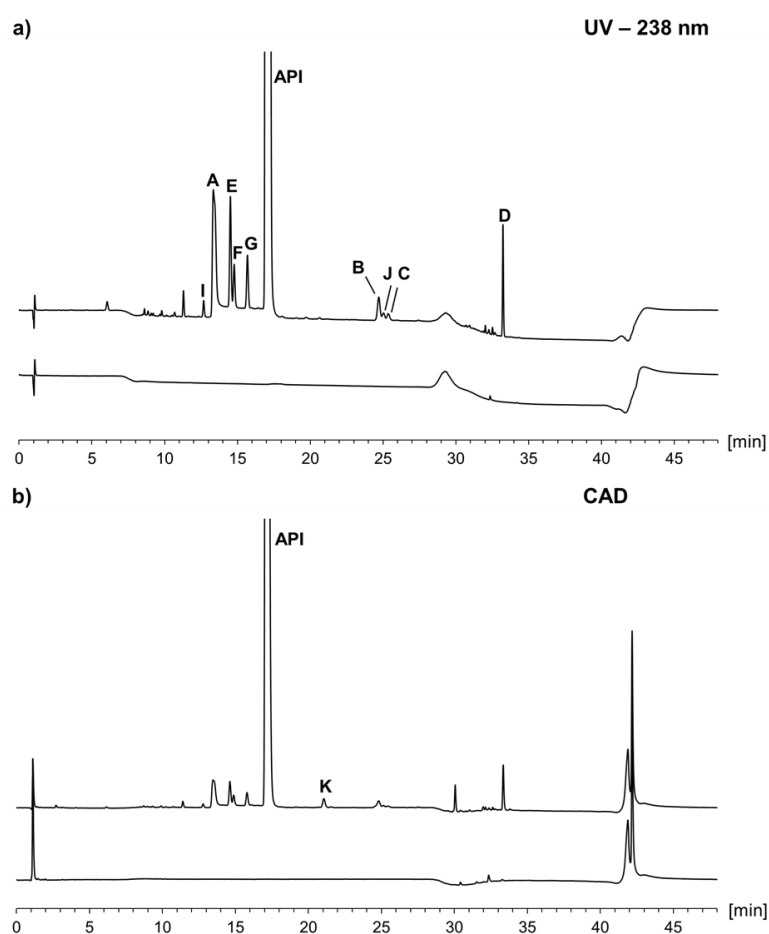
Fig. 6 Chromatogram overlay of the system suitability solution spiked with impurity K and a blank applying the final gradient program and either a) UV detection at 238 nm or b) charged-aerosol detection (for chromatographic details see section 2.5.2)

To check the sensitivity of both detector types, the LOQ for impurity K (CAD) and lovastatin (UV) were determined using the signal-to-noise (S/N) approach [19,23]. Both LOQs obtained with CAD and UV (see Table 3) are significantly lower than the reporting threshold of 0.05 % (m/m) required by ICH guideline Q3A for drug substances with a maximum daily dose of less than 2 g per day [22]. Subsequently, the range for both impurities was investigated from the reporting threshold of 0.001 mg/ml ("low") to a concentration of 120 % of the pharmacopoeial limit ("high"). For this purpose, besides to proof linearity by means of calibration curves with 5 or 6 levels, respectively, in the case of impurity K (n = 3), the accuracy, expressed as recovery rate, and the precision were verified (see Table 3). Although UV detection at 238 nm is more sensitive, as can be seen from the slope of the calibration functions, the CAD for the weak-chromophore impurity K is a proper alternative that allows a determination with comparable precision and accuracy. Using the slope of the CAD´s calibration curve for simvastatin (y = 52.0 x + 0.0533; R^2 = 0.9951), a response factor of 0.96 was calculated. This negligible difference underlines the observations from the inverse gradient compensation in section 3.1.3 and a relative quantification by area comparison as used in the Ph. Eur. is valid.

Table 3
Results from validation experiments for impurity K (dihydrosimvastatin) with the CAD and lovastatin with UV detection applying the final chromatographic conditions (see section 2.5.2)

parameter	level	CAD	UV at 238 nm	
		impurity K	lovastatin	simvastatin
recovery rate [%] (n = 3)	low[a]	97.9	91.6 %	93.3 %
	middle[b]	103.9 %	97.1 %	96.8 %
	high[c]	91.6 %	99.5 %	99.4 %
repeatability RSD (n = 6)	low[a]	1.92 %	0.26 %	0.45 %
	middle[b]	1.11 %	0.11 %	0.12 %
	high[c]	1.60 %	0.090 %	0.11 %
inter-day precision RSD (n = 12)	low[a]	2.14 %	0.26 %	1.03 %
	middle[b]	1.09 %	2.99 %	3.09 %
	high[c]	4.62 %	0.70 %	0.69 %
linearity (n = 3)	y-axis	0.0269	0.278	0.278
	slope	49.73	678.64	668.55
	R^2	0.9974	0.9975	0.9974
LOQ (S/N ≥ 10)	µg/mL	0.35	0.050	n.a.[e]
	[%][d]	0.0175	0.0025	
	ng/column	1.75	0.25	

[a] 0.001 mg/mL of both impurities (≙ reporting threshold of the pharmacopoeial method).
[b] 0.004 mg/mL impurity K and 0.005 mg/mL lovastatin
[c] 0.0096 mg/mL impurity K and 0.012 mg/mL lovastatin (≙ 120 % of the pharmacopoeial limit).
[d] in per cent (m/m) of the API sample solution
[e] not applicable

3.2 Lovastatin hyphenated UV-CAD method

Due to the shared way of synthesis [14,15], the non-chromophore dihydro derivative occurs as an impurity in lovastatin API batches. Since in the case of dihydrolovastatin (impurity E) no *CRS* is available from the EDQM, the same solutions were analysed once with the pharmacopoeial method [12] and then with the adapted UV-CAD method for direct comparison. Analogous to the simvastatin method, phosphoric acid was replaced by 0.05 % (v/v) TFA. By comparing a chromatogram for peak identification and a blank injection, specificity was demonstrated for this method. Furthermore, no difference in elution order, i.e. selectivity, was evident and the system suitability tests (p/v ≥ 3.0 between impurity F and the API; R_s ≥ 5.0 between the API and impurity E) were also met with both methods (see Fig. 7). The resolution between the two critical peak pairs API – impurity E and impurity F – API was better with the new method on the modern LC system (R_s Ph. Eur. method 8.8/2.5 vs. R_s UV-CAD method 11.0/3.2).
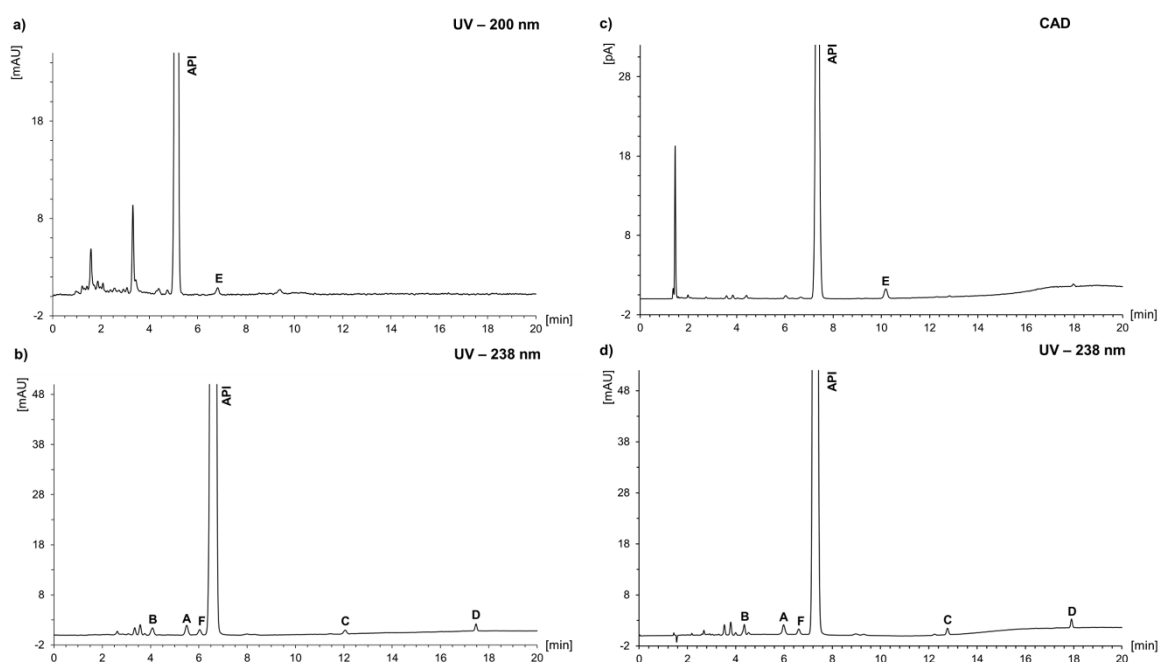
Fig. 7 Comparison of the two methods of the European Pharmacopoeia (left side) with the hyphenated UV-CAD method (right side) using the solution for peak identification
(for chromatographic details see chapter 2.2.6)
a) test for impurity E by isocratic elution with UV detection at 200 nm
b) test for the other related substances by gradient elution with UV detection at 238 nm
c) adapted gradient method using the CAD (60 °C evaporation temperature, 5 Hz, 5 s) for detection of impurity E
d) adapted gradient method using UV detection at 238 nm for the other related substances

However, for the CAD settings, increasing the evaporation temperature to 60 °C was beneficial for the S/N, probably due to the high flow rate of 1.5 mL/min. To compare the accuracy of the two methods without reference substances of the impurity, a 1:200 dilution was used for relative quantification.

The peak area of impurity E from the chromatogram of the solution for peak identification was related to peak area of the lovastatin peak from the chromatogram of the dilution, which corresponds to 0.5 %. The isocratic Ph. Eur. method at 200 nm using the correction factor of 1.6 yielded a content of 0.725 % (n = 6, ± 3.64 % RSD) compared to 0.783 % (n = 6, ± 1.17 % RSD) with the adapted UV-CAD method. Since, analogous to the simvastatin method, impurity E eluted in the gradient after the API at a slightly higher ACN percentage and this theoretically generated a higher detector response, isocratic CAD measurements were carried out with 65 % (v/v) ACN (n = 4 solution for peak identification and 1:200 dilution). The content of 0.784 % (± 1.32 % RSD) determined here complied with the value found in the gradient elution. This deviation in the content can possibly be explained by the significantly poorer sensitivity of UV detection at 200 nm compared to CAD. In the chromatogram of the 0.5 % dilution the lovastatin peak had a S/N of 83.8 using the CAD and only 12.1 at 200 nm with the Ph. Eur. method. In the case of UV detection at 238 nm for the other related substances, there was no significant difference in content between the two methods. Switching to a hyphenated UV-CAD method not only saves time and reagents by using a single method for all related substance, but also seems to be more accurate for the controlling this weak chromophore impurity.

4. Conclusion

This study provides another example of the successful application of hyphenated UV-CAD methods to upgrade existing pharmacopoeial methods. For both APIs, the goal of simultaneously detecting all related substances in only a single run each was achieved by replacing phosphoric acid with the volatile TFA in the mobile phase. Despite the use of a gradient, no inverse compensation with a second pump was necessary to compensate for the different response of the CAD in the case of simvastatin. The omission of this not only simplifies the instrumental setup but also brings better sensitivity for purity control at low concentrations. By systematically investigating robustness of the adapted simvastatin method using DoE the significant factors relating to critical separation were identified and how these can be reasonably adjusted. An expansion of the system suitability test to include the third critical peak pair (impurity B and J) and the CAD´s S/N seems sensible for practical use. Besides the robust performance (also analysed by means of DoE), validation experiments for the CAD demonstrated on the one hand the high sensitivity for the weak chromophore dihydrosimvastatin (LOQ of 1.75 ng/column) and on the other hand a precise and accurate determination was shown for the relevant range. The transfer to the structurally related lovastatin worked without any problems. By using the modern Vanquish™ Flex LC system, improved separation performance was achieved here and a future transfer to a more contemporary shorter column with smaller particles could provide further improvement while reducing run time.

Declaration of competing interest

Supplementary material

Fig. S1 Molecular structures of the UV-active simvastatin specified impurities A-G + I-J

Fig. S2 Molecular structures of the UV-active lovastatin specified impurities A-D + F

a)

S/N

b)

p/v (E-F)

c)

p/v (J-C)

d)
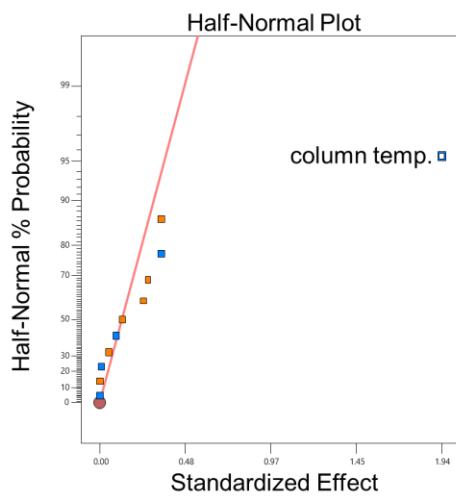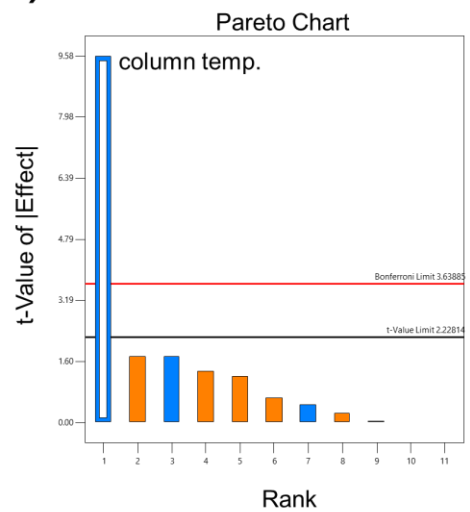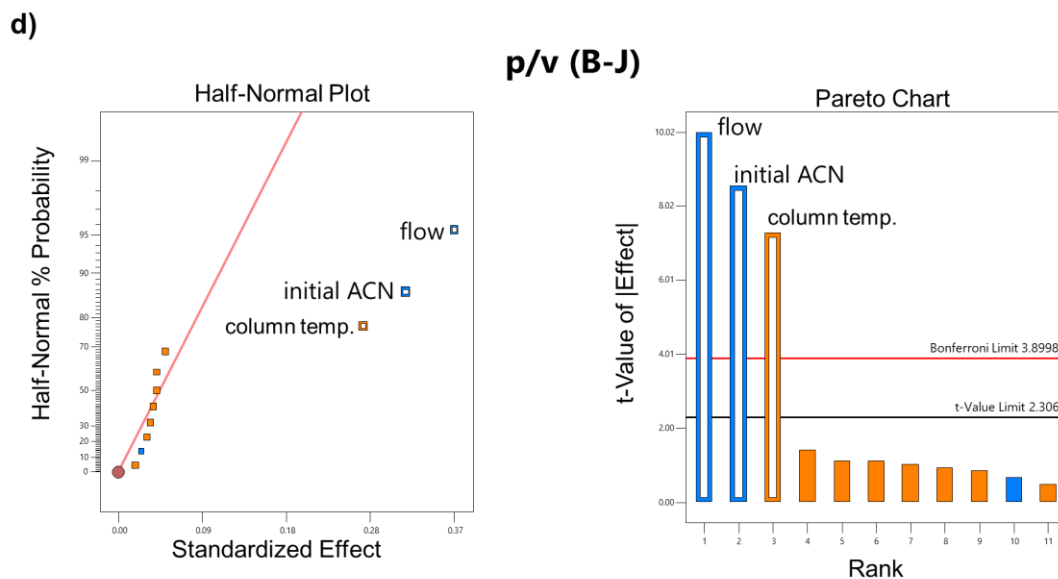
Fig. S3 Half-normal plots and corresponding Pareto charts of the investigated variables a) signal-to-noise ratio (S/N) of impurity K with the CAD, b) peak-to-valley-ratio (p/v) of the impurities E and F, c) p/v of the impurities J and C as well as d) p/v of the impurities B and J for graphically identification of the statistically significant factors

Table S1

Randomized Placket-Burman experimental plan of the robustness study for the simvastatin UV-CAD method with the 7 experimental factors A (TFA concentration in % v/v), B (column temperature in °C), C (evaporation temperature in °C), D (flow rate in mL/min), E (duration of isocratic hold in min), F (initial ACN ratio in % v/v) and G (final ACN ratio in % v/v) as well as the 4 dummy factors H – K (-1, 1)

Std	Run	A	B	C	D	E	F	G	H	I	J	K
7	1	0.055	33	52	0.38	5.1	33	97	+1	-1	+1	+1
10	2	0.045	37	58	0.42	4.1	33	93	+1	-1	+1	+1
6	3	0.045	33	52	0.42	4.1	37	97	-1	+1	+1	+1
9	4	0.055	37	58	0.38	4.1	33	97	-1	+1	+1	-1
4	5	0.045	37	52	0.42	5.1	33	97	+1	+1	-1	-1
8	6	0.055	37	52	0.38	4.1	37	93	+1	+1	-1	+1
3	7	0.055	33	58	0.42	4.1	37	97	+1	-1	-1	-1
11	8	0.055	33	58	0.42	5.1	33	93	-1	+1	-1	+1
1	9	0.055	37	52	0.42	5.1	37	93	-1	-1	+1	-1
5	10	0.045	33	58	0.38	5.1	37	93	+1	+1	+1	-1
2	11	0.045	37	58	0.38	5.1	37	97	-1	-1	-1	+1
12	12	0.045	33	52	0.38	4.1	33	93	-1	-1	-1	-1

Table S2

Data on the separation parameters resolution (R_s) and peak-to-valley ratio (p/v) for the critical peak pair E and F under the conditions analogous to Fig. 4

Fig. 4	Condition	R_s* impurities E – F	p/v* impurities E – F
a)	Gold	1.19	10.64
	BDS	1.44	16.58
b)	Dwell volume	1.44	21.79
c)	40 °C	1.33	10.27
	25 °C	1.48	19.78
d)	Gradient	1.15	9.36

* calculated according to the European Pharmacopoeia

Table S3

Data on the influence of the evaporation temperature on the peak height and signal-to-noise ratio (S/N) of impurity K (0.04 mg/mL) using the CAD (10 Hz data rate, 1 s filter constant)

Evaporation temperature	Height impurity K	S/N* impurity K
50 °C	2.50 pA	165
55 °C	2.54 pA	185
60 °C	2.45 pA	178
65 °C	2.30 pA	168

* calculated according to the European Pharmacopoeia

Table S4
Gradient program for the inverse gradient compensation using
the minimize flow approach and a flow rate of 0.24 mL/min based
on the experimentally determined delay volume of 527.6 µL

t [min]	0.05 % TFA in water	ACN
0 – 0.64	0 %	100 %
0.64 – 5.24	0 %	100 %
5.24 – 6.24	0 → 26.7 %	100 → 73.3 %
6.24 – 26.64	26.7 → 46.7 %	73.3 → 53.3 %
26.64 – 27.64	46.7 → 100 %	53.3 → 0 %
27.64 – 38.64	100 %	0 %
38.64 – 40 64	100 → 0 %	0 → 100 %
40.64 – 48.64	0 %	100 %

Table S5
Measured values of the four dependent variables according to the experimental
design

Std	Run	S/N[a] Impurity K	p/v[b] (E – F)	p/v[b] (B – J)	p/v[b] (J – C)
7	1	75.3	8.92	1.42	4.98
10	2	92.4	6.55	1.96	2.20
6	3	101.5	7.94	1.70	2.28
9	4	108.1	6.82	2.47	2.44
4	5	116.6	9.16	1.85	4.02
8	6	88.9	7.32	2.16	3.80
3	7	118.1	7.76	2.05	2.27
11	8	103.6	9.13	1.46	4.70
1	9	113.8	8.24	2.03	2.37
5	10	114.0	7.17	1.76	3.95
2	11	110.8	7.60	2.00	3.93
12	12	101.5	6.40	2.05	2.20

[a] signal-to-noise ratio
[b] peak-to-valley ratio

Table S6 Overview of the statistical evaluation by ANOVA of the Plackett-Burman Design for the 3 dependent variables showing statistically significant factors

ANOVA for selected factorial model: p/v (E – F)					
Source	Sum of Squares	Degrees of Freedom	Mean Square	F-value	p-Value
Model	9.80	2	4.90	106.77	< 0.0001
B-column temperature	2.60	2	2.60	56.76	< 0.0001
F-ACN initial	7.19	2	7.19	156.77	< 0.0001
Residual	0.4129	9	0.0459		
Cor Total	10.21	11			
Fit Statistics					
Std. Dev.	0.2142		R^2	0.9596	
Mean	7.75		Adjusted R^2	0.9506	
C.V. %	2.76		Predicted R^2	0.9281	
			Adeq. Precision	23.1576	

ANOVA for selected factorial model: p/v (J – C)					
Source	Sum of Squares	Degrees of Freedom	Mean Square	F-value	p-Value
Model	11.25	1	11.25	91.75	< 0.0001
B-column temperature	11.25	1	11.25	91.75	< 0.0001
Residual	1.23	10	0.1226		
Cor Total	12.48	11			
Fit Statistics					
Std. Dev.	0.3502		R^2	0.9017	
Mean	3.26		Adjusted R^2	0.89.19	
C.V. %	10.74		Predicted R^2	0.8585	
			Adeq. Precision	13.5465	

ANOVA for selected factorial model: p/v (B – J)					
Source	Sum of Squares	Degrees of Freedom	Mean Square	F-value	p-Value
Model	0.9207	3	0.3069	75.78	< 0.0001
B-column temperature	0.2160	1	0.2160	53.34	< 0.0001
D-flow	0.4070	1	0.4070	100.5	< 0.0001
F-ACN initial	0.2977	1	0.2977	73.5	< 0.0001
Residual	0.0324	8	0.0041		
Cor Total	0.9531	11			
Fit Statistics					
Std. Dev.	0.0636		R^2	0.9660	
Mean	1.91		Adjusted R^2	0.9533	
C.V. %	3.33		Predicted R^2	0.9235	
			Adeq. Precision	25.9011	

Table S7 Actual equation of the model for the variable p/v (B-J) using the three statistically significant factors column temperature (B), flow rate (D) and initial ACN ratio (F)

p/V (B-J)	**=**
6.00083	
+0.0670833 * B	* column temperature
-9.20833 * D	* flow rate
-0.07875 * F	* initial ACN ratio

References

[1]   K. Zhang, K. L. Kurita, C. Venkatramani, D. Russell, Seeking universal detectors for analytical characterizations, J. Pharm. Biomed. Anal. 162 (2019) 192-204.

[2]   T. Górecki, F. Lynen, R. Szucs, P. Sandra, Universal Response in Liquid Chromatography Using Charged Aerosol Detection, Anal. Chem. 78(9) (2006) 3186-3192.

[3]   S. Grosse, T. Muellner, K. Lovejoy, I. Acworth, P. Gamache, Why use charged aerosol detection with inverse gradient?, Thermo Fisher Scientific Technical note 73449 (2020). https://assets.thermofisher.com/TFS-Assets/CMD/Technical-Notes/tn-73449-cad-inverse-gradient-tn73449-en.pdf.

[4]   K. Zhang, Y. Li, M. Tsang, N. P. Chetwyn, Analysis of pharmaceutical impurities using multi-heartcutting 2D LC coupled with UV-charged aerosol MS detection, J. Sep. Sci. 36 (18) (2013) 2986-2992.

[5]   R. Karongo, T. Ikegami, D. R. Stoll, M. Lämmerhofer, A selective comprehensive reversed-phase×reversed-phase 2D-liquid chromatography approach with multiple complementary detectors as advanced generic method for the quality control of synthetic and therapeutic peptides, J. Chromatogr. A 1627 (2020) 461430.

[6]   P. Sun, X. Wang, L. Alquier, C. A. Maryanoff, Determination of relative response factors of impurities in paclitaxel with high performance liquid chromatography equipped with ultraviolet and charged aerosol detectors, J. Chromatogr. A 1177(1) (2008) 87-91.

[7]   A. Warner, I. Piraner, H. Weimer, K. White, Development of a purity control strategy for pemetrexed disodium and validation of associated analytical methodology, J. Pharm. Biomed. Anal. 105 (2015) 46-54.

[8]   B. Scherer, F.-M. Matysik, Investigations of polymer samples of polyamide 11 concerning the content of monomer, oligomers, and the oxidation stabilizer Irganox 1098 by utilizing inverse gradient HPLC in combination with a triple detection system (diode array detection/mass spectrometry/charged aerosol detection), Talanta Open 3 (2021) 100023.

[9]   R. Pawellek, K. Schilling, U. Holzgrabe, Impurity profiling of l-aspartic acid and glycine using high-performance liquid chromatography coupled with charged aerosol and ultraviolet detection, J. Pharm. Biomed. Anal. 183 (2020) 113149.

[10]   R. Pawellek, U. Holzgrabe, Influence of the mobile phase composition on hyphenated ultraviolet and charged aerosol detection for the impurity profiling of vigabatrin, J. Pharm. Biomed. Anal. 201 (2021) 114110.

[11]   Council of Europe, European Pharmacopoeia, 10.8 edition, Monograph no. 1563 Simvastatin, Strasbourg, France (2022).

[12]   Council of Europe, European Pharmacopoeia, 10.8 edition, Monograph no. 1538 Lovastatin, Strasbourg, France (2022).

[13]   T. Rosen, C. H. Heathcock, The synthesis of mevinic acids, Tetrahedron 42(18) (1986) 4909-4951.

[14]   S. Goswami, A. S. Vidyarthi, B. Bhunia, T. Mandal, A review on lovastatin and its production, J. Biochem. Tech 4 (2012) 581-587.

[15] X. Xinkai, Y. Tang, Efficient Synthesis of Simvastatin by Use of Whole-Cell Biocatalysis, Appl. Environ. Microbiol. 73(7) (2007) 2054-2060.

[16] Council of Europe, Knowledge Database, Simvastatin. Available from: https://extranet.edqm.eu/4DLink1/4DCGI/Web_View/mono/1563 (accessed 22.09.2022)

[17] A. Giaquinto, Z. Liu, A. Bach, Y. Kazakevich, Surface area of reversed-phase HPLC columns, Anal. Chem. 80(16) (2008) 6358-6364.

[18] P. H. Gamache, Charged aerosol detection for liquid chromatography and related separation techniques, 1st edition, John Wiley & Sons, Hoboken, New Jersey, USA (2017).

[19] Council of Europe, European Pharmacopoeia, 10.8 edition, Chapter 2.2. 46 Chromatographic separation techniques, Strasbourg, France (2022).

[20] D. Guillarme, D. T. T. Nguyen, S. Rudaz, J.-L. Veuthey, Method transfer for fast liquid chromatography in pharmaceutical analysis: Application to short columns packed with small particle. Part II: Gradient experiments, Eur. J. Pharm. Biopharm. 68(2) (2008) 430-440.

[21] J. J. Russell, J. C. Heaton, T. Underwood, R. Boughtflower, D. V. McCalley, Performance of charged aerosol detection with hydrophilic interaction chromatography, J. Chromatogr. A 1405 (2015) 72-84.

[22] International Council for Harmonisation of Technical Requirements for Pharmaceuticals for Human Use, Guideline Q3A (R2) Impurities in New Drug Substances (2006).

[23] International Council for Harmonisation of Technical Requirements for Pharmaceuticals for Human Use, Guideline Q2 (R1) Validation of Analytical Procedures (2005).

[24] Y. Vander Heyden, A. Nijhuis, J. Smeyers-Verbeke, B. G. M Vandeginste, D. L Massart, Guidance for robustness/ruggedness tests in method validation, J. Pharm. Biomed. Anal. 24(5–6) (2001) 723-753.

[25] S. L. C. Ferreira, A. O. Caires, T. da S. Borges, A. M. D. S. Lima, L. O. B. Silva, W. N. L. dos Santos, Robustness evaluation in analytical methods optimized using experimental designs, Microchem. J. 131 (2017) 163-169.

[26] M. Jimidar, N. Niemeijer, R. Peeters, J. Hoogmartens, Robustness testing of a liquid chromatography method for the determination of vorozole and its related compounds in oral tablets, J. Pharm. Biomed. Anal. 18(4-5) (1998) 479-485.

3.4. Analytical quality by design: Achieving robustness of an LC-CAD method for the analysis of non-volatile fatty acids

Rasmus Walther[1], Jovana Krmar[1], Adrian Leistner, Bojana Svrkota, Biljana Otašević, Andjelija Malenović, Ulrike Holzgrabe, Ana Protić

[1] These authors contributed equally to this work.

Abstract

An alternative to the time-consuming and error-prone pharmacopoeial gas chromatography method for the analysis of fatty acids (FAs) is urgently needed. The objective was therefore to propose a robust liquid chromatography method with charged aerosol detection for the analysis of polysorbate 80 (PS80) and magnesium stearate. FAs with different numbers of carbon atoms in the chain necessitated the use of a gradient method with a Hypersil Gold C_{18} column and acetonitrile as organic modifier. The risk-based Analytical Quality by Design approach was applied to define the Method Operable Design Region (MODR). Formic acid concentration, initial and final percentages of acetonitrile, gradient elution time, column temperature, and mobile phase flow rate were identified as critical method parameters (CMPs). The initial and final percentages of acetonitrile were fixed while the remaining CMPs were fine-tuned using response surface methodology. Critical method attributes included the baseline separation of adjacent peaks (α-linolenic and myristic acid, and oleic and petroselinic acid) and the retention factor of the last compound eluted, stearic acid. The MODR was calculated by Monte Carlo simulations with a probability equal or greater than 90 %. Finally, the column temperature was set at 33 °C, the flow rate was 0.575 mL/min, and acetonitrile linearly increased from 70 to 80 % (v/v) within 14.2 min.

Graphical abstract

Analysis of non-volatile fatty acids

AQbD

5) Validation & Application
4) Constructing MODR
3) Fine-tuning of the CMPs
2) Fixing practical factors
1) ATP & Scouting phase

Ph. Eur. GC method:
error-prone & time consuming

Polysorbat 80
& Mg stearate

RP HPLC-CAD: more efficient & higher
sensitivity
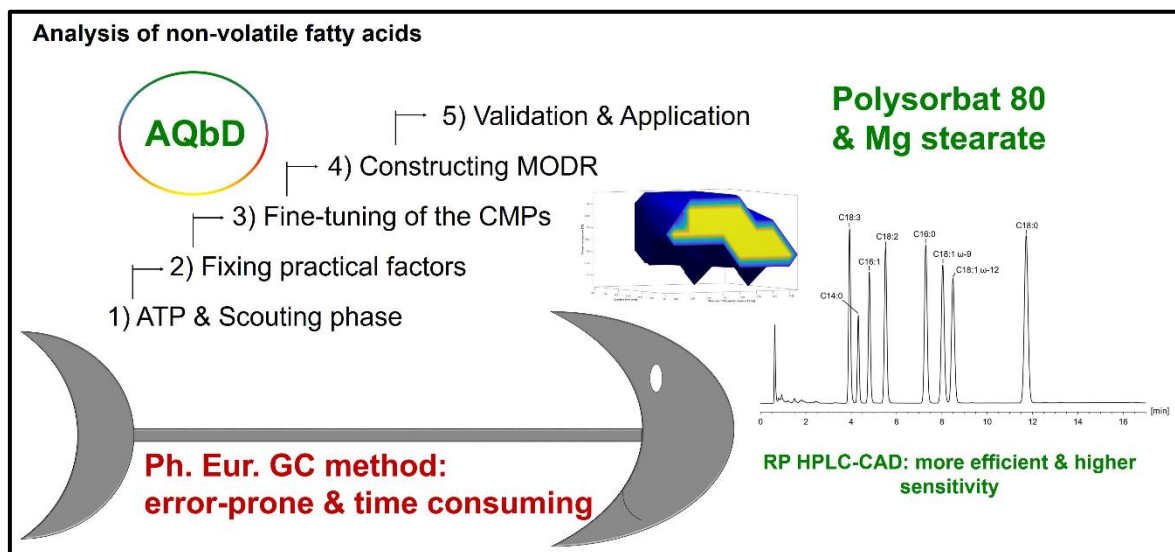
1. Introduction

For decades, pharmaceutical analysis was essentially a discipline in which indispensable chromatographic methods were developed on a trial-and-error basis. In recent years, however, advances in computational tools have increasingly enabled analysts to efficiently select the most appropriate separation conditions, taking into account the entire experimental space. Due to its resource-conscious nature, chemical intelligence has been gaining momentum and is now a key dimension of both the established Pharma 4.0 as well as emerging Pharma 5.0 industry perspectives. As the heart of the pharmaceutical industry, new digital technologies are bringing prosperity, improved process understanding, and better time management across all segments, with a special focus on already overburdened quality control labs [1-4]. A particular benefit is the supply of the more consistent quality method and ultimately patient safety, as failure of the analytical method can have dramatic implications for human health [5]. Consequently, a variety of *in silico* solutions for selecting fit-for-purpose analytical methods have been developed to date.

Analytical Quality by Design (AQbD) is one of the powerful assays in the arsenal of computational tactics that labs with extensive responsibilities and finite resources have been using to develop analytical methods [6-13]. The final result of AQbD is a Method Operable Design Region (MODR), which is a multidimensional space based on the experimental settings that ensure suitable method performance. Changes within the MODR do not need to be submitted to regulatory agencies, which saves time and reduces the potential for analytical method failure in quality control labs [3]. AQbD has been included in the guidelines of the International Conference on Harmonization of Technical Requirements for Pharmaceuticals for Human Use, specifically the ICH Q2 (R2) (analytical validation) and the new ICH Q14 (analytical procedure development) [1,3,14].

Unfortunately, the recognizable systematic approach outlined here is in some respects contrary to the approach used to analyze many excipients in the European Pharmacopoeia (Ph. Eur.). This is particularly problematic when it comes to a large group of excipients counting polysorbates (PS), esters of macrogol or glycerol with various fatty acids (FA), or mineral salts of FAs [15-18]. Typically, the FA composition of these excipients is determined through gas chromatography (GC) after a laborious process of derivatization to the respective volatile methyl esters. According to the monograph 2.4.22 "Composition of fatty acids by gas chromatography" in the Ph. Eur. [19], FAs with chain lengths of 6-24 carbon atoms can be analyzed only if they do not contain thermolabile moieties, such as an epoxy group [20]. The fact that GC analysis endures for about 60 min, requires a larger amount of expensive carrier gases such as helium or hydrogen, and consumes valuable time highlights the need for improvement in this area. In this regard, Ilko et al. [21] developed a liquid chromatography (LC) method with the charged aerosol detector (CAD) as an alternative to the compendial GC method for the analysis of PS80. The CAD's capability to detect analytes irrespective of their chemical structure enabled the convenient analysis of FAs without derivatization, with a shorter runtime of just 18 min. However, the analytical method encountered sensitivity issues with short-chain FAs and was not developed through a systematic risk-based approach. Recent research has explored the suitability of a new generation of CAD instruments for the sensitive detection of non-volatile FAs [22]. This study has taken into account adjustable evaporation temperature, filter constant, and power function value (PFV). The existing knowledge was used in this work to improve the limitations of the previously developed HPLC methods with CAD [21,22] and combine them with the advantages of the AQbD approach. Applying AQbD not only provides an in-depth comprehension of the analytical process, but also ensures the robustness and long life cycle of the methods. These are all attributes that are particularly desirable for general compendial methods such as FA composition. Our aim was therefore to use the AQbD approach to identify the critical factors of the existing methods [21,22] and to optimize them in such a way that a sensitive and, above all, accountable LC-CAD method with appropriate risk management is available. To demonstrate the adequacy of the new method with the Ph. Eur. GC method for the determination of FA composition, a magnesium stearate batch was investigated in addition to a Polysorbate (PS) 80 sample as a further application example (Figure 1).
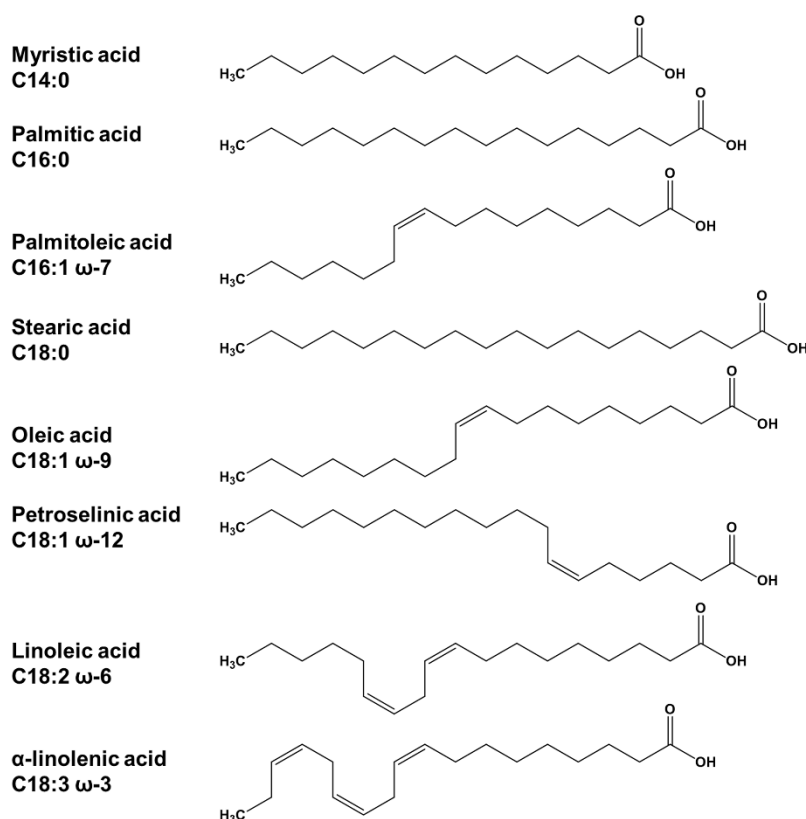
Fig. 1 Common names, lipid numbers, and molecular structures of the analysed non-volatile fatty acids

2. Results and discussion

2.1 Analytical target profile: defining the scope pf the method

AQbD workflow begins by summarizing the characteristics of the analytical method that ideally will be achieved to guarantee the desired quality. The first step of this dynamic procedure thus includes defining the analytical target profile (ATP). The concept of an ATP is in line with the concept of the quality target product profile defined in the ICH Q8 guideline and was recently introduced through the ICH Q14 guideline [3,23]. The ATP involves a description of the method purpose, the selection of an appropriate analytical technique that is able to serve this purpose, and finally, the selection of the quality attributes that are going to be measured along with method performance characteristics. Therefore, the declaration of the ATP represents the base step enabling further definition of desirable analytical method attributes with associated acceptance criteria [3]. In the specific case presented in this study, achieving the baseline separation of eight non-volatile FAs (see Fig. 1) in a sufficiently short analysis run-time posed the purpose of the intended LC-CAD method.

2.2. Design of Experiments in Modeling of Critical Method Attributes

The essence of the ATP was more precisely presented by defining critical method quality attributes, called critical method attributes (CMA), associated with their acceptance criteria. The selection of CMAs refers to a set of chromatographic separation descriptors that are going to be used as a proper indicator of the capability of a method to reach the predefined ATP. In LC, these method attributes are derived from the separation of critical pair of analytes, specific requirements for the peak shape, and/or the number of theoretical plates, etc., and may vary depending on the method purpose [24]. Accordingly, CMAs are influenced by the wide range of LC system operating parameters, which are therefore accordingly denoted as critical method parameters (CMP) [3,6,7,10]. In general, LC method parameters may be classified in a way that all aspects of intended LC analysis, such as sample, mobile phase, detection, or column-related parameters, are properly taken under consideration (see Fig. 2). The analysis of plotted Ishikawa or fish bone diagram followed with an appropriate risk-based approach or based on previous knowledge was used to provide comprehensive method understanding, as well as a scientifically based definition of CMPs. Using an approach known as CNX, important decisions were made about which method parameters should be kept under **C**ontrol, which could be considered **N**oise factors, and finally, which method parameters required e**X**perimental evaluation of the associated acceptable ranges. The parameters that needed to be kept under control were set to constant values. Apart from providing proper insight into the intended method properties, this approach provides inputs for prospective method control strategy [25,26].
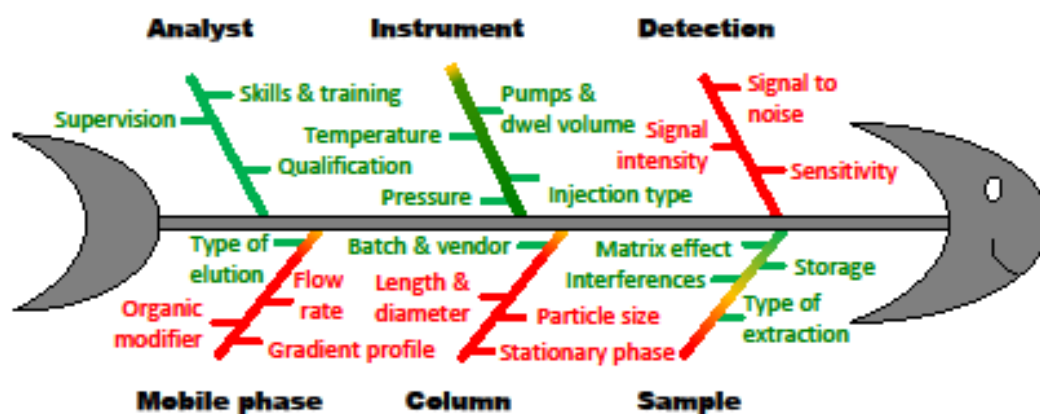
Fig. 2 Fish bone diagram with parameters affecting the quality of LC analyses

Design of Experiments (DoE), as one of the constitutive concepts of the AQbD paradigm, represents an excellent in silico tool for the resource-efficient development of various chromatographic methods. Primarily, DoE provides high-quality information as a consequence to the simultaneous variation of experimental LC-CAD variables. However, when the number of factors to be considered raises, the increase of the cost and the time needed for the analyses follows as well.

This is especially evident when categorical variables (e.g. type of column) are involved. Adjusting all the potentially influential factors, thus, almost certainly ends up with the significant quantity of runs that is impractical to be carried out [27]. Alternatively, since profound background knowledge is available, the parameter optimization can be accomplished through a multistage strategy that includes the following: (1) preliminary scouting of the categorical factors, namely, column chemistry and solvent type; (2) fixing some of the high-risk factors at levels that ensure the fulfillment of practical requirements; (3) fine-tuning of secondary high-risk factors via Response Surface Methodology (RSM) design; (4) construction of the MODR for robust method performance [28]. This sequential strategy provides also independent assessment of potential interactions between the significant factors for a better understanding of the method.

2.2.1 Scouting stage: selection of organic solvent and column type

It is known that the chemistry of the stationary phase and the type of organic modifier are primary factors in determining the retention behavior of compounds in reversed phase (RP) chromatography [24]. In this study, the type of organic modifier (ACN) was selected *a priori*. This decision was supported by the fact that ACN-based mobile phases generally have high elution strength, which is beneficial when working with lipophilic analytes such as FAs. Nevertheless, a better evaporation profile over frequently used MeOH was meaningful since volatility is a very desirable characteristic in terms of the adopted detection technique [29]. On the other hand, regarding the selection of the stationary phase as the core of the chromatographic separation, a screening with four RP columns (different chemistry and different dimensions) was carried out. Using a mix of the homologous series composed of myristic acid, palmitic acid, and stearic acid and the gradient program of Ilko et al. [21] (see Table S1), a C_8, a C_{12}, and two C_{18} columns were compared. Since the Hypersil Gold C_{18} columns showed the best results in terms of retention and peak shapes (see Fig. 3 and Table S3), and at the same time had the lowest level of background current of the CAD, this column was selected for further experiments. Retention times obtained using the other C_{18} core-shell column were notably longer (no elution of stearic acid within the gradient program) and, interestingly, greatest with the C_{12} column (see Fig. 3). Compared to the other columns, this column has the highest carbon load and a considerably higher specific surface area, both of which are factors that influence retention [24]. With the C_8 column, the three FAs were separated but showed inferior peak shapes and worse separation performance (see Table S3).
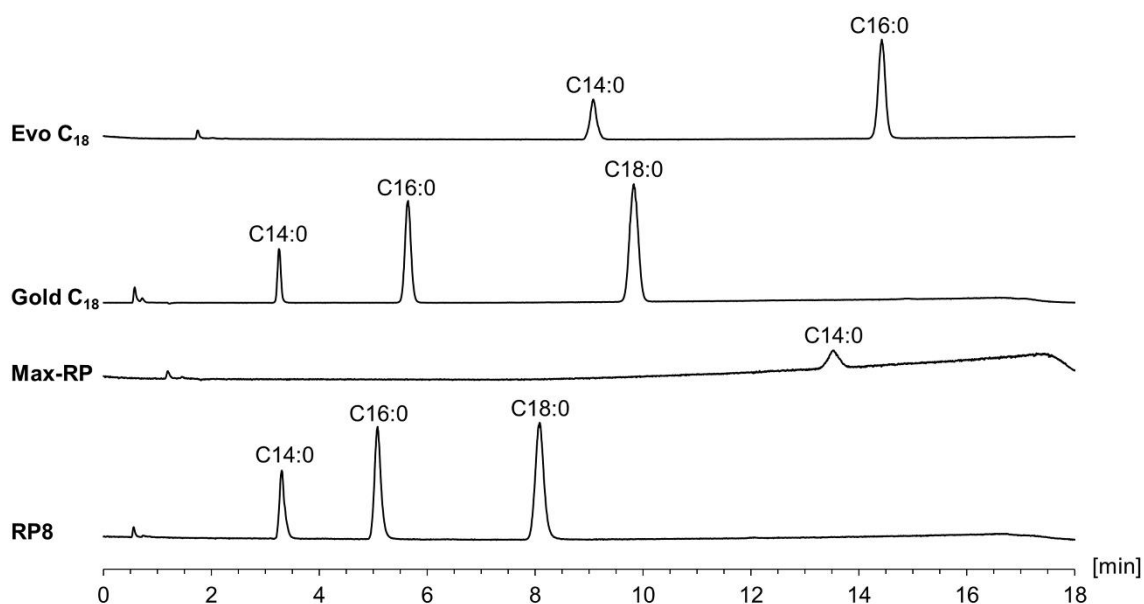
Fig. 3 Chromatogram overlay of the column screening using the gradient program of Ilko et al. [21] (see Table S1)
Injection of the test solution containing myristic acid (C14:0), palmitic acid (C16:0), and stearic acid (C18:0) using the Symmetry Shield RP8 column (100 x 3.0 mm, 3.5 µm), Synergi Max-RP C_{12} column (100 x 4.6 mm, 4 µm), Hypersil Gold C_{18} column (150 x 2.1 mm, 3.0 µm), and the Kinetex Evo C_{18} column (150 x 4.6 mm, 2.6 µm)

2.2.2 Fixing some high-risk factors at reasonable levels

After fixing the stationary phase and the type of organic solvent, it was necessary to optimize the factors of subsequent importance/factors also posing high-risk toward baseline separation.

The addition of formic acid to the mobile phase is on the one hand necessary for the peak shape, on the other hand it affects the CAD's level of background current [29]. The concentration of 0.05 % (v/v) was an acceptable compromise that ensures robust protonation of the FAs and a low level of background current (< 1 pA). A decrease to 0.02 % (v/v) was associated with peak tailing and an increase in the symmetry factor to values above 1.20.

In the next step before optimization by RSM, the initial and final ACN percentage of the gradient program should be defined. Since data from the scouting stage were available, these high-risk factors could be efficiently fixed to meet practical requirements. Thus, the FA test mixture was subjected to a gradient from 65 % (v/v) to 85 % (v/v) ACN in 15 min at 20 °C and 0.7 mL/min. Under these conditions, a baseline separation between all analytes was achieved, but the elution window was relatively wide and a large expenditure of time that preceded the first-eluting peak, i.e. that followed the last-eluting compound, was evident (see Fig. S1a).

To remove empty space before the elution of the least retained FA, the initial and final percentages of ACN in the mobile phase required slight adaptation. It was calculated that at the retention time of the linoleic acid (4.94 min) and the stearic acid (13.23 min), the mobile phase contained approximately 69.8 % (v/v) and 80.8 % (v/v) of ACN, respectively. This calculation was performed using the Equation (1):

$$\varphi_e = \varphi_i + \frac{\varphi_f - \varphi_i}{t_{grad}} * (t_r - t_D) \qquad\qquad \text{Eq. (1)}$$

where φ_e, φ_i, and φ_f are the content of organic solvent at the elution, the beginning of gradient, and the end of gradient, respectively. In the same equation, t_{grad}, t_r, and t_D refer to the gradient time, the retention time of the least (or most) retained analyte, and the dwell time ($\approx$ 1.37 min at 700 µL/min), respectively. For simplicity, the initial ACN percentage was rounded to 70 % (v/v) while the final ACN percentage was rounded to 80 % (v/v). Consequently, the gradient range on Hypersil Gold C_{18} stationary phase was modified from 65 – 85 % (v/v) ACN to 70 – 80 % (v/v) ACN. In the following test run with the modified gradient conditions, acceptable chromatographic behavior was achieved for all the analytes (see Fig. S1b).

2.2.3 Fine-tuning of CMPs via RSM

Once the combination of initial and final percentage of ACN in the mobile phase was set, secondary parameters were optimized to improve the separation. After subjecting model mixture to adopted settings, it was noted that the critical peak pairs were formed by α-linolenic acid and myristic acid (peaks 1 and 2), i.e. oleic acid and petroselinic acid (peaks 6 and 7). Hence, separation criteria, S_{1-2} and S_{6-7} between the adjacent peaks were proclaimed as the first two CMAs. Separation criterion S is recognized a convenient way of measuring the baseline separation in gradient RP-LC. This is achieved by avoiding some of the disadvantages that standard parameters, such as resolution and peak capacity, suffer, according to [30]. S criterion is calculated using Equation (2):

$$s = t_{2,start} - t_{1,end} \qquad\qquad \text{Eq. (2)}$$

In Equation (2) $t_{2,start}$ represents the beginning of the later peak, while $t_{1,end}$ is the end of the former peak of two consecutive peaks ($t_{2,start} > t_{1,end}$). To further fulfill the definition of the ATP, a third CMA was taken into consideration. It was related to the retention of the last-eluting peak, and quantified via the retention factor k.

When observed all together, the satisfactory separation of all critical pairs and the reasonable retention of the last-eluting peak were identified as the goals of utmost importance and the supreme ATP of the proposed method.

To fulfill these pre-defined CMAs, we varied the flow rate (x_1), the gradient time (x_2), and the column temperature (x_3), as variables that, besides the above-considered (categorical and numerical) factors, highly impact the RP-LC behavior [24,31,32]. These factors were thus declared as relevant CMPs and were subjected to RSM experiments. In order to adequately describe the experimental space, registered CMPs were simultaneously varied according to a face-centered Central Composite Design (CCD) requiring 18 runs in total (see Table 1). Broader ranges of the listed factors were used to examine as wide a space as possible. Clearly, these conditions constituted a trade-off between baseline separation and reduced analysis run-time.

Using Equation (2) the first two CMAs, S_{1-2} and S_{6-7}, were calculated and direct modeling of S criteria were attempted. However, this resulted in models with poor predictive performance. One possible reason for the inadequacy of direct modeling could lie in the fact that baseline separation depends on multiple factors (e.g. the size and shape of neighboring peaks). Different assessment of S criterion, in this regard, likely comes to the fore in the case of small time differences. The impact of CMPs on the mentioned CMAs was therefore modeled indirectly, which has the advantage that it does not suffer from faulty estimation of baseline separation [33]. Indirect modeling means that mathematical models were developed for the retention times on the chromatogram that correspond to the end of the first peak and the beginning of the second peak. After developing the mathematical models for the corresponding retention times, they were used to calculate separation criteria S. The baseline separation was achieved when S criterion was greater than zero. On the other hand, the third CMA, k of the last-eluting peak, was modeled directly (Table 1). Since it carried information about the analysis runtime, the goal was to minimize its value.

Table 1
Plan of experiments according to face-centered CCD and acquired values of critical method attributes (CMAs)

critical method parameters			critical method attributes				
flow rate (x_1) [mL/min]	gradient time (x_2) [min]	column temperature (x_3) [°C]	$t_{(\alpha-linolenic)end}$	$t_{(myristic)start}$	$t_{(oleic)end}$	$t_{(petroselinic)start}$	$k_{stearic}$
0.50	8.0	30.00	4.84	4.94	8.99	9.01	15.80
0.70	8.0	30.00	3.53	3.6	6.85	6.85	16.99
0.50	15.0	30.00	4.95	5.07	9.98	10.02	18.78
0.70	15.0	30.00	3.61	3.67	7.47	7.49	19.86
0.50	8.0	40.00	4.31	4.31	7.82	7.82	13.73
0.70	8.0	40.00	3.12	3.12	5.86	5.86	14.64
0.50	15.0	40.00	4.37	4.37	8.47	8.47	15.86
0.70	15.0	40.00	3.15	3.15	6.27	6.27	16.59
0.50	11.5	35.00	4.56	4.61	8.83	8.84	16.41
0.70	11.5	35.00	3.33	3.38	6.66	6.66	17.32
0.60	8.0	35.00	3.84	3.87	7.21	7.21	15.45
0.60	15.0	35.00	3.9	3.95	7.85	7.87	17.88
0.60	11.5	30.00	4.11	4.19	8.22	8.23	18.44
0.60	11.5	40.00	3.62	3.62	7.00	7.00	15.48
0.60	11.5	35.00	3.89	3.93	7.63	7.64	16.65
0.60	11.5	35.00	3.86	3.9	7.57	7.58	16.71
0.60	11.5	35.00	3.85	3.89	7.55	7.57	17.26
0.60	11.5	35.00	3.85	3.91	7.57	7.6	16.87

In order to develop desired RSM models, empirical mathematical functions $y = f(x_1, x_2, x_3)$ were fitted to experimentally acquired data [7,34]. Mathematical models are obtained by applying multiple regression and the least squares method, resulting in polynomial equations. The general form of the polynomial expression is given by Equation (3):

$$y = b_0 + \sum_{i=1}^{3} b_i x_i + \sum_{i=1}^{3}\sum_{j=1}^{3} b_{ij} x_i x_j + \sum_{i=1}^{3} b_{ii} x_i^2 \qquad \text{Eq. (3)}$$

In the present function, *y* is the modeled response value (CMA), x_i indicates independent variable values (x_1, x_2, x_3 represent CMPs as in Table 1), and *b*-s are model coefficients which indicate the magnitude and the trend of respective equation term's influence, with the exception of b_0, which is the intercept. Thus, b_i, b_{ij}, and b_{ii} indicate single-factor, two-factor interaction (where i ≠ j), and second-order value of factor effects [34].

The model development process was governed by the analysis of variance, which compares level-dependent and random error variances and quantifies model quality by the adjusted *coefficient of determination* (*adj. R^2*) [34,35]. A high value of *adj. R^2* implies concurrence of predicted and measured response values in form of explained variance ratio taking into account degrees of freedom [36] and can be tuned by excluding uninformative model terms. Model validation is often performed with the statistical assessment of *lack of fit* ($p > 0.05$), a numerical estimation similarity of residual and experimental variance [31,35].

Obtained mathematical models with quality assessment parameters are presented in Table 2. The mathematical transformations of results were applied in line with the Box-Cox plot results.

Table 2
Generated DoE models which refer to coded factor values are present in tabular form, along with model quality parameters

	$\dfrac{1}{t_{(\alpha-linolenic)end}}$	$\dfrac{1}{t_{(myristic)start}}$	$log(t_{(oleic)end})$	$log\,(t_{(petroselinic)start})$	k_8
b_0	+0.26	+0.26	+0.88	+0.88	+16.89
b_1	+0.041	+0.041	−0.062	−0.062	+0.48
b_2	−2.111 × 10⁻³	−2.196 × 10⁻³	+0.018	+0.019	+1.24
b_3	+0.016	+0.019	−0.035	−0.035	−1.36
b_{12}	/	/	−1.631 × 10⁻³	−1.582 × 10⁻³	/
b_{13}	+3.182 × 10⁻³	+3.317 × 10⁻³	−1.506 × 10⁻³	−1.313 × 10⁻³	/
b_{23}	/	/	−2.369 × 10⁻³	−2.611 × 10⁻³	−0.22
b_{11}	/	/	+4.776 × 10⁻³	+4.493 × 10⁻³	/
b_{22}	/	/	−3.539 × 10⁻³	−3.515 × 10⁻³	−0.33
b_{33}	/	/	/	/	/
R^2	0.9993	0.9993	0.9997	0.9998	0.9902
adj. R^2	0.9991	0.9991	0.9995	0.9996	0.9861
pred. R^2	0.9985	0.9987	0.9991	0.9992	0.9805
lack of fit; p value	0.7790	0.6445	0.9730	0.9650	0.9718

2.3 Computation of the MODR via Monte Carlo Simulations

The combination of CMP values providing an optimal chromatogram could be estimated simply by overlapping the collected response surfaces from generated RSM models, but this method does not follow the risk management approach [35]. Given that the ICH Q8 guideline stated that the design space (DS) is a multidimensional combination of input variable values and parameters that ensure method quality, it is essential to apply probability-based tools for desired response estimation [23]. As postulated in the ICH Q9 and Q14 guidelines, the definition of DS within analytical method development should be accompanied with quality risk analysis as well as setting up of an appropriate risk control strategy [3,26]. In that respect, the zone of theoretical robustness or an MODR needs to be further defined using statistical tools based on the understanding of the CMAs' measurement uncertainty and the quantification of the risk of reaching the predefined ATP [3,24,33,35]. The initial step is the discretization of experimental space and creation of uniformly distributed grid points for gradient time [8:0.35:15], flow rate [0.5:0.01:0.7], and column temperature [30:1:40]. Thus, a total number of combinations of CMPs was 21 × 21 × 11 = 4851. To achieve the assurance of quality in terms of meeting predefined acceptance criteria set by the ATP with desired probability, a Monte Carlo (MC) simulation was performed. It included 5000 iterations to propagate the error in model coefficients' calculation when the error distribution equal to the calculated standard error was added to the estimated model coefficients. In this way response distribution was obtained for each operating condition corresponding to the created 4851 grid points.

The criteria for satisfactory CMAs' values were set as follows: $S_{1-2} > 0$, $S_{6-7} > 0$, and $k_8 < 18.8$, and MODR was computed for the probability of 90 % to meet defined criteria. From the acquired MODR graphical presentation (see Fig. 4), the margins of the safe zone of theoretical method robustness may be extracted, pointing out to the limits to which the reaching of the ATP would not be compromised. The whole MODR central figure is considered as a "safe zone" from which the working point can be selected randomly. However, it is recommendable to select the working point from the central part (illustrated in Fig. 4 in yellow) since the blue colored part represents the edges at risk of falling out of the robust region. Setting up these boundaries is needed for defining a proper method control strategy as required by the ICH Q9 guideline [26]. The working point (0.575 mL/min flow rate, 14.2 min gradient time, and 33 °C column temperature) was further selected from the center of the MODR in order to additionally contribute to method robustness. Fig. 5 shows a chromatogram obtained experimentally at the selected working point.
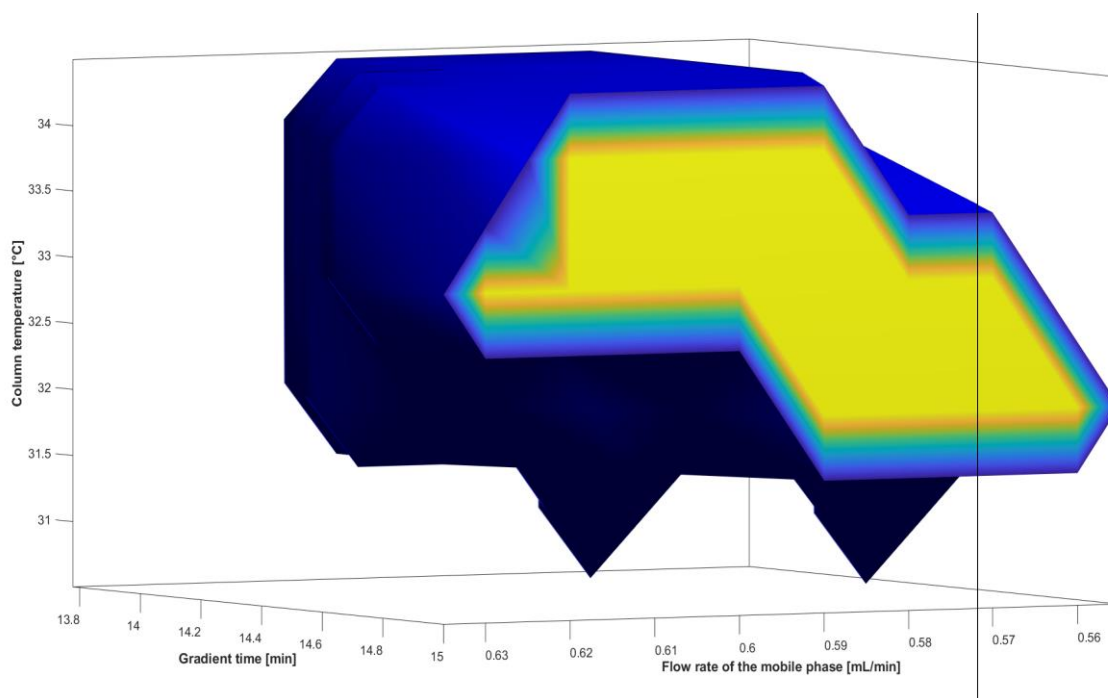

Fig. 4 Graphical representation of MODR obtained using Monte Carlo simulations
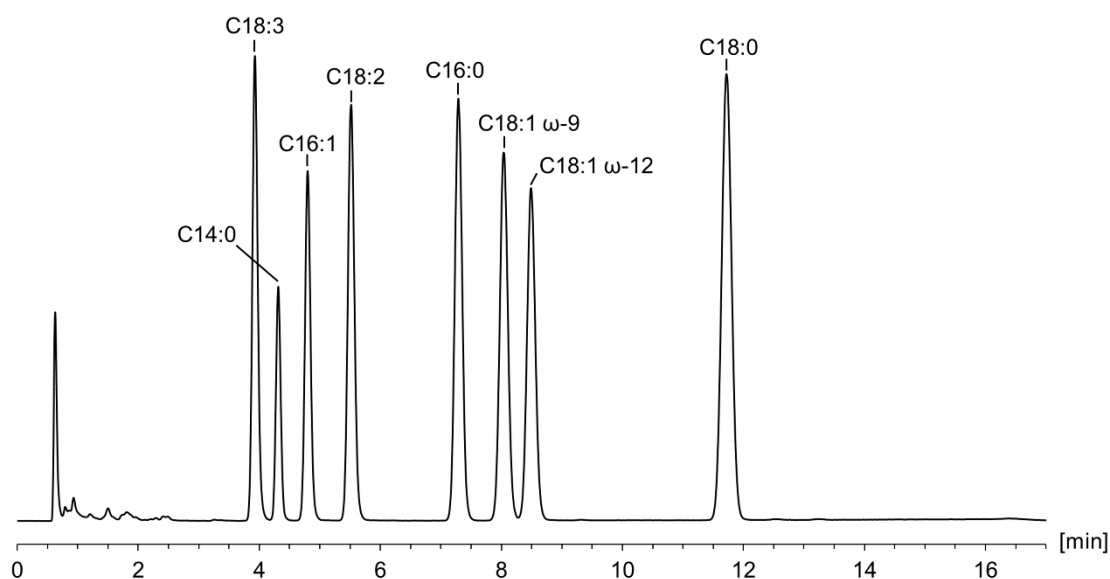
Fig. 5 Experimentally obtained chromatogram at selected working values of CMPs (0.575 mL/min flow rate, 14.2 min gradient time, and 33 °C column temperature) with optimized CAD settings (25 °C evaporation temperature, 3.6 s filter constant, and 5 Hz data collection rate)

2.4 Validation and application

2.4.1 Validation

The final chromatographic method (see section 2.3) was validated with regard to guideline ICH Q2 (R1) [37]. In the context of this, specificity, linearity and range, accuracy, repeatability, and limit of quantitation (LOQ) were investigated. When using the AQbD approach, an experimental evaluation of robustness is not mandatory as long as one works within the MODR framework (see section 2.3) [7,10].

Specificity was demonstrated by analyzing a mixture of the eight FAs of interest, namely α-linolenic acid (C18:3 ω-3), myristic acid (C14:0), palmitoleic acid (C16:1 ω-7), linoleic acid (C18:2 ω-6), palmitic acid (C16:0), oleic acid (C18:1 ω-9), petroselinic acid (C18:1 ω-12), and stearic acid (C18:0). As shown in Fig. 5, all analytes were baseline separated, achieving values of 0.11 or 0.06 for the *S* criterion of the two critical peak pairs α-linolenic acid and myristic acid, and oleic acid and petroselinic acid, respectively. In addition, blank extraction samples were analyzed and checked for possible co-elutions (see Fig. 6).

Linearity and range were also determined. To cover the estimated analyte amount of the samples, concentrations of 1, 25, 50, 75, and 100 µg/mL were injected (n = 3) to obtain calibration curves over a range of two orders of magnitude. Different PFVs were tested, but analogous to Schilling et al. [22], the best coefficients of determination (R^2) were obtained after double logarithmic transformation of concentration and peak area (Table 3). Accuracy was demonstrated by calculating recoveries at concentration levels of 1, 50, and 100 µg/mL for each fatty acid considered (n = 3) using the log–log calibration curves and ranged from 90 % to 108 %.

Relative standard deviations (RSD) for triplicate injections of FA standards (1, 50, and 100 µg/mL) were used to evaluate repeatability. RSD values between 0.05 % and 0.91 % indicated satisfactory precision of the method.

Based on the signal-to-noise (S/N) ratios obtained at the calibration level of 1 µg/mL, dilutions of the FAs were prepared to obtain solutions with a S/N of 10:1. The LOQs for each analyte were less than 2 ng on the column (see Table 3). This improvement compared to the UPLC method [22] is probably due to the lower flow rate (0.575 vs. 1.5 mL/min) and thus lower level of background noise. As expected, the highest value was determined for myristic acid (1.85 ng/column) as the shortest-chain FA examined. This reduced detector response is also evident from the high value of the correction factor compared to the other FAs (with respect to oleic acid).

Table 3
Coefficient of determination (R^2) of the calibration curve (after log–log transformation), correction factor, and LOQ of the investigated FAs

	R^2	slope	y-intercept	correction factor	LOQ (ng/column)
α-linolenic acid	0.9873	0.9350	0.0935	1.01	0.38
myristic acid	0.9995	1.1522	0.0219	1.25	1.85
palmitoleic acid	0.9955	1.0025	0.0529	1.09	0.91
linoleic acid	0.9936	0.9419	0.0937	1.02	0.62
palmitic acid	0.9934	0.9914	0.0921	1.07	0.77
oleic acid	0.9951	0.9231	0.1128	1.00	0.64
petroselinic acid	0.9952	0.9343	0.1089	1.01	0.82
stearic acid	0.9899	0.9540	0.1517	1.03	0.77

2.4.2 Application examples

To investigate the performance of the HPLC-CAD method developed here for the analysis of non-volatile FAs using the AQbD approach, we selected magnesium stearate as another application example in addition to PS80.

In the chromatogram overlay of the PS80 sample with the blank extraction, no interfering peaks with the reagents or other PS80 components were visible (see Fig. 6a), which was considered as evidence of specificity (see above section 2.4.1). In addition to the peaks of the indicated eight FAs, three unknown peaks were detectable at 3.0 min, 9.3 min, and 12.6 min with an S/N of just above 10. If unknown signals appear in future samples, especially if their signals increase, an MS analysis for structure elucidation can be performed with the proposed method without adjustments. These three unknown peaks had a combined percent area of only 0.62 %. As shown in Table 4, the tested batch of PS80 complies with Ph. Eur. FA compositional requirements [15]. As already discussed by Ilko et al. [21], the pharmacopoeial method does not distinguish between the two C18:1 isomers oleic acid (ω-9) and petroselinic acid (ω-12). However, since the percentage content of this additional unknown FA is higher at 6.35 % compared to the PS80 batches examined at that time (< 3 %), it could be useful to introduce a specification for quality control in the future.

Due to poor solubility in water and pure organic solvents, magnesium stearate was dissolved directly in 100.0 mL of a mixture corresponding to the initial gradient conditions and treated for 10 min in an ultrasound bath before analysis. Specificity was similarly ensured by comparison with the chromatogram of the blank sample (see Fig. 6b). In the chromatogram of the test solution, besides a large injection peak and the peaks of palmitic and stearic acid, only one additional unknown peak at the end of the gradient was detected. The high intensity of the injection peak is mainly due to the magnesium ions, which are not retained on the C_{18} column used and therefore do not interfere with the determination of the FAs. A quantitative, chromatographic determination of magnesium ions as an alternative to titration has already been demonstrated for magnesium stearate with the nano quantity analyte detector [38] as another type of aerosol-based detector and would theoretically also be possible using the CAD with, e.g. a suitable mixed-mode column [39]. The investigated Mg stearate sample fulfills the requirements of the Ph. Eur. [18] (see Table 4) and the LC-CAD method should also be a simplification for the other monographed salts of stearic acid (i.e. Na, Ca, Zn, and Al). The advantages are not only time savings (no derivatization and shorter analysis time), but also a less error-prone procedure that does not require toxic boron trifluoride as a catalyst.

Table 4
Results of the LC-CAD analysis of a PS80 and a magnesium stearate sample

PS80			Mg stearate		
Ph. Eur. monograph		LC-CAD	Ph. Eur. monograph		LC-CAD
myristic acid	≤5.0 %	0.21 %			
palmitic acid	≤16.0 %	15.6 %			
palmitoleic acid	≤8.0 %	0.47 %	stearic acid	≥ 40.0 %	69. 3%
stearic acid	≤6.0 %	5.8 %	palmitic acid	n.s. [a]	30.2 %
oleic acid	≥58.0 %	62.1 %	unknown peaks	n.s. [a]	0.5 %
petroselinic acid	n.s. [a]	6.35 %	sum of stearic and	≥ 90.0 %	99.5 %
linoleic acid	≤18.0 %	8.72 %	palmitic acid		
α-linolenic acid	≤4.0 %	0.13 %			
unknown peaks	n.s. [a]	0.62 %			

[a] not specified

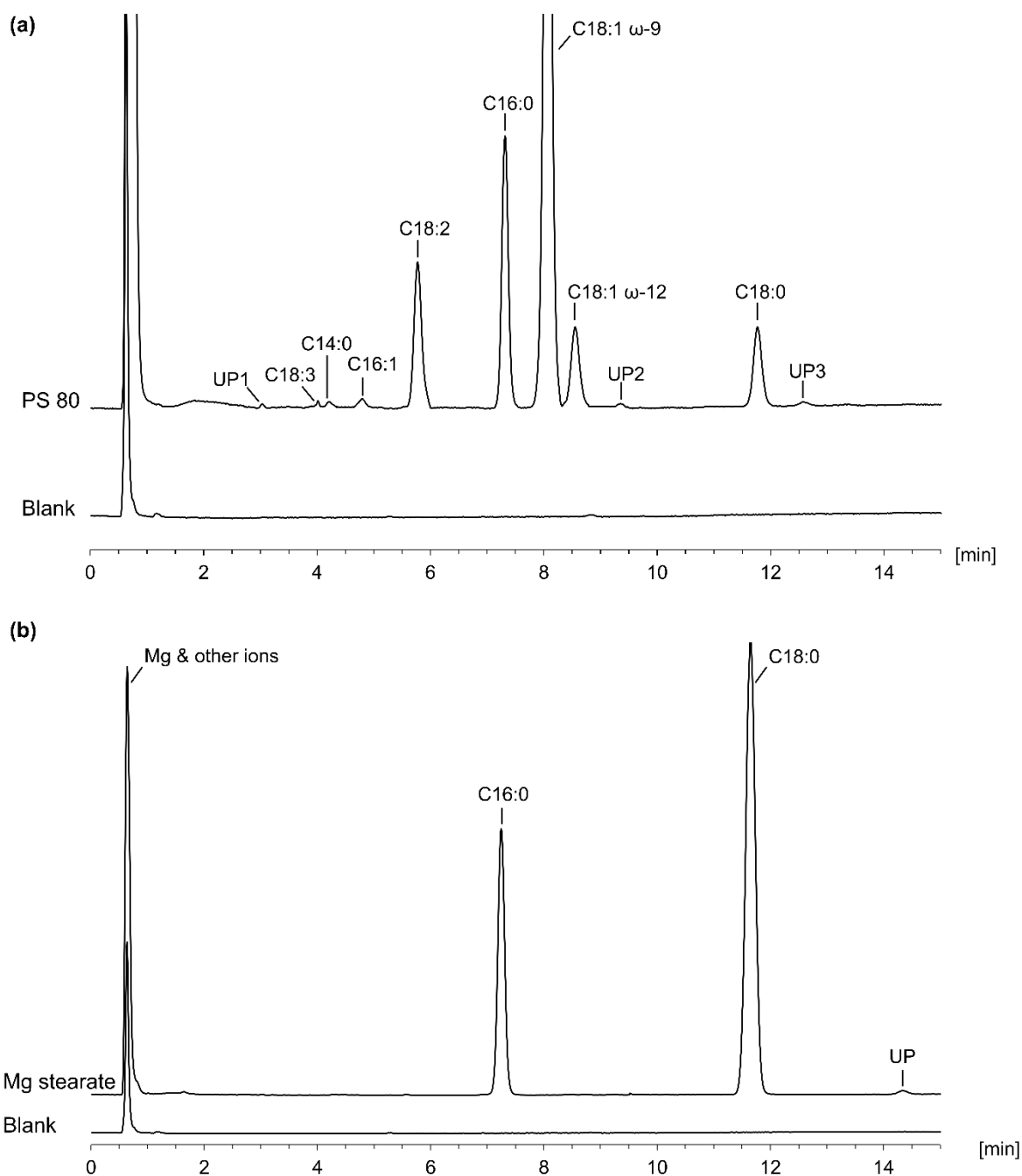**Fig. 6** Chromatogram overlay of the application examples with the corresponding blank extraction sample using the final LC-CAD method (see section 3.3).
(a) Analysis of polysorbate (PS) 80 with three additional unknown peaks (UP) in addition to the specified non-volatile fatty acids (FA).
(b) Analysis of magnesium stearate with another unknown peak in addition to two the main FAs palmitic (C16:0) and stearic acid (C18:0).

3. Material and methods

3.1 Chemicals and reagents

Acetonitrile (ACN) for HPLC (gradient grade, ≥ 99.9 % GC), methanol (MeOH) for HPLC (gradient grade, ≥ 99.9 % GC), *tert.*-butyl methyl ether for HPLC (plus grade, ≥ 99.9% GC), formic acid MS-grade (≥ 99.9 %), palmitic acid (≥ 99 % GC), stearic acid (≥ 98.5 % GC), oleic acid (≥ 99 % GC), petroselinic acid (≥ 95 % GC), linoleic acid (≥ 99 % GC), α-linolenic acid (≥ 99 % GC), palmitoleic acid (≥ 98.5 % GC), PS80 (meets specifications of the Ph. Eur. 10.8), magnesium stearate (meets specifications of the Ph. Eur. 10.8), and magnesium acetate x 4 H_2O (≥ 99 %) were purchased from Sigma Aldrich (Steinheim, Germany). Myristic acid (≥ 99 % GC) and potassium hydroxide for analysis was bought from VWR (Darmstadt, Germany). Ultra-pure water was freshly prepared by a water purification system from Merck Millipore® (Darmstadt, Germany).

3.2 Preparation of solution and samples

3.2.1 Standard solutions for method development

For the preparation of the individual stock solutions, 10.0 mg of the respective FA was exactly weighed and dissolved in 10.0 mL MeOH. For the column screening, a test solution of 0.1 mg/mL each of myristic acid, palmitic acid, and stearic acid in a mixture of water:ACN (25:75, v/v) was used. Additionally, a mixture containing all FAs was prepared at a concentration of 0.1 mg/mL by diluting the stock solutions with the same water/ACN mixture. The obtained solution served as a test solution for scouting and fine-tuning experiments (see sections 2.2.2 and 2.2.3). All stock solutions were stored at -20 °C and used throughout the study. The working solutions were prepared daily. In the validation experiments (see section 2.4.1) and the application examples, a solvent mixture containing water:ACN (30:70 v/v) with 0.05 % (v/v) formic acid was used for all solutions.

3.2.2 Application examples – FA composition in PS80 and in magnesium stearate

Analogous to Ilko et al. [21] a modified saponification and extraction process was employed. In 10.0 mL of a 10 % methanolic (v/v) 1 M KOH solution, 15 mg of the PS80 (n = 3) was incubated at 40 °C for 6 h. Subsequently, 250 μL of this solution was mixed with 50 μL formic acid in a glass centrifuge tube (VWR, Darmstadt, Germany) to obtain an acidic pH value. After addition of 500 μL *tert.*-butyl methyl ether and vortexing, an incubation period of 5 min was applied before centrifuging the tubes at 2700 x *g* for 5 min (EBA 20 centrifuge, Hettich, Tuttlingen, Germany). Finally, the collected organic phase was evaporated under a stream of nitrogen and the residue was dissolved in 1000 μL of the solvent mixture. A blank sample without PS80 was prepared according to the procedure described above. A 0.1 mg/mL test solution was prepared by dissolving 10.0 mg of magnesium stearate in 100.0 mL of the solvent mixture. A reference solution of magnesium acetate x 4 H_2O (0.05 mg/mL) in water was also analyzed.

3.3 HPLC-CAD conditions and equipment

All experiments were performed on a Vanquish™ Flex modular chromatographic system (Thermo Fisher Scientific, Germering, Germany) consisting of a dual pump F (two independent ternary solvent blending flow streams in one housing) with an online vacuum degasser, a thermostatted split sampler, a thermostatted column compartment with an active pre-heater, and a diode array detector in-line with a Vanquish™ Horizon CAD. The CAD was supplied with nitrogen gas from a 1010 Corona Nitrogen generator (Peak Scientific Instruments, Inchinnan, UK) connected to the in-house compressed air system. The instrument was controlled, and runs were processed using the Chromeleon™ 7.3 Chromatography Data System (Thermo Fisher Scientific).

Four different columns were tested: Waters SymmetryShield RP8 (C_8; 100 x 3.0 mm, 3.5 µm), Phenomenex Synergi Max-RP (C_{12}; 100 x 4.6 mm, 4.0 µm), Phenomenex Kinetex Evo C_{18} (150 x 4.6 mm, 2.6 µm), and Thermo Fisher Hypersil Gold C_{18} (150 x 2.1 mm, 3.0 µm). For column testing, the gradient the program of Ilko et al. [21] (see Table S1) was used. Mobile phase consisted of water and ACN, each containing 0.05 % (v/v) formic acid. The flow rate was 0.6 mL/min and the column temperature was set at 30 °C. Test solutions were injected in duplicate.

The face-centered CCD was applied in this study, as an RSM design, in order to obtain mathematical equations, their coefficients, and related standard errors [30]. Experimental factors and their levels varied in CCD are presented in Table S2, while the plan of experiments obtained according to CCD is displayed in Table 1 (see section 2.2.3). Components of the mobile phase were degassed in an ultrasonic bath for 15 min prior to use. After each change of LC conditions, the system was equilibrated for at least 10 column volumes, followed by a blank sample (water:ACN = 25:75, v/v). In order to achieve the best sensitivity, the final tuning of the CAD operating parameters was conducted. The CAD evaporation temperature, filter constant, and data collection rate were varied within following ranges: 20 – 40 °C, 1 – 10 s, and 1 – 10 Hz, respectively.

The final chromatographic conditions consisted of water and ACN each with 0.05 % (v/v) formic acid as mobile phase components and the Hypersil Gold C_{18} column as stationary phase. The column temperature was set to 33 °C and the injection volume to 10 µL at a flow rate of 0.575 mL/min. The percentage of the organic modifier was linearly increased starting from 70 % (v/v) to 80 % (v/v) within 14.2 min. This was followed by a re-equilibration step of 2.8 min. The CAD evaporation temperature was set to 25 °C, the filter constant to 3.6 s, and the data collection rate to 5 Hz. The PFV was set to 1.0 and a log-log transformation was used during validation experiments.

3.4 Tools used for generating RSM and MODR

The sequence of the required experimental runs (Table 1) was obtained by the Design Expert 7.0.0 software (Stat-Ease Inc., Minneapolis, MN, USA); it was also used for fitting mathematical models to the collected results and model quality assessment. In order to determine the zone of theoretical robustness based on developed CCD models, their coefficients, and standard errors MATLAB® R2018b (MathWorks, Natick, MA, USA) software was used. In particular, MATLAB served for indirect modeling of CMAs, grid point discretization, running MC simulations (statistical tool that takes into account the probability of meeting defined quality criteria) and, finally, generating an MODR graphical presentation.

4. Conclusion

Using a risk-based systematic AQbD approach, a robust and trustworthy HPLC-CAD method was developed for the analysis of eight FAs. The performance of the method was ensured within the defined MODR, allowing a long-lasting analytical method lifecycle where changes in chromatographic conditions within the MODR do not require regulatory notification and revalidation. The applicability of the method for the analysis of non-volatile FAs in PS80 and magnesium stearate was demonstrated. Its main limitation is the applicability in the analysis of only non-volatile FAs due to the basic operating principles of CADs. However, the main advantages of the proposed HPLC-CAD method are its less error-prone and time-saving nature compared to the pharmacopoeial GC method, and the higher sensitivity compared to the already existing HPLC-CAD method. The future perspective is the development of uniform sample preparation procedure for FA analysis. The powerful AQbD approach could be used in the optimization of potentially critical process parameters such as the saponification of the polysorbate and the subsequent extraction of the FAs.

Supplementary material

Table S1
Gradient program from Ilko et al. [21] for the separation of fatty acids using water and ACN each with 0.05 % (v/v) formic acid as mobile phases A and B, respectively, at a flow rate of 0.6 mL/min and a column temperature of 30 °C

time [min]	%-A (v/v)	%-B (v/v)
0 – 5	25	75
5 – 15	25 – 15	75 – 85
15 – 18	25	75

Table S2
Investigated levels of the critical method parameters (CMP) for the method optimization by means of design of experiments using a 3 x 3 face-centred central composite design

CMP	low level (-1)	nominal level (0)	high level (+1)
flow rate, X_1 [mL/min]	0.5	0.6	0.7
gradient time, X_2 [min]	8.0	11.5	15.0
column temperature, X_3 [°C]	30.0	35.0	40.0

Table S3
Peak characteristics (retention time (RT), capacity factor (k), symmetry factor (A_s), width at half height ($w_{0.05}$), separation factor (α) and resolution (R_s)) of the column screening experiments

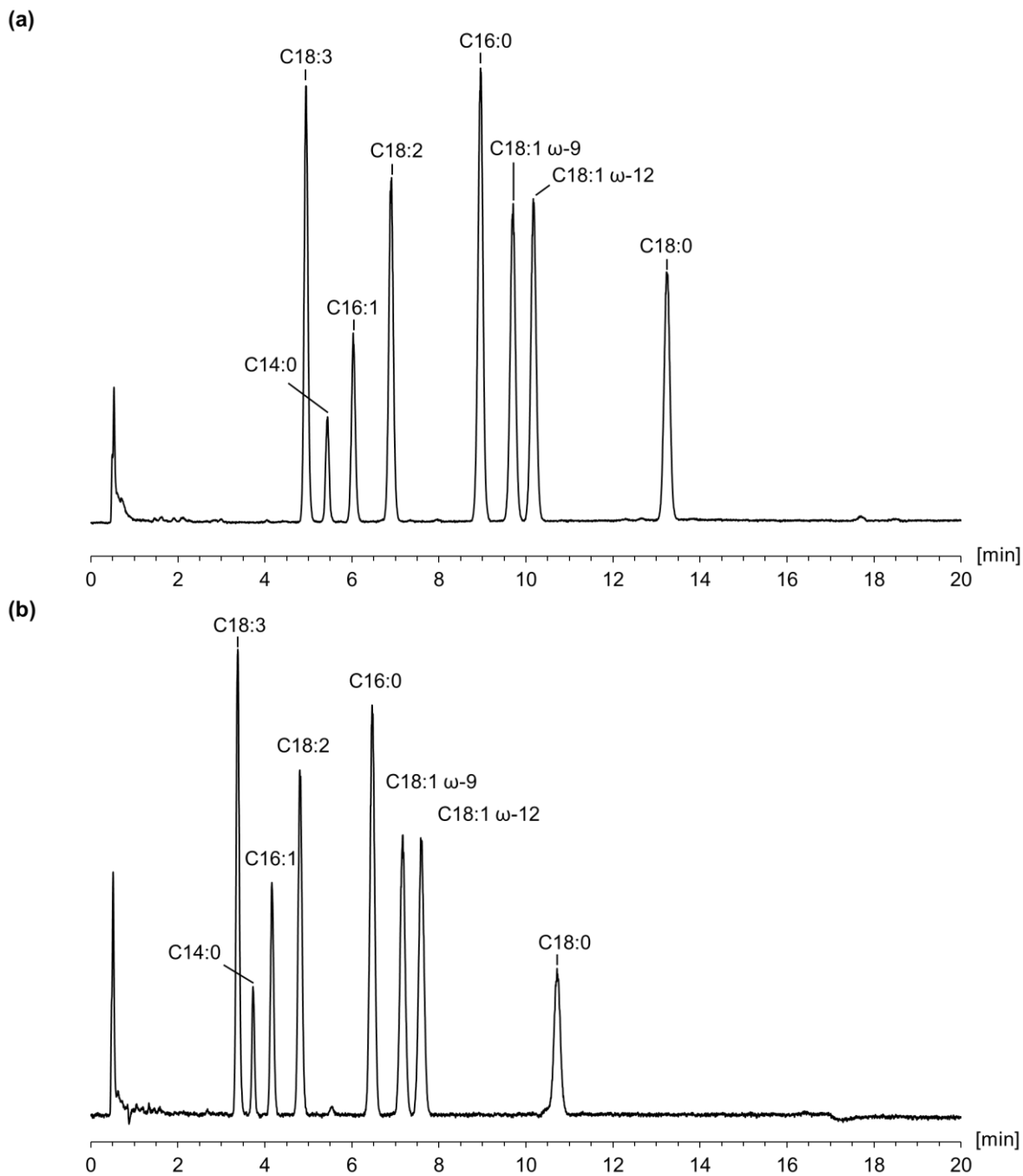| column	peak	myristic acid	palmitic acid	stearic acid	background noise
Symmetry Shield RP8 (100 x 3.0 mm, 3.5 µm)	RT	3.305 min	5.080 min	8.083 min	1.3 pA
	k	4.92	8.10	13.49	
	A_s	1.32	1.14	1.18	
	$w_{0.05}$	0.097 min	0.124 min	0.172 min	
	α	1.65	1.66	n.a. [a]	
	R_s	9.44	12.06	n.a. [a]	
Synergi Max-RP C$_{12}$ (100 x 4.6 mm, 4.0 µm)	RT	13.520 min			2.5 pA
	k	10.31	n.a. [a]	n.a. [a]	
	A_s	1.03			
	$w_{0.05}$	0.222 min			
	α	n.a. [a]			
	R_s	n.a. [a]			
Hypersil Gold C$_{18}$ (150 x 2.1 mm, 3.0 µm)	RT	3.252 min	5.647 min	9.828 min	0.9 pA
	k	4.63	8.77	16.0	
	A_s	1.13	1.01	1.02	
	$w_{0.05}$	0.0690 min	0.121 min	0.180 min	
	α	1.90	1.82	n.a. [a]	
	R_s	14.87	16.39	n.a. [a]	
Kinetex Evo C$_{18}$ (150 x 4.6 mm, 2.6 µm)	RT	9.077 min	14.423 min		1.1 pA
	k	4.19	7.25	n.a. [a]	
	A_s	1.07	1.01		
	$w_{0.05}$	0.127 min	0.144		
	α	1.72	n.a. [a]		
	R_s	23.28	n.a. [a]		

[a] not applicable

(a)

(b)

Fig. S1 Chromatogram of the test solution containing all FAs (0.1 mg/mL) applying a 15 min gradient program with a flow rate of 0.7 mL/min at a column temperature of 20 °C:
(a) linear increase of the ACN percentage from 65 % (v/v) to 85 % (v/v)
(b) linear increase of the ACN percentage from 70 % (v/v) to 80 % (v/v)

References

[1] R. Deidda, S. Orlandini, P. Hubert, C. Hubert, Risk-Based Approach for Method Development in Pharmaceutical Quality Control Context: A Critical Review, J. Pharm. Biomed. Anal. 161 (2018) 110-121.

[2] Industry 5.0. Available from: https://research-and-innovation.ec.europa.eu/research-area/industrial-research-and-innovation/industry-50_en (accessed 27.12.2022).

[3] International Council for Harmonisation of Technical Requirements for Pharmaceuticals for Human Use, Draft Guideline Q14 Analytical Procedure Development (2022).

[4] H. M. Inuwa, A. Ravi Raja, A. Kumar, B. Singh, S. Singh, Status of Industry 4.0 applications in healthcare 4.0 and Pharma 4.0, Mat. Today Proc. 62(6) (2022) 3593-3598.

[5] P. Jackson, P. Borman, C. Campa, M. Chatfield, M. Godfrey, P. Hamilton, W. Hoyer, F. Norelli, R. Orr, T. Schofield, Using the Analytical Target Profile to Drive the Analytical Method Lifecycle, Anal. Chem. 91 (2019) 2577-2585.

[6] P. Borman, P. Nethercote, M. Chatfield, D. Thompson, K. Truman, The Application of Quality by Design to Analytical Methods, Advanstar Communications Inc., Santa Monica, California, USA, (2007).

[7] E. Rozet, P. Lebrun, P. Hubert, B. Debrus, B. Boulanger, Design Spaces for analytical methods, TrAC Trends Anal. Chem. 42 (2013) 157-167.

[8] K. Gkountanas, A. Malenović, Y. Dotsikas, Determination of Bupropion and Its Impurities via a Chaotropic Chromatography Method Following Analytical Quality-by-Design Principles for Method Development, Pharmaceuticals 15 (2022) 1196.

[9] R. Szoleczky, M. Budai-Szűcs, E. Csányi, S. Berkó, P. Tonka-Nagy, I. Csóka, A. Kovács, Analytical Quality by Design (AQbD) Approach to the Development of In Vitro Release Test for Topical Hydrogel, Pharmaceutics 14 (2022) 707.

[10] A. Dispas, H. T. Avohou, P. Lebrun, P. Hubert, C. Hubert, 'Quality by Design' approach for the analysis of impurities in pharmaceutical drug products and drug substances, TrAC Trends Anal. Chem. 101 (2018) 24-33.

[11] G. Park, M. K. Kim, S. H. Go, M. Choi, Y. P. Jang, Analytical Quality by Design (AQbD) Approach to the Development of Analytical Procedures for Medicinal Plants, Plants 11 (2022) 2960.

[12] T. Verch, C. Campa, C. C. Chéry, R. Frenkel, T. Graul, N. Jaya, B. Nakhle, J. Springall, J. Starkey, J. Wypych, T. Ranheim, Analytical Quality by Design, Life Cycle Management, and Method Control. AAPS J. 24 (2022) 34.

[13] T. Tome, N. Žigart, Z. Časar, A. Obreza, Development and Optimization of Liquid Chromatography Analytical Methods by Using AQbD Principles: Overview and Recent Advances. Org. Process Res. Dev. 23 (2019) 1784-1802.

[14] International Council for Harmonisation of Technical Requirements for Pharmaceuticals for Human Use, Draft Guideline Q2 (R2) Validation of Analytical Procedure Development (2022).

[15] Council of Europe, European Pharmacopoeia, 10.8 edition, Monograph no. 0428 Polysorbate 80, Strasbourg, France (2022).

[16] Council of Europe, European Pharmacopoeia, 10.8 edition, Monograph no. 1234 Macrogol stearate, Strasbourg, France (2022).

[17] Council of Europe, European Pharmacopoeia, 10.8 edition, Monograph no. 0495 Glycerol monostearate 40-55, Strasbourg, France (2022).

[18] Council of Europe, European Pharmacopoeia, 10.8 edition, Monograph no. 0229 Magnesium stearate, Strasbourg, France (2022).

[19] Council of Europe, European Pharmacopoeia, 10.8 edition, Chapter 2.4.22. Composition of fatty acids by gas chromatography, Strasbourg, France (2022).

[20] A. N. Grechkin, L. S. Mukhtarova, M. Hamberg, Thermal conversions of trimethylsilyl peroxides of linoleic and linolenic acids, Chem. Phys. Lipids 138(1-2) (2005) 93-101.

[21] D. Ilko, A. Braun, O. Germershaus, L. Meinel, U. Holzgrabe, Fatty Acid Composition Analysis in Polysorbate 80 with High Performance Liquid Chromatography Coupled to Charged Aerosol Detection, Eur. J. Pharm. Biopharm. 94 (2015) 569-574.

[22] K. Schilling, R. Pawellek, K. Lovejoy, T. Muellner, U. Holzgrabe, Influence of Charged Aerosol Detector Instrument Settings on the Ultra-High-Performance Liquid Chromatography Analysis of Fatty Acids in Polysorbate 80. J. Chromatogr. A 1576 (2018) 58-66.

[23] International Council for Harmonisation of Technical Requirements for Pharmaceuticals for Human Use, Guideline Q8 (R2) Pharmaceutical Development (2009).

[24] L. R. Snyder, J. J. Kirkland, J. W. Dolan, Introduction to modern liquid chromatography, 3rd edition, John Wiley & Sons, Hoboken, New Jersey, USA (2010).

[25] G. P. Martin, K. Barnett, C. Burgess, P. D. Curry, J. Ermer, G. S. Gratzl, J. Hammond, J. Herrmann, E. Kovacs, D. J. LeBlond, R. LoBrutto, A. K. McCasland-Keller, P. L. McGregor, P. Nethercote, A. C. Templeton, D. P. Thomas, J. Weitzel, Lifecycle Management of Analytical Procedures: Method Development, Procedure Performance Qualification, and Procedure Performance Verification. Available from: https://www.uspnf.com/sites/default/files/usp_pdf/EN/USPNF/revisions/lifecycle_pdf.pdf (accessed 01.03.2023).

[26] International Council for Harmonisation of Technical Requirements for Pharmaceuticals for Human Use, Guideline Q9 (R1) Quality Risk Management (2023).

[27] T. Tol, N. Kadam, N. Raotole, A. Desai, G. Samanta, A simultaneous determination of related substances by high performance liquid chromatography in a drug product using quality by design approach, J. Chromatogr. A 1432 (2016) 26-38.

[28] L. V. Candioti, M. M. De Zan, M. S. Cámara, H. C. Goicoechea, Experimental design and multiple response optimization. Using the desirability function in analytical methods development, Talanta 124 (2014) 123-138.

[29] P. H. Gamache, Charged aerosol detection for liquid chromatography and related separation techniques, 1st edition, John Wiley & Sons, Hoboken, New Jersey, USA (2017).

[30] J. Stojanović, J. Krmar, A. Protić, B. Svrkota, N. Djajić, B. Otašević, DoE Experimental Design in HPLC Separation of Pharmaceuticals: A Review, Arch. Pharm. 71 (2021) 279-301.

[31]   B. Pasquini, S. Orlandini, S. Furlanetto, R. Gotti, M. Del Bubba, F. Boscaro, B. Bertaccini, M. Douša, G. Pieraccini, Quality by Design as a risk-based strategy in pharmaceutical analysis: Development of a liquid chromatography-tandem mass spectrometry method for the determination of nintedanib and its impurities, J. Chromatogr. A 1611 (2020) 460615.

[32]   L. Ferey, A. Raimbault, I. Rivals, K. Gaudin, UHPLC method for multiproduct pharmaceutical analysis by Quality-by-Design, J. Pharm. Biomed. Anal. 148 (2018) 361-368.

[33]   B. Otašević, J. Šljivić, A. Protić, N. Maljurić, A. Malenović, M. Zečević, Comparison of AQbD and grid point search methodology in the development of micellar HPLC method for the analysis of cilazapril and hydrochlorothiazide dosage form stability, Microchem. J. 145 (2019) 655-663.

[34]   M. A. Bezerra, R. E. Santelli, E. P. Oliveira, L. S. Villar, L. A. Escaleira, Response surface methodology (RSM) as a tool for optimization in analytical chemistry, Talanta 76(5) (2008) 965-977.

[35]   P. Lebrun, B. Govaerts, B. Debrus, A. Ceccato, G. Caliaro, P. Hubert, B. Boulanger, Development of a new predictive modelling technique to find with confidence equivalence zone and design space of chromatographic analytical methods, Chemom. Intell. Lab. Syst. 91(1) (2008) 4-16.

[36]   S. L. C. Ferreira, R. E. Bruns, E. G. P. da Silva, W. N. L. dos Santos, C. M. Quintella, J. M. David, J. B. de Andrade, M. C. Breitkreitz, I. C. S. F. Jardim, B. B. Neto, Statistical designs and response surface techniques for the optimization of chromatographic systems, J. Chromatogr. A 1158(1-2) (2007) 2-14.

[37]   International Council for Harmonisation of Technical Requirements for Pharmaceuticals for Human Use, Guideline Q2 (R1) Validation of Analytical Procedures (2005).

[38]   D. S. Risley, L.-E. Magnusson, P. R. Morow, A. Aburub, Analysis of magnesium from magnesium stearate in pharmaceutical tablet formulations using hydrophilic interaction liquid chromatography with nano quantity analyte detection, J. Pharm. Biomed. Anal. 78-79 (2013) 112-117.

[39]   J. Li, J. A. Stolee, A. Meda, Simultaneous quantitation of inorganic ions in oligonucleotides using mixed-mode liquid chromatography coupled with a charged aerosol detector, J. Pharm. Biomed. Anal. 204 (2021) 114244.

4. FINAL DISCUSSION

The overall aim of the studies performed here was to evaluate the advantages and disadvantages of innovative LC separation and detection techniques for the analysis of weakly chromophore impurities. In addition to the volatility of the mobile phase as a prerequisite for application of the CAD and MS instruments, other factors considerably influence the sensitivity and must thus be carefully selected. In order to facilitate the development of robust methods with a long life cycle and a statistically supported decision-making, software tools are available today that provide valuable support in accordance with the AQbD principles [1].

4.1. MMC for the analysis of carbocisteine API and drug product

With the RP/SAX column material used, a satisfactory separation performance could be achieved in both projects with their different objectives – on the one hand, the quantitative determination of the weakly chromophore main degradation products of the API with the CAD and, on the other hand, the untargeted, qualitative search for unknown impurities in syrup samples using HRMS. As a CAD-compatible mobile phase, the combination of trifluoroacetic acid and formic acid enabled a separation of the diastereomeric carbocisteine sulphoxides comparable to the TBAOH-IPC method and outperformed tributylamine as a volatile substituent (see Fig. 1). The omission of trifluoroacetic acid, which is necessary to improve ionisation efficiency, has reduced the resolution of this peak pair (see Fig. 1). However, since MS coupling involves further separation of the different analytes based on their m/z, some degree of co-elution is less critical (provided ionisation is not significantly affected).
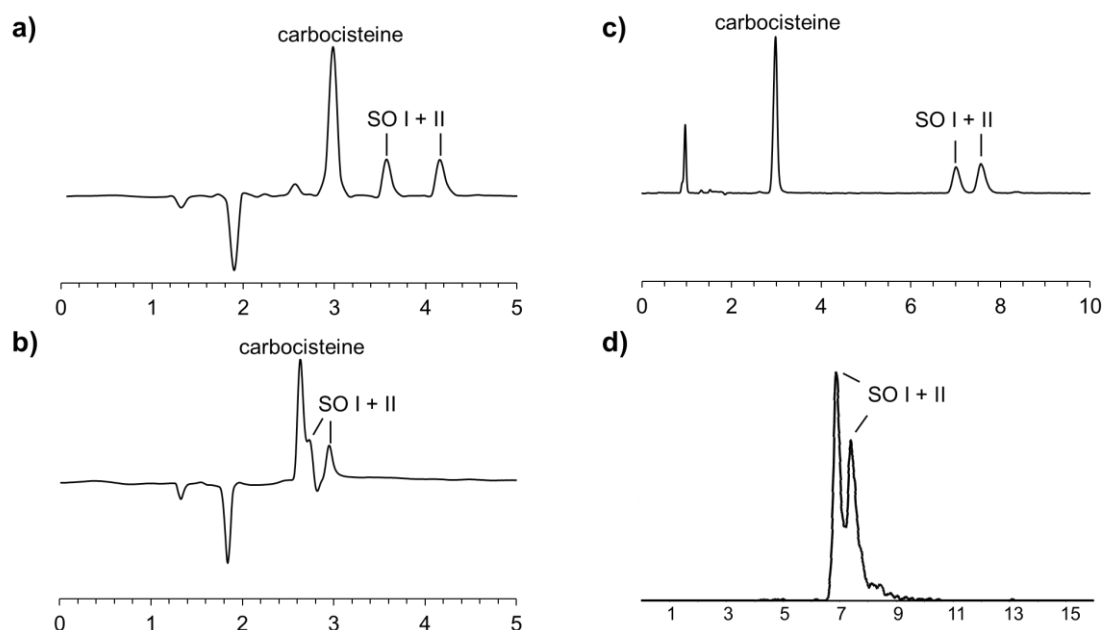

Fig. 1 Sections of the chromatograms illustrating the resolution of the diastereomeric sulfoxides (SO I + II) using ion pair chromatography with 25 mM TBAOH (a) or tributylamine (b) with UV detection at 230 nm and mixed-mode chromatography coupled to the CAD (c) or MS (d)

MMC is undoubtedly a valuable complement to IPC and HILIC for the analysis of polar, charged analytes, although all separation techniques have certain shortcomings (see Table 1) [2,3]. Although the understanding of the underlying separation mechanisms is improving, the multiple nature of interactions ultimately requires experimental verification of whether the Primesep SB column is an alternative to TBAOH for other acidic analytes. If this is the case, coupling with the CAD and/or (HR)MS creates exciting possibilities such as the determination of UV correction factors or identification of new, unexpected impurities that can improve and accelerate the drug development process. Especially for the characterization of finished drug products, which usually contain several physicochemically very different excipients, MMC is able to cover the broad range of very heterogeneous analytes [3].

Table 1
Limitations of ion pair chromatography (IPC), mixed-mode chromatography (MMC) and hydrophilic interaction liquid chromatography (HILIC) for coupling with the CAD or MS [2,3]

	IPC	MMC	HILIC
mobile phase	restricted to volatile IPRs[2]	restricted to volatile buffers/acidic modifiers	
column	altered selectivity due to sticking of the IPR[2]	column bleeding, short lifetime	
sensitivity	IPRs[2] influence background noise/ionization	column bleeding	high CAD response, column bleeding
sustainability	IPRs[2] often toxic	comparable to RP LC	high consumption of organic solvents

[1] cave: solubility organic-rich solvents
[2] IPR: ion-pairing reagents
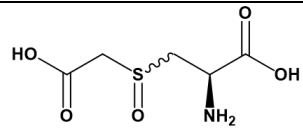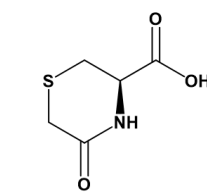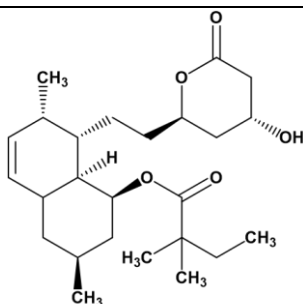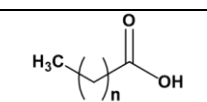
The fact that MMC columns from different manufacturers are not readily interchangeable despite nominally identical functionality probably delays their broader application in pharmacopoeias. For example, despite many advantages, an MMC-CAD method developed back in 2014 for the impurity profile of carbocisteine could not replace the rather unspecific and insensitive thin-layer chromatography test currently used in the Ph. Eur. monograph for ninhydrin-positive compounds [4,5]. The IPC method with TBAOH and detection at a low wavelength (cave: UV-cut off!) could be used as a more generic method for pharmacopoeias or routine quality control.

4.2. Charged aerosol detection for pharmacopoeial purpose

Despite the existing monopoly of a single manufacturer of CAD instruments, corresponding methods for the test for related substances are listed in both the USP and Ph. Eur [6]. The suitability of all new method developed in this work was proven by appropriate validation studies according to the ICH Q2 (R1) guideline [7]. Table 2 summarizes the performance characteristics for the different analytes.

Table 2
Overview of the CAD validation parameters of the analytes studied in this thesis

analyte	range µg/mL	linearity R^2	recovery[a] [%] (m/m)	repeatability[a] [%] RSD	LOQ (ng/column)
carbocisteine sulfoxide	5–17.5	0.9930	101–116	4.03–4.71	17.5–37.5
carbocisteine lactam	5–17.5	0.9953	101	2.52–3.57	42–50
dihydrosimvastatin	1–9.6	0.9974	98	1.92	1.75
various non-volatile fatty acids (chain lengths C_{14}-C_{18})	1–100	0.9873– 0.9995[b]	90–108	0.05–0.91	0.38–1.85

[a] determined at the lower end of the calibration curve
[b] after log-log transformation

When comparing the results, it is obvious that the sensitivity and precision of the MMC method is lower than that of the two RP methods. As already discussed in the chapters, the reasons for this are column bleeding, the higher concentration of ionic additives, the comparatively low percentage of organic solvent and the higher flow rate (see Table 3). Thanks to the zwitterionic character and the associated lower volatility, it was possible to increase the evaporation temperature for the carbocisteine project [8].

On the other hand, a low evaporation temperature and double logarithmic transformation of the data were required for the analysis of fatty acids due to some semi-volatility for satisfactory linearity (see Table 3) [9]. Although the CAD is a non-linear detector, a power function value of 1.0 was sufficient for satisfactory linearity in the other two projects due to the non-volatility and the relatively small concentration range. Depending on the LC separation technique chosen and the properties of the analytes, it is necessary to determine the optimum experimentally, with helpful data and advice in the literature speeding up the procedure [6,10].

Table 3
Comparison of the mobile phase characteristic and CAD settings of the final methods

method	carbocisteine	simvastatin	fatty acids
%-acetonitrile (v/v)	22 %	51–63 %	70–80 %
acidic additive	12 mM FA[a] + 2 mM TFA[b]	6.5 mM TFA[b]	13 mM FA[a]
flow rate	1.2 mL/min	0.4 mL/min	0.575 mL/min
evaporation temperature	65 °C	55 °C	25 °C
filter constant	10 s	5 s	3.6 s
data collection rate	10 Hz	5 Hz	5 Hz
data transformation	1.0 PFV[c]	1.0 PFV[c]	log-log

[a] FA: formic acid
[b] TFA: trifluoroacetcic acid
[c] PFV: power function value

Although highly sophisticated UV-CAD/MS systems (*via* a flow-splitting device) are probably the best strategy for universal detection and complete characterization of even volatile components, the less expensive hyphenation of UV and the CAD is helpful. In addition to the simultaneous detection of UV-active and inactive analytes with only one method, the universal response allows the determination of UV correction factors of unknown impurities and more accurate mass balance studies. With only a minor gradient slope, the dependence of the response on the organic percentage did not falsify the quantification of dihydrosimvastatin, which allows a simplified instrumental set-up and data evaluation. In addition to the analysis of APIs and/or impurities which lack a suitable chromophore, the CAD offers more up-to-date solutions for the characterisation of a variety of excipients [9,10]. Although these are more abundant in many drugs compared to API, many compendial methods are based on inaccurate bulk parameters that are difficult to compare, such as acid value or peroxide value. For quick implementation in pharmacopoeias, method development should follow AQbD principles and, in the best case, general methods for specific classes of excipients can be presented, e.g. as an alternative to existing GC methods.

4.3. Software-assisted LC data evaluation

Depending on the separation issue and the intended application of the method, the effort required for development and validation can vary greatly. In the simplest case of an identity test by matching the retention time, it is sufficient to prove the specificity, e.g. by comparison with a blank sample and determination of the peak purity [7]. Methods for impurity profiling are considerably more elaborate, requiring the separation of many structurally closely related substances and their sensitive detection down to a reporting threshold of 0.03 % (m/m) (daily dose higher than 2 g) in the presence of a large quantity of the API [11]. However, a high degree of robustness is desirable in all methods so that variations that occur (naturally) in practice (room temperature, relative humidity, lot-to-lot variability of reagents, etc.) do not invariably lead to invalid results. The investigation of robustness and the definition of system suitability criteria are therefore strongly recommended in the still valid ICH guideline Q2 (R1) [7]. For an efficient approach, two-stage screening designs have become established in laboratory practice. The use of DoE allows not only the identification of critical factors that must be kept between certain values, but also the statistically sound specification of the limits of the system suitability tests. Since any measurement is associated with a degree of uncertainty, the integration of risk-based approaches into the process of analytical method development is a logical consequence and is therefore addressed in the drafts of the revised ICH Q2 (R2) and new Q14 (R1) guideline [1,12]. To minimize the possibility of method failure, the AQbD approach represents a systematic procedure with the appropriate statistical tools including screening and optimization designs. In a first step, based on existing knowledge all potential influencing factors are visualized in a simple Ishikawa or Fishbone diagram (see Fig. 2). In the further course, more complex mathematical tools are employed to gain a deep understanding of the critical method parameters and attributes. For this purpose, depending on the preference and knowledge of the analyst, various software/statistical programs are available today that allow straightforward planning and evaluation of experiments as part of laboratory routine. A separate investigation of robustness is not necessary at this point since probabilistic simulations can be used to establish the *method operable design region*. Changes within this zone of theoretical robustness allow for flexible adaptation and, moreover, do not have to be reported to the authorities as a change or require re-validation [1,13]. Predictions of mathematical models always represent only an estimate of reality and must be verified experimentally. Furthermore, the validity of the predictions always depends on the correct model being chosen, which requires a good theoretical understanding of the theoretical relationships. The "classical" approach of method development does not lose any validity, of course, since a robust method is created at the end here as well [12].
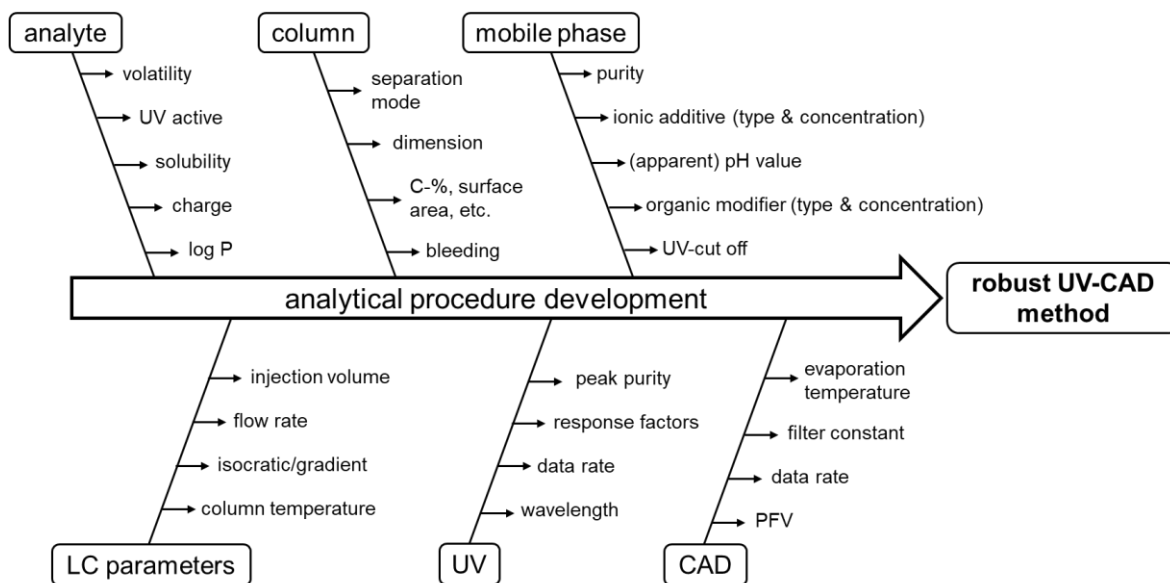
Fig. 2 Example of an *Ishikawa* diagram with analytical procedure parameters that potentially affect the performance of a hyphenated UV-CAD method

Computer-aided data analysis is also indispensable for handling the large amount of information acquired by untargeted HRMS approaches. With multiple ions reaching the detector every second of the chromatographic run and simultaneous MS/MS fragmentation experiments, sophisticated and automated workflows like GUCS are needed to enable straightforward evaluation without the risk of missing relevant information. A randomized sample sequence and of course the selection of the suitable reference sample are pivotal to take full advantage of the GUCS workflow. Despite the demonstrated advantages, the high costs stand in the way of a broader application for stability studies. However, the occurrence of unexpected and (geno-)toxic impurities has highlighted the possibilities of untargeted approaches in combination with software-assisted data evaluation for quality assessment of medicinal products [14].

4.4. References

[1]   International Council for Harmonisation of Technical Requirements for Pharmaceuticals for Human Use, Draft Guideline Q14 Analytical Procedure Development (2022).

[2]   Y. Kazakevich, R. LoBrutto, HPLC for pharmaceutical scientists, 1st edition, John Wiley & Sons, Hoboken, New Jersey, USA (2007).

[3]   K. Zhang, X. Liu, Reprint of Mixed-mode chromatography in pharmaceutical and biopharmaceutical applications, J. Pharm. Biomed. Anal. 130 (2016) 19-34.

[4]   O. Wahl, U. Holzgrabe, Impurity profiling of carbocisteine by HPLC-CAD, qNMR and UV/vis spectroscopy, J. Pharm. Biomed. Anal. 95 (2014) 1-10.

[5]   Council of Europe, European Pharmacopoeia, 11.0 edition, Monograph no. 0885 Carbocisteine, Strasbourg, France (2023).

[6]   K. Schilling, U. Holzgrabe, Recent applications of the Charged Aerosol Detector for liquid chromatography in drug quality control, J. Chromatogr. A 1619 (2020) 460911.

[7]   International Council for Harmonisation of Technical Requirements for Pharmaceuticals for Human Use, Guideline Q2 (R1) Validation of Analytical Procedures (2005).

[8]   K. Petritis, H. Dessans, L. Elfakir, M. Dreux, Volatility evaluation of mobile phase/electrolyte additives for mass spectrometry, LC GC Eur. 15(2) (2002) 98,100,102.

[9]   K. Schilling, R. Pawellek, K. Lovejoy, T. Muellner, U. Holzgrabe, Influence of charged aerosol detector instrument settings on the ultra-high-performance liquid chromatography analysis of fatty acids in polysorbate 80, J. Chromatogr. A 1576 (2018) 58-66.

[10]   P. H. Gamache, Charged aerosol detection for liquid chromatography and related separation techniques, 1st edition, John Wiley & Sons, Hoboken, New Jersey, USA (2017).

[11]   International Council for Harmonisation of Technical Requirements for Pharmaceuticals for Human Use, Guideline Q3 (R2) Impurities in New Drug Substances (2006).

[12]   International Council for Harmonisation of Technical Requirements for Pharmaceuticals for Human Use, Draft Guideline Q2 (R2) Validation of Analytical Procedures (2022).

[13]   T. Tome, N. Žigart, Z. Časar, A. Obreza, Development and Optimization of Liquid Chromatography Analytical Methods by Using AQbD Principles: Overview and Recent Advances. Org. Process Res. Dev. 23 (2019) 1784-1802.

[14]   O. Scherf-Clavel, M. Kinzig, A. Besa, A. Schreiber, C. Bidmon, M. Abdel-Tawab, J. Wohlfart, F. Sörgel, U. Holzgrabe, The contamination of valsartan and other sartans, Part 2: Untargeted screening reveals contamination with amides additionally to known nitrosamine impurities, J. Pharm. Biomed. Anal. 172 (2019) 278-284.

5. SUMMARY

In all the projects presented, it is evident that the selection of suitable separation conditions is only one side of the coin. Equally crucial in the development of methods for the quality assessment of APIs/drugs is the right detection system.

The application of CAD as an alternative to UV detection at low wavelength of the two weak chromophore main degradation products of the very polar, zwitterionic API carbocisteine requires the volatility of the mobile phase. Therefore, as a substitute for the non-volatile ion pairing reagent tetrabutylammonium hydroxide (TBAOH), six different volatile alkylamines as well as a RP/SAX mixed-mode column were evaluated. The best selectivity and separation performance comparable to TBAOH was achieved with the RP/SAX column and a mixture of formic acid and trifluoroacetic acid. For the simultaneous optimisation of the evaporation temperature of the CAD as a function of two chromatographic parameters, a central composite design was chosen and the "desirability function" was subsequently applied for modelling. In addition, column bleeding was investigated with a second RP/SAX column (different batch) with the result that the acetonitrile percentage had to be adjusted and preconditioning by injection of concentrated samples is essential. The final mixed-mode method was finally validated with both columns according to the ICH Q2 (R1) guideline.

Based on this, an MS-compatible method was developed with little effort using an identical RP/SAX column in UPLC dimension for the untargeted analysis by HRMS of two carbocisteine-containing prototype syrup formulations. For a comprehensive characterisation, HRMS and MS/HRMS data were recorded simultaneously by *information dependent acquisition* mode. Based on the exact masses, isotope patterns and an *in silico* plausibility check of the fragment spectra, the prediction of the structures of the unknown impurities was possible. In both syrup samples, which had been stored for nine months at 40 °C and 75 % r.h., two additional impurities of carbocisteine (i.e. lactam of the sulfoxides and disulphide between cysteine and thioglycolic acid) were identified by comparison with the corresponding prototype placebo samples using *general unknown comparative screening*. In addition, the formation of Maillard products by binary mixtures with ^{13}C-labelled sugars was revealed in the sucrose-containing formulation.

For the promising hyphenation of the UV detector with the CAD for the simultaneous detection of all UV-active impurities of the cholesterol-lowering drug simvastatin and the only weak chromophore dihydrosimvastatin, the Ph. Eur. method had to be adapted. Besides replacing phosphoric acid with trifluoroacetic acid, the gradient also had to be adjusted and a third critical peak pair was observed. Based on validation experiments (according to the ICH Q2 (R1) guideline), the suitability of the CAD for sensitive detection (LOQ = 0.0175 % m/m) was proven.

To further investigate the robustness of the adapted method and CAD, a Plackett-Burman design was chosen. None of the factors had a statistically significant effect on the S/N of the CAD in the ranges tested. Regarding the three critical peak pairs, on the other hand, the factors to be controlled were statistically established, so that a targeted correction is possible if the system suitability test is not passed. The idea of employing a hyphenated UV-CAD system was finally applied to the structurally closely related lovastatin and its specified impurity dihydrolovastatin. Here, the CAD showed a significantly better S/N compared to the compendial UV detection at 200 nm.

The suitability of CAD for the analysis of non-volatile fatty acids in polysorbate 80 (PS80) as favourable alternative to the Ph. Eur. GC method (no time-consuming, error-prone and toxic derivatisation) has already been demonstrated. The aim of this project was therefore to develop a robust method with a focus on the AQbD principles, which can be used for the analysis of other excipients with similar fatty acid composition. After the definition of the *analytical target profile* and a risk assessment by means of an Ishikawa diagram, a suitable C$_{18}$ column and the chromatographic framework conditions (formic acid concentration and initial/final gradient conditions) were selected after only few preliminary runs. The remaining critical method parameters were then investigated with the help of DoE and RSM. Using the obtained model equations, Monte Carlo simulations were performed to create the *method operable design region* as a region of theoretical robustness. After validation according to ICH Q2 (R1), the fatty acid composition of a magnesium stearate batch was successfully analysed as a further application example in addition to PS80.

The CAD was able to prove its potential in all the issues investigated in the context of this doctoral thesis. As a cost-effective alternative compared to MS instruments, it thus closes a gap in the quality assessment of APIs or excipients without a suitable chromophore. The easy method transfer to (HR)MS instruments also allows for a unique degree of sample characterisation through untargeted approaches in case of new impurities. For resource- and time-efficient work, the possibilities and limitations of software tools for method development and data evaluation as well as the application of risk-based approaches such as AQbD should also be considered.

6. ZUSAMMENFASSUNG

In allen vorgestellten Projekten wird deutlich, dass die Auswahl geeigneter Trennbedingungen nur eine Seite der Medaille darstellen. Ebenso entscheiden bei der Entwicklung von Methoden zur Qualitätsbeurteilung von Wirkstoffen und Arzneimitteln ist das richtige Detektionssystem.

Die Verwendung des CAD als Alternative zur UV-Detektion bei niedriger Wellenlänge der beiden schwach chromophoren Hauptabbauprodukte des sehr polaren, zwitterionischen Wirkstoffs Carbocystein erfordert die Flüchtigkeit der mobilen Phase. Daher wurden als Ersatz für das nichtflüchtige Ionenpaarreagenz Tetrabutylammoniumhydroxid (TBAOH) sechs verschiedene flüchtige Alkylamine sowie eine RP/SAX Mixed-Mode-Säule untersucht. Die Beste mit TBAOH vergleichbare Selektivität und Trennleistung wurde mit der RP/SAX-Säule und einer Mischung aus Ameisensäure und Trifluoressigsäure erreicht. Für die gleichzeitige Optimierung der Verdampfungstemperatur des CAD in Abhängigkeit von zwei chromatographischen Parametern wurde ein zentral zusammengesetztes Versuchsdesign gewählt und anschließend die *desirability function* zur Modellierung eingesetzt. Darüber hinaus wurde das Säulenbluten mit einer zweiten RP/SAX-Säule (einer anderen Charge) untersucht, mit dem Ergebnis, dass der Acetonitrilanteil angepasst werden musste und eine Vorkonditionierung durch Injektion konzentrierter Proben unerlässlich ist. Die endgültige Mixed-Mode-Methode wurde schließlich mit beiden Säulen gemäß der ICH-Richtlinie Q2 (R1) validiert.

Darauf aufbauend konnte mit geringem Aufwand ein MS-kompatibles Methode mit einer identischen RP/SAX-Säule in UPLC-Dimension für die ungezielte HRMS-Analyse von zwei Carbocystein-haltigen Sirup-Prototypformulierungen entwickelt werden. Für eine umfassende Charakterisierung wurden HRMS- und MS/HRMS-Daten gleichzeitig im *information dependent analysis*-Modus aufgenommen. Anhand der exakten Massen, Isotopenmuster und *In-silico*-Plausibilitätsprüfung der Fragmentspektren war die Vorhersage der Strukturen der unbekannten Verunreinigungen möglich. In den beiden Sirupproben, die neun Monate lang bei 40 °C und 75 % r.F. gelagert worden waren, wurden zwei zusätzliche Verunreinigungen von Carbocystein (sprich das Lactam der Sulfoxide und das Disulfid zwischen Cystein und Thioglykolsäure) durch Vergleich mit den entsprechenden Prototyp-Placeboproben mittels *general unknown comparative screening* identifiziert. Darüber hinaus wurde die Bildung von Maillard-Produkten durch binäre Mischungen mit ^{13}C-markierten Zuckern in der Saccharose-haltigen Formulierung bestätigt. Für die vielversprechende Kopplung des UV-Detektors mit dem CAD zum gleichzeitigen Nachweis aller UV-aktiven Verunreinigungen des Cholesterinsenkers Simvastatin und des nur schwach chromophoren Dihydrosimvastatins musste die Ph. Eur.-Methode angepasst werden.

Neben dem Austausch von Phosphorsäure durch Trifluoressigsäure musste auch der Gradient geändert werden, und es wurde ein drittes kritisches Peakpaar beobachtet. Anhand von Validierungsexperimenten (gemäß der ICH Q2 (R1) Richtlinie) wurde die Eignung des CAD für einen empfindlichen Nachweis (LOQ = 0.0175 % m/m) bewiesen. Um die Robustheit der angepassten Methode und des CAD näher zu untersuchen, wurde ein Plackett-Burman-Design gewählt. Keiner der Faktoren hatte einen statistisch signifikanten Einfluss auf das S/N des CAD in den getesteten Bereichen. Für die drei kritischen Peakpaare hingegen wurden die zu kontrollierenden Faktoren statistisch ermittelt, sodass eine gezielte Korrektur möglich ist, wenn der Systemeignungstest nicht bestanden wird. Die Idee der Verwendung eines kombinierten UV-CAD-Systems wurde schließlich auf das strukturell eng verwandte Lovastatin und dessen spezifizierte Verunreinigung Dihydrolovastatin angewendet. Hier zeigte der CAD ein deutlich besseres S/N im Vergleich zur kompendialen UV-Detektion bei 200 nm.

Die Eignung von CAD für die Analyse von nichtflüchtigen Fettsäuren in Polysorbat 80 (PS80) als vorteilhafte Alternative zur GC-Methode im Ph. Eur. (keine zeitaufwändige, fehleranfällige und toxische Derivatisierung) wurde bereits gezeigt. Ziel dieses Projekts war es daher, eine robuste Methode zu entwickeln, die sich an den Prinzipien des AQbD orientiert und auch für die Analyse weiterer Hilfsstoffe mit ähnlicher Fettsäurezusammensetzung eingesetzt werden kann. Nach der Definition des *analytical target profiles* und einer Risikobewertung mit einem Ishikawa-Diagramms wurden nach nur wenigen Vorversuchen eine geeignete C_{18}-Säule und die chromatographischen Rahmenbedingungen (Ameisensäurekonzentration und Anfangs-/Endbedingungen des Gradienten) ausgewählt. Die übrigen kritischen Methodenparameter wurden dann mit Hilfe von DoE und RSM untersucht. Unter Verwendung der erhaltenen Modellgleichungen wurden Monte-Carlo-Simulationen durchgeführt, um die *Method Operable Design Region* als Zone der theoretischen Robustheit zu erstellen. Nach der Validierung gemäß ICH Q2 (R1) wurde als weiteres Anwendungsbeispiel neben PS80 auch die Fettsäurezusammensetzung einer Magnesiumstearat-Charge erfolgreich analysiert.

Das CAD konnte sein Potential in allen im Rahmen dieser Dissertation untersuchten Fragestellungen unter Beweis stellen. Als kostengünstige Alternative zu MS-Geräten schließt es damit eine Lücke bei der Qualitätsbewertung von Wirk- oder Hilfsstoffen ohne geeignetes Chromophor. Der einfache Methodentransfer auf (HR)MS-Instrumente ermöglicht zudem einen einzigartigen Grad der Probencharakterisierung durch ungezielte Ansätze im Falle neuer Verunreinigungen. Für ein ressourcen- und zeiteffizientes Arbeiten sollten zudem die Möglichkeiten und Grenzen von Softwaretools für die Methodenentwicklung und Datenauswertung sowie die Anwendung risikobasierter Ansätze wie AQbD bedacht werden.

7. APPENDIX

7.1. List of publications

Research papers

- R. Walther, O. Scherf-Clavel, U. Holzgrabe, Method transfer from ion pair chromatography to charged aerosol detector-compatible mixed-mode chromatography: A case study using carbocisteine, J. Chromatogr. Open 1 (2021) 1000014.

- R. Walther, M. Kinzig, A. Zamponi, F. Sörgel, O. Scherf-Clavel, U. Holzgrabe, Identification of low-level impurities in drug prototypes of carbocisteine by means of liquid chromatography-high-resolution mass spectrometry and general unknown comparative screening. Manuscript submitted for publication.

- R. Walther, U. Holzgrabe, Simplification of pharmacopoeial liquid chromatography methods for related substances of statins by hyphenated ultraviolet and charged aerosol detection, J. Pharm. Biomed. Anal. 225(9) (2022) 115218.

- R. Walther, J. Krmar, A. Leistner, B. Svrkota, B. Otašević, A. Malenović, U. Holzgrabe, A. Protić, Analytical quality by design: Achieving robustness of an LC-CAD method for the analysis of non-volatile fatty acids, Pharmaceuticals 16(4) (2023) 478.

- J. Hofmann, P. Spatz, R. Walther, M. Gutmann, T. Maurice, M. Decker, Synthesis and biological evaluation of flavonoid-cinnamic acid amide hybrids with distinct activity against neurodegeneration in vitro and in vivo, Chem. Eur. J. 28(39) (2022) e202200786.

Other publications

- R. Walther, U. Holzgrabe, Qualitätssicherung von Arzneimitteln – Upgrade für Arzneibuchmonographien durch den Charged Aerosol Detektor. Manuscript accepted for publication in PZ Prisma, Avoxa, Eschborn.

7.2. Documentation of authorship

In this section, the individual contribution for each author to the publications reprinted in this thesis is specified. Unpublished manuscripts are handled accordingly.

Autor 1 (RW), Autor 2 (OSC), Autorin 3 (UH)				
Autor	**RW**	**OSC**	**UH**	**∑ in Prozent**
Studiendesign	5%	2.5%	2.5%	10%
Experimentelle Arbeit	30%			30%
Datenanalyse und Interpretation	20%	2.5%	2.5%	25%
Verfassen der Veröffentlichung	22.5%			22.5%
Korrektur der Veröffentlichung		5%	5%	10%
Koordination der Veröffentlichung			2.5%	2.5%
Summe	77.5%	10%	12.5%	100%

Erklärung zur Autorenschaft

Analysis of weakly chromophore impurities by means of liquid chromatography coupled with charged aerosol detection and mass spectrometry

Method transfer from ion pair chromatography to charged aerosol detector-compatible mixed-mode chromatography: A case study using carbocisteine
Rasmus Walther, Oliver Scherf-Clavel, Ulrike Holzgrabe
Journal of Chromatography Open, 2021, 1, 100014

Die Mitautoren der in dieser (teil-)kumulativen Dissertation verwendeten Manuskripte sind sowohl über die Nutzung als auch über die angegebenen Eigenanteile informiert und stimmen dem zu.

Rasmus Walther	Oliver Scherf-Clavel	Ulrike Holzgrabe
Hauptautor/in	**Koautor/in**	**Korrespondenzautor/in**
☒ Verweis: E-Mail hinterlegt	☒ Verweis: E-Mail hinterlegt	☒ Verweis: E-Mail hinterlegt

Würzburg, 2. Mai 2023   _____

(Datum)   Prof. Dr. Ulrike Holzgrabe

Erklärung zur Autorenschaft

Analysis of weakly chromophore impurities by means of liquid chromatography coupled with charged aerosol detection and mass spectrometry

Identification of low-level impurities in drug prototypes of carbocisteine by means of liquid chromatography-high-resolution mass spectrometry and general unknown comparative screening

Rasmus Walther, Martina Kinzig, Annette Zamponi, Fritz Sörgel, Oliver Scherf-Clavel, Ulrike Holzgrabe

Manuscript submitted for publication.

Autor 1 (RW), Autorin 2 (MK), Autorin 3 (AZ), Autor 4 (FS), Autor 5 (OSC), Autorin 6 (UH)							
Autor	**RW**	**MK**	**AZ**	**FS**	**OSC**	**UH**	**∑ in Prozent**
Studiendesign	4%		2%		4%	4%	14%
Experimentelle Arbeit	26%						26%
Datenanalyse und Interpretation	26%						26%
Verfassen der Veröffentlichung	15%						15%
Korrektur der Veröffentlichung		1%	2%	1%	5%	5%	14%
Koordination der Veröffentlichung					1%	4%	5%
Summe	71%	1%	4%	1%	10%	13%	100%

Erklärung zur Autorenschaft

Analysis of weakly chromophore impurities by means of liquid chromatography coupled with charged aerosol detection and mass spectrometry

Identification of low-level impurities in drug prototypes of carbocisteine by means of liquid chromatography-high-resolution mass spectrometry and general unknown comparative screening
Rasmus Walther, Martina Kinzig, Annette Zamponi, Fritz Sörgel, Oliver Scherf-Clavel, Ulrike Holzgrabe
Manuscript submitted for publication.

Die Mitautoren der in dieser (teil-)kumulativen Dissertation verwendeten Manuskripte sind sowohl über die Nutzung als auch über die angegebenen Eigenanteile informiert und stimmen dem zu.

Rasmus Walther	Martina Kinzig	Annette Zamponi
Hauptautor/in	**Koautor/in**	**Koautor/in**
☒ Verweis: E-Mail hinterlegt	☒ Verweis: E-Mail hinterlegt	☒ Verweis: E-Mail hinterlegt

Fritz Sörgel	Oliver Scherf-Clavel	Ulrike Holzgrabe
Koautor/in	**Korrespondenzautor/in**	**Korrespondenzautor/in**
☒ Verweis: E-Mail hinterlegt	☒ Verweis: E-Mail hinterlegt	☒ Verweis: E-Mail hinterlegt

Würzburg, 2. Mai 2023   _____

(Datum)   Prof. Dr. Ulrike Holzgrabe

Erklärung zur Autorenschaft

Analysis of weakly chromophore impurities by means of liquid chromatography coupled with charged aerosol detection and mass spectrometry

Simplification of pharmacopoeial liquid chromatography methods for related substances of statins by hyphenated ultraviolet and charged aerosol detection
Rasmus Walther, Ulrike Holzgrabe
Journal of Pharmaceutical and Biomedical Analysis, 2023, 225, 115218

Autor 1 (RW), Autorin 2 (UH)			
Autor	**RW**	**UH**	**∑ in Prozent**
Studiendesign	5%	5%	10%
Experimentelle Arbeit	30%		30%
Datenanalyse	25%	5%	30%
Verfassen der Veröffentlichung	20%		20%
Korrektur der Veröffentlichung		5%	5%
Koordination der Veröffentlichung		5%	5%
Summe	80%	20%	100%

Erklärung zur Autorenschaft

Analysis of weakly chromophore impurities by means of liquid chromatography coupled with charged aerosol detection and mass spectrometry

Simplification of pharmacopoeial liquid chromatography methods for related substances of statins by hyphenated ultraviolet and charged aerosol detection
Rasmus Walther, Ulrike Holzgrabe
Journal of Pharmaceutical and Biomedical Analysis, 2023, 225, 115218

Die Mitautoren der in dieser (teil-)kumulativen Dissertation verwendeten Manuskripte sind sowohl über die Nutzung als auch über die angegebenen Eigenanteile informiert und stimmen dem zu.

Rasmus Walther	Ulrike Holzgrabe
Hauptautor/in	**Korrespondenzautor/in**
☒ Verweis: E-Mail hinterlegt	☒ Verweis: E-Mail hinterlegt

Würzburg, 2. Mai 2023 _____

(Datum) Prof. Dr. Ulrike Holzgrabe

Erklärung zur Autorenschaft

Analysis of weakly chromophore impurities by means of liquid chromatography coupled with charged aerosol detection and mass spectrometry

Analytical quality by design: Achieving robustness of an LC-CAD method for the analysis of non-volatile fatty acids
Rasmus Walther, Jovana Krmar, Adrian Leistner, Bojana Svrkota, Bilijana Otašević, Andjelija Malenović, Ulrike Holzgrabe, Ana Protić
Pharmaceuticals, 2023, 16(4) 478

Autor 1 (RW), Autorin 2 (JK), Autor 3 (AL), Autorin 4 (BS), Autorin 5 (BO), Autorin 6 (AM), Autorin 7 (UH), Autorin 8 (AP)

Autor	RW	JK	AL	BS	BO	AM	UH	AP	∑ in Prozent
Studiendesign	1.5%	1.5%	1.5%				1.5%	1.5%	7.5%
Experimentelle Arbeit: HPLC	15%		10%						25%
Experimentelle Arbeit: Modelling		15%		5%		2.5%			22.5%
Datenanalyse und Interpretation	5%	5%	2.5%	2.5%					15%
Verfassen der Veröffentlichung	5%	5%	2.5%	2.5%	2.5%			2.5%	20%
Korrektur der Veröffentlichung							2.5%	2.5%	5%
Koordination der Veröffentlichung							2.5%	2.5%	5%
Summe	26.5%	26.5%	16.5%	10%	2.5%	2.5%	6.5%	9%	100%

Erklärung zur Autorenschaft

Analysis of weakly chromophore impurities by means of liquid chromatography coupled with charged aerosol detection and mass spectrometry

Analytical quality by design: Achieving robustness of an LC-CAD method for the analysis of non-volatile fatty acids
Rasmus Walther, Jovana Krmar, Adrian Leistner, Bojana Svrkota, Bilijana Otašević, Andjelija Malenović, Ulrike Holzgrabe, Ana Protić
Pharmaceuticals, 2023, 16(4) 478

Die Mitautoren der in dieser (teil-)kumulativen Dissertation verwendeten Manuskripte sind sowohl über die Nutzung als auch über die angegebenen Eigenanteile informiert und stimmen dem zu.

Rasmus Walther

Hauptautor/in

☒ Verweis: E-Mail hinterlegt

Jovana Krmar

Hauptautor/in

☒ Verweis: E-Mail hinterlegt

Adrian Leistner

Koautor/in

☒ Verweis: E-Mail hinterlegt

Bojana Svrkota

Koautor/in

☒ Verweis: E-Mail hinterlegt

Bilijana Otašević

Koautor/in

☒ Verweis: E-Mail hinterlegt

Andjelija Malenović

Koautor/in

☒ Verweis: E-Mail hinterlegt

Ulrike Holzgrabe

Korrespondenzautor/in

☒ Verweis: E-Mail hinterlegt

Ana Protić

Korrespondenzautor/in

☒ Verweis: E-Mail hinterlegt

Würzburg, 2. Mai 2023

(Datum)

_____

Prof. Dr. Ulrike Holzgrabe